POLITECNICO DI MILANO

SCHOOL OF INDUSTRIAL AND INFORMATION ENGINEERING

MASTER DEGREE IN CHEMICAL ENGINEERING

# KINETIC MODELING AND ANALYSIS OF METHANE COMBUSTION IN MILD OXY-FUEL CONDITIONS.

Candidate:

**Fabio DE CAPITANI  850344**

Advisor:

**Prof. Tiziano FARAVELLI**

Co-advisor:

**Ing. Alessandro STAGNI**

Academic Year 2016 – 2017

*To my family*

# Acknowledgements

In principio, il mio più profondo ringraziamento va al Professor Tiziano Faravelli per il continuo supporto e gli stimolanti confronti durante tutto il percorso di Tesi, che hanno permesso di ampliare la mia conoscenza, la mia esperienza e le mie abilità in ambiti non solo legati all'ingegneria. Un enorme grazie va anche ad Alessandro Stagni per la grande pazienza e disponibilità con le quali mi ha supportato durante questi quindici mesi. Grazie per gli innumerevoli incontri dai quali ho avuto la possibilità di apprendere ogni volta qualcosa di nuovo, motivandomi a non arrendere mai la voglia di imparare. Un ringraziamento va anche a Matteo Pelucchi per il supporto datomi attraverso le numerose idee e suggerimenti conferitomi durante gran parte del lavoro svolto. Vorrei, anche, ringraziare tutto il gruppo CRECK del Politecnico di Milano, in particolare Isabella, Giancarlo, Paulo, Magnus e i Professori Alessio Frassoldati, Alberto Cuoci e Eliseo Ranzi.

Grazie ai miei compagni di corso Riccardo Brazzoli e Jaspreet Singh con i quali, in questi cinque anni, ho condiviso gioie, risate, sofferenze e importanti traguardi. Ringrazio anche tutti i compagni con i quali ho condiviso l'aula tesisti oltre alle tante risate e pause pranzo insieme. In particolare Matteo Mensi, Erica Quadarella, Paolo Guida, Francesca Gallone, Federica Zamarian e Ayoub El Ziani. Grazie anche a tutti i colleghi del Politecnico per i momenti passati insieme, sia di studio che di svago. Grazie, inoltre, agli amici di sempre che hanno reso più leggeri questi anni di impegno e sacrifici.

Il più profondo ringraziamento va alla mia famiglia per avermi reso ciò che sono. In primis ai miei genitori per l'incondizionato supporto morale ed economico negli

studi, per tutti gli insegnamenti e, soprattutto, per aver sempre creduto in me. Grazie a mia sorella, Francesca, per essere stata sempre presente e per essere la mia tifosa numero uno. Grazie anche ai miei nonni e a mia nonna per avermi sempre motivato e sostenuto e un grazie anche a tutti i miei zii e cugini.

Un ringraziamento speciale va alla mia fidanzata, Marina, per avermi dato e per aver condiviso con me i migliori anni della mia vita. Grazie per il sostegno, il sacrificio e il supporto nei momenti di difficoltà, ma, soprattutto, grazie per l'amore incondizionato che ha reso ogni istante unico e indimenticabile.

<div align="right">Milano, 21 Dicembre 2017</div>

# Conferences

**De Capitani, F.**, Stagni, A., Pelucchi, M., Faravelli, T., De Joannon, M., Sabia, P., Lubrano Lavadera, M. A Kinetic Study of the Oscillating Combustion of Hydrogen and Syngas in Well-stirred Reactors, 3rd General Meeting and Workshop on SECs in Industry of SMARTCATs Action, October 25-27, 2017, Prague.

# Contents

# Abstract

T HE use of combustion for the production of energy must comply with increasingly stringent regulations, pushing towards higher efficiencies and lower emissions of pollutant compounds. In this scenario, the research towards newer fuels and burning technologies assumes a key importance. Among several processes of the petrochemical industry, steam cracking is definitely one of the most energy intensive. In this context, the European project Horizon 2020 IMPROOF has the aim to develop novel furnaces to drastically improve the energy efficiency by at least 20%, simultaneously reducing the emissions of greenhouse gases and $NO_x$ per ton of ethylene produced with at least 25%. For this purpose, oxy-combustion, in presence of high $H_2O$ and $CO_2$ dilution levels, has been identified as the solution to minimize the amount of $NO_x$ produced. The use of alternative fuels as bio-gas and bio-oil constitutes the solution to decrease the greenhouse gases thanks to their vegetable origin.

The purpose of the present Thesis is the development of a detailed kinetic mechanism able to predict the behavior of methane combustion in MILD oxy-fuel conditions. In fact, methane is at the basis of the combustion kinetics for all hydrocarbon and, simultaneously, it can be fed as fuel in steam cracking furnaces. On the basis of a huge collection of experimental data in the conditions of interest, the kinetic model previously developed by CRECK Modeling group at Politecnico di Milano has been opportunely modified in order to include the conditions of interest. This process has been supported by the "Aramco" mechanism, considered as a reference for the kinetic modeling of combustion of hydrocarbon up to 4 carbon atoms.

The performances of the obtained mechanism have been successfully verified

in a broad range of experimental data within ideal reactors, including perfectly-stirred reactors, plug-flow reactors and premixed laminar flames. Moreover, the model has been used to analyze the oscillating oxy-combustion of methane within Continuous Stirred Tank Reactors (CSTR). Such phenomenon, for these devices, has been observed frequently during the combustion of several hydrocarbon. Therefore, in this Thesis, a kinetic study has been performed with the purpose to identify the causes of such undesirable phenomenon. The preliminary analysis has interested simpler fuels like hydrogen and syngas. In such a way, the competition between branching and third-body reaction for the hydrogen radical consumption through the interaction with oxygen molecules has been identified as the main cause of the inhibition of reactivity and, thus, also of the oscillations onset. On the other hand, in case of methane, the oscillations are determined by the competition among the branching reaction between H and $O_2$ and all the termination reactions responsible of the H and OH radicals consumption. This has been demonstrated by introducing the "branching ratio". It is defined as the ratio between the branching reaction rate and the sum of the rates of all the termination channels. The system is able to achieve steady-state conditions when branching outweighs termination reactions, i.e. when the "branching ratio" assumes a constant value higher than 1. At the same time, maps characterizing the operating conditions suitable to the onset of oscillatory limit cycles have been developed for the three fuels.

# Sommario

L A produzione di energia tramite processi di combustione è al giorno d'oggi sottoposta a limiti di legge sempre più restrittivi, che spingono verso maggiori efficienze e minori emissioni di sostanze inquinanti. In questo scenario, la ricerca verso nuovi combustibili e nuove tecnologie di combustione assume un ruolo di primo piano. Tra i vari processi dell'industriale petrolifera, lo steam cracking è sicuramente uno tra i più energivori. In questo contesto, il progetto europeo Horizon 2020 IMPROOF ha il compito di sviluppare forni innovativi con lo scopo di migliorare l'efficienza energetica del 20%, abbattendo, allo stesso tempo, almeno il 25% delle emissioni totali di gas serra e $NO_x$ per tonnellata di etilene prodotta. A tal fine, l'ossicombustione in presenza di alti livelli di diluizione attraverso vapore acqueo e anidride carbonica (MILD) è stata identificata come una possibile tecnologia per soddisfare tali obiettivi. Infatti, l'ossicombustione in presenza di alti livelli di diluizione con $H_2O$ e $CO_2$, è stata identificata come la soluzione per minimizzare la quantità di $NO_x$ prodotti. L'impiego di combustibili alternativi come bio-gas e bio-oli, invece, rappresenta la soluzione per abbattere le emissioni di gas serra grazie alla loro origine vegetale.

Lo scopo della presente Tesi è lo sviluppo di un meccanismo cinetico dettagliato in grado di replicare il comportamento dell'ossicombustione in condizioni MILD per il metano. Tale combustibile è, infatti, alla base della cinetica di combustione di tutti gli idrocarburi e, allo stesso tempo, può essere impiegato come materia prima nei forni per lo steam cracking. Sulla base di una vasta raccolta di dati sperimentali in condizioni simili a quelle d'interesse, il modello cinetico precedentemente sviluppato dal gruppo di ricerca CRECK Modeling del Politecnico di Milano, è stato opportunamente modificato in modo da includere le condizioni

di interesse. In supporto, è stato utilizzato il meccanismo "Aramco", considerato come il punto di riferimento per la modellazione cinetica della combustione di idrocarburi fino a 4 atomi di carbonio.

Le prestazioni del meccanismo ottenuto sono state quindi verificate con successo in un ampio range di dati sperimentali su reattori ideali, tra cui reattori perfettamente miscelati, reattori a flusso e fiamme premiscelate. Inoltre il modello è stato utilizzato per analizzare il comportamento oscillante dell'ossidazione di metano all'interno di reattori continui perfettamente miscelati. Tale fenomeno, per questi reattori, risulta essere molto frequente nell'ossidazione di diversi idrocarburi. Perciò, in questa Tesi, è stato condotto uno studio cinetico con lo scopo di identificare le cause di tale indesiderato fenomeno. Lo studio preliminare dello stesso è partito dai combustibili più semplici come idrogeno e syngas. In questo modo, la competizione chimica tra la reazione di branching e di terzo corpo per il consumo di radicali idrogeno per interazione con molecole di ossigeno è stata identificata come principale causa dell'inibizione della reattività e, quindi, anche dell'insorgere delle oscillazioni, per questi due combustibili. Per il metano, invece, è stato trovato che le oscillazioni sono determinate dalla competizione tra la reazione di branching tra H e $O_2$ e tutte le reazioni di terminazione responsabili del consumo di radicali H e OH. Questo è stato dimostrato attraverso l'introduzione del "branching ratio", ovvero il rapporto tra la velocità della reazione di branching e la somma di tutte le velocità delle reazioni di terminazione. Il sistema è in grado di raggiungere le condizioni stazionarie quando il branching prevale sulle terminazioni, cioè quando il "branching ratio" assume valore costante e maggiore di 1. Allo stesso tempo, per tutti e tre i combustibili è stato anche possibile generare delle mappe caratterizzanti le condizioni operative favorevoli all'insorgere dei cicli limite oscillatori.

# List of Figures

XVIII

XXIII

# List of Tables

# Nomenclature

**Roman Symbols**

| | |
|---|---|
| D | Oxygen Dilution Ratio [-] |
| P | Pressure [Pa] |
| T | Temperature [K] |
| Z | Carbon Dioxide Dilution Ratio [-] |

**Acronyms**

| | |
|---|---|
| CFD | Computational Fluid Dynamics |
| CSTR | Continuous-flow Stirred Tank Reactor |
| EGR | Exhaust Gas Recirculation |
| GHG | GreenHouse Gases |
| LFL | Lower Flammability Limit |
| LFS | Laminar Flame Speed [cm/s] |
| LOL | Lower Oscillating Limit |
| $NO_x$ | Nitrogen Oxides |
| PFR | Plug Flow Reactor |
| $PM_{10}$ | Particulate Matter of maximum dimension of 10 micrometer |
| PSSA | Pseudo-Stationary State Approximation |

| | |
|---|---|
| $SO_x$ | Sulphur Oxides |
| UFL | Upper Flammability Limit |
| UOL | Upper Oscillating Limit |

**Greek Symbols**

| | |
|---|---|
| $\Phi$ | Equivalence Ratio [-] |
| $\tau$ | Residence Time [s] |

**Subscripts**

| | |
|---|---|
| $i$ | Species subscript |
| $j$ | Reaction subscript |

**Mathematical Symbols**

| | |
|---|---|
| $K_{eq}$ | Equilibrium constant |

CHAPTER *1*

Introduction

## 1.1 Novel steam cracking furnaces

S TEAM cracking is the most important process for the worldwide production of ethylene. It is based on the pyrolysis of a hydrocarbon mixture, typically virgin naphtha, in the presence of steam [1]. Due to its very simple structure, ethylene is the largest of the basic chemical building blocks. That is why, it is involved in the production of a high number of molecules: polyethylene and ethylene oxide are two representative examples [2]. In 2013, the world ethylene production capacity was around 145 million tons per year and the expected demand for 2020 is about 200 million tons per year [3]. Therefore, the ethylene yearly produced is extremely high and it is continuously growing over the years. To face this production growth, companies must increase their capacity production as well as they should build new plants.

Although steam cracking technology can be considered mature, the complexity of the process and the harsh operating conditions allow the implementation of innovations, especially in providing heat. In fact, steam cracking is one of the most energy intensive processes of the chemical industry. Globally, it uses approximately the 8% of the sector's total primary energy [4]. The steam cracking

furnace, also known as steam cracker, is the unit around which the process is built. Here, the breaking of the hydrocarbon molecules contained in the feedstock stream occurs inside the so-called pyrolysis coil. The operating temperature at which this process works is about 1150 K [1, 5]. Therefore, due to the high endothermicity of the involved reactions, a huge amount of heat must be provided by the furnace. Here, the combustion of a range of fuels occurs from natural gas to crude oil. The choice is related to economic and practical reasons. Air is typically used as oxidizer; therefore, nitrogen is fed together with oxygen, making possible the formation of Nitrogen Oxides ($NO_x$) [6]. Flames generated must have a high radiating power: therefore, combustion occurs under operating conditions able to maximize production of species with high radiating efficiency. Among them, carbonaceous particles are present [7]; they easily provide fouling on the external surface of the pyrolysis coil causing a reduction of the performance of the furnace in heat transport. Therefore, frequent maintenance is required to remove the deposited coke and to restore the initial "clean" operating conditions of the unit. All of these operations are expensive in terms of time and money.

"Integrated Model guided PROcess Optimization of steam cracking Furnaces", better known as IMPROOF, is a European project whose purpose is the identification of all the aspects of such process which can be improved. Its final objective is the drastic enhancement of the energy efficiency of steam cracking furnaces by at least 20%, in a cost-effective way, while simultaneously reducing emissions of greenhouse gases and $NO_x$ per ton of ethylene produced by at least 25%. The result will be the realization of future generation furnaces which can be then adapted to different applications [8]. Improving the energy efficiency has an immediate pay-out because energy cost counts for approximately 70% of production costs in typical ethane-based plants [9].

IMPROOF has proposed several innovative solutions whose implementation can allow the achievement of the purposes above shown:

- Novel refractory and emissive materials. Their properties must maximize the amount of radiations reflected with respect to the ones adsorbed and transmitted [10–12].

- Novel design and novel modeling of the furnace. This point is based on the development of a full 3D high-fidelity Computational Fluid Dynamics (CFD) model. In this way, the strong turbulent flows can be accurately simulated along with the complex cracking kinetics and the coke deposited inside the reactor [13, 14].

- Alternative to the fossil fuels. The main advantage is represented by the lower amount of greenhouse gases emitted. In fact, since such species are already partially oxidized, the CO and $CO_2$ produced will be rather low [15].

- Oxy-fuel combustion. The air is replaced by pure oxygen as oxidizer. In this way, the amount of $NO_x$ produced can be drastically reduced. Nitrogen is still present since it can derive from furnace leakages along with traces in the oxygen due to the non-perfect air separation. Furthermore, these operating conditions allow the reduction of the coke deposition. In parallel, since the oxy-fuel combustion is characterized by a high temperature increase, water and/or carbon dioxide will be added to the fuel feed. They behave as diluents, keeping small the temperature drop. As consequence, the effects of such species on the combustion must be investigated.

The objective of this Thesis is obtaining a comprehensive kinetic characterization of the MILD oxy-fuel combustion. In particular, since the chemistry of such process is based on methane, a detailed kinetic mechanism for its oxy-combustion in presence of high dilution levels of $CO_2$ and $H_2O$ has been developed and validated in a wide range of operating conditions.

## 1.2  Combustion chemistry

From a general point of view, combustion can be defined as a gas phase chemical process [16, 17]. It can be identified by two reactive paths responsible of the fuel conversion: the oxidation and the pyrolysis. The first requires the presence of an oxidizer, typically oxygen, while the second is based on the interactions between the fuel molecules. The most thermodynamically stable products are water and carbon dioxide. In parallel, a high amount of heat is released because of the exothermic nature of such process. In addition, also electromagnetic waves are generated in different wavelengths which define chromatic feature of the flame. Indeed, the conversion of the main reactants into the major products ($H_2O$ and $CO_2$) passes through hundreds of intermediate species involved in thousands of reactions. Therefore, it is a very complicated process which can be further understood considering both kinetic and thermodynamic features [18].

**Thermodynamics of combustion process**

Thermodynamics is the science which describes the energy exchanged between a delimited system and the environment. Once defined some initial conditions, it identifies the direction through which a system spontaneously evolves, i.e. the

equilibrium state [19]. This is the most stable point which a generic system approaches after a theoretically infinite time. It depends only on the initial and the final state. Therefore, it does not provide information regarding the mechanism or the velocity through which this passage occurs. In chemistry, the equilibrium state is defined "dynamic"; in fact, concerning a reversible chemical reaction, the equilibrium condition is represented by the equality between the forward and the backward reaction rates. This means that no variation in reactants and products concentration can be observed even if both the direct and the inverse reactions are happening within the system.

From a physical point of view, fixed the temperature, T, and the pressure, P, the equilibrium condition is characterized by a minimum of the Gibbs free energy. Therefore, its differential is null:

$$dG_{T,P} = 0 \tag{1.1}$$

The Gibbs free energy is a thermodynamic potential which depends on temperature, pressure and quantity of matter:

$$dG = -SdT + VdP + \sum_{i=1}^{NC} \mu_i \cdot dn_i \tag{1.2}$$

where $n_i$ indicates the moles of the $i-th$ species, $\mu_i$ indicates the chemical potential of the $i-th$ species and $NC$ is the number of all the species present in the system under analysis. Since the equilibrium condition is defined once fixed a temperature and a pressure:

$$dG_{T,P} = \sum_{i=1}^{NC} \mu_i \cdot dn_i \tag{1.3}$$

Coupling with the definition of equilibrium condition, the following expression is obtained:

$$\sum_{i=1}^{NC} \mu_i \cdot dn_i = 0 \tag{1.4}$$

The infinitesimal degree of progress, $\lambda$, of a generic reaction $j$ is defined as the ratio between the infinitesimal variation of the moles of the $i-th$ species involved in reaction $j$ and the corresponding stoichiometric coefficient $v_i$:

$$d\lambda = \frac{dn_i}{v_i} \tag{1.5}$$

Therefore, expression 1.5 can be substituted within the (1.4) obtaining

$$d\lambda \left( \sum_{i=1}^{NC} \mu_i \cdot v_i \right) = 0 \tag{1.6}$$

Since the infinitesimal variation of the degree of progress is arbitrary, the equilibrium condition is reduced to:

$$\sum_{i=1}^{NC} \mu_i \cdot v_i = 0 \tag{1.7}$$

The chemical potential can be related to the fugacity:

$$d\mu_i = R \cdot T \cdot dln\left( f_i \right) \tag{1.8}$$

which can be integrated between the system state and a reference state (at the same temperature of the system and, typically, for the $i - th$ pure component. Since combustion is a gas-phase chemical process, the reference aggregation state is the ideal gas state at a pressure $P_r$ equal to 1 bar):

$$\int_{T,P_r,x_i=1}^{T,P,x} d\mu_i = \int_{T,P_r,x_i=1}^{T,P,x} R \cdot T \cdot dln\left( f_i \right) \tag{1.9}$$

$$\mu_i\left( T, P, x \right) - \mu_i\left( T, P_r \right) = R \cdot T \cdot ln\left( \frac{f_i(T, P, x)}{f_i(T, P_r)} \right) \tag{1.10}$$

The argument of the natural logarithm identifies the activity, $a_i$. It is defined as the ratio between the fugacity of the $i - th$ species at the system conditions and the fugacity of the same compound at the chosen reference state.

$$\mu_i\left( T, P, x \right) = \mu_i\left( T, P_r \right) + R \cdot T \cdot ln\left( a_i\left( T, P, P_r, x \right) \right) \tag{1.11}$$

Substituting this last expression into (1.7):

$$\sum_{i=1}^{NC} v_i\mu_i\left( T, P, x \right) = \sum_{i=1}^{NC} v_i\mu_i\left( T, P_r \right) + \sum_{i=1}^{NC} v_i \cdot R \cdot T \cdot ln\left( a_i\left( T, P, P_r, x \right) \right) = 0 \tag{1.12}$$

Involving the logarithmic properties, the last term can be rewritten:

$$\sum_{i=1}^{NC} v_i\mu_i\left( T, P_r \right) + R \cdot T \cdot ln \prod_{i=1}^{NC} \left( a_i\left( T, P, P_r, x \right)^{v_i} \right) = 0 \tag{1.13}$$

Since the chemical potential involved in the previous equation is referred to the

ideal $i - th$ pure component, it is equal to the molar Gibbs free energy of that species: $\mu_i(T, P_r) = g_i(T, P_r)$.

$$\sum_{i=1}^{NC} \upsilon_i g_i(T, P_r) + R \cdot T \cdot ln \prod_{i=1}^{NC} (a_i (T, P, P_r, x)^{\upsilon_i}) = 0 \qquad (1.14)$$

The first term indicates the Gibbs free energy change of the generic reaction, $\Delta G_R^0$. It is defined as the variation of the Gibbs free energy which occurs when the reactants, at the stoichiometric conditions, are totally converted into products at the reference conditions.

$$\Delta G_R^0(T, P_r) + R \cdot T \cdot ln \prod_{i=1}^{NC} (a_i (T, P, P_r, x)^{\upsilon_i}) = 0 \qquad (1.15)$$

The argument of the logarithm is defined as the equilibrium constant of the reaction of concern, $K_{eq}$ .

$$\Delta G_R^0(T, P_r) + R \cdot T \cdot ln (K_{eq}) = 0 \qquad (1.16)$$

$$K_{eq} = exp \left( -\frac{\Delta G_R^0 (T, P_r)}{R \cdot T} \right) \qquad (1.17)$$

Therefore, the equilibrium constant can be computed through the Gibbs free energy change of reaction at the reference conditions. At the same time, it can be also computed through the exploitation of the activities. This requires the definition of the reference state. Since combustion occurs in the gaseous phase and the temperatures are high enough to assume the ideal gas hypothesis, the activity of the $i - th$ species can be written equal to the partial pressure of the species itself. Considering a generic reaction:

$$aA + bB \leftrightarrow cC + dD \qquad (1.18)$$
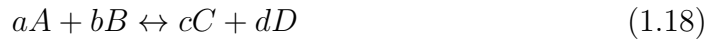
the equilibrium constant becomes:

$$K_{eq,p} = \frac{y_{C,eq}^c \cdot y_{D,eq}^d}{y_{A,eq}^a \cdot y_{B,eq}^b} \cdot P^{(c+d-a-b)} \qquad (1.19)$$

If molar concentrations are used, the next writing can be obtained:

$$K_{eq,c} = \frac{(C_{C,eq})^c \cdot (C_{D,eq})^d}{(C_{A,eq})^a \cdot (C_{B,eq})^b} \qquad (1.20)$$

The link between the two previous constants is shown below:

$$K_{eq,c} = K_{eq,p} \cdot (R \cdot T)^{a+b-c-d} \tag{1.21}$$

The two quantities are exactly coincident only when the number of moles among reactants are the same of products, therefore when $a + b = c + d$.

$K_{eq}$ is an important thermodynamic property which defines the concentration of each species once reached the corresponding equilibrium state. Therefore, if a reaction has an equilibrium constant lower than one, the reactants equilibrium conversion will be very small. Therefore, once defined initial conditions, the thermodynamic equilibrium represents a unique constraint which other phenomena must respect.

Dealing with combustion, different stoichiometric parameters must be introduced [20]:

- The equivalence ratio, $\Phi$, indicates the ratio between the moles of fuel and its stoichiometric moles computed as a function of the global combustion reaction which involves that fuel:

$$\Phi = \frac{n_{fuel}}{n_{fuel,stoichiometric}} \tag{1.22}$$

For example, considering methane combustion in pure oxygen, the global reaction is:

$$CH_4 + 2\,O_2 \rightarrow CO_2 + 2\,H_2O \tag{1.23}$$
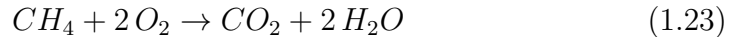
Therefore, studying an initial mixture with 1 mol of methane and 0.2 mol of oxygen, the stoichiometric amount of methane can be evaluated through the proportion:

$$1 : 2 = n_{fuel,stoichiometric} : n_{O_2} \tag{1.24}$$

Solving as a function of methane:

$$n_{fuel,stoichiometric} = \frac{1 \cdot n_{O_2}}{2} = \frac{1 \cdot 0.2}{2} = 0.1\,mol \tag{1.25}$$

Thus, the equivalence ratio becomes:

$$\phi = \frac{1}{0.1} = 10$$

- A similar quantity is represented by $\lambda$; it indicates the ratio between the

amount of oxidizer and the corresponding stoichiometric one:

$$\lambda = \frac{n_{oxidizer}}{n_{oxidizer,stoichiometric}} \tag{1.26}$$

The following relation is valid:

$$\lambda = \frac{1}{\phi} \tag{1.27}$$

- In case of air as oxidizer, another parameter can be used, i.e. "air excess" (A.E.) which is computed as follows:

$$A.E. = \frac{n_{air} - n_{air,stoichiometric}}{n_{air,stoichiometric}} \cdot 100 \tag{1.28}$$

It indicates the percentage of air in excess with respect to the stoichiometric quantity.

**Kinetics of combustion process**

Kinetics is the science that defines the rates through which a system evolves from its initial condition to the corresponding equilibrium state [21]. In chemistry, the reaction rate is the quantity of interest. It represents the moles of reactant converted per unit of volume and unit of time. It can be computed as the product of two functions:

$$R(T, C_i) = k(T) \cdot f(C_i) \quad \left[\frac{kmol}{m^3 \cdot s}\right] \tag{1.29}$$

- $k(T)$ is the kinetic constant of the reaction, and, generally, it is function only of temperature. An exception is made for "third-body" reactions. In such case, also the dependence on gas concentration of the system has to be taken into account. The expression typically used to compute this quantity is the modified form of the Arrhenius equation:

$$k = A \cdot T^n \cdot \exp\left(-\frac{E_{act}}{R \cdot T}\right) \tag{1.30}$$

where:

$A$      is the pre-exponential factor; it is proportional to the number of collisions between reactants molecules.

$n$      indicates the exponent of the temperature. It is introduced to better fit experimental data.

$E_{act}$      is the activation energy of the reaction. When reactants molecules collide, the energy associated to the collision must be at least equal to this quantity in order to convert them into products.

$R$      is the universal gas constant; its value is $8.314 \frac{J}{mol \cdot K}$.

The exponential factor is a quantity between 0 and 1. It represents the fraction of collisions among reactant molecules which are effective. A collision can be considered effective when the molecules involved are correctly oriented and the impact energy is at least equal to the activation energy; in this way, the transition state is formed and reactants can be converted into products.

- $f(C_i)$, is a function of the molar concentrations of species involved in the corresponding chemical reaction. This quantity is represented by the product of the reactants concentrations elevated to their stoichiometric coefficients. Therefore, given the generic Reaction (1.23), the function for the forward path is:

$$f(C_i)_{forward} = (C_A)^a \cdot (C_B)^b \tag{1.31}$$

and for the backward one is:

$$f(C_i)_{backward} = (C_C)^c \cdot (C_D)^d \tag{1.32}$$

This structure can be considered valid only if referred to elementary reactions. Since, the investigated reactions belong to combustion detailed kinetic schemes, they can be all considered as elementary. Therefore, the above writing can be considered as valid for the purposes treated. Being combustion a gas-phase process, the molar concentration can be computed using the ideal gas law:

$$C_i = \frac{P \cdot y_i}{R \cdot T} \tag{1.33}$$

where:

$P$      is the system pressure measured in $[Pa]$.

$y_i$      is the molar fraction of the i-th species.

$R$      is the universal gas constant: $8.314 \frac{J}{mol \cdot K}$.

$T$      is the temperature of the system in $[K]$.

Since at equilibrium conditions the forward reaction rate matches the backward:

$$k_{forward} \cdot (C_{A,eq})^a \cdot (C_{B,eq})^b = k_{backward} \cdot (C_{C,eq})^c \cdot (C_{D,eq})^d \tag{1.34}$$

Rearranging this last writing, the equilibrium constant, $K_{eq,c}$, is found:

$$K_{eq,c} = \frac{k_{forward}}{k_{backward}} = \frac{(C_{C,eq})^c \cdot (C_{D,eq})^d}{(C_{A,eq})^a \cdot (C_{B,eq})^b} \qquad (1.35)$$

Therefore, the link between kinetics and thermodynamics is then obtained.

In combustion, third-body reactions are quite important, especially for recombination processes [20, 22]. Due to the exothermicity of this kind of reactions, the species produced are energetically excited and, consequently, very unstable. Owing to the small dimensions of the molecules as well as to the low number of vibrational motions on which distribute the excess of energy, they need to an external support in order to be stabilized. Therefore, there are two possible paths:

- The external dissipation of energy by collision with a "third body"; this is represented by any molecule present in the system.

- The excited species can come back to the original reactants if the energy is not delocalized efficiently.

Third-body reactions have a kinetic constant which is dependent on pressure, too. This dependence appears in the molar concentration of the third body itself, typically indicated through "$[M]$". This quantity can be evaluated using the ideal gas law as follows:

$$[M] = \frac{P}{R \cdot T} \cdot \sum_{i=1}^{NC} y_i \cdot \varepsilon_i \qquad (1.36)$$

The difference with respect to Equation (1.33) is represented by the summation term. This is characterized by the product of the molar fraction of each species and its third-body efficiency $\varepsilon_i$ [23,24]. This represents the tendency of the $i-th$ species to stabilize the molecule produced in the relative reaction. $NC$ indicates the number of all the species involved in the reaction environment.

In Figure 1.1, the typical behavior of the kinetic constant of a third-body reaction is shown.

Three regions can be recognized:

- A pressure window within the kinetic constant linearly changes with pressure. Here, this quantity can be recognized as "low-pressure limit" or $k_0$.

- When pressure overcomes an upper threshold, the kinetic constant becomes pressure independent. Here, it is called "high-pressure limit" or $k_\infty$.

- For intermediate pressures, the kinetic constant of third-body reactions has a complex behavior that deviates from the linear one. Its value must be evalu-
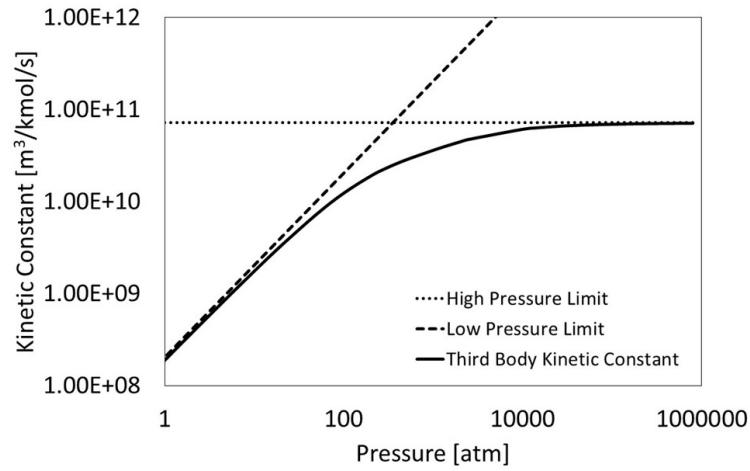
**Figure 1.1:** Third-body kinetic constant (solid line), low-pressure limit or $k_0$ (dashed line) and high-pressure limit or $k_\infty$ (dotted line) as a function of pressure. These curves have been obtained for the generic reaction $A + B(+M) \leftrightarrow AB(+M)$.

ated using empirically derived expressions in order to better fit experimental data. This topic will be better described in chapter 2.

The pressure range where the kinetic constant of third-body reactions reduces with the pressure decrease is called "fall-off" region.

Furthermore, as depicted in Figure 1.2, with the increase of temperature, the third-body kinetic constant curve is shifted to the right. Therefore, the "fall-off" region is extended along with the pressure window where the kinetic constant has a complex behavior with the pressure itself.
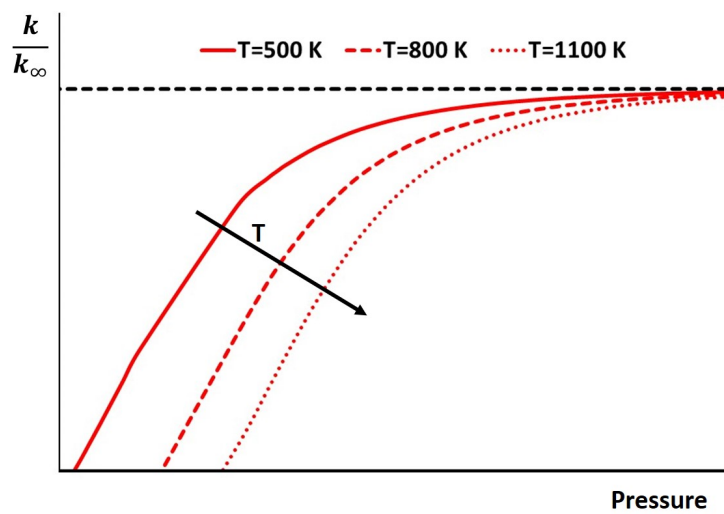


**Figure 1.2:** Temperature dependence of the ratio between the third-body kinetic constant and the high-pressure limit. The solid line indicates 500 K, the dashed 800 K and the dotted 1100 K.

11

Below the high-pressure limit, the presence of a third body enhances the order of the reaction by a value of one. In fact, it behaves as a reactant and as a product for all intents and purposes. Its concentration must be included in the evaluation of the kinetic constant and it depends on the third-body efficiencies of the species present in the system. In the region of pressure independence, the reaction order is calculated without considering the third body presence.

In addition to the reaction rate, chemical kinetics provides also the mechanism through which the system converts the reactants into the more stable products from the thermodynamic point of view. Therefore, combustion is characterized by a radical chain mechanism which involves thousands of reactions that can be collected in four groups:

- Initiation; here, one or two neutral molecules are converted into one or more radicals. A radical is a chemical species which comes from the homolytic scission of a covalent bond of a stable molecule. The electrons shared in such bond are equally distributed between the two parts of the original particle. As a result, a radical is formed by at least one odd electron. This feature provides high instability and, therefore, the radical is able to easily react with other molecules or radicals. Since a bond breakage is involved, this kind of reaction is endothermic and the activation energy is typically high. For this reason, an ignition is required to begin the combustion process.

- Propagation collects all the reactions for which the balance on radicals is preserved. As a result, no net production or destruction of radicals occurs. Below there is an example of a propagation reaction.

$$OH + CO \leftrightarrow CO_2 + H \tag{1.37}$$

- An important role in the combustion process is covered by branching reactions. They are responsible of the increase of the overall number of radicals in the system. Starting from a radical and a neutral molecule, two or more of them are obtained as products of this reaction. The most typical example is the branching reaction which involves a hydrogen radical and an oxygen molecule:

$$H + O_2 \leftrightarrow OH + O \tag{1.38}$$
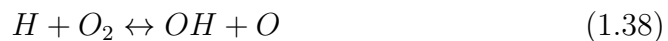
Among products, there are two radicals, but O has a triplet ground state electronic configuration which shows two unpaired electrons at the valence orbital, making it equivalent to a bi-radical. Hence, from a theoretical point of view three radicals are obtained starting from one. At net, there is the

production of two radicals.

- Termination, finally, is the last category of reactions recognizable in a radical chain mechanism. It is characterized by the interaction between radicals producing stable molecules. Therefore, the impact on the system reactivity is negative, since it favors the reduction of the overall number of radicals. Reactions of this kind are exothermic because chemical bonds are formed.

$$CH_3 + H \ (+M) \leftrightarrow CH_4 \ (+M) \tag{1.39}$$
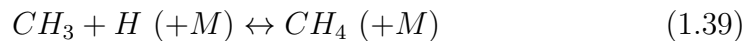
**Flammability limits**

Once described the main thermodynamic and kinetic aspects, the concept of flammability limits must be explained to complete this introduction on the combustion process [20].

As mentioned in the previous section, initiation reactions require an external source of energy to occur. Once the mechanism is initiated, propagation and branching reactions allow the proceeding of the process. But this second step happens only if the fuel-oxidizer-diluent mixture has a suitable composition allowing the flame to propagate in space and time. Therefore, for a given fuel, oxidizer and diluent, a triangular diagram can be experimentally obtained. As an example, the flammability diagram for a ternary mixture constituted by methane, oxygen and nitrogen is shown in Figure 1.3 [25].

In the triangular area, there is a closed region called flammability field. It is delimited by one side of the triangle and two curves known as flammability limits curves. They are distinguishable into:

- Lower Flammability Limit (LFL); it indicates the minimum fuel concentration in the mixture able to guarantee the combustion occurrence. Below this curve the excess of oxidizer inhibits the reaction, avoiding the propagation of heat and radicals and favoring termination reactions.

- On the other hand, the Upper Flammability Limit (UFL) indicates the maximum fuel concentration able to propagate the combustion. Above this concentration, although ignition presence, fuel is too concentrate than oxidizer to allow flame spreading.

The flammability field is influenced by the variation of the operating conditions. Increasing the temperature, the extension of the region is increased because a higher number of mixtures is able to provide combustion due to the higher energy available in the system.
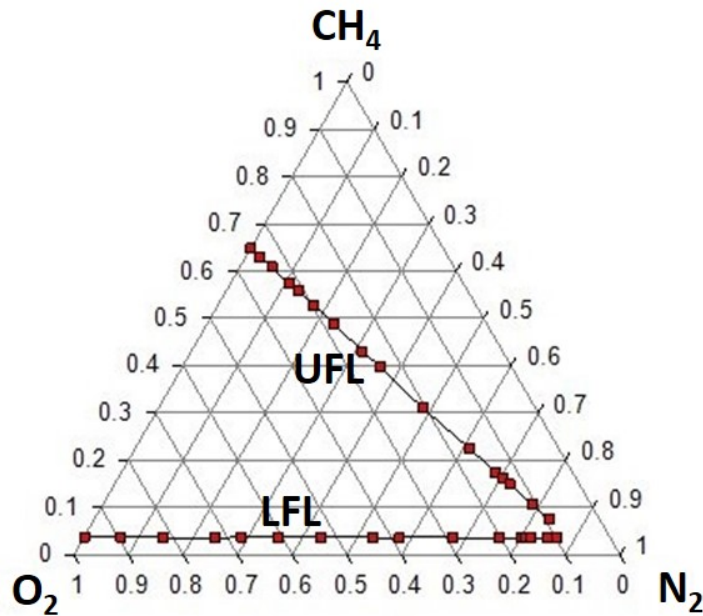
**Figure 1.3:** Triangular diagram for the flammability field of a $CH_4/O_2/N_2$ mixture.

Also, the increase of pressure provides the enlargement of the field; in particular, this can be observed highly for the UFL since the temperature increase of the fuel-rich mixture by compression is significant. In case of LFL such effect is negligible. Moreover, using a diluent with a relatively high specific heat, the flammability region is reduced. This is related to the more effective heat absorption which prevents the heat propagation after ignition occurs. In this way, a lower number of mixtures is able to favor the flame spatial and temporal spreading.

Finally, it is important to describe also the concept of auto-ignition temperature of a fuel in presence of oxygen. This is the minimum temperature at which the fuel spontaneously interacts with the oxygen molecules, initiating the combustion. No external ignition are required because the temperature itself represents the source of energy which initiates the process. The reaction occurs uniformly, involving the whole volume occupied by the reacting mixture. Therefore, no flame front is observable.

**Combustion products**

As conclusion of this introduction, an analysis of the possible products of the combustion process must be performed. From a thermodynamic point of view, the most stable products are carbon dioxide and water. Unfortunately, in the real systems, thermodynamic equilibrium is not always approached. Even if it is

reached, combustion does not occur producing only these two products. There-fore, along with $CO_2$ and $H_2O$, other species are present at the end of the reaction or at the outlet of the reactor.

In order to better understand this topic, a classification of the thousands of reactions which constitute the combustion process has to be done. Actually, two paths can be always recognized in presence of an hydrocarbon fuel and an oxidizer:

- Oxidation route: it is characterized by the set of reactions responsible of the conversion of the C-H bonds into C-O and H-O bonds. As shown in Figure (1.4), such process is characterized by the interaction between the fuel molecules with the oxygen. The reactants are principally transformed into $H_2O$ and $CO_2$. In addition to these two, other intermediate products can survive at the end of the process, thanks to their relatively high stability. Among them, CO must be highlighted. Its conversion to carbon dioxide is kinetically slow and if the reaction has an equivalence ratio higher than one, oxygen isn't enough to allow its further oxidation. Secondarily, methanol and formaldehyde are examples of products of intermediate oxidation of the original fuel.
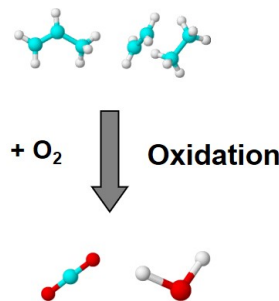


**Figure 1.4:** Oxidation route: C-H bonds are converted into C-O and O-H bonds. Colors are used to indicate elements: light blue for carbon atoms, red for oxygen and white represents the hydrogen atoms.

- Pyrolysis, instead, is the collection of reactions which are responsible of the cleavage of C-C bonds as depicted in Figure (1.5). The main products are, therefore, unsaturated molecules whose interaction with other hydrocarbon species contributes to the production of longer chain hydrocarbon molecules. They constitute the so-called "soot". It is the name used to indicate all the carbonaceous particles generated from the condensation of the aromatic molecules. These can be defined as by-products of the combustion process.
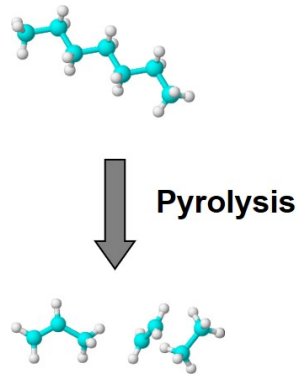
**Figure 1.5:** Pyrolysis route: the C-C bonds breaking forms smaller hydrocarbon molecules. From alkanes, alkenes are recovered and by the latter, alkynes are obtained.

In addition to the two previous categories of products, another can be included. It is related to the oxidation of species not always present in the feed stream to the reactor. For example, if air is used as source of oxygen in the reactor, the $N_2$ oxidation can occur producing the so-called "Thermal-$NO_x$" and "Prompt-$NO_x$". The Nitrogen Oxides can be obtained also from the oxidation of nitrogen atoms contained in the hydrocarbon chains of the fuel. In this case, they are named "Fuel-$NO_x$". Figure (1.6) shows a schematic representation of the mechanisms through which the $NO_x$ can be produced.
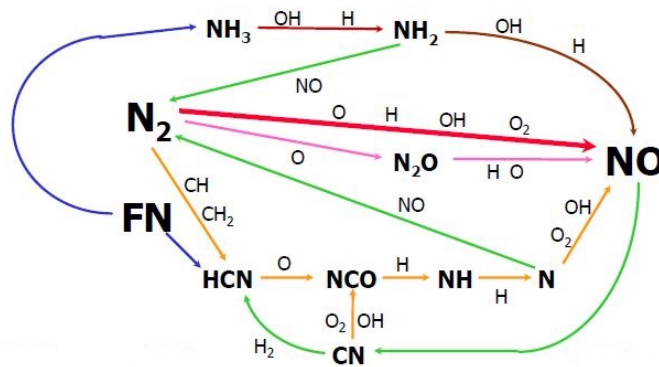


**Figure 1.6:** Schematic representation of the different mechanisms through which $NO_x$ are produced.

The same considerations can be done also for S atoms. Their oxidation produces Sulphur Oxides ($SO_x$).

With the exception of water, all the combustion products are undesired and they are considered pollutants for both the earth and the human health [26, 27]. For this reason, the today's research is moving toward innovative operating conditions of combustion as well as alternative fuels in order to minimize the emissions.

## 1.3 MILD oxy-fuel combustion

Conventional fuels typically used for combustion processes are obtained from fossil sources. They have been significantly exploited thanks to their high calorific power, which made them particularly suitable for the production of energy [28]. After the industrial revolution, the interest in fossil fuels exploded and a massive extraction of oil, coke and natural gas started growing during the years [29]. The high exploitation of these raw materials in combustion provided the emission of very high amount of Greenhouse-Gases (GHG) in the atmosphere [30, 31]. Over the years, negative consequences such as increase in the earth's temperature has been observed. This has caused the occurrence of weather instability, increase of the ocean levels and ice melting in the North and South Poles [26, 32].

In parallel to GHG, particulate matter is of concern, too. From an environmental point of view, these small particles interact with water, favoring nucleation and generating the so called "smog" [33]. This is typical of highly urbanized areas, where these emissions constitute a serious concern. Another effect of soot is on human health. Because of their small size, under $10\,\mu m$ ($PM_{10}$), soot particles are under the "inhalable threshold" for human beings. Therefore, they are easily introduced into the human body, where they interact negatively with the circulatory and the respiratory systems [34]. Moreover, recent studies have confirmed the presence of carcinogenic substances in the carbonaceous particulate making them very dangerous [27]. Through the same process, such particles can further increase their size. In Figure 1.7, the schematic representation of the synthesis process of carbonaceous particles is provided. For quite high time intervals, there is a gas-solid interaction which causes the production of particles which cause fouling in the structure [35].
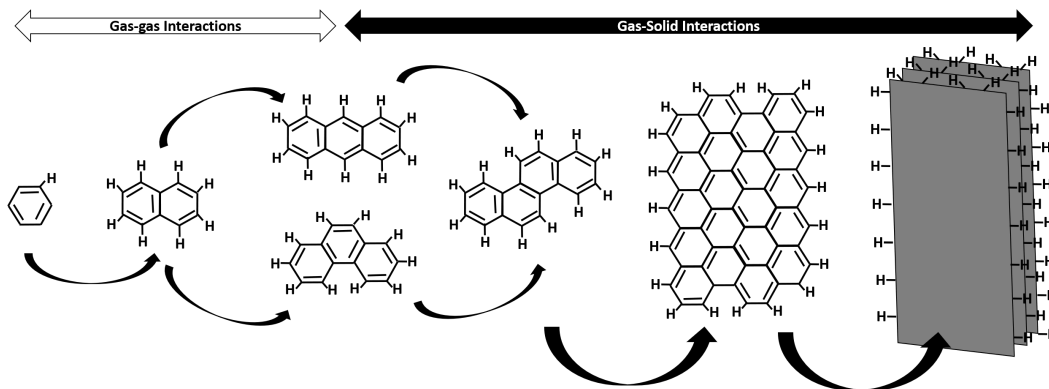


**Figure 1.7:** Schematic description of the graphene production.

This phenomenon on mechanical devices generates an efficiency reduction of the

unit where combustion occurs. The main consequence is the continuous start and stop of the units, to perform structural maintenance. This causes time and money waste; thus, the aim is to minimize the frequency of such operations working in operating conditions able to minimize the production of carbonaceous particles.

This brief analysis motivates the existence of several international laws, continuously imposing more stringent constraints on burners emissions [36]. Therefore, the industrial and academic interest is in studying new methods to perform combustion, with the purpose of minimizing pollutants production. At the same time, with an attention on the foreseen availability of fossil fuels, a second purpose is maximizing the efficiency of combustion devices to minimize fuel consumption.

In this Thesis, the methane combustion in MILD oxy-fuel conditions is investigated. Such combustion mode comes from the coupling of the MILD and the oxy-combustion. In the following chapters, the description of these two types of process is observed.

## 1.3.1 MILD combustion

In this current section, a deep analysis of the "Moderate or Intense Low-oxygen Dilution combustion", known as "MILD" combustion is presented. This combustion mode is able to provide several advantages, deriving from many particular operating conditions.

MILD combustion is characterized by a strong pre-heating of the reactants. This is performed by diluting fuel and oxidizer with hot exhaust gases. This modifies the original composition of the system, possibly pushing the mixture outside of the flammability limits. Therefore, to ignite the system, a temperature higher than the fuel self-ignition temperature is required. Auto-ignition allows a uniform temperature throughout the system. In addition, the maximum allowable temperature increase with respect to the initial one during the combustion is lower than the mixture self-ignition temperature (in Kelvin) [37]. This means that such process evolves in a rather narrow temperature range, which could be placed in an intermediate region between the very fast kinetics of the oxidative undiluted conditions and the relatively slow kinetics linked to low temperature self-ignition regimes. Figure 1.8 shows the typical operating conditions of the methane MILD combustion in air. It depicts the dependence of the temperature on the dilution ratio of the exhaust recycled gases [38]. Due to the particular operating conditions, the flame becomes green and in general less visible than in conventional flames, meaning that different wavelengths of the electromagnetic waves are emitted [39]. A first advantage in performing MILD combustion is the relatively low amount

$$K_r = \frac{\dot{m}_{exhaust}}{\dot{m}_{exhaust} + \dot{m}_{air}}$$
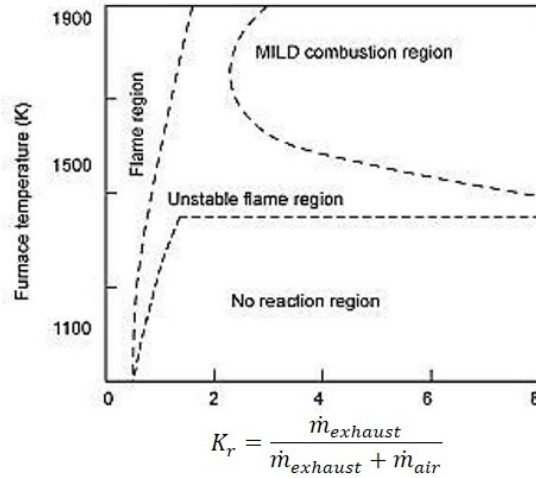
**Figure 1.8:** Temperature as a function of recycle ratio of exhausted gases. MILD combustion is characterized by a high dilution levels with operating temperatures in the 1300-1900 K.

of $NO_x$ produced. The high dilution levels minimize the temperature rise in the reactor. Indeed, system temperature is always below 2000 K which is a threshold above which the production of "Thermal-$NO_x$" occurs in a time interval of few milliseconds [6, 40]. The diluent is usually constituted by $H_2O$ and $CO_2$, with a close to 2 : 1 ratio, recycled from the burner outlet; such composition derives from the global combustion equation:

$$CH_4 + 2\,O_2 \leftrightarrow CO_2 + 2\,H_2O \tag{1.40}$$
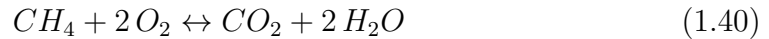
where the amount of water produced is double than the carbon monoxide [39]. Due to their high specific heats, a better temperature control is allowed. The recycle of such gases is known as Exhaust Gas Recirculation (EGR). The last, but not least, advantage provided by the high dilution is the very small amount of carbonaceous particulate produced. This is a positive aspect for devices such as furnaces, where the minimization of carbonaceous particles deposition allows to keep the thermal-exchange efficiency rather constant during the time.

In conclusion, MILD combustion represents a very innovative and beneficial solution. In fact, it can be classified as a clean combustion thanks to the reduction of $NO_x$ emitted of about 50% [41]. At the same time, due to the uniform temperature throughout the burner and thanks to the recycle of waste heat of flue gases, an increase of about 30% in thermal efficiency is guaranteed [39]. For these reasons, MILD combustion is considered as one of the new-generation of clean and efficient combustion technologies.

### 1.3.2   Methane combustion in MILD oxy-fuel conditions

Unfortunately, the solution described in the previous section is not suitable to be implemented in a steam cracking furnace. In fact, the amount of $NO_x$ emitted are still high and not suitable to fulfill the increasingly more stringent constraints imposed by recent laws [36].

The innovation investigated in this Thesis is the adoption of pure oxygen as oxidizer, instead of air. The absence of nitrogen within the combustion process results in a drastic reduction of the amount of $NO_x$ produced (since air leakages in the furnace are always present, traces of such pollutants can still find in the off gases).

Even if this solution is very effective in reducing emissions, it can not be adopted due to the strong temperature increase owing to the exothermicity of the process. In the case of conventional combustion, nitrogen would act as a thermal diluent avoiding extreme temperature peaks. Therefore, performing an oxy-combustion within a steam cracker, the melting of the pyrolysis coils along with damaging of the furnace itself occurs. The only way to control the temperature increase is the adoption of the same technology used also in MILD combustion: EGR. Thus, exhaust gases are recycled from the outlet of the burner to keep the furnace temperature sufficiently high to perform steam cracking and, at the same time, low enough to guarantee the unit integrity. This is guaranteed by the relatively high specific heat of the mixture recycled, since it is mostly constituted by $H_2O$ and $CO_2$.

Therefore, combustion performed in MILD oxy-fuel conditions [42] allows to reduce emissions from steam cracking furnaces. In the following chapters, the development of a kinetic scheme able to predict experimental MILD oxy-fuel combustion results will be discussed. The investigated fuel is methane. Two reasons are connected to this choice. First, methane can be used directly as fuel for the steam cracking furnaces. Second, combustion of higher hydrocarbon molecules is based on the chemistry of the methane oxidation. As a result, the development of a mechanism for the combustion in MILD oxy-fuel conditions of whatever hydrocarbon fuel requires a reliable kinetic scheme for the methane itself.

CHAPTER $2$

# Experimental and numerical tools

I N this second chapter, the attention is focused on the description of how `OpenSMOKE++` works. The `OpenSMOKE++` framework consists of a collection of several C++ libraries conceived to manage large and detailed kinetic schemes in numerical simulation of reactive flows [43]. In parallel, BzzMath libraries [44] are used by the code to solve systems of equations which represent the combustion process inside different systems: ideal reactors, laminar premixed flames, counter flow flames etc. It has been developed by the CRECK Modeling research group at "Politecnico di Milano" [45].

This represents the tool around which this thesis work is based. In fact, it is used for the simulation of several systems for the development and the validation of a kinetic scheme able to model the methane oxy-combustion in presence of water and carbon dioxide as diluents. In addition, `OpenSMOKE++` is equipped with several Post-Processing tools which allow to perform several analysis on the results: sensitivity and rate of production analysis are two examples.

In order to perform a simulation, different elements must be provided to the code. In the following sections, all the elements of the `OpenSMOKE++` framework which will be used in the Thesis will be described in detail.

## 2.1 Ideal reactors

Chemical reactions take place within suitable devices called reactors. Such systems can assume different configurations to face several operating conditions, both for the nature of the process and for the chemical species involved. In general, there are three functions which each reactor must fulfill; first of all, it must guarantee a residence time long enough to let the reaction occur. Then, in order to favor the interaction among the involved molecules, the reactor must mix at the molecular level the reactants and provide, at the same time, the heat needed by the reaction to take place.

Therefore, two asymptotic operating regimes can be identified: the perfectly-stirred and the plug-flow. The reactors which work in such conditions are defined ideal. In fact, these configurations can be realized only theoretically.

The combustion process is carry out in several kinds of reactors with a huge range of fluid dynamics arrangements. In the present Thesis, since kinetic studies must be performed, the purpose is the simulation of very simple systems as ideal reactors which are easy to be modeled and where the chemistry cover the most important role. In this way, it is relatively easier conduce analysis on the kinetic mechanisms and consider in the background the other phenomena.

In the next subsections, a detailed description of the different kinds of ideal reactors is provided. A description of the way real reactors are built up in laboratories and operated in order to approach such conditions is also provided.

### 2.1.1   Batch reactor

Batch reactor is a tank where the perfectly-stirred regime is guaranteed by a mixer. This ensures uniform conditions throughout the reactor volume in terms of composition, temperature and pressure. It is defined as "batch" because it is closed to the material exchange. Therefore, it operates in a discontinuous regime: at the beginning, the reactants are loaded in the system in a single charge and, at the same time, they are mixed and eventually heated to start-up the reactivity. Then, the involved chemical reactions occur until the final conditions are approached. At the end, the final mixture is discharged and the unit is cleaned up for the following cycle.

In combustion, reactors which can be modelled as "batch" are typically adopted to study ignition times of fuel-oxidizer mixtures. This quantity is used to measure the reactivity of a generic fuel by varying the operating conditions in terms of pressure and temperature.

Inside the `OpenSMOKE++` suite, a variety of batch reactors can be solved, either at constant pressure, assigned or variable volume, in isothermal or adiabatic conditions, or, even, with heat exchange with external environment. The conservation equations [43] of species are solved in terms of mass fractions ($\omega$):

$$\hat{\rho} \cdot \frac{d\omega_i}{dt} = MW_i \cdot \sum_{j=1}^{NR} \upsilon_{i,j} \cdot r_j \quad (i = 1, ..., NS) \tag{2.1}$$

where $MW_i$ represents the molecular weight of the $i - th$ species $\left[\frac{kg}{kmol}\right]$, $\hat{\rho}$ the massive density of the mixture $\left[\frac{kg}{m^3}\right]$, $r_j$ the rate of the $j - th$ reaction $\left[\frac{kmol}{m^3 \cdot s}\right]$ and $\upsilon_{i,j}$ the stoichiometric coefficient of the i-th species in the j-th reaction.

The conservation equation of energy is written directly in terms of temperature. For constant-pressure reactors:

$$\hat{\rho} \cdot \hat{C}_p \cdot \frac{dT}{dt} = -\sum_{i=1}^{NC} \sum_{j=1}^{NR} \upsilon_{i,j} \cdot r_j \cdot \tilde{H}_i + \frac{\dot{Q}}{V} \tag{2.2}$$

while for constant-volume reactors:

$$\hat{\rho} \cdot \hat{C}_p \cdot \frac{dT}{dt} = -\sum_{i=1}^{NS} \sum_{j=1}^{NR} \upsilon_{i,j} \cdot r_j \cdot \left( \tilde{H}_i - RT \right) - \frac{P}{V} \cdot \frac{dV}{dt} + \frac{\dot{Q}}{V} \tag{2.3}$$

In the expression reported above, NS indicates the number of species and NR the number of reactions available in the kinetic mechanism. $\dot{Q}$ represents the power exchanged with the environment, typically expressed using the global heat exchange coefficient $U \left[\frac{W}{m^2 \cdot K}\right]$, the exchange surface area $A \left[m^2\right]$ and the temperature of the environment $T_{env}$: $\dot{Q} = U \cdot A \cdot (T_{env} - T) \left[W\right]$.

### 2.1.2 Continuous-flow Stirred Tank Reactor

A second reactor which works in a perfectly-stirred regime is the Continuous-flow Stirred Tank Reactor (CSTR) which is an open ideal reactor. It is an idealization that proves useful in describing laboratory experiments and can often be used in modeling practical devices. Gases enter the reactor with a mass flow rate $\dot{m}$, temperature $T^{inlet}$ and massive composition $\omega_i^{inlet}$. Once inside the reactor, the gases mix instantaneously and perfectly, which means that temperature and composition within the reactor volume are uniform. Typical CSTRs realized for laboratories experiments are vessels, typically made of quartz, in which the inlet flow rate is provided through a four-nozzle stirrer. Its configuration is able to exploit the force exerted by the flux to make this device rotate. Figure 2.1 shows

a schematic representation of such solution. This is able to guarantee a very high
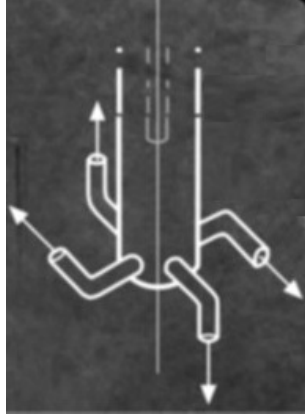


**Figure 2.1:** Schematic representation of the four-nozzle stirrer.

degree of mixing and to approach the ideal uniform conditions within the reactor. For this reason, the reactor can be assumed as a zero-dimensional reactor since the fluid properties do not vary with a spatial coordinate, but, eventually, only with time.

OpenSMOKE++ framework also includes the possibility to study chemical reactions in such kind of reactors, both in steady-state and unsteady conditions. Moreover, the reactor can be adiabatic, isothermal or it can exchange heat with the external environment.

The conservation equations of species and energy are reported in the unsteady form [43]:

$$\hat{\rho} \cdot \frac{d\omega_i}{dt} = \hat{\rho} \cdot \frac{\omega_i^{inlet} - \omega_i}{\tau} + MW_i \cdot \sum_{j=1}^{NR} v_{i,j} \cdot r_j \quad (i = 1, ..., NS) \qquad (2.4)$$

$$\hat{\rho} \cdot \hat{C}_p \cdot \frac{dT}{dt} = \hat{\rho} \cdot \frac{\sum_{i=1}^{NS} x_i^{inlet} \left( \tilde{H}_i^{inlet} - \tilde{H}_i \right)}{MW_{mix}^{inlet} \cdot \tau} - \sum_{i=1}^{NS} \sum_{j=1}^{NR} v_{i,j} \cdot r_j \cdot \tilde{H}_i + \frac{\dot{Q}}{V} \qquad (2.5)$$

In the equation reported above, $\tau$ is the residence time of the reactor, which is defined as:

$$\tau = \frac{\hat{\rho} \cdot V}{\dot{m}} \quad [s] \qquad (2.6)$$

In steady conditions, Equations (2.4) and (2.5) become a system of non-linear algebraic equations, since the unsteady terms are identically equal to zero.

### 2.1.3 Plug Flow Reactor

The plug-flow hydrodynamic condition is characteristic of the Plug Flow Reactor (PFR ). It is a tubular device which can be assumed as an ideal reactor because the two following fluid dynamics properties are assured:

- A perfect mixing along the radial coordinate of the tube; this means that all the properties, such as temperature, pressure and composition, can be assumed uniform over the cross section of the reactor.

- Instead, along the axial coordinate, mixing is ideally absent. This means that in such direction, the flowing fluid can be subdivided into pockets of infinitesimal length, each one isolated from the one which precedes and follows it.

Therefore, the properties of the fluid are dependent only on the axial coordinate, but not on the radial one. This kind of reactor can be modeled as a monodimensional reactor.

In order to make a real reactor work in plug-flow regime, it is necessary to introduce the material Peclet number. This dimensionless number is computed as the ratio between the convective and diffusive rate of the species in the reactor. In particular, two types of this quantity can be recognized:

- the radial Peclet number:

$$Pe_r = \frac{\langle v \rangle \cdot D}{\Gamma_{i,r}} \tag{2.7}$$

    where

| | |
|---|---|
| $\langle v \rangle$ | indicates the convective velocity with which the fluid is flowing through the tubular unit. |
| $D$ | is the reactor diameter. It coincides with the characteristic length along which the material diffusion occurs. |
| $\Gamma_{i,r}$ | is the radial material diffusivity of the $i - th$ species. |

    In order to approach in the reality the plug-flow configuration, this number has to be close to zero. Therefore, the velocity through which the species are diffusing radially must be infinitely higher than the convection speed in order to have a perfect radial mixing.

- On the contrary, the axial Peclet number is defined as follows:

$$Pe_a = \frac{\langle v \rangle \cdot L}{\Gamma_{i,a}} \tag{2.8}$$

Since, in this case, the material diffusion is investigated along the axial co-ordinate, the corresponding characteristic length is the reactor length $L$. On the other hand, $\Gamma_{i,a}$ represents the axial diffusivity of the $i-th$ species. Thus, in a real device, the plug-flow regime is approached only when also this quantity tends to infinite. This means that each species must diffuse axially with a velocity infinitely lower than the convective velocity. In this way, an axial perfectly segregated flux can be realized.

From the previous two expressions, the solution to realize a real tubular reactor which behaves as a PFR can be reached geometrically. In fact, very long tubes with a very small cross section are the typical devices used in laboratory to approach the ideal conditions of the plug-flow regime.

The `OpenSMOKE++` framework allows the simulation of such reactors, in isothermal or adiabatic conditions or with prescribed heat exchange with the external environment. The conservation equations of species and energy are written with respect to the spatial coordinate $z$ [43].

$$\hat{\rho} \cdot v \cdot \frac{d\omega_i}{dz} = MW_i \cdot \sum_{j=1}^{NR} v_{i,j} \cdot r_j \quad (i = 1, ..., NS) \tag{2.9}$$

$$\hat{\rho} \cdot v \left( \hat{C}_p + \frac{v^2}{T} \right) \frac{dT}{dz} = -\sum_{i=1}^{NS} \sum_{j=1}^{NR} v_{i,j} r_j \cdot \tilde{H}_i - v^2 \cdot MW_{mix} \sum_{i=1}^{NS} \sum_{j=1}^{NR} v_{i,j} r_j + \frac{U \cdot P_c}{A_c} (T_{env} - T) \tag{2.10}$$

where $v$ is the velocity $\left[ \frac{m}{s} \right]$, $P_c$ and $A_c$ are, respectively, the perimeter and the area of the cross section surface $[m]$.

### 2.1.4  Premixed laminar flame speed

In combustion, there are other devices, in addition to those above described, used to define some important properties of a fuel, suitable for several purposes such as kinetic studies. The premixed laminar flame speed (LFS) is one of the most representative examples. It is a rigorously defined fundamental property of the mixture investigated, embodying and, thereby, manifesting the net effects of its diffusivity, exothermicity and reactivity [46].

Such quantity can be obtained experimentally using an open burner. It is constituted by a perforated plate, realized in a metallic porous material, through which a fuel-oxidizer-diluent mixture is passing from the premixing zone to the combustion chamber. In the first, the fuel is efficiently mixed with the oxidizer and an eventual added diluent. In the second part, thanks to an external ignition,

combustion occurs. From the ignition point, a front flame develops and propagates through the whole volume occupied by the flammable mixture. Then, since the reactants are continuously fed in the chamber from the metallic plate, the flame tends to stabilize on it. This happens only if the volumetric flow rate are relatively small. The premixed laminar flame speed represents the velocity through which the reactants must be provided through the burner in order to keep fixed in the space the front of the flame. Such speed constitutes the boundary condition which separates two events experimentally observable. If the inlet flow rate is smaller than the one which corresponds to the laminar flame speed, the back diffusion of the species involved in the system stabilizes the front of the flame on the perforated plate. This structure is able to avoid back propagation of the flame itself in the equipment, preventing its damaging. On the other hand, if the inlet velocity exceeds the laminar flame speed, due to the too high convective flow rate of the reactants, the flame is extinguished.

`OpenSMOKE++` suite has an utility able to compute such quantity performing a monodimensional simulation of the device. It is based on the solution of a system of equations written as a function of time and axial coordinate $z$. Four are the classes of equations solved [47]:

- Continuity equation:

$$\frac{\partial \hat{\rho}}{\partial t} + \frac{\partial (\hat{\rho} \cdot v)}{\partial z} = 0 \tag{2.11}$$

- Momentum:

$$\frac{\partial (\hat{\rho} \cdot v_z)}{\partial t} + \frac{\partial (\hat{\rho} \cdot v_z \cdot v_z)}{\partial z} = -\frac{\partial P}{\partial z} - \nabla \tau_z + \hat{\rho} \cdot g_z \tag{2.12}$$

  where $P$ is the pressure $[Pa]$, $g_z$ is the component along the axial axis $z$ of the Gravity of the Earth $\left[\frac{m}{s^2}\right]$ and $\tau_z$ is the z component of the viscous stress tensor $[Pa]$.

- Energy:

$$\hat{\rho}\hat{C}_p\frac{\partial T}{\partial t} + \hat{\rho}\hat{C}_p v_z \frac{\partial T}{\partial z} = -\frac{\partial \dot{Q}}{\partial z} - \frac{\partial \dot{Q}_{rad}}{\partial z} - \sum_{i=1}^{NS} \hat{C}_{p.i} \cdot \omega_i \cdot J_i \cdot \frac{\partial T}{\partial z} - \sum_{i=1}^{NS}\sum_{j=1}^{NR} v_{i,j} \cdot r_j \cdot \tilde{H}_i \tag{2.13}$$

  where $\dot{Q}$ is the heat exchanged with the external environment per unit of time and area $\left[\frac{W}{m^2}\right]$; $\dot{Q}_{rad}$ is the heat exchanged through radiation per unit of time and area $\left[\frac{W}{m^2}\right]$; $J_i$ is the diffusive flux $\left[\frac{kg}{m^2 \cdot s}\right]$ of the $i - th$ species.

- Species mass balance:

$$\frac{\partial \left( \hat{\rho} \cdot \omega_i \right)}{\partial t} + \frac{\partial \left( \hat{\rho} \cdot \omega_i \cdot v_z \right)}{\partial z} = -\frac{\partial}{\partial z} \left( \hat{\rho} \cdot \Gamma_i \cdot \frac{\partial \omega_i}{\partial z} \right) + MW_i \cdot \sum_{j=1}^{NR} v_{i,j} \cdot r_j \quad (2.14)$$

where $\Gamma_i$ is the material diffusivity of the $i-th$ species $\left[ \frac{m^2}{s} \right]$.

Therefore, the transport equations which model the system are solved forcing some constraints. Along with the Danckwerts boundary conditions imposed to the ordinary differential equations system, an additional information is imposed by the program to indicate the axial coordinate at which the ignition occurs. In particular, in this arbitrary position a temperature increase of about 10-12 K than the inlet stream indicates the point where the front flame must stabilize. In this way, the problem is properly bounded and once the solution converges the laminar flame speed is obtained as result.

In addition, also the evaluation of the flammability limits of a whatever mixture can be obtained computationally through the laminar flame speed evaluation. In fact, assuming $5 \frac{cm}{s}$ as the minimum velocity at which the flame can propagate after an ignition, the compositions which represent the upper and the lower flammability limits can be defined [48]. In this way, without experiments, the flammability field of every fuel can be readily estimated, saving both money and time which would be lost through real experiments [25].

## 2.2 Kinetic Model

The core of each simulation is represented by the kinetic model. It is the fundamental tool which is able to describe the chemical interactions of the molecules involved in a defined system. These are described both from a chemical point of view, but also from a physical one. Therefore, this first element includes all the aspects which describe the production or destruction of a species as well as its capacity to move through a mixture, along with its tendency to exchange energy with the surrounding.

In order to describe all these phenomena, a very high number of parameters must be provided. They are collected inside three files. The first includes the kinetic mechanism; the second is a thermodynamic database and the last contains coefficients for the transport properties computation. In the following sections a detailed analysis of these elements is performed.

## 2.2.1 Kinetic mechanism

In case of combustion, the kinetic mechanism is a collection of thousands of reactions which describe the chemical interactions of hundreds of species. The structure of the schemes developed by CRECK Modeling group is modular and hierarchical. These concepts can be better understood looking at the Figure 2.2. As shown, there are different subsystems, called modules, each containing a set of reactions related to the corresponding family of species. Moreover, the modules for smaller species are always present in the set of reactions for larger species since the chemistry of the latter is based on the former. In fact, through pyrolysis reactions, hydrocarbon molecules break into smaller whose chemistry must be involved in the overall kinetic mechanism. Therefore, it is possible to add or remove some of these modules as a function of operating conditions of interest.
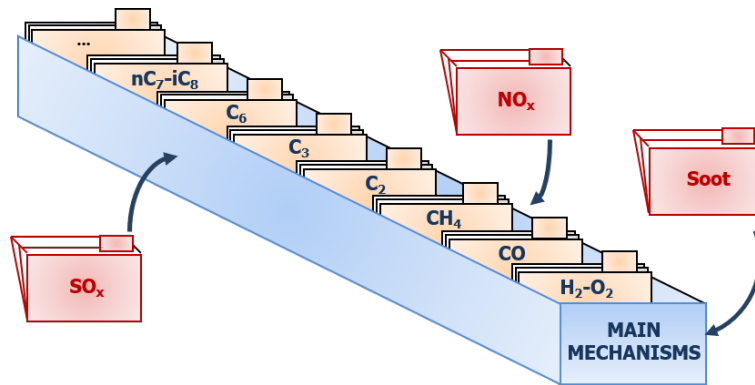


**Figure 2.2:** Description of the hierarchy and modularity of the CRECK modeling kinetic schemes.

The format through which the schemes are written is known as CHEMKIN. CHEMKIN is a software package developed during the eighties at Sandia National Laboratories [49]. It was born as a research project for the numerical modeling of reactive fluxes. Its purpose was to facilitate the formulation, solution, and interpretation of problems involving elementary gas-phase chemical reactions in ideal systems. It provides a flexible and powerful tool for incorporating complex chemical kinetics into simulations of fluid dynamics. They invented a standard language through which write the kinetic mechanisms in order to include all the kinds of reaction. Thanks to its completeness, all the software developed in the following years have used as reference the CHEMKIN format. Therefore, programs as `OpenSMOKE++` have an interpreter which is able to "read" the kinetic schemes written in such language and convert them into a series of files suitable to interface with the relative code.

The development of a kinetic mechanism able to describe the methane oxy-combustion in presence of high dilution levels of $CO_2$ and $H_2O$ has started from the state-of-the-art POLIMI kinetic mechanism "C1C3HT-1412". Such terms indicate that the mechanism contains the reactions involving all the hydrocarbon molecules with a chain length between one to three carbon atoms ("C1C3"). "HT" stays for High Temperature, i.e. the chemistry involved regards only the high temperature mechanism. This particular feature has been selected since the fuel investigated is methane and its chemistry is characterized by a dynamics which can be described by the same reactions both at low and at high temperature. "1412" indicates the publication date of such scheme: December 2014. The considered kinetic model, finally, is constituted by 84 species which interact through 1698 reactions.

The formulation of a kinetic scheme must contain not only the values representing the reactions involved in the chemical kinetic mechanism, but also additional information about the reaction type. During the simulation of reacting flow systems, they are implemented by the code into equations which allow the evaluation of the forward kinetic constant. There are different expressions to calculate such quantity as a function of kind of reaction itself [50]:

- If the kinetic constant depends only on temperature, the Arrhenius equation is used:

$$k_f = A \cdot T^{\alpha} \cdot \exp\left(-\frac{E_{act}}{R \cdot T}\right) \qquad (2.15)$$

  Therefore, in the kinetic scheme, the parameters which must be provided along with the reaction equation are three: the pre-exponential factor $A$, the $\alpha$ factor and, finally, the activation energy $E_{act}$.

- In case of third-body reactions, the kinetic constant depends also on pressure. As described in Chapter 1, three different kinetic constants can be used:

  - for very small pressures, the so-called "low-pressure limit" or $k_0$ is adopted to compute the forward kinetic constant. It can be evaluated using the modified Arrhenius expression multiplied by a correction factor:

$$k_f = k_0 \cdot [M] = A_0 \cdot T^{n_0} \cdot \exp\left(-\frac{E_{act,0}}{R \cdot T}\right) \cdot [M] \qquad (2.16)$$

    Therefore, $A_0$, $n_0$ and $E_{act,0}$ are the first three parameters which must be involved in the kinetic scheme for the reaction under analysis. The correction factor is represented by the molar concentration of the system

gas phase. It can be computed by recalling the ideal gas law:

$$[M] = \sum_{i=1}^{NC} \frac{P \cdot y_i}{R \cdot T} \varepsilon_i \tag{2.17}$$

As already explained, $\varepsilon_i$ represents the third-body efficiency of the $i - th$ species. It indicates its capability of distributing the energy released by the reaction over its vibrational degrees of freedom. In the kinetic scheme, such parameters must be provided only for the species for which those values are different from one. Finally, since these efficiencies are dependent on the specific reaction, they must be specified for each of them.

– When pressure becomes higher than an upper threshold, the dependence of the kinetic constant on pressure itself vanishes. It can be evaluated always through the modified form of Arrhenius equation. Therefore, in the kinetic scheme also the Arrhenius parameters for the "high-pressure limit", also known as $k_\infty$, must be provided. They are $A_\infty$, $n_\infty$ and $E_{act,\infty}$. The forward kinetic constant coincides with $k_\infty$ and no correction factor must be included:

$$k_f = k_\infty = A_\infty \cdot T^{n_\infty} \cdot \exp\left(-\frac{E_{act,\infty}}{R \cdot T}\right) \tag{2.18}$$

– For intermediate pressures, the forward kinetic constant for third-body reactions has a complex behavior. There are several methods of representing the rate in the "fall-off" region. For the gas-phase kinetics three of them are typically used. All are based on the following equation:

$$k_f = k_\infty \cdot \frac{k_0 \cdot [M]}{k_\infty + k_0 \cdot [M]} \cdot F \tag{2.19}$$

It depends on both the "high-pressure limit" and the "low-pressure limit" kinetic constants. Also the molar concentration of the third body is included and it must be computed by taking into account the enhanced third-body efficiencies. In addition, a correction factor $F$ is present. Depending on the method chosen for the evaluation of the kinetic constant, such parameter can be computed in different ways.

∗ In case of Lindemann approach [51] the correction factor is unity.

∗ Through the Troe form [52], F is given by

$$\log{(F)} = \left[ 1 + \left[ \frac{\log{(P_r)} + c}{n - 0.14 \cdot (\log{(P_r)} + c)} \right]^2 \right]^{-1} \cdot \log{(F_{cent})} \quad (2.20)$$

The constants in Equation (2.20) are

$$P_r = \frac{k_0 \cdot [M]}{k_\infty} \quad (2.21)$$

$$c = -0.4 - 0.67 \cdot \log{(F_{cent})} \quad (2.22)$$

$$n = 0.75 - 1.27 \cdot \log{(F_{cent})} \quad (2.23)$$

$$F_{cent} = (1 - \alpha)\exp{\left( -\frac{T}{T^{***}} \right)} + \alpha\exp{\left( -\frac{T}{T^*} \right)} + \exp{\left( -\frac{T^{**}}{T} \right)} \quad (2.24)$$

The four parameters $\alpha$, $T^{***}$, $T^*$ and $T^{**}$ must be specified as auxiliary inputs to the kinetic mechanism in correspondence of the relative third-body reaction.

∗ The approach taken at SRI International by Stewart [53] is in many way similar to that taken by Troe, but the function $F$ is approximated differently. It is given by

$$F = d \left[ a \cdot exp{\left( -\frac{b}{T} \right)} + exp{\left( -\frac{T}{c} \right)} \right]^X \cdot T^e \quad (2.25)$$

where

$$X = \frac{1}{1 + (logP_r)^2} \quad (2.26)$$

In this case, in addition to the six Arrhenius parameters, three for the "low-pressure limit" $k_0$ and three for the "high-pressure limit" $k_\infty$, the parameters $a$, $b$, and $c$ must be provided in the kinetic scheme. The $d$ and $e$ terms are used to increase the flexibility of the equation. They can be considered parameters that define a weak-collision efficiency factor. Therefore, they can be introduced in case of strong-collision rate parameters computation.

The `OpenSMOKE++` code is able to evaluate the kinetic constants for third-body reactions through all these three methods. Depending on the parameters provided, it selects the corresponding approach for the evaluation of the $F$ correction factor. The value obtained in case of high or small pressure is the same evaluated using the procedure described in the two previous points. In fact, if the pressure is sufficiently high,

$F$ tends to 1 and $k_0 \cdot [M]$ tends to infinity. Therefore, in the Equation (2.19), only $k_\infty$ survives. Conversely, when pressure is very small, at the denominator of (2.19), $k_0 \cdot [M]$ can be neglected with respect to $k_\infty$; at the end, since $F$ is about 1 in this case, the kinetic constant computed in such a way is equal to $k_0 \cdot [M]$.

In addition to third-body, there are other reactions whose kinetic constants depend on pressure. In this case, the PLOG function [54] can be used to evaluate them. Indeed, for each of these reactions, the Arrhenius parameters are provided for different values of pressure. They are characteristic of each reaction and they are defined as a function of the experimental procedure performed for the definition of such quantities. The `OpenSMOKE++` code interpolates between the two kinetic constants evaluated at the two adjacent pressures with respect to the operating pressure of the simulated system.

### 2.2.2 Thermodynamic database

In addition to the kinetic scheme, the kinetic model is completed by two additional databases. The first is the thermodynamic database [55, 56]; it is the collection of the 7-coefficients NASA polynomials for each species used to evaluate the expression as a function of temperature of three gas-phase properties: the specific heat at constant pressure, the enthalpy and entropy of formation. These data are important in order to compute the equilibrium constant useful to evaluate, for each reaction, the backward kinetic constant, $k_b$. It is linked to the forward through the following correlation:

$$K_{eq,c} = \frac{k_f}{k_b} \tag{2.27}$$

Since $k_f$ can be computed through the parameters provided in the kinetic file, $k_b$ can be found using only the previous correlation. Therefore, the equilibrium constant must be computed. This can be done through the following equation:

$$K_{eq,p} = \exp\left(-\frac{\triangle G_R^0(T)}{R \cdot T}\right) \tag{2.28}$$

where $\triangle G_R^0$ is the Gibbs' free energy change associated to the generic reaction R. The relation between $K_{eq,p}$ and $K_{eq,c}$ is:

$$K_{eq,p} = K_{eq,c} \cdot (R \cdot T)^{\triangle n} \tag{2.29}$$

where $\triangle n$ represents the sum of the stoichiometric coefficients of the products minus the stoichiometric coefficients of the reactants:

$$\triangle n = \sum_{i=1}^{Products} v_i - \sum_{j=1}^{Reactants} v_j \qquad (2.30)$$

The Gibbs' free energy change of reaction can be computed using the the Gibbs' free energy change of formation of reactants and products as shown below:

$$\triangle G_R^0(T) = \sum_{i=1}^{Products} v_i \cdot \triangle G_{f,i}^0(T) - \sum_{j=1}^{Reactants} v_j \cdot \triangle G_{f,j}^0(T) \qquad (2.31)$$

The Gibbs' free energy of formation of a generic species $i$ is defined as the variation of this thermodynamic quantity related to the reaction which produces the $i - th$ species starting from the elements which constitute it:

$$\triangle G_{f,i}^0(T) = G_i^0(T) - \sum_{k=1}^{Elements} v_k \cdot G_k^0(T) \qquad (2.32)$$

where $v_k$ represent the stoichiometric coefficient of the $k - th$ element in the concerned reaction in order to make equal to 1 the stoichiometric coefficient of the $i - th$ species itself.

In order to compute the Gibbs' free energy of each species involved in (2.32), the thermodynamic definition of this property can be used:

$$G^0(T) = H^0(T) - T \cdot S^0(T) \qquad (2.33)$$

At this point, the enthalpy and entropy must be calculated at the generic temperature T. The following expressions must be used:

$$H^0(T) = H^0(T_{ref}) + \int_{T_{ref}}^{T} C_p^0(T)dT \qquad (2.34)$$

$$S^0(T) = S^0(T_{ref}) + \int_{T_{ref}}^{T} C_p^0(T)d\ln T \qquad (2.35)$$

Finally, to complete the previous two equations, the expression of the specific heat at constant pressure as a function of temperature must be defined:

$$C_p^0(T) = R \cdot \left(a_1 + a_2 \cdot T + a_3 \cdot T^2 + a_4 \cdot T^3 + a_5 \cdot T^4\right) \qquad (2.36)$$

The last three equations involve some parameters they can be derived experimentally or through theoretical calculations (ab initio or group additivity). In literature, there are some thermodynamic databases within which these quantities are listed. In order to increase the computational accuracy, two correlations are provided, one for the high and one for the low temperature. The temperature threshold which divides these two regimes changes between the species.

This distinction is related to the different behavior of the specific heat as a function of temperature in these two intervals.

Therefore, in the thermodynamic file, for each species, fifteen values must be provided:

- The first represents the temperature threshold just introduced.

- Then, 7 parameters are provided. These are related to the low-temperature range. The first five are the specific heat coefficients $a_1$ to $a_5$. The last two correspond to $H^0\left(298\,K\right)$ and $S^0\left(298\,K\right)$. 298 K is identified as the reference temperature for the low-temperature regime.

- The last 7 are related to the high-temperature region. As above, the first five values are the $a_1$ to $a_5$ specific heat coefficients. The last two are $H^0$ and $S^0$ evaluated at the reference temperature which coincides with the boundary between the high and the low temperature regimes.

In order to better understand the procedure followed for the computation of the thermodynamic properties for each species, an example is here provided; considering $H_2O$, the elements which form this molecule are the hydrogen and the oxygen. In nature, at a reference temperature of 298 K and at 1 bar of pressure, they are present inside the $O_2$ and $H_2$ molecules. The corresponding aggregation state is the gaseous one. Therefore, the reaction equation which describes the water production, balanced as above described, is:

$$H_2 + \frac{1}{2}\,O_2 \leftrightarrow H_2O \tag{2.37}$$

The Gibbs' free energy of formation of water is thus given by:

$$\triangle G^0_{f,H_2O}\left(T\right) = G^0_{H_2O}(T) - G^0_{H_2}\left(T\right) - \frac{1}{2}G^0_{O_2}\left(T\right) \tag{2.38}$$

The Gibbs' free energy at the generic temperature T must be computed involving the enthalpy and entropy as described in the Equation (2.33). To calculate these last two quantities, Equation (2.34) and (2.35) must be used. Therefore, two integrals must be solved once defined the reference temperature: 298 K if

the operating temperature at which the system is studied belongs to the low-temperature; the low-to-high temperature threshold in case of high temperature regime.

Typically, when `OpenSMOKE++` interprets the thermodynamic file, it computes the integrals above seen, both with 298 K and with the low-to-high boundary temperature, obtaining coefficients that must be implemented inside temperature dependent expressions which are provided in a dimensionless form:

$$\frac{H(T)}{R \cdot T} = A_H + B_H \cdot T + C_H \cdot T^2 + D_H \cdot T^3 + E_H \cdot T^4 + \frac{F_H}{T} \qquad (2.39)$$

$$\frac{S(T)}{R} = A_S \cdot \ln(T) + B_S \cdot T + C_S \cdot T^2 + D_S \cdot T^3 + E_S \cdot T^4 + F_S \qquad (2.40)$$

The A to F constants are computed both for the high and for the low temperature regions. Also the specific heat at constant pressure is rearranged including the universal gas constant as follows:

$$C_p(T) = A + B \cdot T + C \cdot T^2 + D \cdot T^3 + E \cdot T^4 \quad \left[\frac{J}{kg \cdot K}\right] \qquad (2.41)$$

### 2.2.3 Transport properties

The last database needed to complete the kinetic model contains the transport properties of all the species involved in the mechanism. In particular, the following six parameters are provided [50, 54]:

- The first is a number which indicates the geometrical configuration of a species: 0 for atoms, 1 for linear molecules and 2 for non linear molecules.

- The Lennard-Jones potential well depth $\frac{\varepsilon}{k_B}$ $[K]$. It is a measure of the attraction strength of two interacting particles.

- The Lennard-Jones collision diameter $\sigma$ $\left[\mathring{A}\right]$. It is the distance at which the inter-molecular potential between two particles is zero. Therefore, it tells how close two non bonded particles can get.

- The dipole moment $\mu$ $[D]$. It is a measure of the polarity of a chemical bond within a molecule. It is zero for neutral molecules and for atoms.

- The polarizability $\alpha$ $\left[\mathring{A}^3\right]$. This property indicates the ability of a molecule to form instantaneous dipoles. Therefore it represents also the dynamical response of a bound system to external force fields.

- The rotational relaxation collision number $Z_{rot}$ at 298 K. This parameter indicates the number of collisions that a particle excited rotationally takes in order to deactivate.

These six quantities are used to estimate the fitting coefficients for the correlations used to compute the thermal conductivity $\lambda$, viscosity $\mu$, binary diffusivity $\Gamma_{ij}$ and thermal diffusion ratio $\theta_{ij}$ as a function of temperature. Therefore, in the interpreted file, the parameters for the following expressions will be used:

$$\lambda(T) = \exp\left[A_\lambda + B_\lambda \cdot \log(T) + C_\lambda \cdot \log^2(T) + D_\lambda \cdot \log^3(T)\right] \quad \left[\frac{W}{m \cdot K}\right] \quad (2.42)$$

$$\mu(T) = \exp\left[A_\mu + B_\mu \cdot \log(T) + C_\mu \cdot \log^2(T) + D_\mu \cdot \log^3(T)\right] \quad \left[\frac{kg}{m \cdot s}\right] \quad (2.43)$$

$$\Gamma_{ij}(T) = \frac{\exp\left[A_\Gamma + B_\Gamma \cdot \log(T) + C_\Gamma \cdot \log^2(T) + D_\Gamma \cdot \log^3(T)\right]}{P\,[bar]} \quad \left[\frac{m^2}{s}\right] \quad (2.44)$$

$$\theta_{ij} = A_\theta + B_\theta \cdot T + C_\theta \cdot T^2 + D_\theta \cdot T^3 \quad [-] \quad (2.45)$$

### 2.2.4   Interpretation of the kinetic scheme

In the previous sections, the description of the three files which form a kinetic model has been provided. They contain the parameters required to calculate thermodynamic, kinetic and transport properties. Since they are written in CHEMKIN format, they need to be interpreted in order to make them suitable to be used by the different solvers. Therefore, in the `OpenSMOKE++` suite there is a utility which allows to pre-process the model [43]. In this way, a folder is generated as output, containing the same elements present in the three raw files. The difference stays in the extension which is suitable to allow the interaction with the `OpenSMOKE++` libraries. In addition, the Pre-Processor creates also files where the coefficients for the thermodynamic and transport properties expressions above seen are listed. Therefore, in case of enthalpy and entropy, for each species the parameters for the evaluation of these quantities as a function of temperature are present. The same for the A to D values for the equations which goes from (2.42) to (2.45). Therefore, the interpreted kinetic model is recover and it represents the first element necessary to perform a simulation of a generic system.

## 2.3   Simulation

The interpreted kinetic model, which is formed by the kinetic, thermodynamic and transport files, represents the tool which is able to describe the chemistry

and physics of a generic system. At the same time, also the transport properties are defined and they are able to describe both the mass and the energy transfer in a system. All the quantities involved in these files are only the coefficients which must be introduced in the expressions as a function of temperature and pressure for the evaluation of the different system properties. In order to perform a simulation, different information must be clearly defined in an input file:

- The type of reactor or flame to simulate. Within `OpenSMOKE++`, there are different devices which can be selected. They are ideal reactors or flame: well-stirred reactors, plug-flow reactors, counter-flow flames and premixed laminar flames are some examples. Along with this first information, also the boundary conditions are required: isothermal or non-isothermal, adiabatic, constant volume, constant pressure etc. Depending on these properties, the code set the system of equations that represents the model of the system to simulate. In addition, some geometrical parameters of the unit must be provided to fully characterize the reactor.

- As a function of reactor type, the inlet or initial properties of the reactive mixture must be provided. In particular, its composition, temperature and pressure must be specified. They represent also the initial conditions for the system of equations which describe the reactor itself.

- Depending on the kind of species introduced in the unit to simulate, the suitable interpreted kinetic model must be included in the simulation itself.

Once compiled properly the input file with all the elements required to totally characterize the reactor or the flame, the simulation is initialized and, now, it can be performed. Therefore, in this way the boundary conditions to the system of transport equations describing the related unit are defined. To run a simulation, a proper utility must be selected and executed. There is one utility for each reactor or flame which can be simulated. It contains the transport equations which characterize the system: mass balances, energy balance and momentum balance. Once coupled the input file with the corresponding solver, the simulation can be performed; thus, the equations are solved and an output folder containing the results is generated. They are present both in ASCII and XML formats, the latter serving as an input for the post-processing utilities available in `OpenSMOKE++`. They are introduced in the next section.

## 2.4 `OpenSMOKE++` **Post-Processor**

The `OpenSMOKE++` Post-Processor is the numerical tool which allows the analysis and interpretation of the results from a kinetic point of view. It requires some inputs:

- The simulation results are provided through the service files generated at the end of the simulation.

- The interpreted kinetic model must be involved in order to perform different kinds of analysis.

In the next sections, the three possible available options are described in detail.

### 2.4.1 Profiles

Through this first option, different properties of the reactor or flame simulated can be analysed [43]. Typically, it represents the first approach to the results analysis; in fact, it allows to investigate, through several diagrams, the behavior of the different parameters as a function of a selected independent variable: time, pressure, temperature, conversion, geometrical parameter of the reactor etc. For example, Figure shows the the methane conversion as a function of time for a Plug-Flow Reactor (PFR).
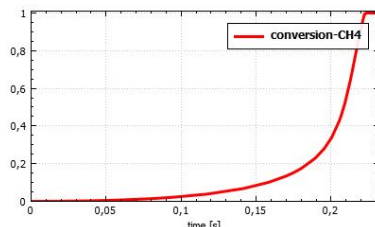


**Figure 2.3:** Methane conversion as a function of time for a plug-flow reactor.

### 2.4.2 Rate Of Production Analysis (ROPA)

The Rate Of Production Analysis, or simply ROPA, is an important tool to understand kinetic aspects in the simulation of reactive flows [43]. This analysis determines the contribution of each reaction to the production or consumption of a selected species $i$. A first available function is represented by the ROPA bars. The software returns a window containing a series of horizontal bars. Each one is associated to a correspondent reaction along with a number which represents its net rate. Depending on the sign of this parameter, the bar will have a related color: red for positive rates, which corresponds to a production of the i-th species,

and blue in case of consumption. Finally, each of these horizontal bars has a specific length proportional to the corresponding reaction rate and, as a function of this quantity, they are stacked in a decreasing order. In the Figure 2.4, the ROPA for the H radical is shown. The numbers on the left indicate the number of the reaction in the kinetic mechanism involved in the post-processing. From a physical point of view, through such analysis, the most relevant reactions which control the chemistry in a specific selected time instant can be identified. In the example reported, reaction 5 is the most important path for the consumption of the H radical; in fact, the corresponding bar is the longest, its color is blue and the net production rate is negative.
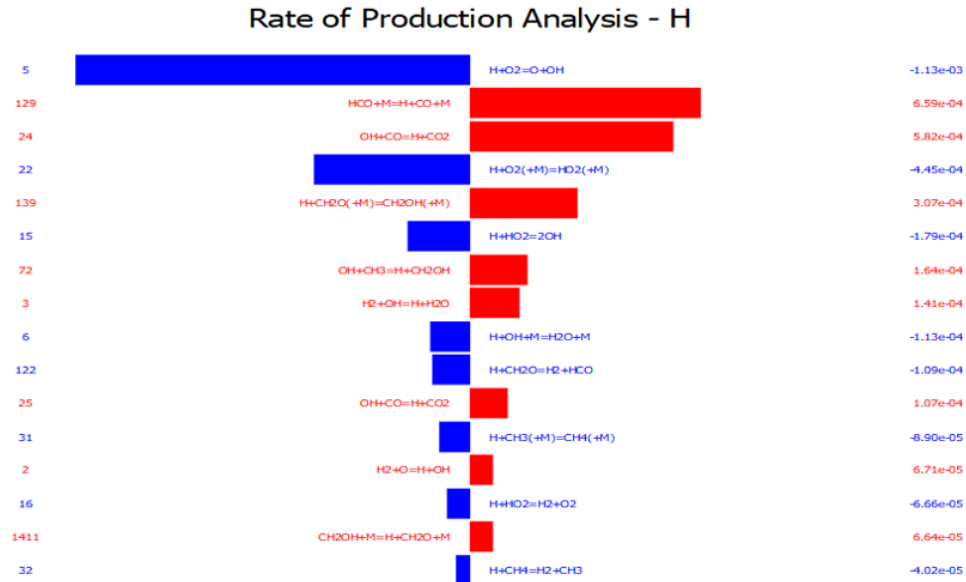


**Figure 2.4:** ROPA for the H radical.

Through ROPA, it is possible to find the overall rate of production, consumption or the net one for a selected species. The program will compute the following three quantities:

- the formation rate, $\dot{c}_i$, is computed in this way:

$$\dot{c}_i = \sum_{j=1}^{Reactions} v_{ij}^f \cdot r_j^b + \sum_{j=1}^{Reactions} v_{ij}^b \cdot r_j^f \tag{2.46}$$

where $v_{ij}^f$ is the stoichiometric coefficient of the $i-th$ reactant in the backward $j-th$ reaction; $r_j^b$ is the rate of the backward reaction which produces the $i-th$ species itself. Instead, $v_{ij}^b$ is the stoichiometric coefficient of the $i-th$ product in the forward $j-th$ reaction; $r_j^f$ represents the rate of the forward

reaction which produces the $i - th$ species. This quantity is conventionally positive.

- Similarly, the destruction rate, $\dot{d}_i$ is:

$$\dot{d}_i = \sum_{j=1}^{Reactions} v_{ij}^f \cdot r_j^f + \sum_{j=1}^{Reactions} v_{ij}^b \cdot r_j^b \qquad (2.47)$$

where $v_{ij}^f$ is the stoichiometric coefficient of the $i - th$ reactant in the forward $j - th$ reaction; $r_j^b$ is the rate of the backward reaction which produces the $i - th$ species itself. $v_{ij}^b$ is the stoichiometric coefficient of the $i - th$ product in the backward $j - th$ reaction; $r_j^f$ represents the rate of the forward reaction which produces the $i - th$ species. Differently from the previous case, this quantity is negative.

- Finally, the net formation rate is calculated. It is simply the sum between creation and destruction terms:

$$\dot{c}_i + \dot{d}_i \qquad (2.48)$$

A positive value means that the analysed species is producing, otherwise, it is consuming.

The last option included in the Rate Of Production Analysis is the flux analysis. For any species with respect to any atomic element available in the kinetic mechanism, the corresponding reaction path diagram is automatically generated. It is drawn according to the width and the depth parameters specified by the user, which are used to control its complexity and the level of detail. In particular, the first parameter indicates the maximum number of arrows leaving from each node. The depth parameter is an integer which specifies the maximum number of levels to be drawn. Figure 2.5 shows an example to better illustrate the capabilities of the reaction path diagram generator.
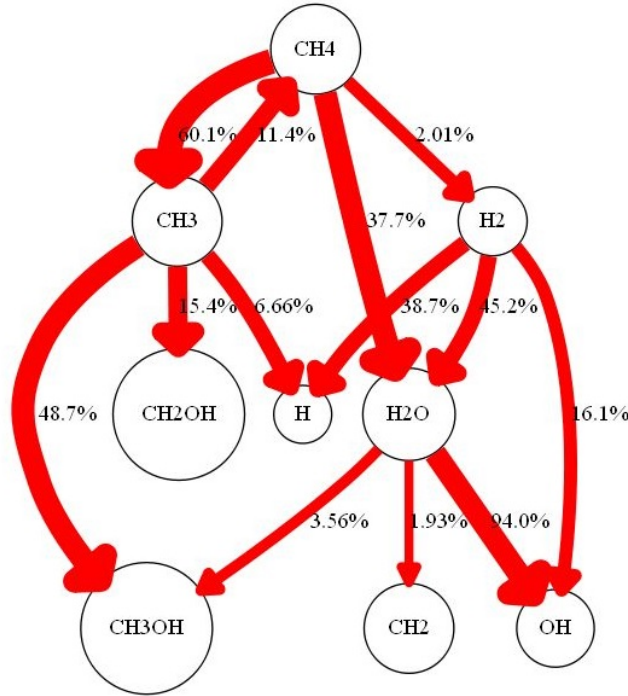
**Figure 2.5:** Flux analysis generated for the H element starting from methane molecule.

### 2.4.3 Sensitivity Analysis

The last function of the Post-Processor is the sensitivity analysis [43]. In order to perform this kind of study, in the input file created before the simulation, the user must provide the name of the species he wants to investigate through this kind of post-processing. It is a very important tool for kinetic studies because it allows the quantitative understanding of how the numerical solution of the governing equations depends on the several parameters contained in the model of the system of concern. There are three coefficients of the reaction rate as a function of which the first-order sensitivity coefficients are calculated: pre-exponential factor, activation energy and kinetic constant. The output generated by a sensitivity analysis is a window which contains bars depicted through the same logic described for the ROPA. In this case the number that corresponds to each reaction and, consequently, to each bar is the first-order sensitivity coefficient. This parameter, called $s_{ij}$, is computed as follows:

$$s_{ij} = \frac{\partial y_i}{\partial \alpha_j} \tag{2.49}$$

where $y$ is the vector of unknown terms as a function of which the equations of the model that represents the simulated system are written. $\alpha$ is the vector of variables with respect to which the analysis is performed. In the bars diagram the

sensitivity coefficients are, in general, normalized as a function of the maximum one. Figure 2.6 shows the sensitivity analysis evaluated for methane concentration within a CSTR.
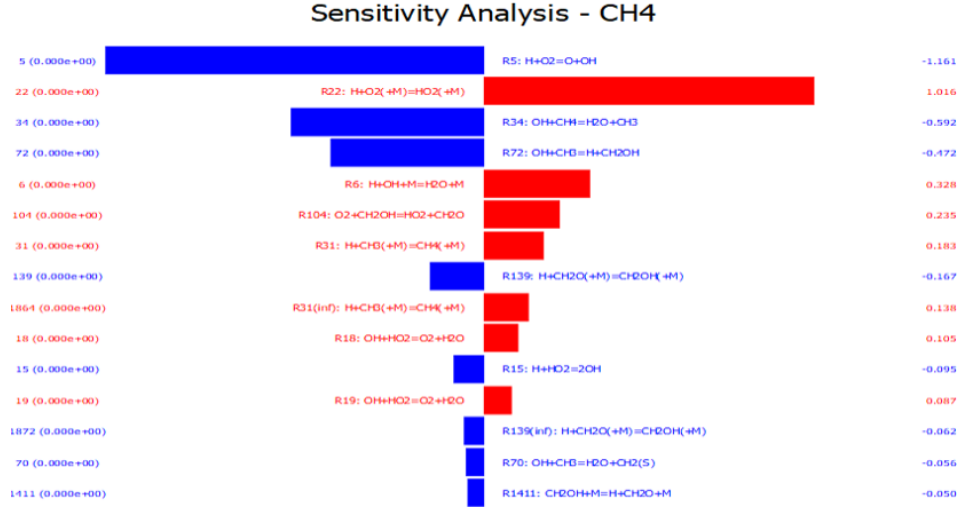


**Figure 2.6:** Sensitivity Analysis conduced on methane in a CSTR.

Considering for example the first reaction, if the forward path is favored, it will cause the reduction of the methane concentration in the reactor. In fact, this process is the main source of reactivity of a combustion process. Therefore, it is responsible of the increase of the active radicals in the system. As a result, the $CH_4$ molar fraction will decrease.

CHAPTER *3*

# Kinetic modeling of methane combustion in MILD oxy-fuel conditions

I N the present chapter, the development of a kinetic mechanism able to describe the methane combustion in MILD oxy-fuel conditions is performed starting from the state-of-the-art POLIMI scheme "C1C3HT-1412". The collection of a rather high number of experimental data is the necessary condition for the beginning of such kind of work. They must interest several operating conditions in terms of pressure, temperature, equivalence ratios and dilution levels. Only in this way, it is possible to test the existing model and understand how to modify it in order to make it suitable to replicate the behavior of the oxy-combustion of methane in presence of high dilution levels of $CO_2$ and $H_2O$. In parallel, also the comparison with other available kinetic schemes is performed in order to find the improvement points of the developing model. At the end of such work, the final kinetic mechanism is obtained and in order to assume it as correct, robust and reliable, it must replicate the experimental data in all the different operating conditions.

## 3.1 Experimental data collection

The long way which drives from the "raw" kinetic mechanism to the validated one starts with the experimental data collection. The method followed in performing such process is based on the research in the literature of results concerning the methane oxy-combustion in presence of different dilution levels of $H_2O$ and $CO_2$. Several conditions in terms of pressure, temperature and equivalence ratio have been found. Only ideal reactors have been selected. In fact, the MILD oxy-methane combustion is a relatively innovative solution, not yet applied in industrial scale and most of the available experimental data have been obtained only in laboratories where reactors are typically operated in such a way as to replicate ideal conditions. Moreover, since the purpose of the work is the development of a kinetic scheme, ideal reactors are devices which allow to perform kinetic studies, decoupling all the phenomena not related to the chemistry. In addition to the published data, CRECK Modeling group have obtained other new experimental results given by affiliated laboratories. In particular, "Istituto di Ricerche sulla Combustione, IRC" placed in Naples [57] and the "CNRS, National Center for Scientific Research" of Nancy [58].

All the data have been collected in three groups as a function of the reactor type within they have been obtained: plug-flow reactor, well-stirred reactor and premixed laminar flame speed. In Table 3.1, a resume of all the operating conditions of the experimental data investigated in this Thesis is provided.

| Reactor | Fuel | Oxidizer | $\Phi$ | Diluent | Dilution | $T_{inlet}$ | P |
|---------|------|----------|--------|---------|----------|-------------|---|
| LFS | $CH_4$ | $O_2$ | 0.5/1/1.5 | $H_2O$ | 0-60% | 298-373 K | 1 atm |
| | | | 0.5-1.5 | $CO_2$ | | | 1/2/3 bar |
| | | | 0.6/1/1.4 | $H_2O$-$CO_2$ | | | 1 atm |
| PSR | $CH_4$ | $O_2$ | 0.5 | $CO_2$ | 90% | 800-1250 K | 1.1 atm |
| | | | 1.5 | $H_2O$-$N_2$ | | | 1.1 atm |
| PFR | $CH_4$ | $O_2$ | 0.124 | $H_2O$-$CO_2$ | 96% | 800-1300 K | 1 atm |
| | | | 3.89 | $CO_2$-$N_2$ | 99.85% | 1200-1800 K | 1 atm |

**Table 3.1:** Operating conditions of the experimental data collected for three reactors: Laminar Flame Speed (LFS), Perfectly-Stirred Reactor (PSR) and Plug-Flow Reactor (PFR).

## 3.2 "POLIMI C$_1$-C$_3$ 1412" simulation

Chapter 2 provided a description of the kinetic mechanism recently developed by the CRECK Modeling research group of "Politecnico di Milano", i.e. "POLIMI C$_1$-C$_3$ 1412". In this section, experimental data are compared with results from numerical simulation carried out with the `OpenSMOKE++` suite in order to prove the capability of such kinetic mechanism to predict important combustion features

typical of the MILD oxy-fuel conditions. Therefore, for each ideal reactor type, the corresponding input file has been initialized. Then, the simulations have been performed and, at the end, the different output files generated by the program have been processed in order to compare them with the results of the real experiments.

The new conditions investigated are characterized by the presence of high dilution through water and carbon dioxide. They are species with a relatively high specific heat at constant pressure, but also a quite high third-body efficiency, especially for $H_2O$. The original model tested, as better described below, is not always good in predicting the real behavior of such process. Therefore, in the following sections, the effects caused by such diluents are fully explained.

### 3.2.1 Premixed laminar flame speed

Several experimental results have been found in literature regarding the premixed laminar flame speed. Such property is important in order to fully characterize a flammable mixture [46]. Therefore, the comparison of the simulated results with experimental data will give important information about the goodness of the involved kinetic scheme. Finally, to perform a robust and complete testing of the "POLIMI C$_1$-C$_3$ 1412" model, different initial pressures and temperatures of several compositions of methane based mixtures have been investigated.

**Methane oxy-combustion in presence of CO$_2$ and/or H$_2$O**

Mazas et al., during 2010 [59], performed several experiments evaluating the premixed laminar flame speed for methane oxy-combustion in presence of $H_2O$ and $CO_2$ as diluents. All the mixtures were investigated at atmospheric pressure with reactants inlet temperature of 373 K. In Figure 3.1, the experimental apparatus used to recover such data is depicted.
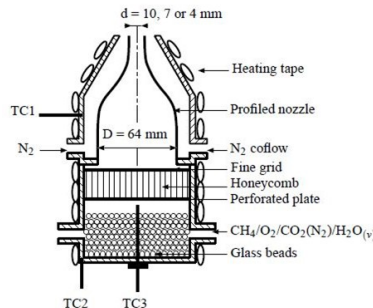


**Figure 3.1:** Schematic of the experimental set-up: detailed view of the burner.

The experiments have been divided in two parts. First of all, the analysis of the effects of the single diluents were considered. In Table 3.2, the compositions of

the first two mixtures investigated are listed.

| Mixture | Diluent | Equivalence Ratio | Diluent Molar Fraction |
|---|---|---|---|
| $CH_4/O_2$ | $H_2O$ | 0.5 - 1 - 1.5 | 0 - 0.4 |
| $CH_4/O_2$ | $CO_2$ | 0.5 - 1 - 1.5 | 0 - 0.5 |

**Table 3.2:** Operating conditions for methane-oxygen mixtures.

For each one, an equivalence ratio for lean, stoichiometric and rich conditions has been selected. Therefore, the laminar flame speed has been computed for increasing molar fractions of water or carbon dioxide. As a result, the comparison between experimental and simulated with "POLIMI $C_1$-$C_3$ 1412" data is reported in Figure 3.2.



**Figure 3.2:** Experimental (symbols) and computed (lines) premixed laminar flame speeds of $CH_4/O_2/H_2O$ and $CH_4/O_2/CO_2$ mixtures as a function of molar fraction of the corresponding diluent ($H_2O$ and $CO_2$ respectively). For each mixture, three equivalence ratios are investigated: 0.5, 1 and 1.5. The inlet temperature is 373 K and the operating pressure is of 1 atm.

The model is quite good in predicting the experiments for $\Phi = 0.5$. Passing to the rich conditions through the stoichiometric ones, the computed data are overestimating the real behavior of the system.

The increase of the diluent molar fraction keeps the error between the two data almost constant except for the case with $CO_2$ and equivalence ratio of 1.5. Only in this case, the error seems to reduce with the increase of the amount of diluent in the inlet mixture. Consequently, in addition to the effects of the water and carbon dioxide over the kinetics of the process, also the replacement of air with pure oxygen as oxidizer must be investigated. In fact, always in rich conditions, when the molar fraction of the diluent is zero, the difference between the observed and the predicted laminar flame speed is quite high.

Finally, performing a comparison between the two diluents, for the same equivalence ratio the flame containing water is faster than carbon dioxide. Therefore, the influence of the latest over the laminar flame speed is more important than $H_2O$.

A second set of experimental data have been obtained by Mazas et al. They investigated the laminar flame speed for $CH_4/O_2$ mixtures in presence of both water and carbon dioxide as diluents. For these experiments, the dilution ratio ($D$) has been introduced to describe the relative amount of moles of oxygen with respect to the total moles of the $CO_2$-$O_2$ mixture:

$$D = \frac{O_2}{O_2 + CO_2} \tag{3.1}$$

In Table 3.3, the compositions of the mixtures investigated are listed.

| Mixture | Diluent Ratio | Equivalence Ratio | H$_2$O molar fraction |
|---------|---------------|-------------------|------------------------|
| CH$_4$/O$_2$/CO$_2$ | 0.52 | 0.7 - 1 - 1.4 | 0 - 0.3 |
| CH$_4$/O$_2$/CO$_2$ | 0.72 | 0.6 - 1 - 1.4 | 0 - 0.4 |

**Table 3.3:** Operating conditions for methane-oxygen-carbon dioxide mixtures.

As done in the previous analysis, lean, stoichiometric and rich conditions have been examined for each $O_2$-to-$CO_2$ dilution ratio. The laminar flame speeds have been evaluated for increasing water molar fractions. Figure 3.3 shows the comparison between the experimental laminar flame speeds and the ones obtained from the simulation with "POLIMI C$_1$-C$_3$ 1412" kinetic mechanism.
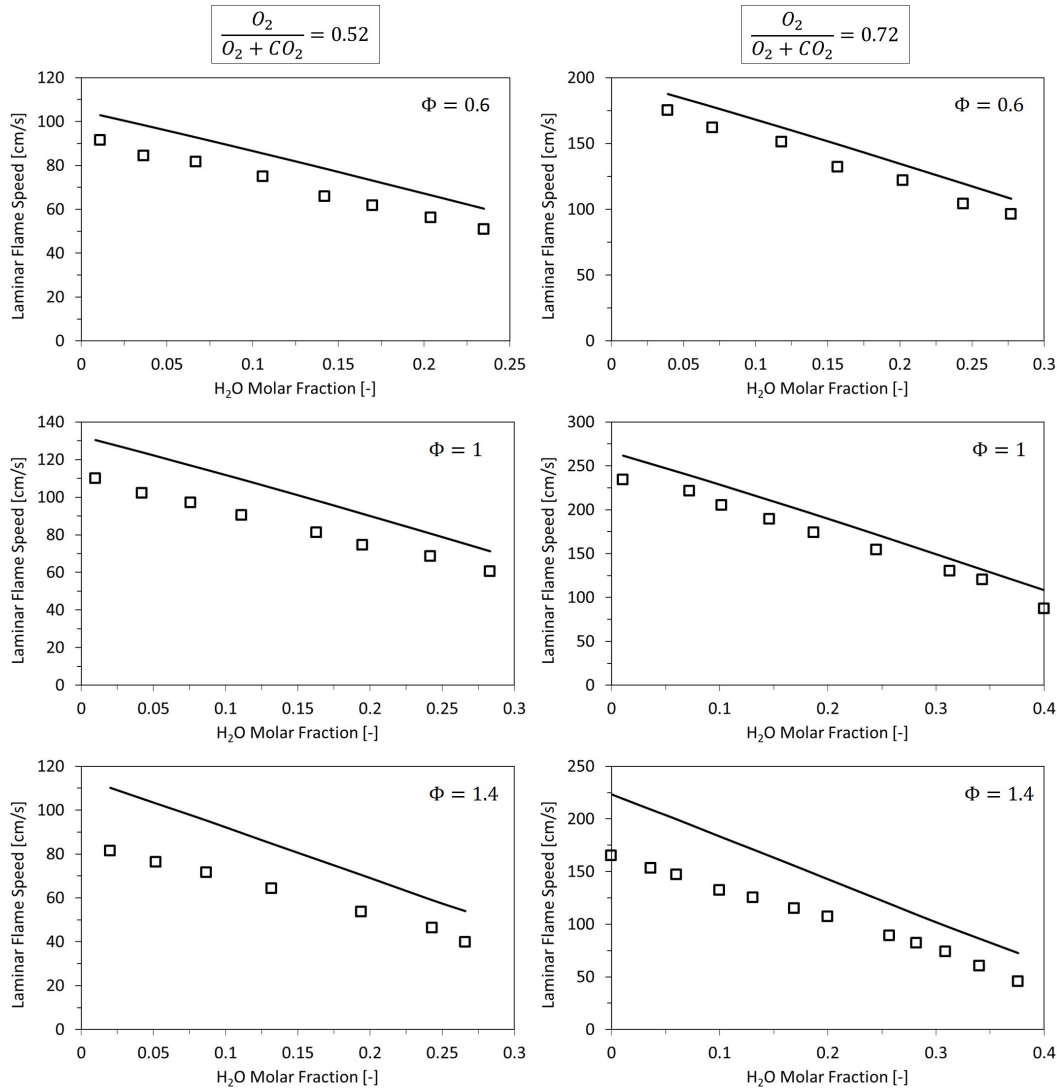
**Figure 3.3:** Experimental (symbols) and computed (lines) laminar flame speeds of $CH_4/O_2/CO_2/H_2O$ mixtures as a function of water molar fraction. Two $O_2$-to-$CO_2$ diluent ratios have been considered: 0.52 and 0.72. For each one, three equivalence ratios have been investigated: 0.6, 1 and 1.4.

In this case, the combined effect of water and carbon dioxide can be analysed. Considering at first the dilution ratio equal to 0.52, since the amount of carbon dioxide in the oxidizer mixture is around 50%, the total dilution level including water is quite high. Therefore, an error between experimental and computed results is observable at lean conditions. Such deviation increases for increasing the equivalence ratio.

Instead, considering a lower amount of $CO_2$ in the oxidizer (dilution ratio of 72%), for the same $\Phi$, the model better agrees with experimental data. Therefore, the effect of carbon dioxide is rather strong and its presence tends to decrease the reactivity inside the flame. The same influence is also provided by water: increas-

ing its molar fraction in the inlet mixture, the laminar flame speed is drastically reduced.

**Methane oxy-combustion in presence of CO$_2$ at different unburned gas temperatures**

In the present section, the "POLIMI C$_1$-C$_3$ 1412" mechanism is tested for the oxy-combustion of several methane based mixtures in presence of carbon dioxide at different inlet temperatures. The high dilution level of the experiments allows to reduce the temperature increase preserving the integrity of the apparatus.

In order to perform such kind of analysis, several experimental studies from the literature have been considered. Konnov et al. [60] measured the laminar flame speed as a function of equivalence ratio at an inlet temperature of 298 K. The amount of carbon dioxide inside the inlet mixture is defined through the dilution ratio $D$, Section (3.2.1). In this case, $D$ is equal to 0.3155.

In Figure 3.4, a schematic representation of the experimental apparatus adopted by Konnov is reported [61].
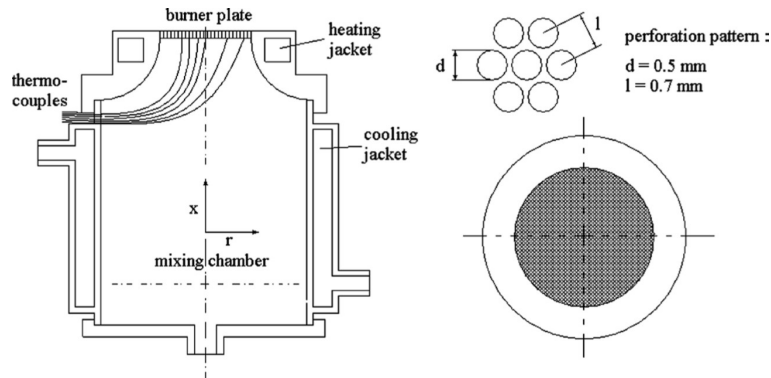


**Figure 3.4:** Left: the heat flux burner; right: top view of the burner head showing the perforation pattern of the plate.

Coppens et al. [62] measured laminar flame speeds for $CH_4/O_2/CO_2$ mixtures with the same dilution ratio, at a higher inlet temperature ($T = 323\,K$) for equivalence ratios between 0.5 to 1.5.

Mazas et al. [59] investigated $CH_4/O_2/CO_2$ mixtures ($\Phi = 0.5 - 1.5$) at an inlet temperature of 373 K and a molar fraction of carbon dioxide of 40%. In both these last two experiments, the laminar flame speed has been evaluated as a function of equivalence ratio.

The comparison between experimental data and POLIMI predictions is reported in Figure 3.5.
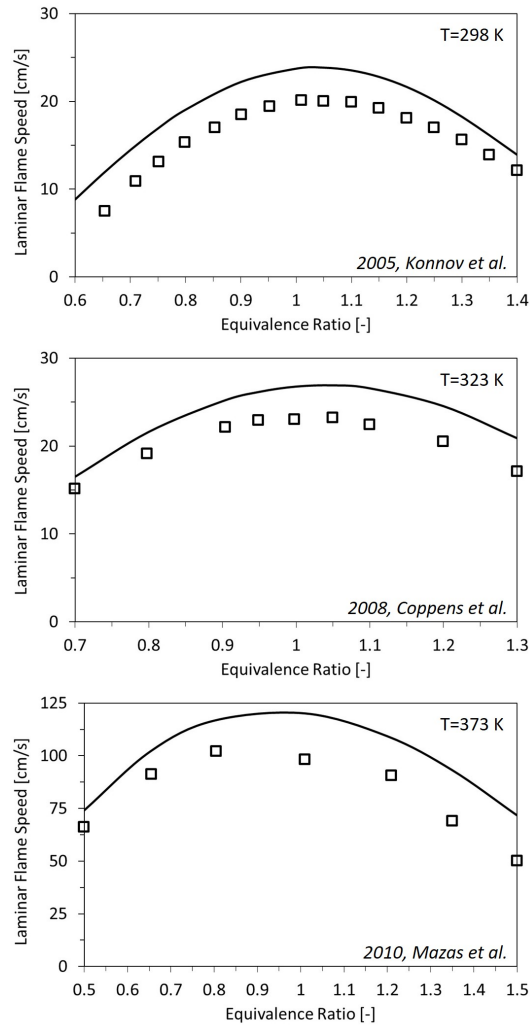
**Figure 3.5:** Propagation speed in $CH_4/O_2/CO_2$ flames as a function of equivalence ratio. In each diagram, squares represent the experimental data and lines indicate the results of the "POLIMI $C_1$-$C_3$ 1412" kinetic model simulations. The tests at 298 K and 323 K correspond to a mixture with a dilution ratio of 0.3155, while the last contains a carbon dioxide molar fraction of 40%.

The first comparison can be done between Coppens and Konnov experiments because they adopted the same dilution ratio. Laminar flame speed increases by increasing the inlet temperature. In fact, the higher temperature causes the increase of the flame temperature and, consequently, also of the speed of the back diffusion processes responsible of the front flame propagation towards the burner plate. This results in a greater velocity through which the reactants must be fed to prevent such phenomenon.

The test conducted at 373 K, presented by Mazas et al., shows a very high laminar flame speed if compared with the other cases. In fact, in addition to the increased inlet temperature of the mixture, the lower amount of $CO_2$ ensures a

higher burning velocity. This can be proven comparing the two mixtures as shown below:

- In case of dilution ratio of 0.3155 the amount of diluent contained can be computed as follows:

$$y_{CO_2} = \frac{1 - D}{1 + \frac{O_2}{2}\Phi} \qquad (3.2)$$

Such expression can be obtained assuming an amount of moles for the $CO_2/O_2$ mixture equal to one; as consequence, the oxygen in such equation is equal to the dilution ratio. Concerning the minimum and maximum equivalence ratio analysed, 0.6 and 1.4, the corresponding percentages of $CO_2$ are 62.5% and 56%, respectively.

- On the contrary, for the inlet temperature of 373 K, the molar fraction of carbon dioxide is always equal to 40%.

The coupled effect of high temperature and lower dilution justifies the high value of the laminar flame speed in the case from Mazas.

Despite a 10-30% overestimation, the "POLIMI C$_1$-C$_3$ 1412" kinetic model captures the effects of temperature, dilution ratio and equivalence ratio. In fact, it is able to replicate the qualitative behavior of the laminar flame speed with the temperature. At the same time, it is able to reproduce quite well the "parabolic" trend of such property with the $\Phi$.

Specifically, the POLIMI model overestimates consistently the data at temperature equal to 298 K. Good agreement is observed at lean conditions for the higher temperature cases. Greater deviations are observed for increasing the equivalence ratio. Concluding, these results suggest the need for a revision of the kinetic model.

**Effect of pressure over the laminar flame speed**

Xie et al., in 2013, investigated the effects of pressure on the laminar flame speed of several $CH_4/O_2/CO_2$ mixtures [63]. The inlet temperature was kept equal to 300 K at three different pressures: 1, 2 and 3 bar. In this case the dilution ratio ($Z$) is defined as a function of the amount of carbon dioxide inside the $O_2$-to-$CO_2$ mixture:

$$Z = \frac{CO_2}{O_2 + CO_2} \tag{3.3}$$

Comparing this quantity with the corresponding one seen Section (3.2.1), the following relation can be obtained:

$$Z = 1 - D \tag{3.4}$$

The operating conditions analysed in the experiments are summarized in Table 3.4.

| P (bar) | Z | Φ |
|---------|---|---|
| 1 | 0.4/0.5/0.6/0.7 | 0.4 to 1.6 |
| 2 | 0.4/0.5/0.6/0.7 | 0.4 to 1.6 |
| 3 | 0.5/0.6/0.7 | 0.6 to 1.6 |

**Table 3.4:** Operating conditions investigated for the $CH_4/O_2/CO_2$ mixtures.

All these mixtures are simulated through the "POLIMI $C_1$-$C_3$ 1412" kinetic model. The comparison with the experimental data is reported in Figure 3.6. Three graphs are presented, one for each pressure. The laminar flame speed is plotted as a function of equivalence ratio for different dilution ratios $Z$.

As shown, for the same dilution and equivalence ratio, the laminar flame speed decreases for increasing pressure. On the other hand, for a given pressure, the laminar flame speed decreases for increasing amount of $CO_2$. When $Z$ assumes values of 0.7, the laminar burning velocity becomes very small if compared with the case at $Z$ equal to 0.4 (around the 13% both for experimental and simulated results). Once again, it is evinced the inhibiting effect of the carbon dioxide over the reactivity of the flame.

The "POLIMI $C_1$-$C_3$ 1412" is able to predict the qualitative experimental trend. Once again, the model seems to fulfill better under lean conditions.

**Figure 3.6:** Experimental (symbols) and calculated (lines) laminar burning velocities of the $CH_4/O_2/CO_2$ mixtures as a function of equivalence ratio, at 1, 2 and 3 bar and for different carbon dioxide dilution ratios (Z). Solid lines correspond to the data computed through "POLIMI $C_1$-$C_3$ 1412".

## 3.3 "AramcoMech1.3" mechanism simulation

"AramcoMech1.3" represents the reference $C_0$-$C_4$ kinetic mechanism for combustion applications. It was developed starting from 2012 at the "Combustion Chemistry Centre" at the National University of Ireland in Galway (NUIG). Its optimization was based on theoretical and experimental determination of the rate constants, while the validation over a broad range of conditions.

The mechanism was systematically developed moving from the hydrogen oxidation [64] up to the $C_4$ hydrocarbon molecules [65–68], including also the oxygenated fuels [65,69]. For each reaction involved in the model, an accurate search of parameters within the literature was carried out identifying the most accurate

kinetic coefficients through experimental measurements, theoretical calculations or from a coupling of them. An optimization process carried out over a huge number of experimental data allowed to propose the best parameters for each elementary step. Figure 3.7 shows the schematic representation of the process followed during the development of "AramcoMech1.3".
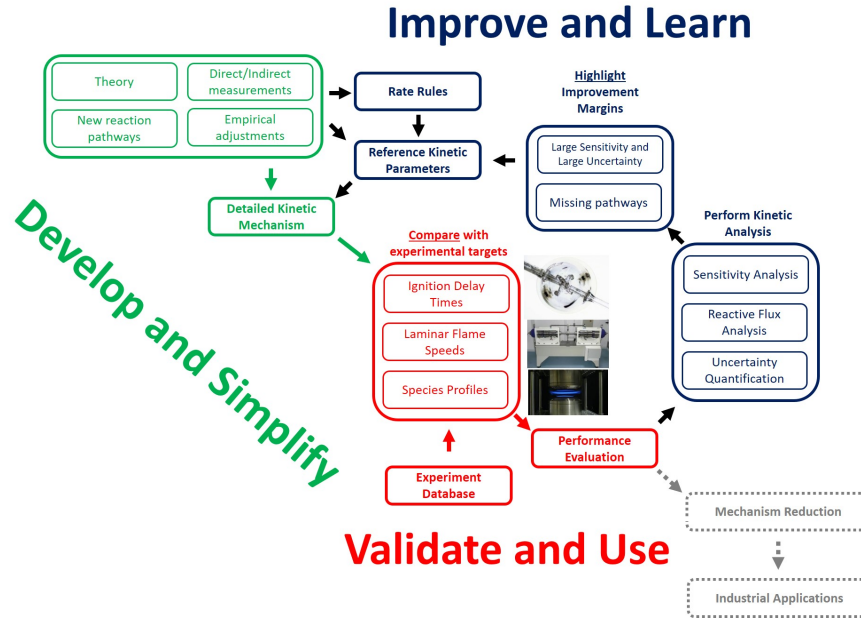


**Figure 3.7:** Schematic representation of the procedure for a kinetic mechanism development.

In addition, Olm et al. [70, 71] simulated several experimental data obtained for hydrogen and syngas mixtures through different kinetic mechanisms. By doing so, they showed that "AramcoMech1.3" is the model which works in the best way in all the reactors and conditions investigated, in comparison with all the other kinetic models available in literature.

The experimental data investigated in this Thesis have been found in rather recent literature works because they have been obtained in innovative conditions close to the MILD oxy-methane combustion. For this reason, they have not been included in the validation process of the "AramcoMech1.3" kinetic model. Therefore, this section presents a testing of the Aramco mechanism performed through the same datasets previously discussed for the "POLIMI $C_1$-$C_3$ 1412" kinetic model.

**Methane oxy-combustion in presence of CO₂ and/or H₂O**

The same $CH_4/O_2/H_2O$ and $CH_4/O_2/CO_2$ mixtures investigated by Mazas at al. have been simulated also with the "AramcoMech1.3". In Figure 3.8, the results obtained are shown in comparison with those recovered in Section (3.2.1) with "POLIMI $C_1$-$C_3$ 1412" model and with the experimental data.
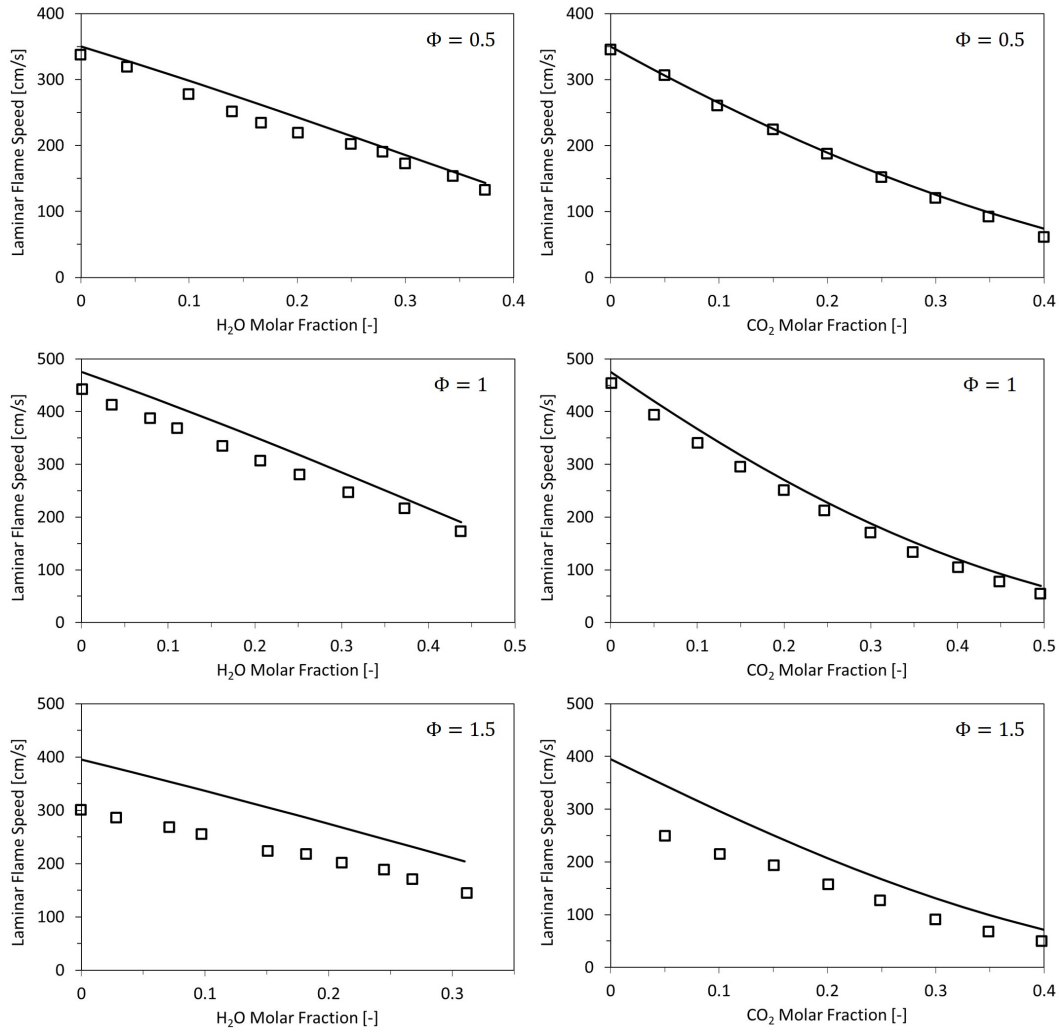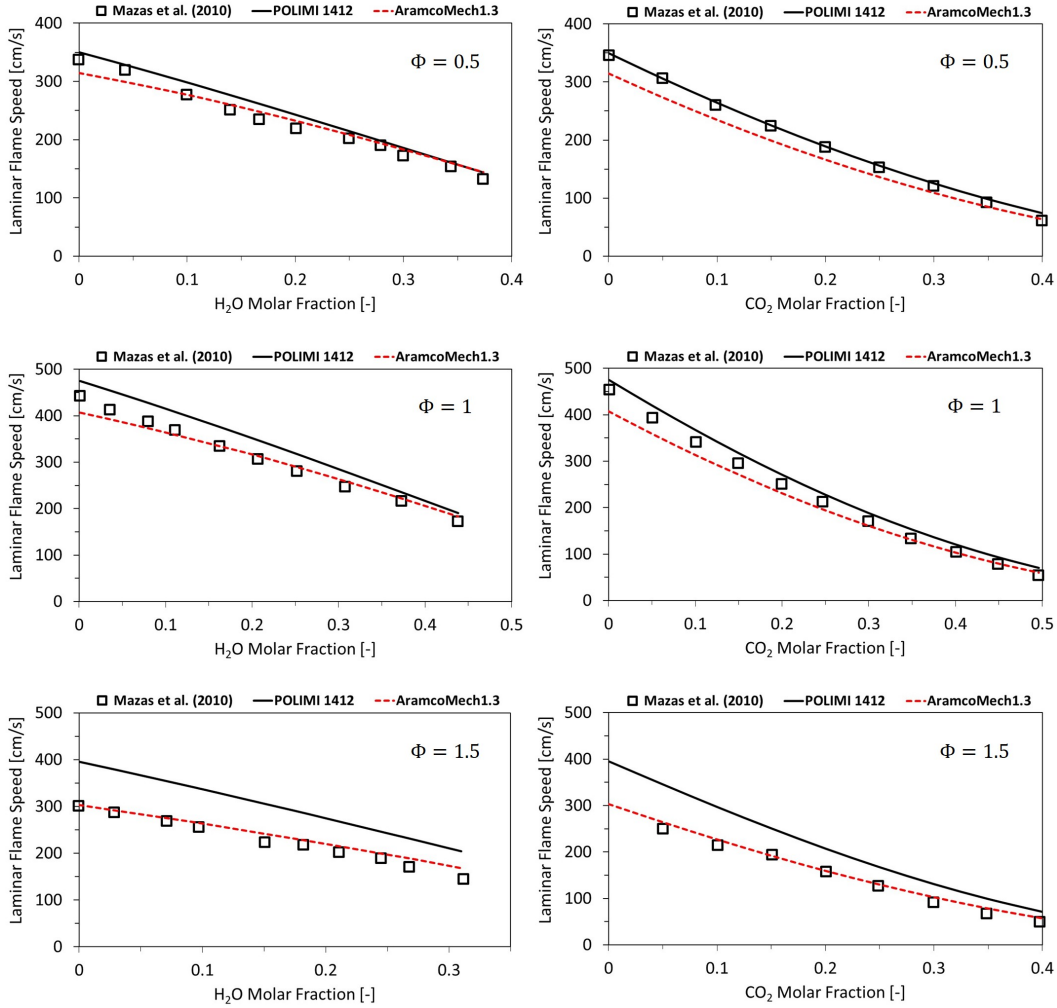


**Figure 3.8:** Experimental (symbols) and computed (lines) premixed laminar flame speeds of $CH_4/O_2/H_2O$ and $CH_4/O_2/CO_2$ mixtures as a function of molar fraction of the corresponding diluent ($H_2O$ or $CO_2$ respectively). For each mixture, three equivalence ratios are investigated: 0.5, 1 and 1.5. The inlet temperature is 373 K and the operating pressure is of 1 atm. The red dashed lines represent the "AramcoMech1.3" kinetic model and the black solid ones the "POLIMI $C_1$-$C_3$ 1412" mechanism.

As shown, this second mechanism is able to predict rather well the experimental data in lean, stoichiometric and rich conditions. The positive aspect is represented by the very good fitting of the real laminar flame speeds at a higher than one equivalence ratio, where the "POLIMI $C_1$-$C_3$ 1412" is bad.

In Figure 3.9, the laminar flame speed has been investigated for $CH_4/O_2/H_2O/CO_2$ mixtures. As in the previous section, the same two dilution ratios have been considered: 0.52 and 0.72.

$$\frac{O_2}{O_2 + CO_2} = 0.52 \qquad\qquad \frac{O_2}{O_2 + CO_2} = 0.72$$
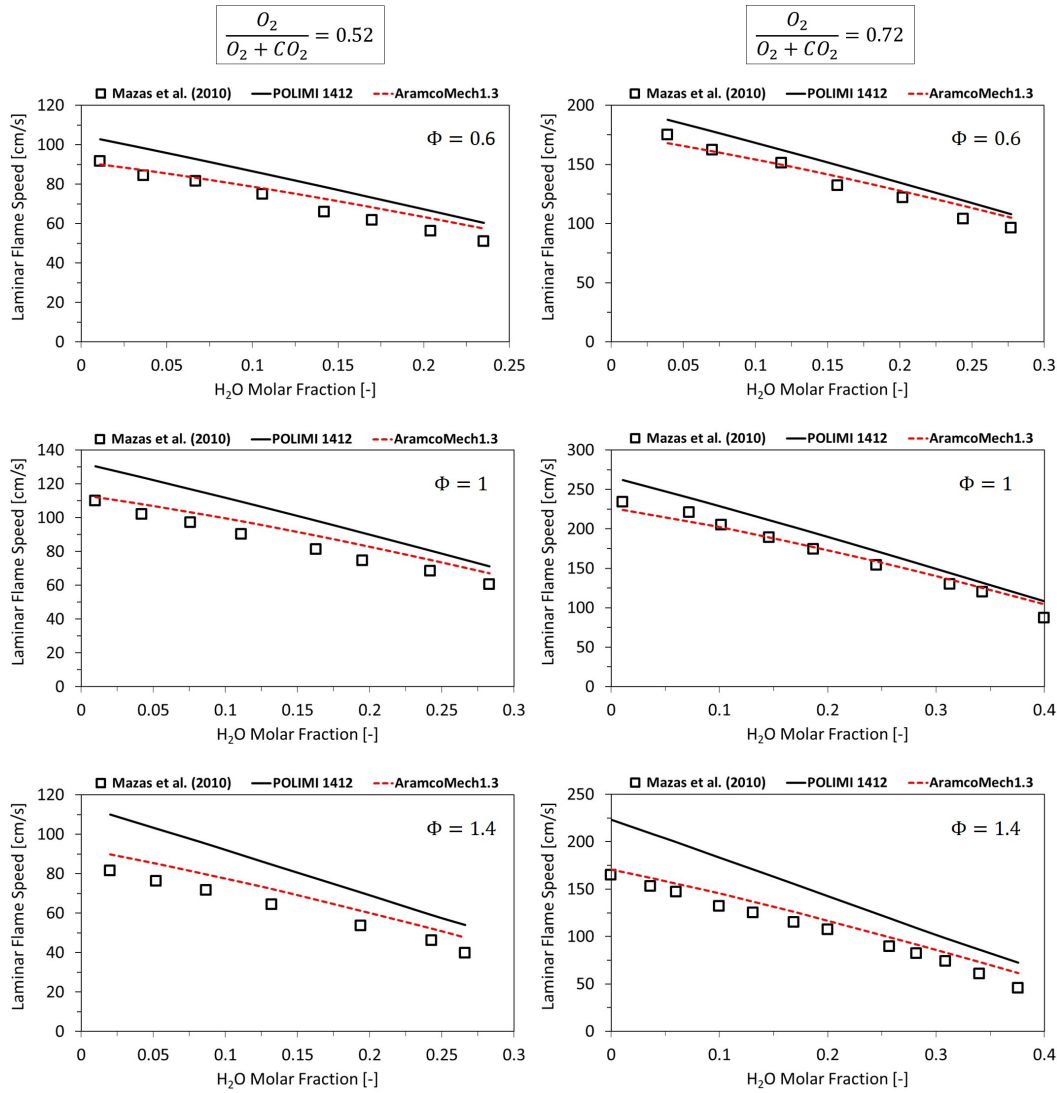


**Figure 3.9:** Experimental (symbols) and computed (lines) laminar flame speeds of $CH_4/O_2/CO_2/H_2O$ mixtures as a function of water molar fraction. Two $O_2$-to-$CO_2$ diluent ratios have been considered: 0.52 and 0.72. For each one, three equivalence ratios have been investigated: 0.6, 1 and 1.4. The red dashed lines represent the "AramcoMech1.3" kinetic model and the black solid ones the "POLIMI $C_1$-$C_3$ 1412" mechanism.

The same analysis performed for Figure 3.8 can be done also for Figure 3.9. In fact, the "AramcoMech1.3" model is better than "POLIMI $C_1$-$C_3$ 1412" in all the three conditions investigated, i.e. for equivalence ratios of 0.6, 1 and 1.4. Only for the fuel-enriched mixture and dilution ratio $D$ equal to 52%, thus for high dilution levels, there is a small error with respect to the experimental data. Therefore, the Aramco mechanism is better than POLIMI in predicting the effects

over the premixed laminar flame speed in several dilution conditions through water and carbon dioxide. Consequently, on this base a kinetic comparison of the two schemes must be performed in order to modify the "POLIMI $C_1$-$C_3$ 1412" and make it suitable to reproduce such behavior.

**Methane oxy-combustion in presence of $CO_2$ at different unburned gas temperatures**

Comparisons of "AramcoMech1.3" with experimental data of Konnov, Coppens and Mazas are reported in Figure 3.10.
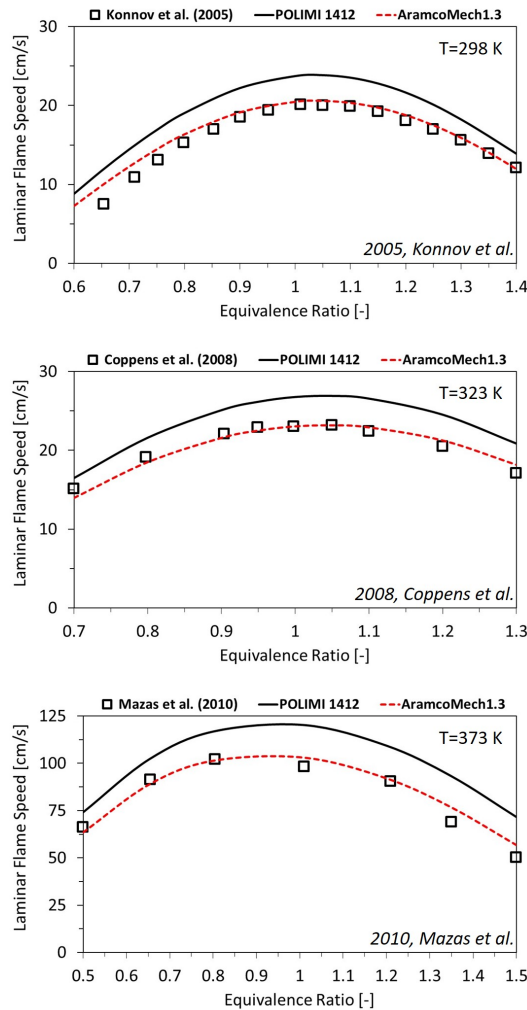


**Figure 3.10:** Propagation speed in $CH_4/O_2/CO_2$ flames as a function of equivalence ratio. In each graph, squares represent the experimental data, the black solid lines indicate the results obtained through the simulation of the "POLIMI 1412" kinetic scheme and the red dashed lines represent the "AramcoMech1.3" model.

The Aramco mechanism is able to better fit the experimental data for the whole equivalence ratio range at any temperatures. Therefore, it can be considered as a reliable starting point for explain combustion features at MILD oxy-methane

conditions.

**Effect of pressure over the laminar flame speed**

Finally, the last testing of the "AramcoMech1.3" has been performed for the evaluation of the premixed laminar flame speeds at different pressures. Therefore, the same conditions investigated by Xie et al., presented in Section (3.2.1), have been simulated with such mechanism. In Figure 3.11, the computed results are shown in comparison with those obtained with "POLIMI $C_1$-$C_3$ 1412", always in relation to the experimental data.
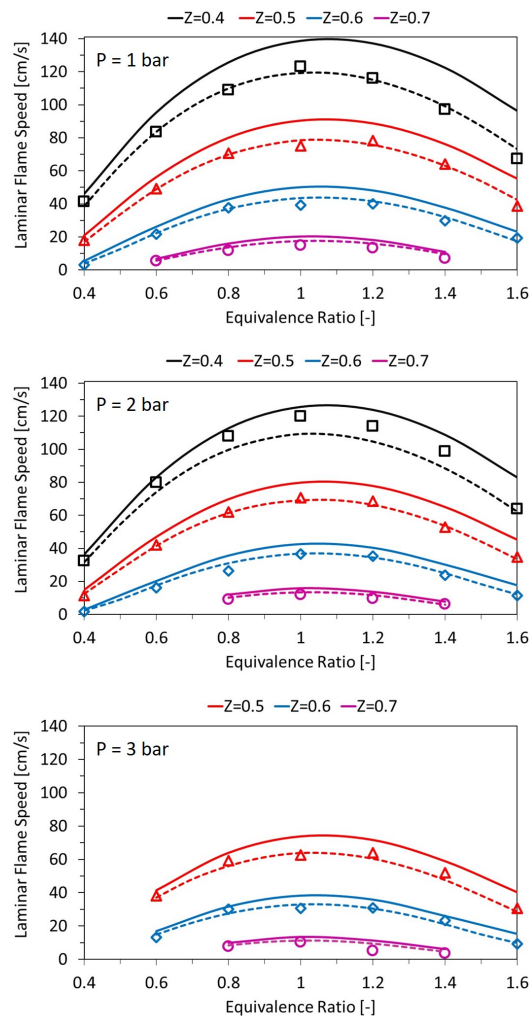


**Figure 3.11:** Experimental (symbols) and calculated (lines) laminar burning velocities of the $CH_4/O_2/CO_2$ mixtures at 1, 2 and 3 bar and different carbon dioxide dilution ratios (Z). Solid lines represent data computed through "POLIMI $C_1$-$C_3$ 1412", while dashed lines depict the results of the "AramcoMech1.3" kinetic model.

Also in this case, the "AramcoMech1.3" is better than "POLIMI $C_1$-$C_3$ 1412" in predicting the laminar flame speeds at different pressures and at several dilution

ratios. Same deviation is observed for the case at pressure equal to 2 bar and Z equal to 0.4. The kinetic reasons behind different behaviors of "AramcoMech1.3" and "POLIMI C$_1$-C$_3$ 1412" mechanisms at the investigated conditions are discussed in the next section.

## 3.4 "POLIMI C$_1$-C$_3$ 1412" and "AramcoMech1.3" kinetic comparison

In the previous sections, several experimental data for the methane oxy-combustion in presence of high dilution levels of CO$_2$ and/or H$_2$O have been compared with "POLIMI C$_1$-C$_3$ 1412" and "AramcoMech1.3" kinetic mechanisms. In particular, laminar flame speed cases have been analysed mainly in light of the relevance of such property in the real combustion systems [46]. Overall, "AramcoMech1.3" showed a better agreement with experimental data than POLIMI and this section provides kinetic insights of the differences between these two kinetic models.

**Methyl-methyl radicals recombination**

First of all, in order to perform a reliable, efficient and suitable sensitivity analysis, the relevant operating conditions must be accurately chosen. The previous sections highlighted that the major deviations of "POLIMI C$_1$-C$_3$ 1412" kinetic mechanism from experimental data are at stoichiometric and rich conditions. Therefore, among all the cases investigated, those obtained for equivalence ratios higher and equal to 1 are taken into account. Moreover, both the high and the low dilution levels have been considered in order to perform a complete analysis.

Comparative sensitivity analysis of "AramcoMech1.3" and "POLIMI C$_1$-C$_3$ 1412" mechanisms are presented in the following. The output variable is the mass flow rate which is directly related to the laminar flame speed ($s_L$) through the mass density $\hat{\rho}$ and the cross section area $A$:

$$s_L = \frac{\dot{m}}{\hat{\rho} \cdot A} \tag{3.5}$$

Several sensitivity analysis have been performed for both the mechanisms, investigating different water and carbon dioxide molar concentrations along with several operating pressures and temperatures. Below, only two representative analysis have been reported with the purpose of highlight the main differences between the two kinetic models tested.

The first analysis has been conducted for the CH$_4$/O$_2$/CO$_2$/H$_2$O mixtures investigated by Mazas et al. at an inlet temperature of 373 K and at atmospheric pressure. As seen in the previous sections, only the composition and the nature of

the diluent adopted changes. In Figure 3.12, the sensitivity analysis performed at a water molar fraction of 0.04, equivalence ratio of 1.4 and oxygen dilution ratio $D$ equal to 0.72 is reported.

**POLIMI C$_1$-C$_3$ 1412**

| Reaction | Value |
|---|---|
| $O_2 + H = O + OH$ | 0.510 |
| $CH_3 + CH_3 = H + C_2H_5$ | 0.095 |
| $H + CH_3 (+M) = CH_4 (+M)$ | - 0.075 |
| $HCO + M = CO + H + M$ | 0.074 |
| $OH + CH_3 = H_2 + CH_2O$ | - 0.060 |
| $CH_4 + H = H_2 + CH_3$ | - 0.058 |

**AramcoMech1.3**

| Reaction | Value |
|---|---|
| $O_2 + H = O + OH$ | 0.561 |
| $HCO + M = CO + H + M$ | 0.099 |
| $OH + CH_3 = H + CH_2OH$ | 0.098 |
| $H + CH_3 (+M) = CH_4 (+M)$ | - 0.084 |
| $CH_4 + H = H_2 + CH_3$ | - 0.049 |
| $HCO + OH = H_2O + CO$ | - 0.040 |
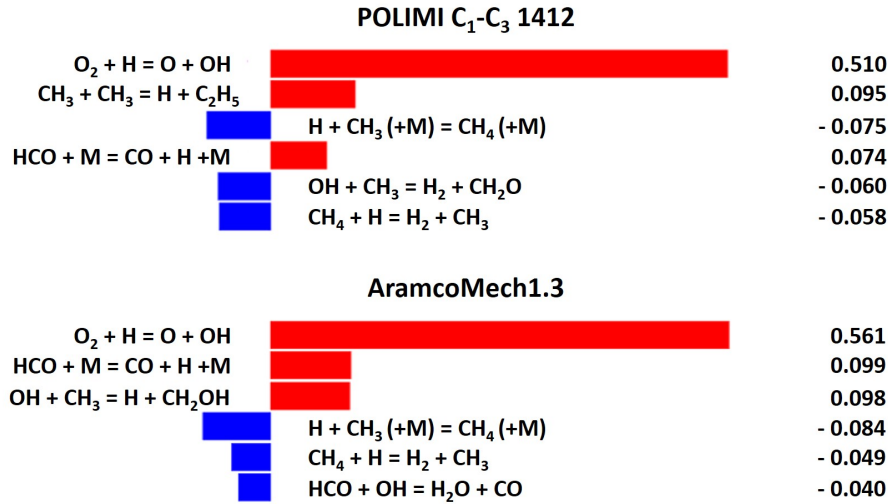
**Figure 3.12:** Comparison of the sensitivity analysis conduced at a water molar fraction of 0.04 for "POLIMI C$_1$-C$_3$ 1412" and "AramcoMech1.3" kinetic models.

Such figure is representative of all the sensitivity analysis conducted for the different cases investigated by Mazas et al. Only the first reactions are reported since they are the most important in influencing the laminar flame speed. From a comparison of the results, the main difference observed is the presence of the methyl-methyl radicals recombination/disproportionation for the "POLIMI C$_1$-C$_3$ 1412" kinetic model:

$$CH_3 + CH_3 \leftrightarrow H + C_2H_5 \tag{3.6}$$
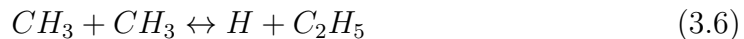
Such reaction converts two rather stable radicals (CH$_3$) into a hydrogen (H) and an ethyl radical (C$_2$H$_5$). The latter is a rather unstable species which rapidly decomposes to give a molecule of ethylene and and a new H radical. This can be proven by observing the Rate Of Production (ROP) analysis reported in Figure 3.13. The same output file is generated performing such analysis both with the "AramcoMech1.3" and "POLIMI C$_1$-C$_3$ 1412" kinetic schemes. Here, the ethyl radical decomposition is the fastest reaction involving such species.

| Reaction | Value |
|---|---|
| $H + C_2H_4 (+M) = C_2H_5 (+M)$ | - 0.059 |
| $H + C_2H_6 = H_2 + C_2H_5$ | 0.030 |
| $CH_3 + CH_3 = H + C_2H_5$ | 0.014 |
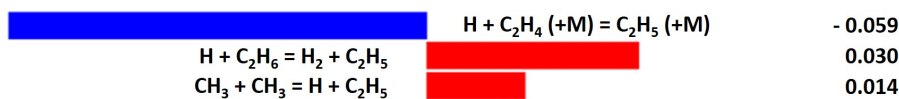
**Figure 3.13:** ROP analysis for the ethyl radical.

Therefore, from a methyl-methyl recombination, a C$_2$H$_4$ molecule is obtained along with two H radicals. The latter is the most reactive species observable during a combustion reaction. As soon as it is produced, it immediately reacts through several pathways. Among them, the most relevant one is the branching reaction. The H atom converts an oxygen molecule into an hydroxyl and an oxygen triplet radical as described by the following expression:

$$H + O_2 \leftrightarrow OH + O \tag{3.7}$$
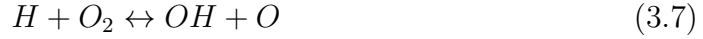
The triplet ground state electronic configuration of $\ddot{O}$ explains its large instability. The triplet configuration shows two unpaired electrons at the valence orbitals, making O equivalent to a bi-radical. Therefore, through the branching reaction, the system reactivity is increased because three active radicals are obtained from one. This is also demonstrated by all the sensitivity analysis studied; in fact, in each one the branching reaction is placed at the first position with the highest and positive sensitivity coefficient. Therefore, its impact over the laminar flame speed is extremely important. As consequence, if such reaction was disadvantaged, the mixture burning velocity would be highly decreased. This is due to the lower amount of radicals developed by this process which would decrease the back diffusion of the front of the flame.

Therefore, the methyl-methyl recombination appears as one of the most important reactions in influencing the laminar flame speed for the "POLIMI C$_1$-C$_3$ 1412" kinetic mechanism. In addition, since its sensitivity coefficient is positive, it represents, thus, the main cause of the overestimation of the laminar flame speed than both experimental data and "AramcoMech1.3" results.

For the sensitivity analysis obtained through the Aramco model, Reaction (3.6) does not appear in the first 20 reactions. Therefore, its kinetic constant is such that it does not influence in an effective way the laminar flame speed. At place of the analysed reaction, there is the following:

$$OH + CH_3 \leftrightarrow H + CH_2OH \tag{3.8}$$

This appears with a positive sensitivity coefficient, hence it has a positive impact over the burning velocity due to the presence of the H radical among the products. But unlike the CH$_3$-CH$_3$ recombination, the second radical produced, CH$_2$OH, does not impact the reactivity as the C$_2$H$_5$ decomposition. Looking at the corresponding ROP analysis reported in Figure 3.14, CH$_2$OH decomposes to form formaldehyde (CH$_2$O) and HO$_2$ ($\sim 65\%$).

| | | |
|---|---|---|
| OH + CH$_3$ = H + CH$_2$OH | | 0.153 |
| | O$_2$ + CH$_2$OH = HO$_2$ + CH$_2$O | - 0.100 |
| | H + CH$_2$O (+M) = CH$_2$OH (+M) | - 0.049 |
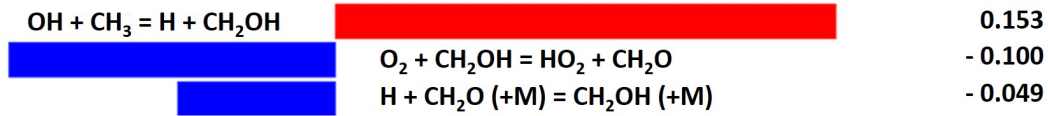
**Figure 3.14:** Rate Of Production Analysis for the CH$_2$OH radical.

The competing decomposition channel through third-body reaction would increase the laminar flame speed through the production of a H radical. These competitions explain the lower impact of Reaction (3.8) on the laminar flame speed compared to (3.6).

The second sensitivity analysis reported has been performed for a CH$_4$/O$_2$/CO$_2$ mixture tested by Xie et al., with an equivalence ratio of 1.4 and a carbon dioxide dilution ratio of 60%. The inlet temperature is 300 K and the operating pressure is 3 atm. The most sensitive reactions are reported in Figure 3.15 for both "POLIMI C$_1$-C$_3$ 1412" and "AramcoMech1.3".

**POLIMI C$_1$-C$_3$ 1412**

| | | |
|---|---|---|
| O$_2$ + H = O + OH | | 0.502 |
| OH + CH$_3$ = H$_2$O + CH$_2$S | | 0.075 |
| HCO + M = CO + H +M | | 0.069 |
| | H + CH$_3$ (+M) = CH$_4$ (+M) | - 0.066 |
| | H + OH + M = H$_2$O + M | - 0.059 |
| | OH + CH$_3$ = H$_2$ + CH$_2$O | - 0.052 |
| | O$_2$ + H (+M) = HO$_2$ (+M) | - 0.052 |
| CH$_3$ + CH$_3$ = H + C$_2$H$_5$ | | 0.050 |

**AramcoMech1.3**

| | | |
|---|---|---|
| O$_2$ + H = O + OH | | 0.802 |
| | H + CH$_3$ (+M) = CH$_4$ (+M) | - 0.193 |
| OH + CH$_3$ = H + CH$_2$OH | | 0.165 |
| | H + OH + M = H$_2$O + M | - 0.079 |
| HCO + M = CO + H +M | | 0.065 |
| | CH$_4$ + H = H$_2$ + CH$_3$ | - 0.061 |
| | CH$_4$ + OH = H$_2$O+ CH$_3$ | - 0.061 |
| HO$_2$ + CH$_3$ = OH + CH$_3$O | | 0.049 |
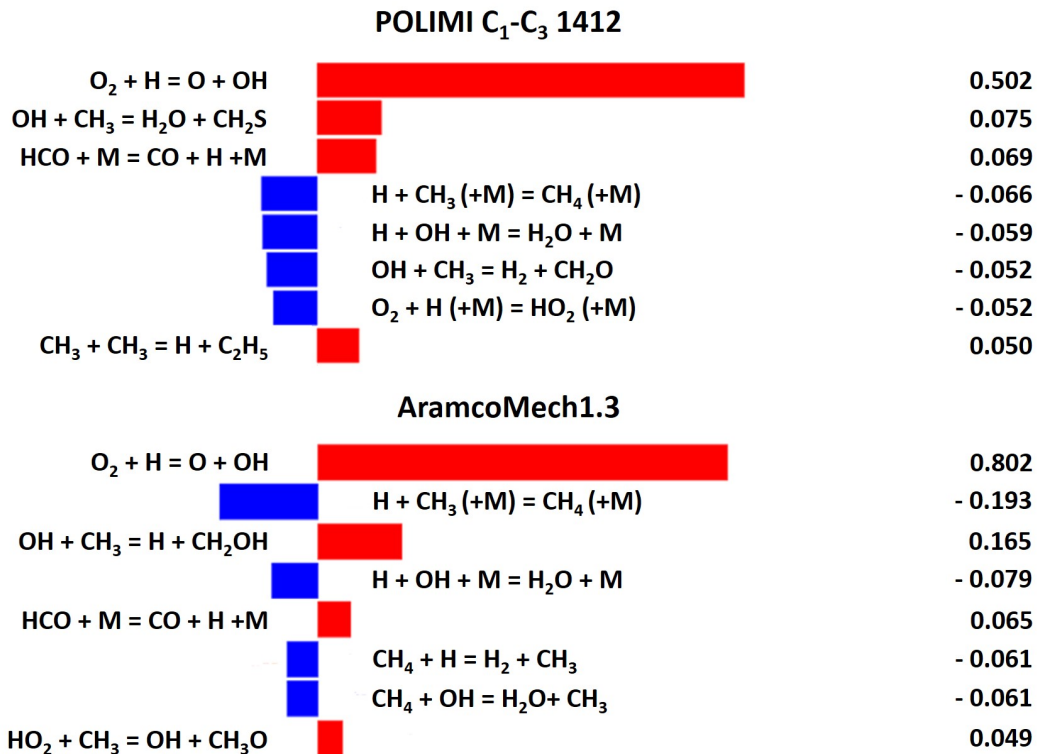
**Figure 3.15:** Sensitivity analysis conduced for the laminar flame speed using the "POLIMI C$_1$-C$_3$ 1412" and the "AramcoMech1.3" kinetic models. The operating conditions investigated are characterized by an inlet temperature of 300 K and a pressure of 1 atm.

Also in this case, the methyl-methyl recombination appears only for the "POLIMI C$_1$-C$_3$ 1412" kinetic mechanism even if with a lower ranking than in the Mazas

conditions. Among the reactions limiting the laminar flame speed predicted by the "AramcoMech1.3" there are the H-abstractions from methane, consuming two reactive radicals to yield $CH_3$:

$$CH_4 + H \leftrightarrow CH_3 + H_2 \qquad (3.9)$$

$$CH_4 + OH \leftrightarrow CH_3 + H_2O \qquad (3.10)$$
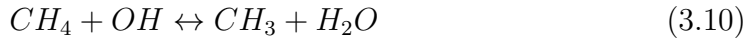
Figure 3.16 shows the comparison of the kinetic constants of these two processes for the investigated mechanisms; negligible differences are observable for both the forward and backward paths.
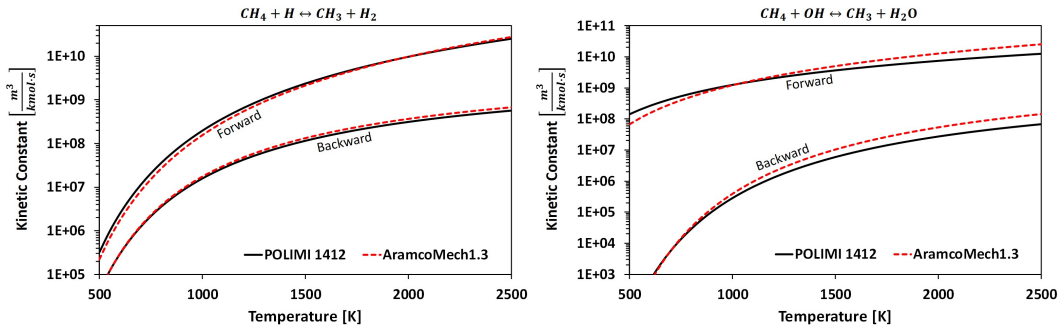


**Figure 3.16:** Forward and backward kinetic constants as a function of temperature for $CH_4 + H \leftrightarrow CH_3 + H_2$ (left) and $CH_4 + OH \leftrightarrow CH_3 + H_2O$ (right) reactions computed using the parameters contained in "POLIMI C$_1$-C$_3$ 1412" (solid black lines) and "AramcoMech1.3" (dashed red lines) models.

This means that this path is somehow overwhelmed by alternative pathways in "POLIMI C$_1$-C$_3$ 1412". As shown in Figure 3.15, in the same positions of the two methane decomposition for "AramcoMech1.3", the recombination reaction between an hydroxyl and a methyl radical is present:

$$OH + CH_3 \leftrightarrow H_2 + CH_2O \qquad (3.11)$$
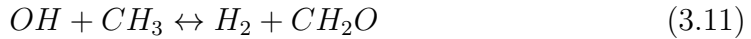
In addition, also the third-body propagation reaction between the hydrogen radical and an oxygen molecule producing an HO$_2$ radical can be observed:

$$H + O_2(+M) \leftrightarrow HO_2(+M) \qquad (3.12)$$
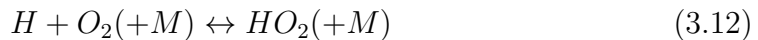
Figure 3.17 shows the comparison of the kinetic constants of these four paths computed using parameters taken from "POLIMI C$_1$-C$_3$ 1412" for (3.12) and (3.11) and from "AramcoMech1.3" for (3.9) and (3.10).
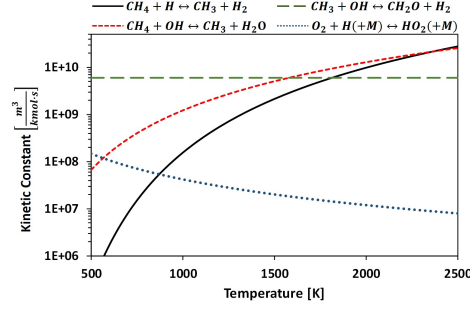
**Figure 3.17:** Kinetic constants as a function of temperature.

For high temperatures, above 2000 K, the reactions belonging to the sensitivity analysis of Aramco mechanism acquire higher importance than those of the POLIMI, in terms of kinetic constants. From the comparison of the two reactions which contain the OH radical among reactants, the reaction rate of (3.10) is higher than the (3.11), due to the greater kinetic constant and the higher molar concentration of the $CH_4$ than methyl radicals:

$$k_{CH_4+OH} > k_{CH_3+OH} \qquad C_{CH_4} > C_{CH_3} \qquad (3.13)$$

Therefore, extending to the reaction rates:

$$r_{CH_4+OH} = k_{CH_4+OH} \cdot C_{CH_4} \cdot C_{OH} > k_{CH_3+OH} \cdot C_{CH_3} \cdot C_{OH} = r_{CH_3+OH} \quad (3.14)$$

A similar analysis can be performed for Reaction (3.9) and (3.12). With respect to the previous case, the molar concentration of oxygen is typically higher than methane of a factor between 2-4; however, Figure (3.17) shows that the kinetic constant of the third-body reaction is 2-3 order of magnitude lower than the (3.9):

$$k_{CH_4+H} >> k_{O_2+H(+M)} \qquad C_{CH_4} \leq C_{O_2} \qquad (3.15)$$

Therefore, in terms of reaction rates results:

$$r_{CH_4+H} = k_{CH_4+H} \cdot C_{CH_4} \cdot C_H > k_{O_2+H(+M)} \cdot C_{O_2} \cdot C_H = r_{O_2+H(+M)} \quad (3.16)$$

As conclusion, the two reactions observed in the sensitivity analysis obtained with the "AramcoMech1.3" show higher reaction rates than those of the "POLIMI $C_1$-$C_3$ 1412". This contributes to keep the laminar flame speed predicted by the first model smaller, allowing to the Aramco mechanism to well predict the experimental data.

## 3.5 From "POLIMI C$_1$-C$_3$ 1412" to "POLIMI 1612"

As clearly described by the sensitivity analysis shown in the previous section, the main difference between the two kinetic mechanisms investigated is Reaction (3.6) playing a major role in "POLIMI C$_1$-C$_3$ 1412" model. This pathway has been identified as the main reason of the laminar flame speed overestimation with respect to the experimental data. Therefore, a review of literature information concerning this reaction has been carried out to verify the reliability of the adopted parameters. The first paper found investigates the different pathways allowable for two methyl radicals recombination over the temperature range 1200-2400 K. In this work, Davidson et al. [72] showed that the main reaction at typical flame temperatures is the recombination (3.6) analysed in the previous section immediately followed by the consecutive step based on the ethyl radical decomposition:

$$CH_3 + CH_3 \leftrightarrow H + C_2H_5 \tag{3.17}$$

$$C_2H_5(+M) \leftrightarrow H + C_2H_4(+M) \tag{3.18}$$
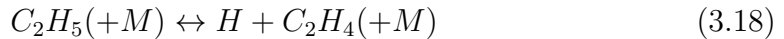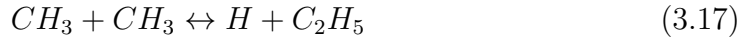
Therefore, this paper confirms that the pathway predicted by the POLIMI kinetic scheme for the CH$_3$-CH$_3$ reaction is correct. Thus, the difference with respect to the "AramcoMech1.3" must be found in the kinetic constant adopted for such reaction. Therefore, since in this last kinetic mechanism there are the literature references for each kinetic reaction, that correspondent to the reaction of interest has been taken. The relative paper, published by Stewart et al. [73], shows the derivation of the kinetic constant for the methyl-methyl recombination reaction. In Table 3.5, the Arrhenius parameters for the reaction of concern contained in the "POLIMI C$_1$-C$_3$ 1412" kinetic scheme and in the analysed literature work are reported.

| Source | $A \left[ \frac{m^3}{kmol \cdot s} \right]$ | $\alpha$ | $E_{act} \left[ \frac{cal}{mol} \right]$ |
|---|---|---|---|
| "POLIMI C$_1$-C$_3$ 1412" | $1.4 \cdot 10^{11}$ | 0.0 | 14000 |
| Stewart et al. | $3.1 \cdot 10^{11}$ | $-0.362$ | 13372.5 |

**Table 3.5:** Arrhenius parameters for the mehtyl-methyl recombination reaction at atmospheric pressure contained in the "POLIMI C$_1$-C$_3$ 1412" kinetic model and in Stewart's paper [73].

In order to better understand the differences between the two kinetic rate constants, they have been plotted as a function of temperature. In Figure 3.18, the corresponding diagram is depicted.
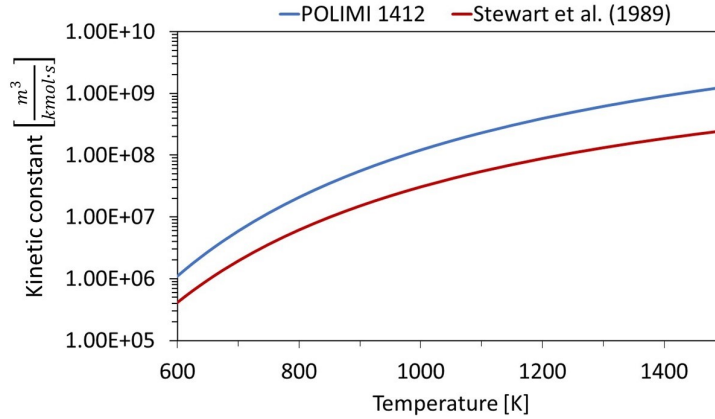
**Figure 3.18:** Kinetic constant for the methyl-methyl recombination as a function of temperature using the parameters provided by "POLIMI $C_1$-$C_3$ 1412" (blue line) and Stewart et al. [73] (red line).

As shown, the rate constant adopted in the "POLIMI $C_1$-$C_3$ 1412" kinetic mechanism is about 3-5 times higher than the values suggested by Stewart et al. This observation confirms the hypothesis according to which the methyl-methyl recombination reaction is the cause of the laminar flame speed overestimation.

In order to adjust the original kinetic mechanism, the Arrhenius parameters for the methyl-methyl recombination have been updated implementing those provided by Stewart et al., together with the pressure logarithmic expression reported in Table 3.6.

| $CH_3 + CH_3 \leftrightarrow H + C_2H_5$ | $A \left[\frac{cm^3}{mol \cdot s}\right]$ | $\alpha$ | $E_{act} \left[\frac{cal}{mol}\right]$ |
|---|---|---|---|
| 0.01 atm | $4.74 \cdot 10^{12}$ | 0.105 | 10664.3 |
| 0.1 atm | $2.57 \cdot 10^{13}$ | $-0.096$ | 11406.1 |
| 1 atm | $3.1 \cdot 10^{14}$ | $-0.362$ | 13372.5 |
| 10 atm | $2.15 \cdot 10^{10}$ | 0.885 | 13532.5 |
| 100 atm | $1.032 \cdot 10^2$ | 3.23 | 11236.1 |

**Table 3.6:** Arrhenius parameters for the methyl-methyl recombination. PLOG approach is used to exploit the pressure dependence of the kinetic constant.

The second important modification to the starting "POLIMI $C_1$-$C_3$ 1412" kinetic mechanism deals with the thermodynamic and the transport properties. In fact, the innovative highly diluted operating conditions investigated in this thesis enhance the importance of water and carbon dioxide. An example is represented by the laminar flame speed analysed in the previous sections: by adding few percentages of such diluents a strong impact can be observed. Therefore, all the thermodynamic and transport properties of the POLIMI mechanism have been compared with the values reported in the Burcat's database [74]. Due to a very de-

tailed coupling of experimental and theoretical determinations of thermodynamic properties, Burcat's database has been and still is a reference for kinetic models. More recent developments of the same approach are available in the ATCT database at Argonne National Laboratory.

The modified kinetic model thus obtained will be referred to as "POLIMI 1612", from here on.

## 3.6 From "POLIMI 1612" to "POLIMI 1702"

Before moving to the complete validation of the new mechanism, a first test of "POLIMI 1612" was done in order to understand the impact of the modifications introduced on the capability of reproducing the experimental flame speeds already analysed in the previous sections.

As an example, only the effect of modification on the $CH_4/O_2/H_2O/CO_2$ data by Mazas et al., at atmospheric pressure and inlet temperature of 373 K have been simulated. This dataset has been chosen to the intermediate operating conditions within the whole validation range. Figure 3.19 shows three different equivalence ratio conditions ($\Phi = 0.6 - 1 - 1.4$) with two different dilution ratios ($D = 0.52 - 0.72$).

Despite the modifications and the improvements in the performance of the "POLIMI 1612" compared to the "POLIMI $C_1$-$C_3$ 1412", deviations are still observed. The $C_0$-$C_4$ mechanism from NUIG [69] still shows the best performances. For this reason the "AramcoMech1.3" was adopted and implemented as the new core mechanism within the POLIMI kinetic framework.

Due to the complexity and intrinsic hierarchy of the extensive kinetic mechanism such as "POLIMI $C_1$-$C_3$ 1412", the implementation of a new core mechanism requires a careful, modular and methodical procedure. A thorough re-validation was performed for different types of fuels, and pollutants subsets, under different conditions and reactors. Further improvements are still being introduced within the activity of the CRECK Modeling group regarding especially higher than $C_3$ hydrocarbon molecules.

These additional improvement strongly rely on the adoption of more updated, and formally more accurate, theoretical and experimental parameters, extensively used to derive rate rules and lumped rate constants.

A recently reviewed by Klippenstein [75], advances in theoretical kinetics and computational capabilities allow to determine kinetic based theoretical parameters with a high degree of accuracy. An effective use of such information in standard kinetic model development procedures constitute one of the present challenges of

combustion.
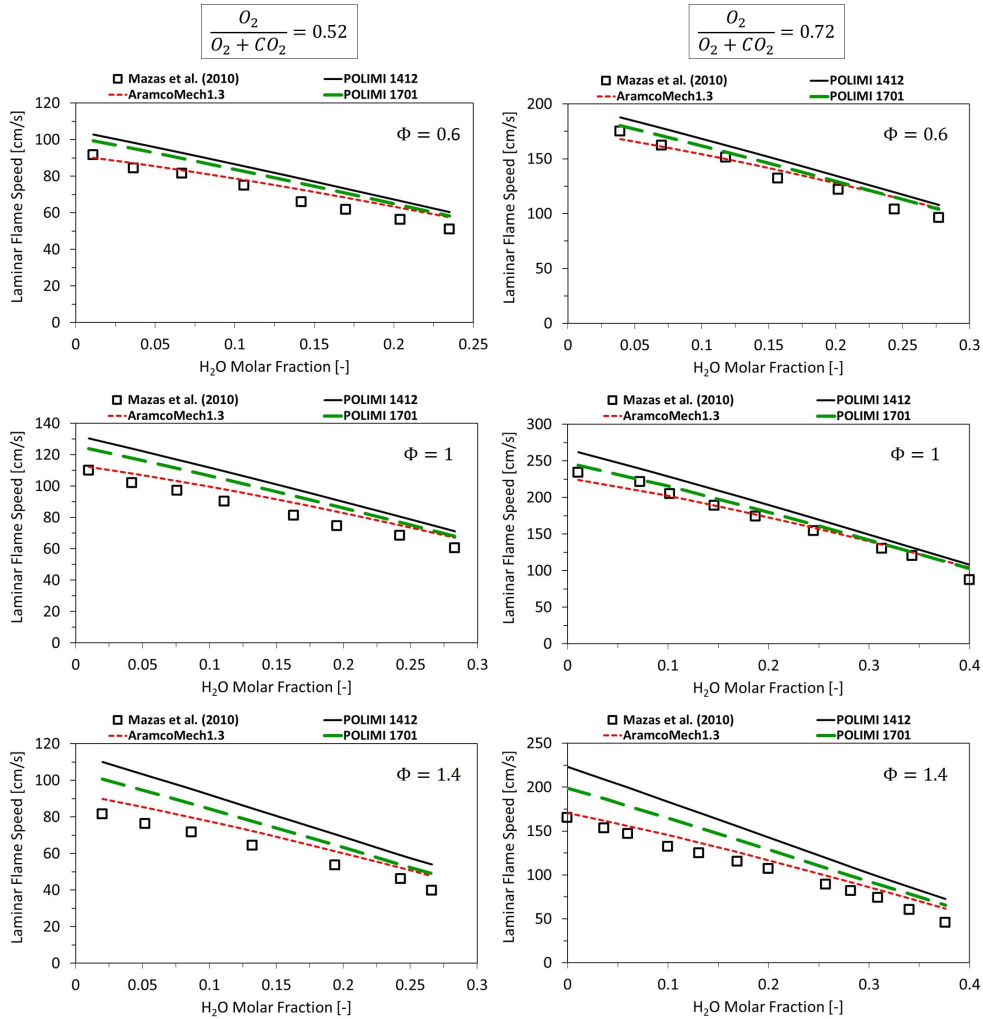


**Figure 3.19:** Experimental (symbols) and computed (lines) laminar flame speeds for the $CH_4/O_2/H_2O/CO_2$ mixtures as a function of water molar fraction is reported. The 52% and 72% dilution ratios have been tested. For each one 0.6, 1 and 1.4 equivalence ratios have been considered. The black solid lines represent the results obtained from the "POLIMI $C_1$-$C_3$ 1412" kinetic mechanism, the red small dashed the "AramcoMech1.3" and, finally, the green large dashed lines the "POLIMI 1701" scheme.

In the next section, the validation of the obtained "POLIMI 1702" kinetic mechanism is carried out considering that the experimental data investigated in this Thesis are rather recent and not tested during the "AramcoMech1.3" development.

## 3.7 "POLIMI 1702" validation

The "POLIMI 1702" model predictions are here compared with the same experimental targets already discussed in section (3.2.1).

### 3.7.1 Premixed laminar flame speed

The first step of the validation process is the simulation of the experimental data regarding the laminar flame speed. In all the proposed figures, the simulated with "POLIMI 1702" and "POLIMI $C_1$-$C_3$ 1412" results are compared with the experimental data.

**Methane oxy-combustion in presence of $CO_2$ and/or $H_2O$**

Figure 3.20 and 3.21 highlight the improved performances of the new kinetic model in predicting the conditions investigated by Mazas et. al. The laminar flame speed for equivalence ratios equal and higher than one is no longer overestimated. Therefore, the problems observed for "POLIMI $C_1$-$C_3$ 1412" mechanism have been fixed.
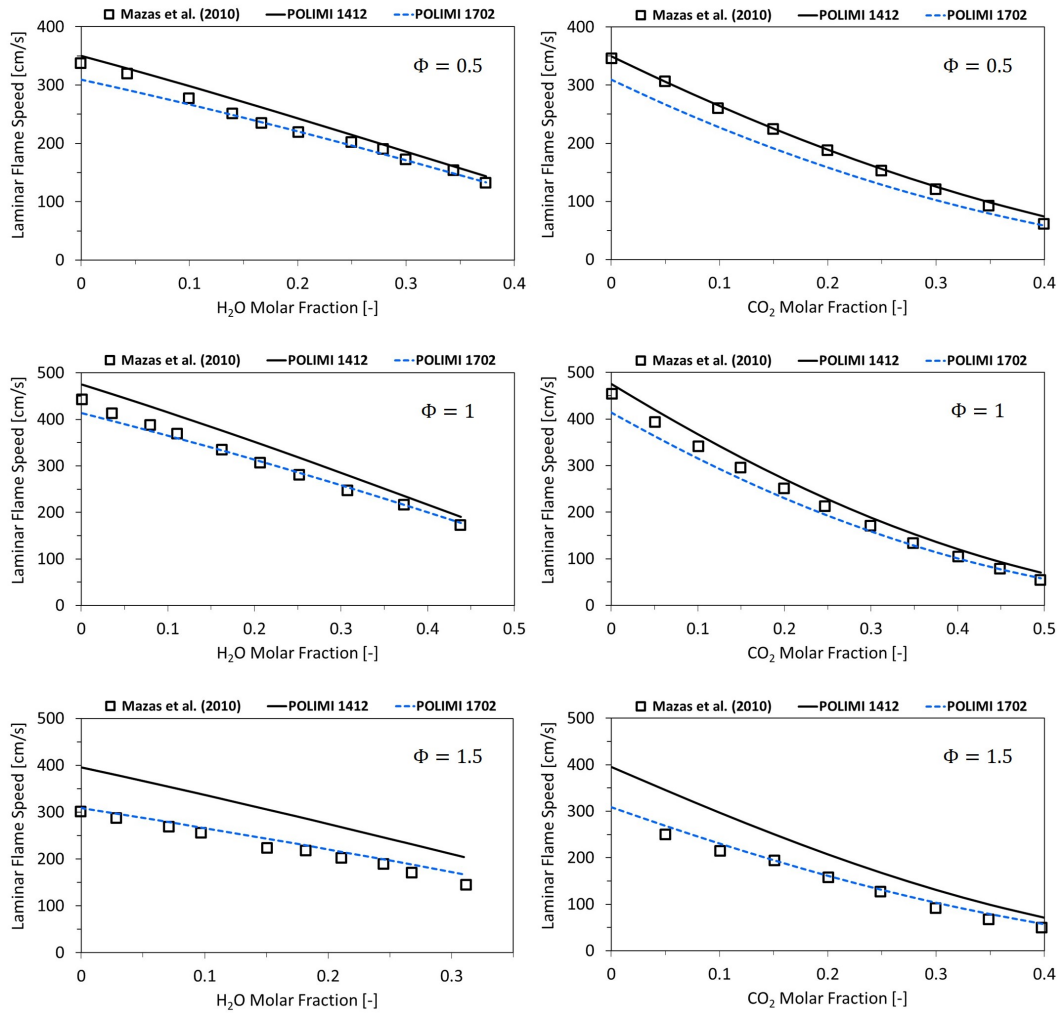
**Figure 3.20:** Experimental (symbols) and computed (lines) premixed laminar flame speeds of $CH_4/O_2/H_2O$ and $CH_4/O_2/CO_2$ mixtures as a function of molar fraction of the corresponding diluent ($H_2O$ or $CO_2$ respectively). For each mixture, three equivalence ratios are investigated: 0.5, 1 and 1.5. The inlet temperature is 373 K and the operating pressure is of 1 atm. The blue dashed lines represent the "POLIMI 1702" kinetic model and the black solid ones the "POLIMI $C_1$-$C_3$ 1412" mechanism.

**Figure 3.21:** Experimental (symbols) and computed (lines) laminar flame speeds of $CH_4/O_2/CO_2/H_2O$ mixtures as a function of water molar fraction. Two $O_2$-to-$CO_2$ diluent ratios have been considered: 0.52 and 0.72. For each one, three equivalence ratios have been investigated: 0.6, 1 and 1.4. The blue dashed lines represent the "POLIMI 1702" kinetic model and the black solid ones the "POLIMI $C_1$-$C_3$ 1412" mechanism.

**Methane oxy-combustion in presence of CO$_2$ at different unburned gas temperatures**

Figure 3.22 shows the good agreement with experimental data obtained at different inlet temperatures ($T = 298\,K,\,323\,K,\,373\,K$) by Konnov, Coppens and Mazas.
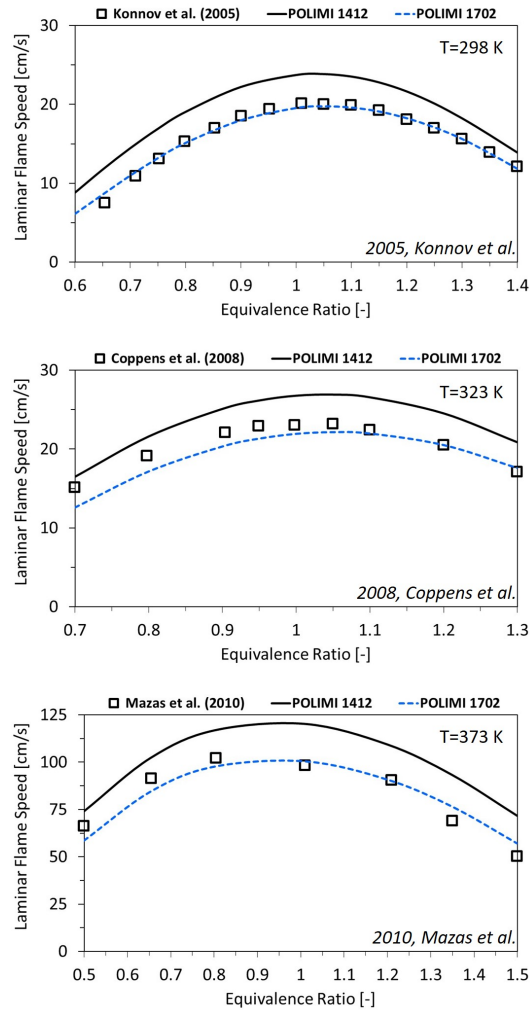


**Figure 3.22:** Propagation speed in CH$_4$/O$_2$/CO$_2$ flames as a function of equivalence ratio. In each graph, squares represent the experimental data, the black solid lines indicate the results obtained through the simulation of the "POLIMI 1412" kinetic scheme and the blue dashed lines represent the "POLIMI 1702" model.

**Effect of the pressure over the laminar flame speed**

Figure 3.23 shows the improvements of "POLIMI 1702" also for experimental data obtained by Xie et al., for a pressure variation from 1 to 3 bar.
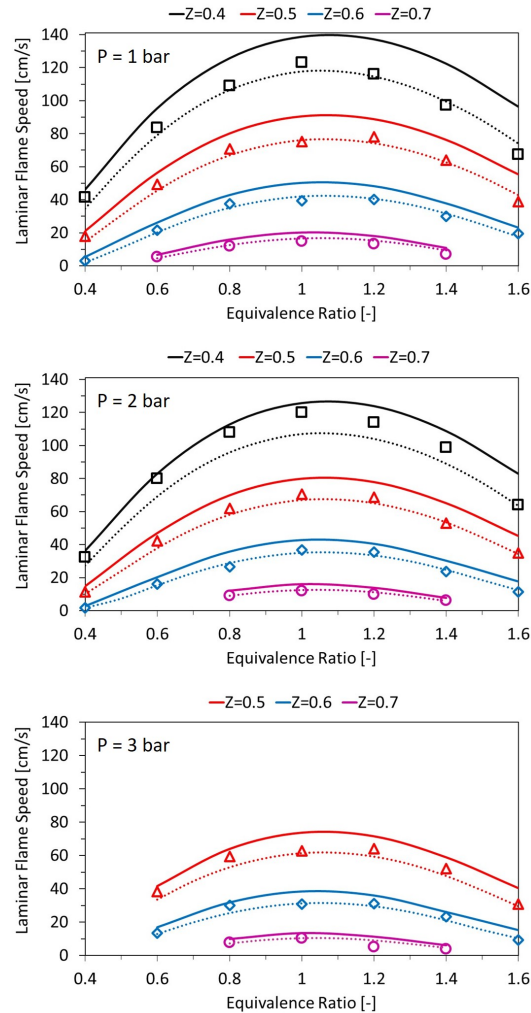


**Figure 3.23:** Experimental (symbols) and calculated (lines) laminar burning velocities of the $CH_4/O_2/CO_2$ mixtures at 1, 2 and 3 bar and different carbon dioxide dilution ratios (Z). Solid lines represent data computed through "POLIMI $C_1$-$C_3$ 1412", while dotted lines the results of the "POLIMI 1702" kinetic model.

**Conclusion**

Figures from 3.20 to 3.23 highlight the improved performances of the "POLIMI 1702" mechanism over the validation for laminar flame speed under conditions nearest to methane combustion in MILD oxy-fuel conditions.

### 3.7.2 Plug Flow Reactor

In addition to the laminar flame speed, also experimental data from other facilities are here discussed to extend the operating conditions and further verify the reliability of the kinetic model.

Bendtsen et al. [76] measured species profiles from the combustion of a $CH_4/O_2/H_2O/N_2$ mixture at atmospheric pressure with an equivalence ratio of 0.12. The composition is reported in Table 3.7.

| Species | Molar Fraction |
|---------|----------------|
| $CH_4$ | 0.00228 |
| $O_2$ | 0.0369 |
| $H_2O$ | 0.04 |
| $CO_2$ | 0.92082 |

**Table 3.7:** Composition of the mixture studied by Bendtsen et al. [76].

Figure 3.24 shows the experimental data for different species with the simulation results from "POLIMI $C_1$-$C_3$ 1412" and "POLIMI 1702" kinetic mechanisms.

The new model better predicts the overall reactivity and intermediate species profiles. Some deviations within experimental uncertainty are however highlighted for formaldehyde.
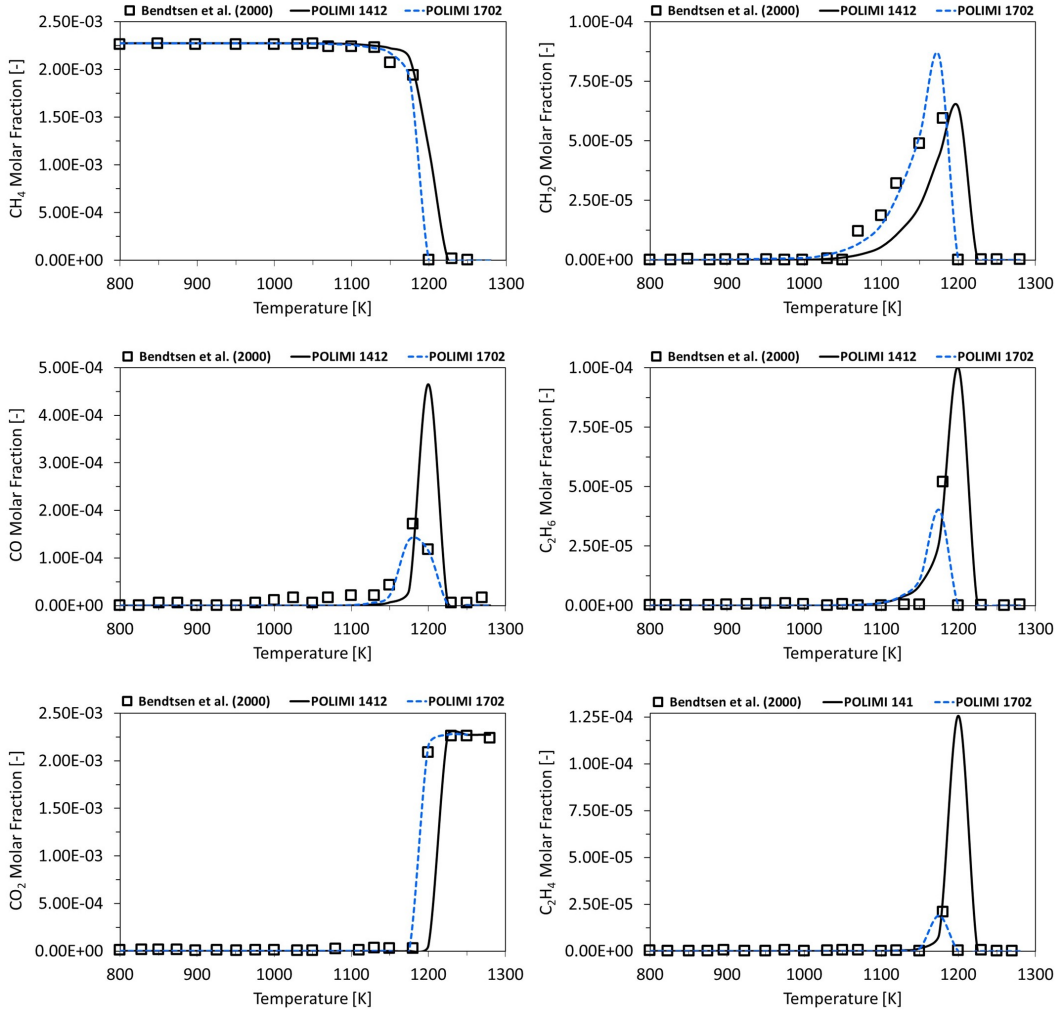
**Figure 3.24:** Experimental (squares) and computed (lines) molar fractions of different species as a function of inlet temperature of the mixture. The black solid lines indicate the "POLIMI $C_1$-$C_3$ 1412", while the blue dashed ones the "POLIMI 1702" kinetic scheme.

The second work considered for the validation of the "POLIMI 1702" kinetic mechanism is the one by Glarborg et al. [77]. They investigated a $CH_4/O_2/CO_2/N_2$ mixture at an equivalence ratio of 3.89 and at atmospheric pressure. In Table 3.8, the corresponding composition is reported.

| Species | Molar Fraction |
|---------|----------------|
| $CH_4$  | $9.83 \cdot 10^{-4}$ |
| $O_2$   | $5.05 \cdot 10^{-4}$ |
| $CO_2$  | $0.952$ |
| $N_2$   | $4.65 \cdot 10^{-2}$ |

**Table 3.8:** Mixture composition investigated by Glarborg et al. [77].

The comparison between experimental data and the simulated results for CO

is reported in Figure 3.25.
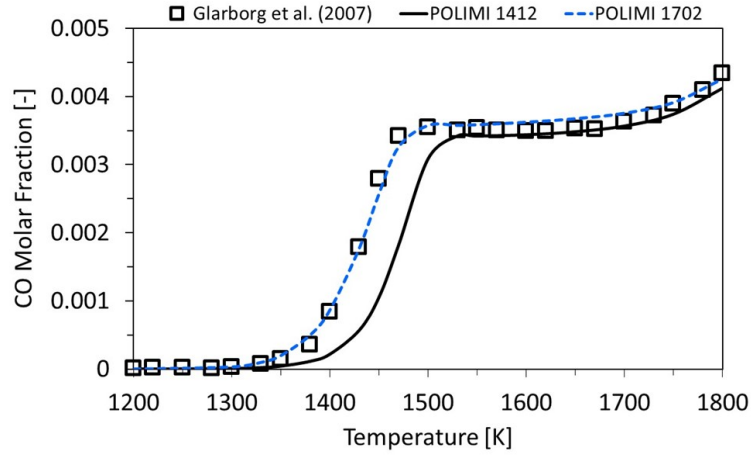


**Figure 3.25:** Carbon monoxide molar fraction as a function of inlet temperature of the mixture. The squares are the experimental data; they are compared to the results of the simulation through the "POLIMI 1702" (blue dashed line) and the "POLIMI $C_1$-$C_3$ 1412" (black solid line) kinetic mechanisms.

Also in this case, as seen for Bendtsen et al. work, the "POLIMI 1702" predicts very well the trend of the CO. The old model shows some consistent delay of about 50 K.

### 3.7.3 Perfectly Stirred Reactor

Unpublished experimental data in PSR have been provided by the "Istituto di Ricerche sulla Combustione, IRC" of Naples [78]. Some of these data have been presented during the recent COST "3rd General Meeting and Workshop on SECs in Industry of SMARTCATs Action" held in Prague [79].

As described in Figure 3.26, the reactor used to perform such experiments [80] is fed by four-jet nozzle, allowing the immediate mixing of the reactants, approaching the ideal conditions of a PSR within the reactor volume.
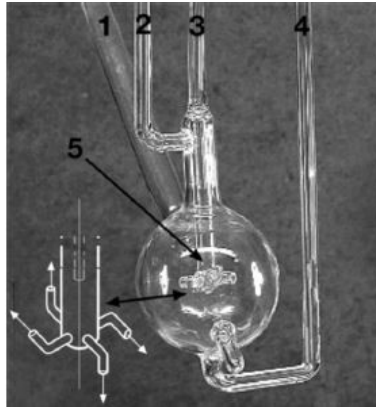


**Figure 3.26:** Jet stirred flow reactor used in the experimental analysis carried out in the Naples laboratory of IRC. (1) Thermocouple duct; (2) oxidizer/diluent duct; (3) fuel inlet; (4) exhaust gases outlet; (5) reactant premixing sections. About this last element, a schematic representation is also reported.

The atmospheric pressure Jet Stirred Reactor was used to investigate a mixture composed by $CH_4/O_2$ with 90% of $CO_2$ dilution. Two equivalence ratios have been analysed: 1 and 1.5. The molar fraction of reactant, intermediate and product species have been analysed for varying the inlet temperature ($T = 800 - 1200\,K$). The data are compared with the results form the "POLIMI 1702" model in Figure 3.27. The model correctly replicates the experimental observations.

**CH$_4$/O$_2$/90%CO$_2$**
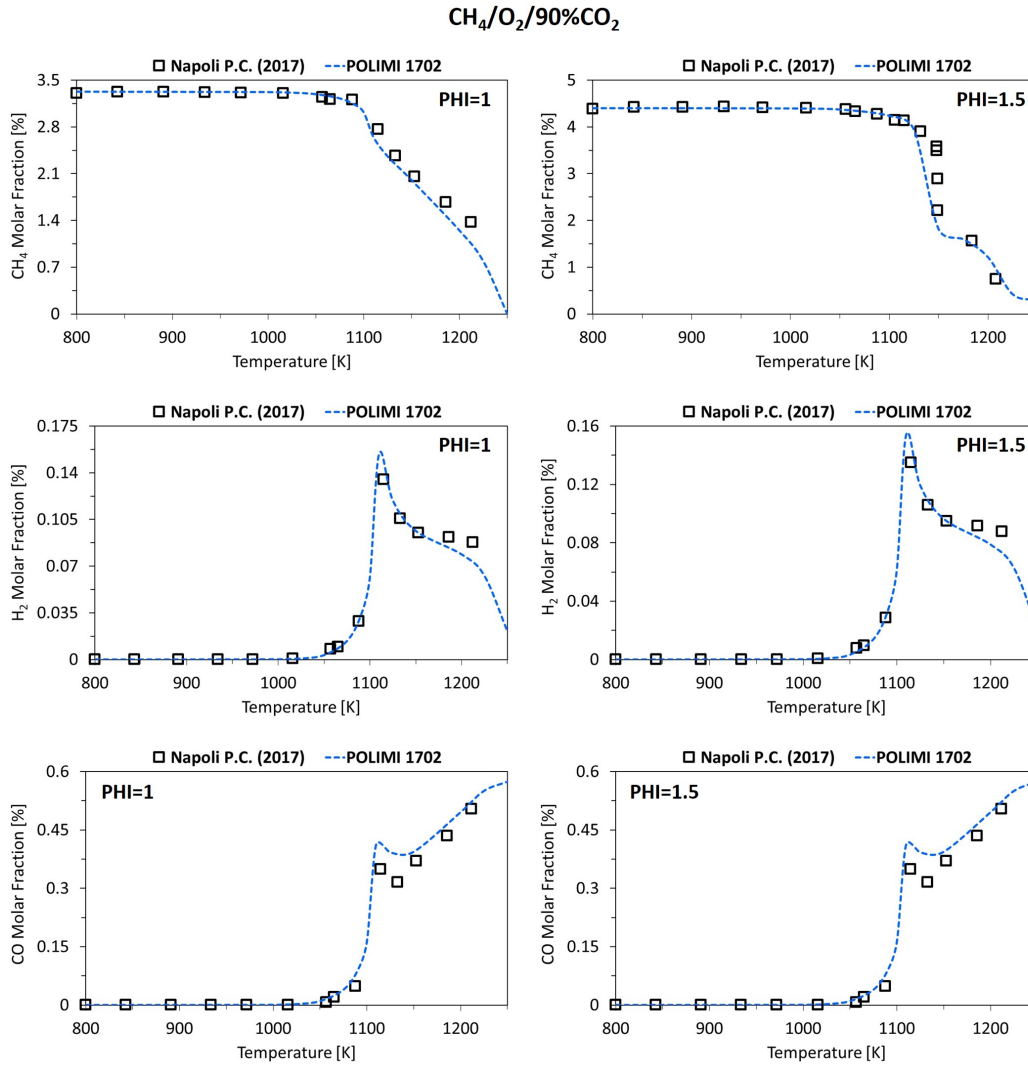


**Figure 3.27:** Experimental (squares) and computed (line) molar fraction of CH$_4$, H$_2$ and CO as a function of inlet mixture temperature at equivalence ratio equal to 1 and 1.5. The blue dashed lines represent the results of the "POLIMI 1702" simulation.

Then, CH$_4$/O$_2$ mixtures have been also tested for the same equivalence ratios ($\Phi = 1/1.5$) under a dilution with a mixture composed by 45% of H$_2$O and 55% of N$_2$. Figure 3.28 shows the comparison between experimental data and model results, highlighting good agreement all over the temperature range investigated.

**CH$_4$/O$_2$/45%H$_2$O-55%N$_2$**
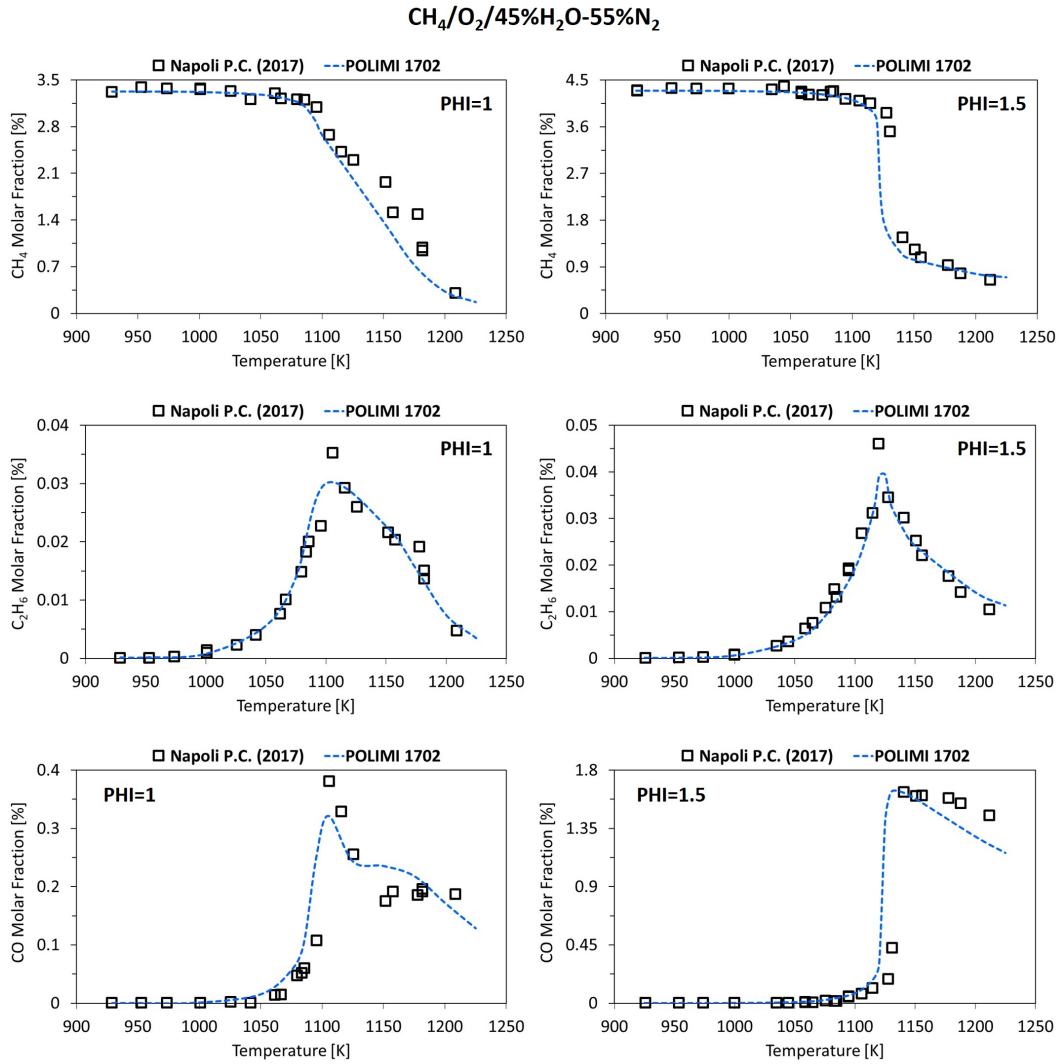


**Figure 3.28:** Experimental (squares) and computed (line) molar fraction of CH$_4$, C$_2$H$_6$ and CO as a function of inlet mixture temperature at equivalence ratio equal to 1 and 1.5. The blue dashed lines represent the results of the "POLIMI 1702" simulation.

Some delay is observed in terms of overall reactivity. Part of this discrepancy has to be attributed to oscillating behaviors observed for temperatures higher than 1100 K. Therefore, both computationally and experimentally, the molar fractions are determined through a time weighed average, at the cost of some loss in accuracy. Figure 3.29 highlights the capacity of the "POLIMI 1702" kinetic model to predict the temperature range at which oscillations are detected within $\pm 20\,K$.
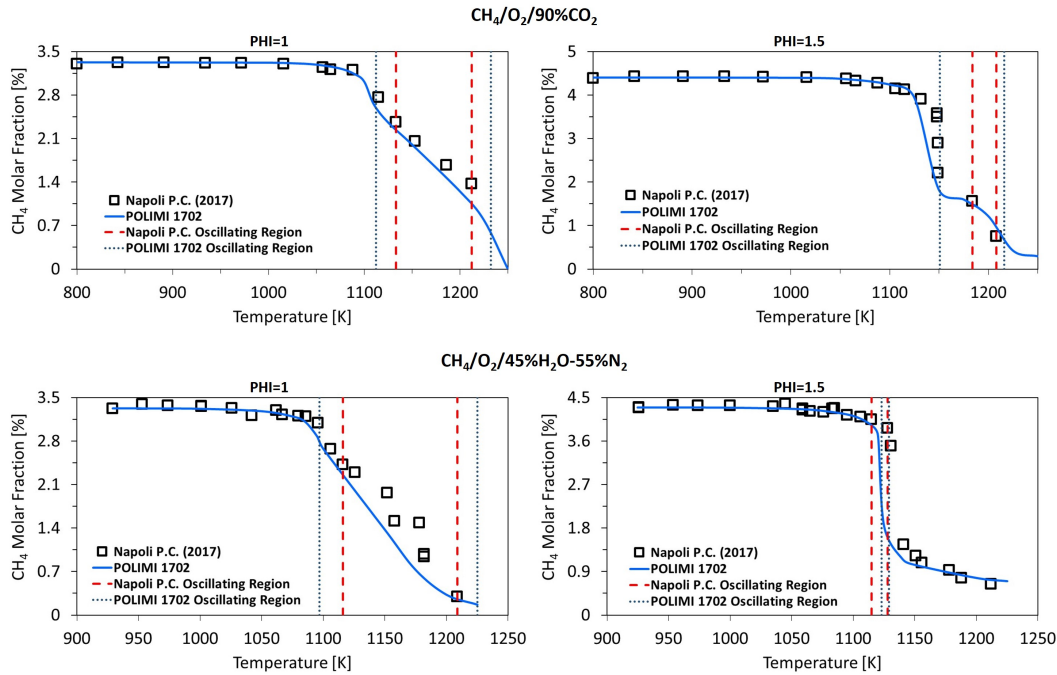
**Figure 3.29:** Experimental (red dashed lines) and computed (blue dotted lines) range of temperatures where oscillating combustion occurs in the Jet Stirred Reactor analysed.

## 3.8   Conclusions

In this third chapter, the detailed description of the "POLIMI 1702" development on the basis of the "POLIMI $C_1$-$C_3$ 1412" kinetic mechanism has been shown. The thermodynamic and transport properties files have been updated based on the Burcat's database. The kinetic scheme has been updated starting from the "AramcoMech1.3". The procedure followed has been based on the adjustment of such mechanism in order to make it suitable to be implemented in the already existing POLIMI framework. The new model has been validated over a wide range of conditions of interest for MILD oxy-fuel combustion.

The "POLIMI 1702" model proved to be reliable in predicting the innovative operating conditions for the following sections.

CHAPTER $4$

# Oscillating combustion in well-stirred reactors

I N Chapter 1, when the aim of this Thesis was introduced, it has been observed how one of the most important features of this process is its exothermicity. The amount of heat released per unit of fuel mass is rather high and conversion of internal energy into heat is the conceptual basis of the large adoption of combustion for energy purposes (transport, industry, domestic application...). Steam cracking furnaces are a representative example. As already seen, IMPROOF [8] has the objective to optimize such units, increasing the heat transfer efficiency and reducing the total amount of pollutants emitted. This can be realized through the MILD oxy-fuel combustion. In the previous chapter, the development of a detailed kinetic mechanism able to replicate such conditions has been shown. In the section related to the validation of the "POLIMI 1702" scheme in jet-stirred reactors, the presence of oscillations has been observed in some temperature conditions. This is, certainly, undesired since it corresponds to a periodic extinction and re-ignition of the mixtures fed to the facilities. In fact, if such phenomenon occurred in a furnace, the heat would be discontinuously provided to the pyrolysis coil. As consequence, the hydrocarbon molecules cracking would not be effective and the overall conversion and selectivity of the process would be unsustainable. At the same time, problems in the process control would be observed. In fact,

in case of very high frequency of the oscillations, the temperature variation could be lower than the thermocouple sensitivity. In this way, the control system is not able to detect the discontinuous heat supply.

Therefore, the investigation of the fundamental reasons behind such phenomenon is of relevance. From a kinetic modeling perspective, the goal is to minimize such instabilities by defining proper operating conditions.

## 4.1 Dynamic Continuous-flow Stirred Reactors

In Chapter 2, a brief introduction about CSTR has been provided. They are zero dimensional ideal reactors characterized by a perfect mixing throughout the reactor volume. Therefore, all the mixture properties such as temperature, pressure and composition can be assumed uniform. The system is characterized by the presence of a mass exchange with the external environment. This is realized through an inlet and an outlet flow rate. They are responsible of the continuous reactants supply and products removal. An important parameter must be defined for such reactor: the residence time, $\tau$. It represents the ratio between the reactor volume and the volumetric flow rate exchanged by the reactor:

$$\tau = \frac{V}{\dot{Q}} \quad \left[\frac{m^3}{\frac{m^3}{s}}\right] = [s] \tag{4.1}$$

The oscillating combustion occurs only within this type of reactor. In fact, it is the result of the interaction between the chemistry and the fluid dynamics of the unit. Such phenomenon, indeed, is characterized by permanent oscillations. Therefore, once they are stabilized, they repeat exactly during the time with the same dynamics. Since in these conditions the achievement of the steady state does not occur, the process will be studied through dynamic CSTRs. A generic conservation equation is defined as:

$$Acc = In - Out + Prod \tag{4.2}$$

where the accumulation term is different from zero and periodically changes during time. In addition, in order to simplify the complexity of the oscillating phenomenon, the reactors are assumed to work in isothermal conditions. In this way, the effects of the temperature variation during the oscillating reactions are neglected, focusing the attention on kinetic features. Equation 4.3 represents the mass balance written for the generic $i - th$ species, as implemented in

OpenSMOKE++:

$$\frac{d\left(\hat{\rho} \cdot \omega_i\right)}{dt} = \frac{\hat{\rho}_0}{\tau}\left(\omega_i^0 - \omega_i\right) + \sum_{i=1}^{NR} v_{ij} \cdot r_j \cdot MW_i \qquad (4.3)$$

where:

$\hat{\rho}$ is the mass density of the mixture inside the reactor and of the outlet flow, measured in $\left[\frac{kg}{m^3}\right]$.

$\hat{\rho}_0$ is the mass density of the inlet flow $\left[\frac{kg}{m^3}\right]$.

$\omega_i$ is the mass fraction of the $i-th$ species in the reactor volume and in the outlet flow.

$\omega_i^0$ is the mass fraction of the $i-th$ species in the flow entering the reactor.

$v_{ij}$ is the stoichiometric coefficient of the $i-th$ species in the $j-th$ reaction.

$r_j$ represents the rate of the $j-th$ reaction whose unit of measure is $\left[\frac{kmol}{m^3 \cdot s}\right]$.

$MW_i$ is the molecular weight of the $i-th$ species measured in $\left[\frac{kg}{kmol}\right]$.

The equation just described represents the mass balance. A similar expression can be obtained in molar terms by substituting the mass density with the molar density and the molar fractions with the mass fractions. In such a way, the final expression does not contain the molecular weight in the production term.

$$\frac{d\left(\widetilde{\rho} \cdot y_i\right)}{dt} = \frac{\widetilde{\rho}_0}{\tau}\left(y_i^0 - y_i\right) + \sum_{i=1}^{NR} v_{ij} \cdot r_j \qquad (4.4)$$

where the symbol $\sim$ is used to indicate the molar base.

Both in the mass and in the molar balances, in the right-hand term of the equation, two contributions can be distinguished:

- The "convective" contribution is related to the material exchange of the reactor with the external environment. It is function of the inlet and the outlet molar fraction of the species considered along with the residence time: $\frac{\widetilde{\rho}_0}{\tau}\left(y_i^0 - y_i\right)$.

- The second contribution to molar variation is the "kinetic" part. It is influenced only by the chemistry. It is function of the rates of the reactions in which the species of concern is involved: $\sum_{i=1}^{NR} v_{ij} \cdot r_j$.

## 4.2 Hydrogen

Before discussing methane and higher hydrocarbons, attention has to be given to the $H_2/O_2$ subset, as it plays a major role for every heavier fuel chemistry. In this chapter, the oscillating oxidation of the hydrogen is studied. In particular, a deep analysis of the operating conditions which allow the establishment of permanent "limit cycles" is performed. This process is realized starting from the well-stirred reactors investigated in literature by Baulch et al. around the 1990 [81–83]. They considered a $550\,cm^3$ CSTR operated in non-isothermal conditions. In a pressure interval of 10-20 torr and a temperature range of 670-690 K, they observed the establishment of oscillations through the measurement of the temperature and the concentration of some species as hydrogen, water and OH radicals. They investigated also different inlet compositions in terms of equivalence ratio along with several residence times in the range of 0.7 to 8 s.

On this basis, a perfectly stirred reactor with the same volume, but operating in isothermal conditions, has been simulated in order to observe the same oscillating phenomenon. Certainly, the ranges of temperature, pressure and residence time which delimit the oscillations are different because the temperature is assumed constant and, thus, the effects of heat release and removal are completely neglected.

In the following sections, a deep description of the hydrogen oscillating combustion will be provided, together with a detailed kinetic analysis of the mechanism through which the hydrogen is converted to water, in order to define the criticism and relevant pathways. All the reactors analysed in the following sections have a fixed volume of 550 cm³ [82, 83].

### 4.2.1 Limit cycle

Concerning the hydrogen oxidation in isothermal well-stirred reactors at 0.1 atm, the temperature window between 753 K and 843 K identifies the oscillating field for a stoichiometric mixture. In Figure 4.1, the temporal profile of the hydrogen and water molar fraction is shown. During the time, several limit cycles can be observed. Each one can be recognized by the presence of two regions:

- The "kinetic" part is the first. It is confined in the time interval where the ignition occurs. The controlling phenomenon is the chemistry which prevails on the convection.

- Instead, the "convective" part is related to the time interval where the convection is controlling. In this region, indeed, there is a reactants accumulation
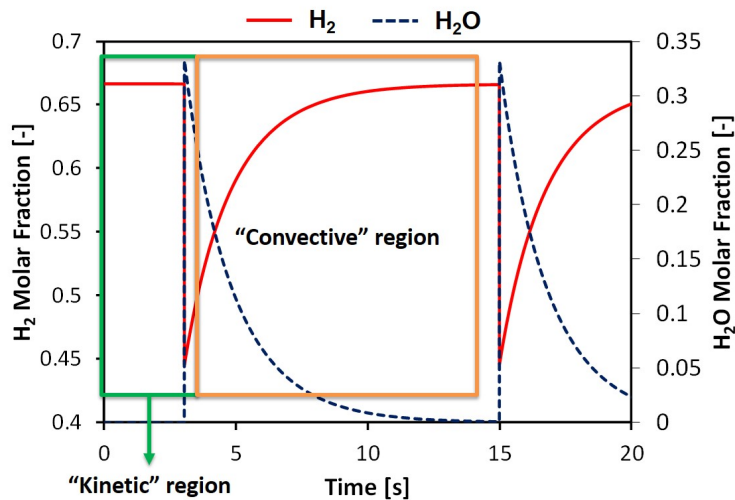
**Figure 4.1:** Hydrogen and water molar fraction as a function of time. The "kinetic" and "convective" regions are depicted. The operating temperature is 755 K and the pressure is 0.1 atm. The inlet mixture is in stoichiometric conditions.

and products removal from the reactor. Here, the chemistry contribution is very small and it can be neglected.

Each limit cycle terminates as soon as the system reactivity increases such that a new consumption of the reactants occurs.

### 4.2.2 Kinetic mechanism

In the present section, the analysis of the kinetic mechanism on which the hydrogen combustion is based are investigated. In particular, the causes of the oscillating phenomenon are explained through the study of the competing paths acting in the system. For these purposes, the Rate Of Production (ROP) Analysis available in the `OpenSMOKE++` Post-Processor will be widely employed.

In order to understand completely the process, the first point to consider is the chemistry which occurs at the very beginning of the process. Only one reaction takes place: the initiation between a hydrogen and an oxygen molecule.

$$H_2 + O_2 \rightarrow H + HO_2 \tag{4.5}$$

An initial accumulation of H and $HO_2$ radicals can be observed. Since the former is the most reactive species, it rapidly reacts with oxygen whose initial concentration in the reactor is high. Two are the possible paths in competition with one other:

$$H + O_2 \rightarrow O + OH \tag{4.6}$$

87

$$H + O_2(+M) \rightarrow HO_2(+M) \tag{4.7}$$
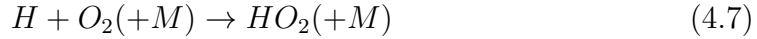
Through Reaction (4.7), another $HO_2$ radical is produced. Conversely, the (4.6) produces OH and O radicals. This is a branching reaction since from one radical, three more are obtained. In fast, O behaves as a double radical. They interact with $H_2$ through the following reactions:

$$H_2 + OH \rightarrow H_2O + H \tag{4.8}$$

$$H_2 + O \rightarrow OH + H \tag{4.9}$$

The (4.9) is a propagation: the double radical O converts the hydrogen molecule into OH and H. Reaction (4.8) is the main reaction responsible of the hydrogen molecules conversion and the principal step for water production.

On the other hand, the $HO_2$ can follow several paths depending on the radical with which it interacts:

$$H + HO_2 \rightarrow 2\,OH \tag{4.10}$$

$$H + HO_2 \rightarrow H_2 + O_2 \tag{4.11}$$

$$OH + HO_2 \rightarrow H_2O + O_2 \tag{4.12}$$

$$O + HO_2 \rightarrow OH + O_2 \tag{4.13}$$
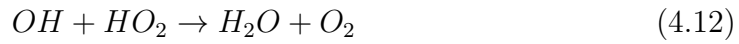
Among them, (4.11) and (4.12) are termination reactions. In fact, they involve two radicals producing two stable molecules, reducing the overall system reactivity. Instead, (4.10) is a propagation reaction since two radicals are converted in two other radicals. The last one converts into a OH and an oxygen molecule an O and a $HO_2$ radicals, thus reducing the number of radicals since from three, only one is obtained. Hence, it can be classified as a middle ground between a termination and a propagation.

Therefore, after a very small time interval during which chemistry is mainly controlled by the initiation Reaction (4.5), the principal mechanism responsible of $H_2$ and $O_2$ conversion into water is characterized by the set of reactions from (4.6) to (4.13). Among all the species involved, the crucial one can be identified in the H atom. In fact, it is formed by one nucleus coupled with only one odd electron which makes such radical particularly reactive. Before system ignition, the main reactions responsible of such species decomposition are the (4.6) and the (4.7). These are two alternative paths whose competition is extremely important in influencing the system behavior. In order to better understand this property, the kinetic mechanism shown can be divided in two competing channels.

**"Chain branching"**

The first one is called "chain branching". It is responsible of the increase in system reactivity. Three reactions can be identified. They form a cycle based on the H radical. Through the branching Reaction (4.6), the hydrogen atom is transformed with an oxygen molecule into two radicals O and OH. The resulting O atom then reacts quickly by Step (4.9), returning a hydrogen atom and producing a second OH radical. At this point, two OH radicals have been gained by the system. The Reaction (4.8) rapidly converts them into two H atoms and two water molecules. This is an autocatalytic process: going through the cycle, one H atom produces three H radicals. This constitutes "chain branching": considering the limit condition in which no termination reactions take place, the exponential increase of reactivity becomes clear: three radicals can then become nine, then 27 etc.

Furthermore, in order to find the rate of the overall cycle, the kinetics of the three involved reactions must be investigated. In Figure 4.2, the reaction rates as a function of time are shown.
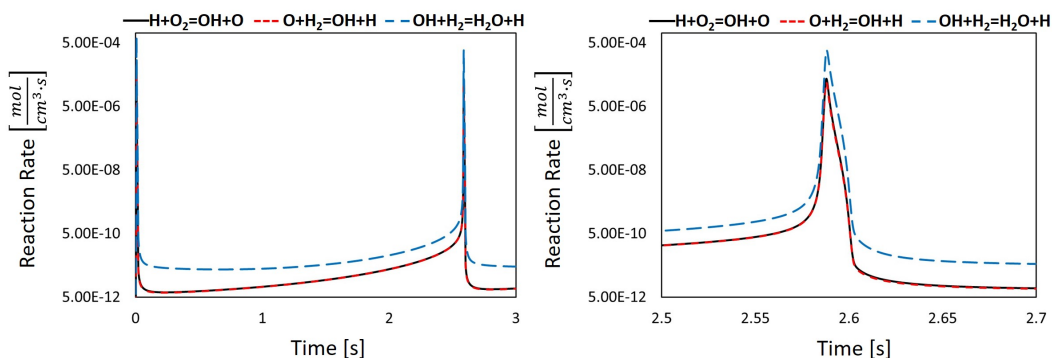


**Figure 4.2:** Rates of the reactions involved in the "chain branching" cycle as a function of time.

While the hydrogen consumption through OH is the fastest process, the other two paths have the same speed. Therefore, a Pseudo-Stationary State Approximation (PSSA) can be adopted for the OH radical, since its consumption rate is more rapid with respect to its production. In Figure 4.3, a schematic representation of the cycle is provided.
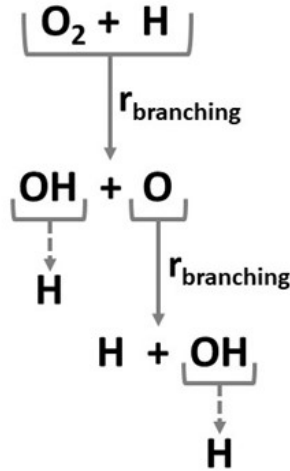
**Figure 4.3:** Chain branching cycle. The dashed lines indicate the $H_2 + OH$ reaction which is much faster than branching. The O radical is consumed by the hydrogen with a reaction rate equal to the branching one.

As depicted, the conversion of the hydroxyl radical into a H atom is immediate. Conversely, the conversion of the O double radical happens through a reaction rate which can be assumed equal to the branching one as demonstrated by Figure 4.2. As a result, from the consumption of one H radical, three are produced and the overall cycle has a rate which can be computed as follows:

$$r_{ChainBranching} = 2k_{branching} \left[O_2\right] \left[H\right] \tag{4.14}$$

The factor of two just mirrors the increase from one to three of the H atom.

**"Chain termination"**

If these were the only reactions, the production rate of the H radical would simply increase exponentially, leading to ignition for all experimental conditions. But this does not happen because of the competition between the branching process with the termination channel. This is responsible of the inhibition of the catalytic cycle through Step (4.7). It is the alternative process to the branching Reaction (4.6). Through this path, H and $O_2$ are converted into $HO_2$ radicals. This can be considered as a "termination" step since the product obtained is a very stable radical if compared with H, OH and O. In addition, Step (4.7) is a third-body reaction. This is suggested by the presence of the M species in the reaction equation. Its role is to remove energy from the $HO_2$ molecule produced. If such process does not occur sufficiently rapidly, then the radical simply redissociates back to the relative reactants. The "third body" is any species to which the newly

formed $HO_2$ radical can transfer energy by collision.

$$H + O_2 \leftrightarrow HO_2^* \xrightarrow{+M} HO_2 \tag{4.15}$$
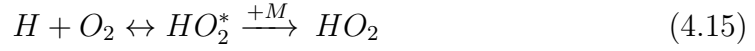
The species with which such molecule is most likely to collide are those present in the highest concentrations: the $H_2$ and $O_2$ continuously provided to the reactor, any added inert gas introduced as a diluent and water produced during the reaction. All the radicals which appear in the system do not contribute significantly to this stabilization process since they are present at concentrations lower by several orders of magnitude. One further, and very important, point is that the different species with which $HO_2$ may collide are not equally efficient at storing sufficient energy to induce the stabilization process. For this reason, each species has a related "third-body efficiency" ($\varepsilon_i$). In particular, in the "POLIMI 1702" kinetic mechanism, a collision with $H_2O$ is approximately ten times more likely to stabilize a radical than a collision with $O_2$. For Reaction (4.7) oxygen has a third-body efficiency equal to 1, water of 10 and hydrogen of 1.3. Diluents as helium and argon have an efficiency lower than one: 0.64 and 0.5 respectively. As already explained in Chapter 1, the kinetic constant of a third-body reaction depends not only on temperature, but also on the concentration of the gas-phase mixture. In this quantity a correction factor is present which is function of the third-body efficiencies of the involved species, along with their molar fraction:

$$[M] = \frac{P}{R \cdot T} \sum_{i=1}^{NC} y_i \cdot \varepsilon_i \tag{4.16}$$

This expression explains that the rate of the third-body Reaction (4.7) changes with the composition. This means that as the $H_2$ and $O_2$ are converting into water, the kinetic constant of the third-body reaction increases. Therefore, the weight of the (4.7) with respect to the branching (4.6) dynamically evolves during the time as shown in Figure 4.4.
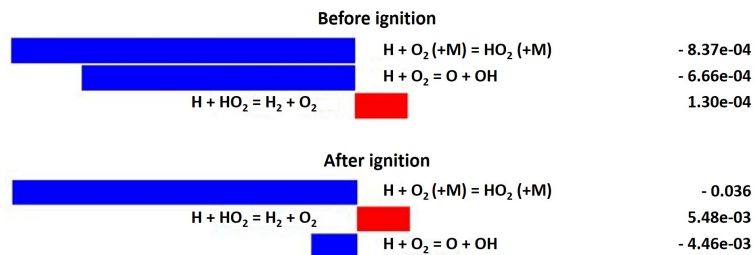


**Figure 4.4:** ROPA around the ignition of the mixture. It highlights the variation of the weight of the third-body reaction with respect to branching.

Rate of Production Analysis - $HO_2$

| | |
|---|---|
| H + O$_2$ (+M) = HO$_2$ (+M) | 9.78e-03 |
| H + HO$_2$ = 2 OH | - 7.89e-03 |
| H + HO$_2$ = H$_2$ + O$_2$ | - 1.50e-03 |
| OH + HO$_2$ = H$_2$O + O$_2$ | - 2.25e-04 |
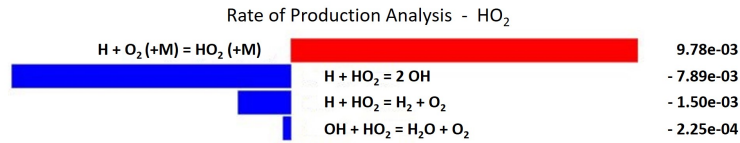
**Figure 4.5:** Rate of Production Analysis for the $HO_2$ radical in the "kinetic" region.

This is crucial in the explanation of the oscillatory features in a CSTR. The "termination chain" is completed with all the processes which involve the radical $HO_2$. The most relevant paths are the (4.10), (4.11) and (4.12) as shown in Figure. While the first is a propagation, the second and the third are terminations. In Figure 4.6, a schematic representation of the cycle is shown.

$$O_2 + H \ (+M)$$
$$r_{ThirdBody}$$
$$HO_2 \ (+M)$$
$$+H \qquad +H \qquad +OH$$
$$2 \ OH \qquad H_2O+O_2$$
$$H_2+O_2$$
$$2 \ H$$
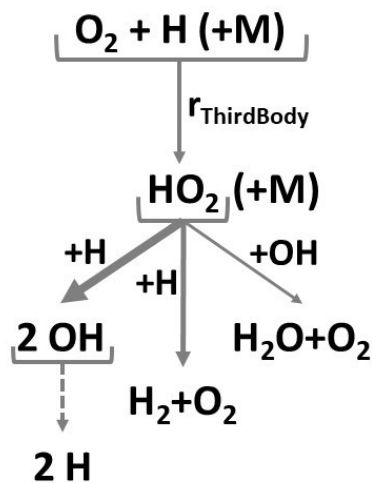
**Figure 4.6:** Mechanism of the termination chain. Only the path on the left allows to close the H cycle.

As depicted, the only way to return to H atom is the Reaction (4.10). Through this process, two hydrogen radicals are consumed, obtaining two further H atoms. At net, no increase in the amount of radicals is observed. Studying the behavior of the kinetic constants of these three reactions as a function of temperature, the different thicknesses of the arrows connected to the $HO_2$ radical in Figure 4.6 can be explained. Figure 4.7 shows how the propagation Reaction (4.10) is more favored than the other two for all the temperatures.
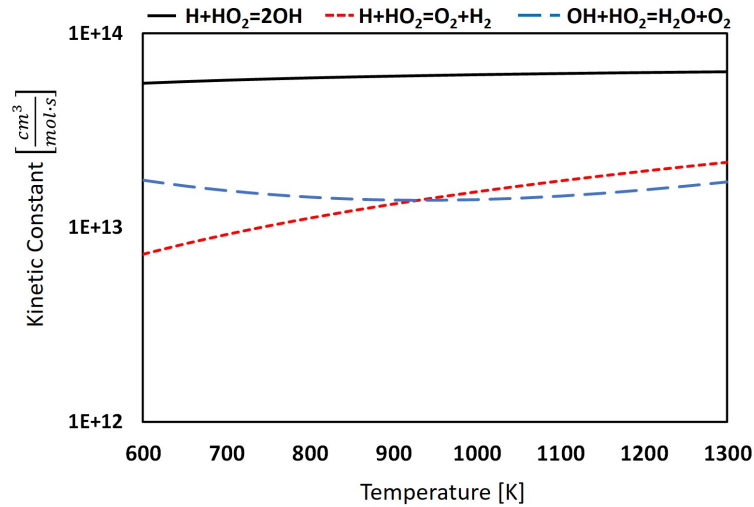
**Figure 4.7:** Kinetic constants of the three main reactions responsible of the $HO_2$ radical consumption as a function of temperature.

Its weight reduces with the increase of the temperature since the termination reaction which involves an H radical grows highly with temperature. Therefore, the overall weight of the termination reactions is progressively higher with the temperature.

Comparing the two pathways, while the branching chain allows a production of three H radicals from one consumed, the termination chain can, instead, generate at maximum two of them, but consuming other two. So, the first process is able to increase strongly the system reactivity, but the second preserves or reduces the overall number of radicals. Therefore, the competition between the branching Reaction (4.6) and the corresponding third-body one (4.7) controls the overall behavior of the system. This is responsible both of the mixture ignition and of the oscillations as explained in the following sections.

### 4.2.3 $H_2/O_2$ ignition: switch from slow to fast reaction

In combustion, a fuel-oxidizer mixture can ignite spontaneously if temperature is higher than the auto-ignition one. This represents the boundary between slow and fast reaction. Therefore, if the temperature is such that the system reactivity is high enough, the ignition of the mixture occurs and a fast conversion of the reactants can be observed. This is connected to the competition between branching and termination channels. In the previous section, the main difference between these two paths had been described. Step (4.6) is responsible of the exponential growth of the H radicals and, thus, of the development of reactivity. Conversely, the Reaction (4.7) produces $HO_2$ molecules causing a reduction of hydrogen radi-

cals concentration and, at the same time, the inhibition of the system. Therefore, the competition of these two channels can be used to define the operating conditions at which the switch from slow to fast reaction is observed. In Figure 4.8, the comparison of these two cases is provided through the time behavior of $H_2$ and H molar fractions.
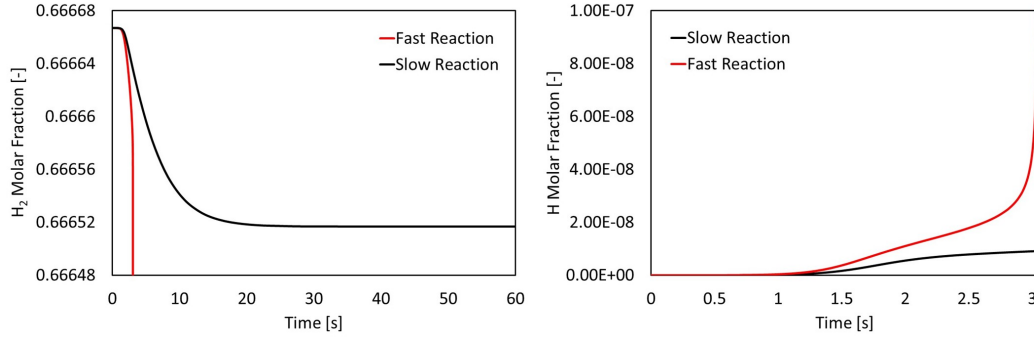


**Figure 4.8:** $H_2$ and H molar fractions as a function of time. The red lines represent the trend for the fast reaction case, while the black ones the slow.

From a mathematical point of view, the auto-ignition temperature can be predicted through the study of the hydrogen radical material balance. In order to recover an analytical expression which can predict, with a relatively small error, the ignition of the system, the reduced mechanism shown in Figures 4.3 and 4.6 can be adopted. Therefore, assuming a PSSA for the OH and O radicals, the material balance for the H atom in a dynamic CSTR can be written as follows [84]:

$$\frac{d[H]}{dt} = k_{initiation}[H_2][O_2] + 2k_{Branching}[H][O_2] - k_{ThirdBody}[H][O_2] - \frac{[H]}{\tau} \quad (4.17)$$

Assuming the Pseudo Stationary State Approximation also for this radical, the following expression can be obtained:

$$[H] = -\frac{k_{initiation}[H_2][O_2]}{2k_{Branching}[O_2] - k_{ThirdBody}[O_2] - \frac{1}{\tau}} \quad (4.18)$$

The ignition of the system can be assumed as an infinite increase of the H radical concentration. This can be proven by the evaluation of the temporal molar fraction profile of H proposed in Figure 4.8. Therefore, the condition which can be adopted is the zeroing of the denominator of (4.18). Thus, the final equation used to localize the system ignition on a P-T diagram is:

$$(2 \cdot k_{Branching} - k_{ThirdBody}) \cdot [O_2] - \frac{1}{\tau} = 0 \quad (4.19)$$

Such expression depends on temperature, pressure and initial composition of the

mixture, along with the residence time of the reactor. Thus, once fixed the inlet composition, the pressure and the reactor residence time, the ignition temperature can be obtained.

Moreover, the (4.19) is very accurate only with a reduced kinetic mechanism for hydrogen combustion. Using this expression to predict the ignition, Figure (4.9) shows that the maximum error with respect to the experimental results is around 10 K.
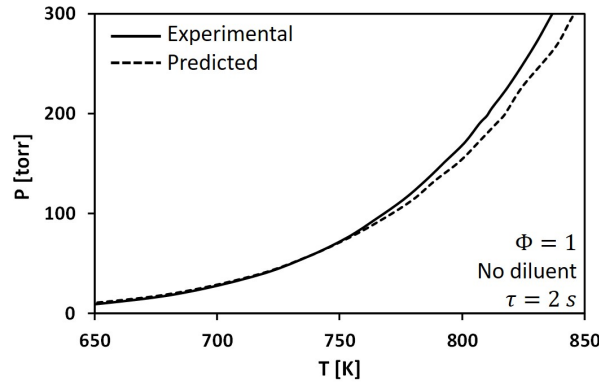


**Figure 4.9:** Experimental (solid line) and predicted (dashed line) P-T ignition curves.

In order to find a better model, a more detailed and complicated kinetic mechanism should be adopted. Such complications prevent the development of an analytical expression similar to that in (4.18). Therefore, the model obtained above can be assumed sufficiently accurate to find an approximate ignition temperature, once fixed the other system parameters.

In order to investigate the influence of the residence time on the ignition of the flammable mixture, a comparison between a batch and a perfectly stirred reactor with the same volume is performed. Once fixed the operating conditions in terms of pressure and composition for a $H_2/O_2$ mixture, the corresponding ignition temperature can be found in a batch reactor of equal volume of the CSTR of interest. The first can be assumed as a perfectly-stirred reactor with an infinite residence time. Considering the perfect gas law, the connection between this last quantity and the molar flow rate can be expressed by the following writing:

$$P \cdot \frac{V}{\tau} = \dot{n} \cdot R \cdot T \tag{4.20}$$

A batch reactor is, therefore, characterized by a zero molar flow rate, since it is closed to material exchange. Thus, the way to evaluate the ignition temperature is to investigate several batch simulations, by changing the operating temperature, the minimum one which shows a sharp peak of the H, OH and O radicals

molar fractions respectively. Similarly, at the same time instant, the hydrogen and oxygen molar fractions show a fast decrease, while water grows rapidly. The ignition delay can be defined as the time interval needed to observe such phenomena. If the CSTR of interest has a residence time which is lower than the ignition delay of the corresponding batch reactor, the explosion of the mixture can not be observed. This means that the time needed by the system to develop a reactivity sufficient to initiate the fast reaction is too high if compared with the interval spent by the molecules in the reactor. In this case, only a smooth decrease of the $H_2$ and $O_2$ molar fraction can be observed until the stationary state achievement. Indeed, in the PSR, the ignition temperature is higher of some degrees than in the batch reactor in order to make the radicals production faster with respect to the rate through which they are removed from the system. Thus, as the residence time is decreased, the ignition temperature is increased because the molar flow rate is higher as justified by the Equation (4.20). This concept is clearly reported in Figure 4.10: the P-T explosion curve of a stoichiometric mixture of $H_2/O_2$ is shifted to higher temperatures as the residence time is reduced from 2 to 0.1.
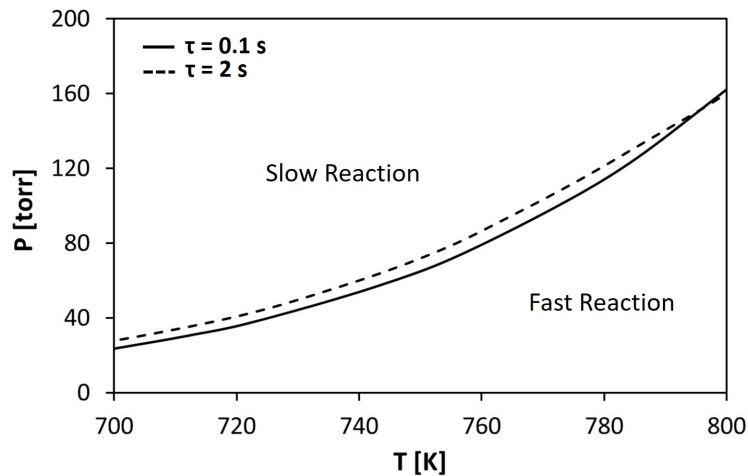


**Figure 4.10:** P-T explosion curve for a stoichiometric $H_2/O_2$ mixture at two residence times: 0.1 s and 2 s.

Moreover, such figure shows that the ignition temperature increases with pressure. Therefore, as pressure grows, the temperature needs to be increased in order to develop the sufficient reactivity to allow the switch from slow to fast reaction. This can be explained comparing the kinetic constants of the branching and the third-body processes as depicted in Figure 4.11.
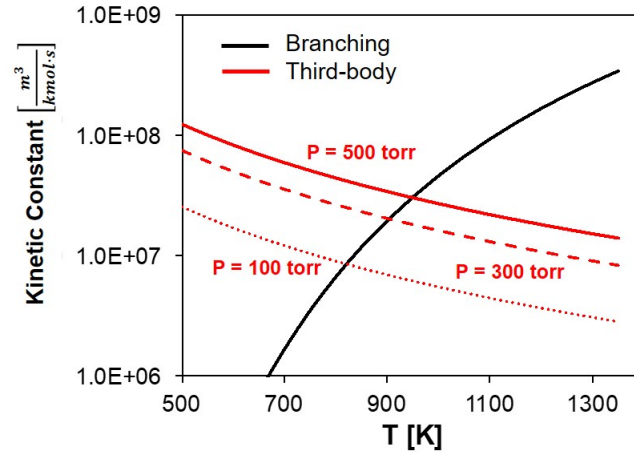
**Figure 4.11:** Pressure and temperature behavior of the third-body and branching kinetic constants at different pressures.

Once fixed a temperature, by increasing pressure, the weight of the third-body reaction over the branching one grows. Therefore, H atoms are preferentially converted into $HO_2$ radicals. In this way, the amount of active species as H, OH and O released in the system are progressively lower. At the same time, the produced $HO_2$ tend to consume such species causing a double inhibition of the system reactivity. In fact, the main reactions involved are only propagation or termination processes which avoid an exponential increase of the amount of active radicals.

### 4.2.4 Inhibition of the system: from fast to slow reaction

In the previous section, the kinetic description of the causes which allow the switch from slow to fast reaction of a $H_2/O_2$ mixture has been provided. Considering a batch reactor with a stoichiometric mixture of hydrogen and oxygen at a pressure of 0.1 atm, a temperature immediately successive to the system ignition is selected: 753 K. In Figure 4.12, the $H_2$ molar fraction is reported as a function of time. The interesting aspect is related to the partial conversion of the reactant. Therefore, after the switch from slow to fast reaction, a rapid reduction of hydrogen occurs until a molar fraction of about 0.45. Then, the curve keeps rather flat; in fact, the conversion proceeds very slowly due to the switch to the slow reaction. In this section, the kinetic analysis of the phenomenon which causes the inhibition of the system is performed.
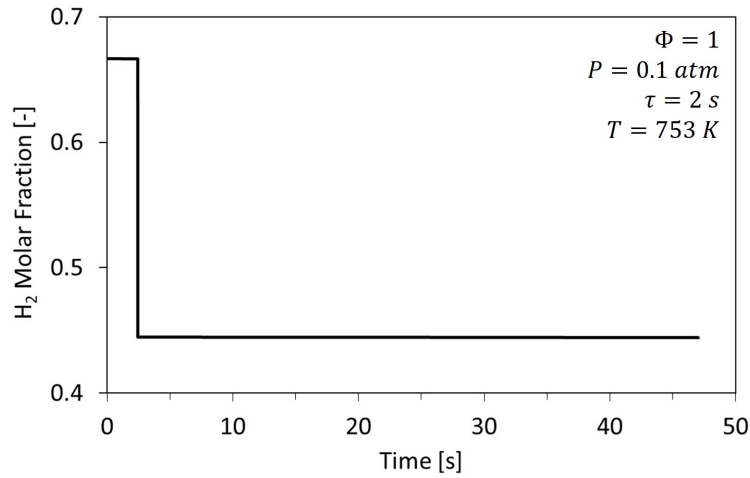
**Figure 4.12:** Hydrogen molar fraction as a function of time.

In order to better understand the behavior of the system, the temporal profiles of the O, OH and $HO_2$ radicals are reported in Figure 4.13.
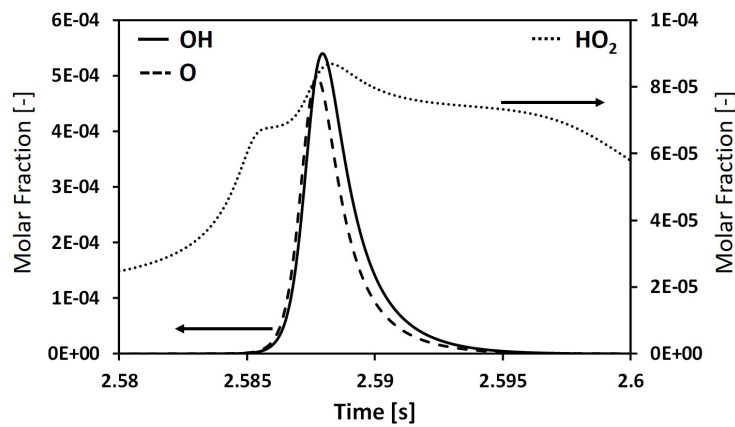


**Figure 4.13:** OH (solid line), O (dashed line) and $HO_2$ (dotted line) radicals molar fraction as a function of time around the ignition of the system.

The peaks of the O and OH radicals indicate the time location of the system ignition. Therefore, in correspondence of these points, the $H_2$ and, consequently $O_2$, molar fractions are reducing, while water is producing and accumulating in the reactor volume. This is responsible of the progressive increase of the importance of the third-body reaction over the branching one as shown in Figure 4.14. As a consequence, the maximum molar fraction of $HO_2$ is delayed with respect to the active radicals peaks.
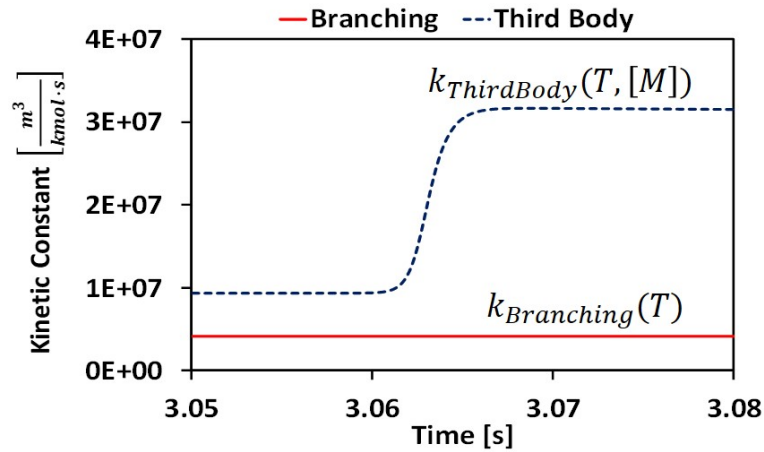
**Figure 4.14:** Temporal trends of the branching and third-body kinetic constants in the neighborhood of the mixture ignition.

Therefore, once $HO_2$ molecule is produced, it interacts mainly with H and OH radicals. Through the Step (4.10) two OH radicals are released and immediately converted into H atoms. This reaction, as already seen, is a propagation which does not increase the amount of radicals. Conversely, the terminations (4.11) and (4.12) are responsible of the removal from the system of two H radicals, causing a strong reduction of the system reactivity. These processes are the cause of the inhibition of the fast reaction, which switches back to the slow regime. Without termination steps, it is sufficient to ignite the system to allow the total conversion of the reactants. Even if during the occurrence of the reaction, water is producing and the weight of the branching process is progressively reducing, the paths starting from $HO_2$ are only of propagating nature, thus sustaining continuously the fast reaction. This can be proven by modifying the kinetic scheme, i.e. by removing both the terminations which involve $HO_2$ to give water, hydrogen and oxygen molecules. In Figure 4.15, the comparison of the time profile of the $H_2$ molar fraction obtained with the complete and the modified kinetic mechanism is reported. Therefore, the total conversion of hydrogen is observed.
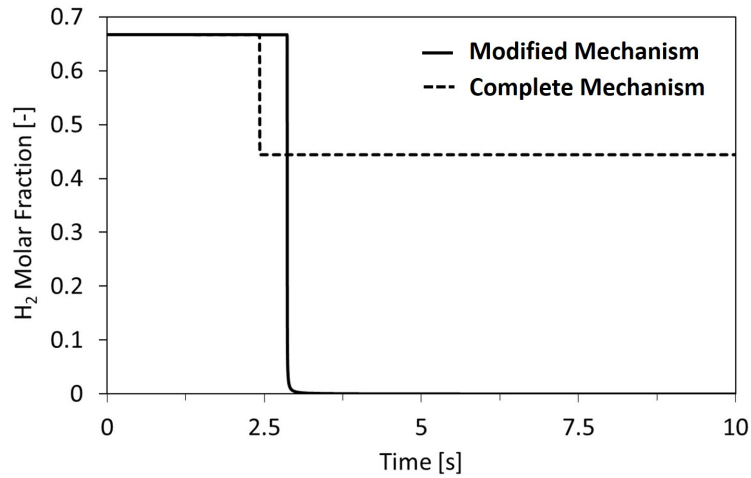
**Figure 4.15:** $H_2$ molar fraction as a function of time computed through the complete (dashed line) and modified (solid line) kinetic mechanism.

The same phenomenon can be analysed in an equivalent CSTR. The difference lies in the presence of a continuous feed of fresh reactants in the reactor. As observed for the batch, after ignition, in a time interval of few milliseconds there is the rapid decrease of the hydrogen and oxygen concentration. This can be observed in Figure 4.16, where the $H_2$ molar fraction profile is shown.
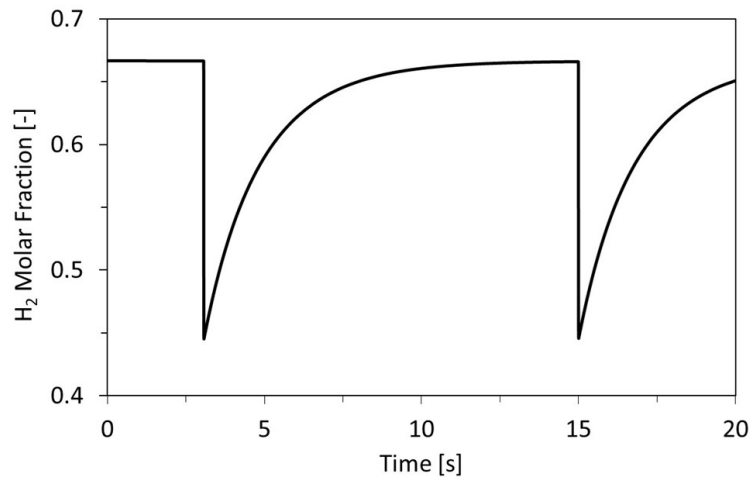


**Figure 4.16:** Hydrogen molar fraction as a function of time.

Around 2.5 s, immediately after the ignition, the switch from fast to slow reaction can be observed by the presence of a minimum in the curve which is different from zero. In the successive instants, an increase of the amount of $H_2$ in the reactor is observed. This can be explained involving the material balance of the dynamic PSR. When the system is inhibited by the branching-termination competition, the "kinetic" term responsible of the hydrogen consumption becomes smaller than the

"convective" one. This means that the rate through which the reactants, $H_2$ and $O_2$, are introduced in the reactor is higher than their consumption.

$$\left| \frac{\rho^0}{\tau} \left( y_i^{in} - y_i \right) \right| >> \left| \sum_{j=1}^{NR} v_{i,j} \cdot r_j \right| \tag{4.21}$$

Therefore a growth in the hydrogen and oxygen molar fraction can be observed, while water is progressively removed. This coincides with the "convective" region of the limit cycle. For the two-thirds of the time interval interested by convection, a function proportional to the $\exp\left(-\frac{time}{\tau}\right)$ can be used to approximate the re-accumulation of the hydrogen within the reactor volume. This expression derives from the integration of the dynamic CSTR material balance by neglecting the "kinetic" contribution. Figure 4.17 shows the overlap between the temporal profile of the hydrogen molar fraction obtained in a batch reactor and in a CSTR at the same temperature and pressure.
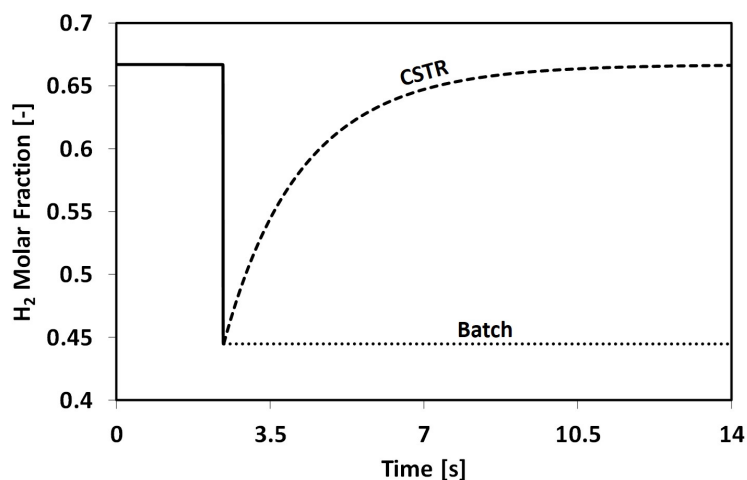


**Figure 4.17:** Temporal profile of the $H_2$ molar fraction in a CSTR and a batch reactor for the same temperature (755 K) and pressure (0.1 atm).

In the well-stirred reactor, when the "convective" term prevails on the "kinetic" one, the hydrogen re-accumulates in the system.

In case of a batch reactor, as seen above, a residual reactivity is still present in the system after the inhibition. This allows a very slow conversion of the reactants as shown in Figure 4.17 by the straight line with a negative slope near to zero. Instead, in a CSTR, the residual reactivity is completely removed by the fresh reactants fed. They interact with the small amount of radicals still present in the reactor. Since the branching-termination equilibrium is shifted to the inhibition path, as soon as a radical H reacts with an oxygen molecule, the

HO$_2$ is preferentially produced. This is related to the water influence which favors the third-body reaction with respect to the branching one. The radicals produced are then involved mainly in the termination Steps (4.11) and (4.12) responsible of the H radicals consumption. Therefore, the inlet flow rate of H$_2$ and O$_2$ leads to the complete disappearance of the active radicals in the reactor. In this way, the inhibition of the reactivity occurs, and the switch from the "kinetic" to the "convective" region can be observed. This is synonym of fast to slow transition.

### System inhibition: oscillations vs steady-state

In the "convective" region, the reactants accumulation can be observed. Then two cases can be recognized: either the stationary state achievement or the beginning of an oscillatory phenomenon.

Once fixed the reactor temperature and pressure, the controlling parameter is the residence time. A threshold representing the boundary between these two conditions exists. For a temperature of 753 K, changing the residence time from 10 s to 11 s, the system stops to oscillate and all the species reach a steady-state molar fraction. The increase of $\tau$ corresponds to a decrease of the volumetric and, consequently, of the molar flow rate. In this way, the speed through which the reactants are fed to the reactor is slower: for the same time instant, the H$_2$ and O$_2$ concentration is lower, while the water molar fraction is higher. Conversely, the amount of water in the reactor volume is higher and its inhibiting effect is stronger than the case at lower residence time. In Figure 4.18, the hydrogen and H$_2$O molar fraction profile for the two residence times are compared.
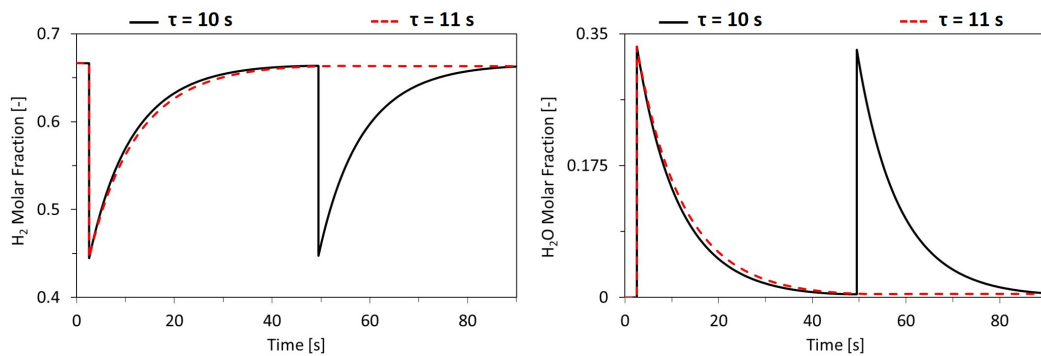


**Figure 4.18:** Hydrogen (left) and water (right) molar fraction as a function of time for two residence times: 10 s (solid black lines) and 11 s (dashed red lines).

In case of $\tau$ equal to 10 s, H$_2$ profile shows a higher concentration for the same time instant. Therefore, the consumption rate of such reactant as well as the oxygen is higher because the corresponding reaction rates are proportional to their

concentrations. Likewise, the minimum of water is located at a lower concentration. This increases the weight of the branching with respect to the third-body reaction, allowing the development of a higher reactivity in the reactor. So, in the case of higher flow rate, a new ignition can be observed since the switch from slow to fast reaction can occur. In case of higher residence time, the rate through which the reactants are introduced in the reactor is slower. This means that the amount of radicals developed is smaller than the other case. Therefore, a slow increase of the "kinetic" term occurs up to match the "convective" one, guaranteeing in this way the steady state. This condition has been defined as "1 ignition steady state". Figure 4.19 shows for the same temperature and pressure, the behavior of the $\frac{OH}{HO_2}$ and the $\frac{O}{HO_2}$ ratios as a function of residence time measured at the second ignition of the system.
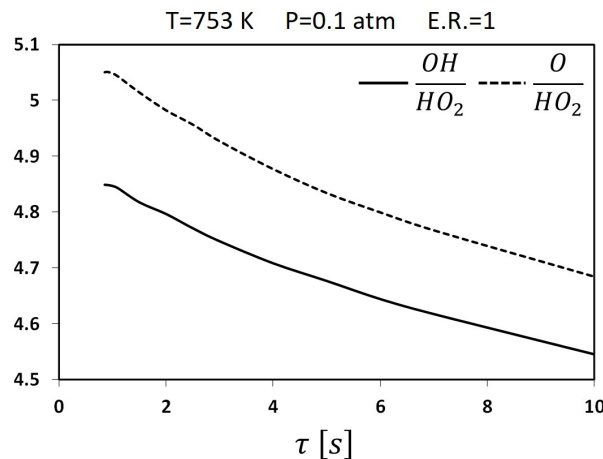


**Figure 4.19:** $\frac{OH}{HO_2}$ and $\frac{O}{HO_2}$ ratios as a function of residence time.

Such quantities reduce with the increase of $\tau$ testifying the higher weight of the third-body reaction over the branching one. This demonstrates the larger relative production of $HO_2$ with respect to more active radicals as O and OH, favored by the higher amount of water in correspondence of the following ignition. Figure 4.20 confirms such concept showing the increasing minimum molar fraction of $H_2O$ for higher residence times.

Thus, above the upper-threshold residence time, the third-body reaction is favored enough to avoid a new switch from slow to fast reaction. In this way, the "kinetic" term slowly increases up to a value equal to the "convective" contribution. Hence, the stationary state is reached. This concept is valid only for temperatures close to the ignition of the mixture.
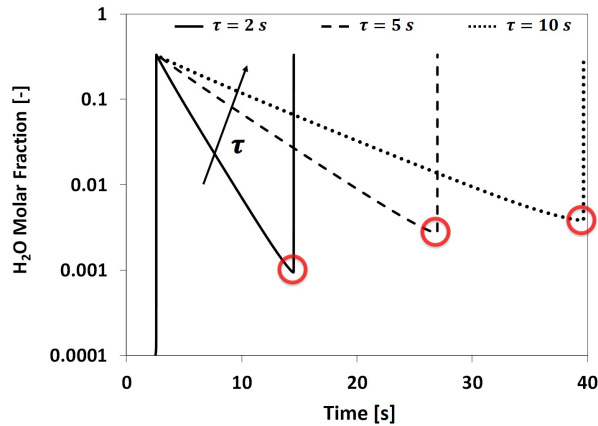
**Figure 4.20:** Water molar fraction as a function of time for three residence times: 2 s (solid line), 5 s (dashed line) and 10 s (dotted line). The red circles indicate the location of the $H_2O$ minimum for the three cases.

A further analysis can show the inhibiting effect of the higher amount of water in correspondence of the steady state achievement for high residence times. This is based on the evaluation of the ignition times of the mixtures taken at several time instants of the "convective" region. In order to perform such study, an isothermal batch reactor at the same temperature and pressure conditions is adopted. The two cases considered at the beginning of this section are again considered. For a temperature of 753 K and 0.1 atm of pressure, thus, the selected residence times are 10 and 11 s. Figure 4.21 shows the mixtures taken from the "convective" regions of the two simulations which are then analysed within corresponding batch reactors. The blue crosses indicate those mixtures which give slow reaction. Therefore, no switch from slow to fast reaction occurs. The test performed at 10 s shows one red triangle. This is the first mixture able to show a fast ignition within the batch reactor.
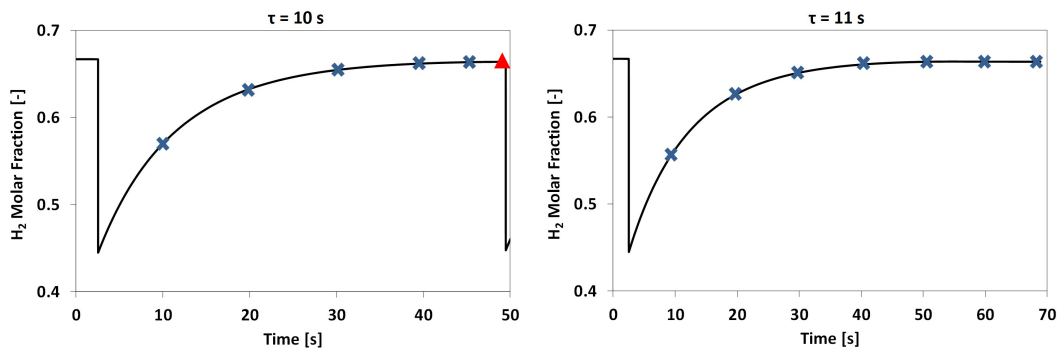


**Figure 4.21:** Temporal $H_2$ molar fraction profile obtained in well-stirred reactors at 753 K and 0.1 atm for 10 s and 11 s residence times. The symbols represent the mixtures simulated within batch reactors in the same conditions of temperature and pressure. The blue crosses indicate the slow reaction, while the red triangle represents the first mixture which ignites.

Hence, in the CSTR, after a small time interval proportional to the ignition delay measured in the batch reactor, a new transition from slow to fast chemistry occurs, thus initiating the oscillating phenomenon. Conversely, for the case at 11 s, no red crosses are present. Therefore, the stationary state is achieved in the PSR. The difference with respect to 10 s is related to the lower reactivity developed during the "convective" region. It is caused by the higher water molar fraction kept in the reactor as consequence of the lower molar flow rate exchanged with the environment.

**Lower Oscillating Limit**

In the previous sections, the kinetic analysis which allows to identify the ignition of a $H_2/O_2$ mixture has been discussed. Then, also the investigation of the system behavior after the switch from slow to fast reaction has been considered. Once fixed the operating pressure and the residence time, the Lower Oscillating Limit (LOL) can be identified as the minimum temperature at which the establishment of periodic "limit cycles" can be observed. This parameter is strongly affected by the operating conditions of the reactor, firstly by the residence time. In fact, as seen above (Figure 4.18), for the same temperature and pressure, by varying the time spent by the molecules in the reactor, it is possible to pass from the oscillating to the steady-state condition.

The properties of the P-T curve representing the LOL for the stoichiometric mixture of $H_2$ and $O_2$ are here investigated. Therefore, once selected a residence time, the Lower Oscillating Limit is a monotonously increasing curve. Figure 4.22 shows the pressure-temperature diagram where LOL obtained in a PSR with a residence time of 2 s is shown. The inlet mixture is formed by hydrogen and oxygen at stoichiometric conditions.
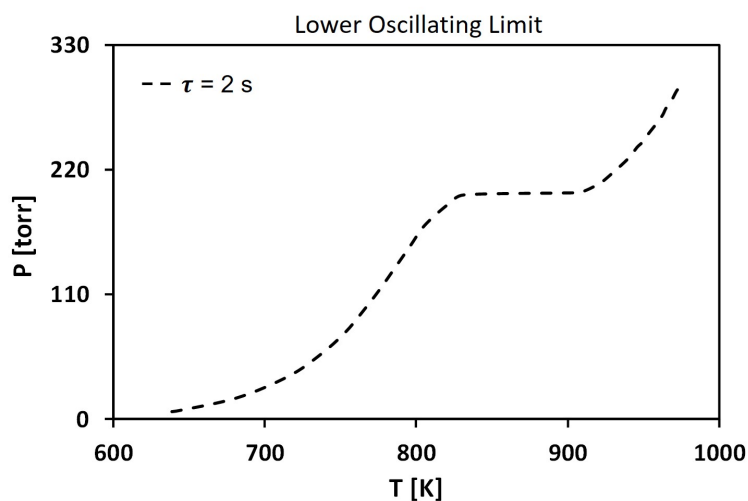
**Figure 4.22:** Lower Oscillating Limit for a stoichiometric mixture of $H_2$ and $O_2$ for a residence time of 2 s.

Specifically, at higher pressures, the corresponding temperature is located at larger temperatures. This is controlled by the competition of the branching and the third-body reaction. This concept can be qualitatively observed in Figure 4.23.
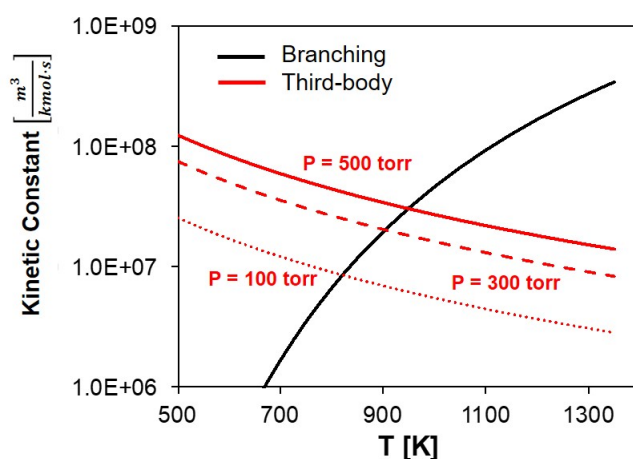


**Figure 4.23:** $H+O_2$ branching (black line) and third-body (red lines) kinetic constants as a function of temperature and pressure.

In fact, with pressure increasing, the intersection point between the two kinetic constants is shifted to higher temperatures. This is due to the stronger importance of the third-body reaction with respect to the branching for the same temperature. Such feature is related to the pressure dependence of the kinetic constant of the Reaction (4.7).

106

**Inlet composition**

The LOL is also affected by the influence of the inlet composition. There are different behaviors assumed by the P-T curve delimiting the oscillating field. The first aspect investigated is the influence of the addition of a diluent. Different cases can be taken into account as a function of third-body efficiency of the species added. Nitrogen is a neutral third body since it has the same capacity to remove energy from the excited $HO_2$ radical as the oxygen molecule. So, keeping the equivalence ratio equal to 1, but introducing such diluent, the kinetic constant of the third-body reaction is reduced. In fact, the molar concentration of the $H_2$ ($\varepsilon_{H_2} = 1.3$) is lower than the mixture formed only by hydrogen and oxygen. So LOL is shifted to lower temperatures for the same pressure. The higher the amount of nitrogen in the inlet mixture, the lower the temperature at which the oscillations occur. If $N_2$ is replaced by water, the effect generated by the diluent is opposite. In fact, the $H_2O$ third-body efficiency is 10, so the kinetic constant of the third-body reaction is drastically increased by the introduction of a small amount of such species. As a result, the Lower Oscillating Limit is then shifted to higher temperatures. An example is proposed; for a pressure of 0.1 atm, the presence of 10% of nitrogen causes the ignition temperature to decrease from 752 K to 751 K; conversely, the same amount of water shifts the LOL to 783 K from 752 K.

**Equivalence ratio**

The influence of the variation of also the equivalence ratio is considered. By increasing such quantity, the inlet molar fraction of hydrogen is higher, while that of the oxygen is reduced. In this way, the third-body kinetic constant is slightly increased. It is expected an higher LOL temperature than the stoichiometric case. From the simulations, actually, the observed phenomenon is opposite: changing for example the equivalence ratio from 1 to 1.3, the ignition temperature is increased of about 1 K. This effect is related to the amount of H radicals produced. In particular, since the molar fraction of $H_2$ is higher, the consumption of OH and O through $H_2$ molecule (Reaction (4.8) and (4.9)) is faster. As a result, the hydrogen radicals released is increased than the stoichiometric case. On the other hand, the hydroxyl and oxygen radicals are less. Figure 4.24 shows such concept. Moreover, if the H atoms are more concentrated, for the same weight of the third-body reaction over the branching one, the amount of radicals involved in the Step (4.6) is higher.

T=800 K   P=0.1 atm   $\tau = 2\,s$
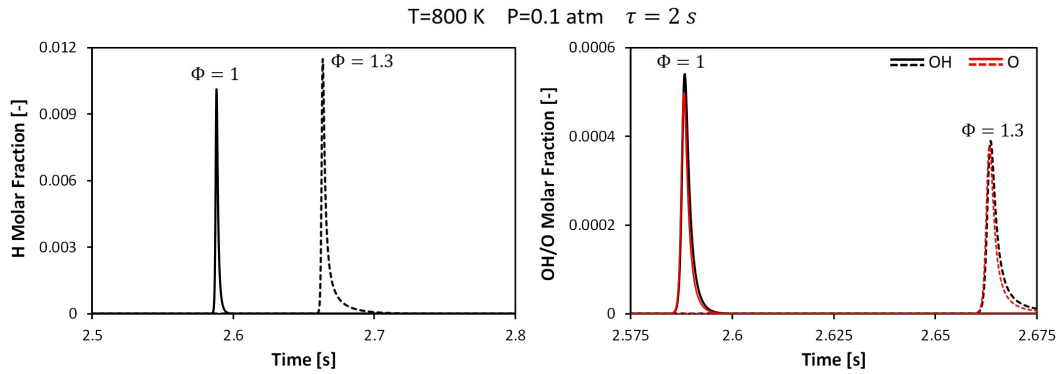
**Figure 4.24:** H, OH and O molar fractions as a function of time at two equivalence ratios: 1 (solid lines) and 1.3 (dashed lines).

In this way, for the same temperature, the developed reactivity is enhanced guaranteeing the ignition at lower temperatures. The same considerations can be done for the opposite case; when the equivalence ratio is lower than one, the hydrogen inlet molar fraction is lower than the stoichiometric mixture. Thus, oxygen is more concentrated and the third-body kinetic constant is lower because the species with the highest third-body efficiency is less. Even if the expected ignition temperature is lower, the real behavior shows an increased LOL. Also in this case, since the $H_2$ present in the reactor is lower, also the amount of H atoms produced is smaller. On the other hand, the OH and O radicals are more concentrated as confirmed by Figure 4.25.

T=800 K   P=0.1 atm   $\tau = 2\,s$
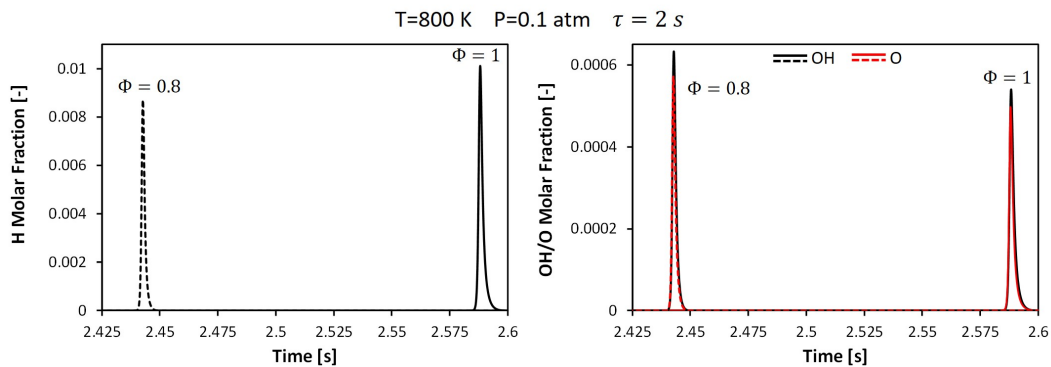
**Figure 4.25:** H, OH and O molar fractions as a function of time at two equivalence ratios: 1 (solid lines) and 0.8 (dashed lines).

Therefore, at 752 K, which is the ignition temperature of the stoichiometric mixture, the amount of hydrogen radicals released is not enough to develop a sufficiently high reactivity. A higher operating temperature is required to allow such condition. Considering an equivalence ratio of 0.8, the required temperature to observe the system ignition is 753 K. In fact, 1 degree more is able to guarantee

the development of the sufficient pool of radicals in order to ignite the system.

### 4.2.5 From Lower to Upper Oscillating Limit

In the previous section, the analysis of the location in a P-T diagram of the Lower Oscillating Limit has been described. In addition, the influence of several parameters on the LOL has been investigated. Increasing the temperature starting from the ignition one, the effects on the oscillations is investigated.

A stoichiometric $H_2/O_2$ mixture in a CSTR with $\tau = 2\,s$ at 0.1 atm is assumed as an example. In Figure 4.26, the hydrogen molar fraction is shown as a function of time in four oscillating cases: at 753 K, which is the Lower Oscillating Limit, 785 K and 815 K which are two intermediate temperatures and 842 K which represents the Upper Oscillating Limit (UOL). This is the maximum temperature above which the system stops to oscillate.
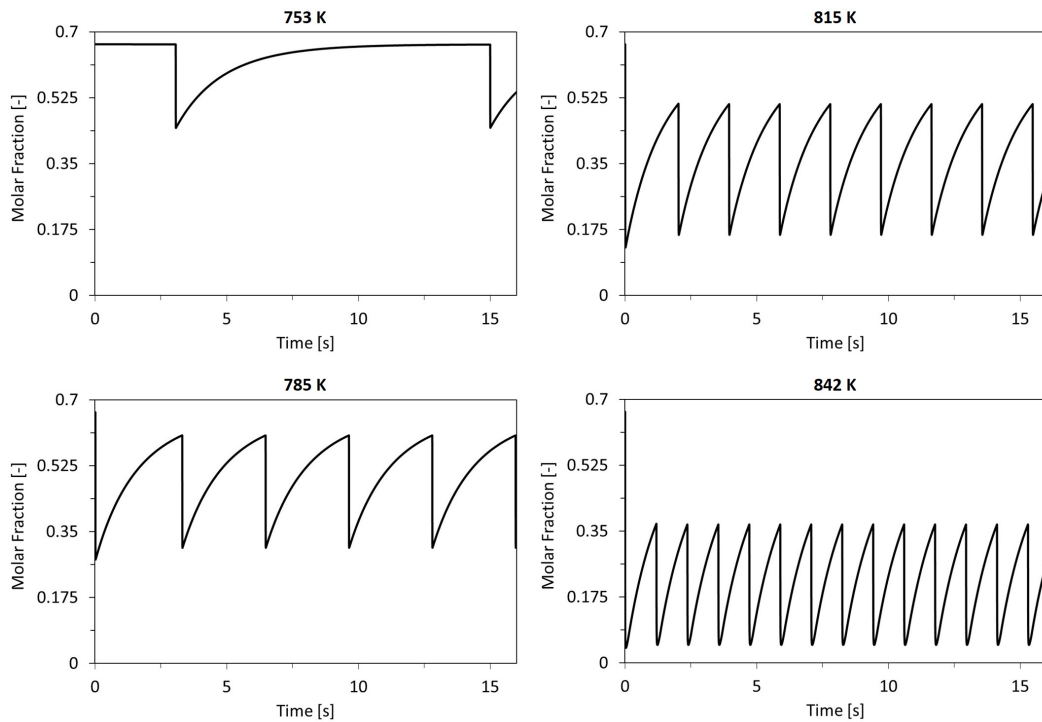


**Figure 4.26:** Hydrogen molar fraction profiles as a function of time at four temperatures: 753 K, 785 K, 815 K and 842 K.

As depicted, with the increase of temperature, defined the other parameters, the frequency of the oscillations increases. In parallel, as expectation, the time at which the first ignition occurs is shorter and the reactants conversion is higher. Also in this case, the reason has to be found in kinetics. At higher temperatures, for the same pressure, the weight of the branching over the third-body reaction

is higher as clearly shown in Figure 4.23. In order to have the inhibition of the system reactivity in correspondence of each ignition, a larger amount of $H_2O$ is required to increase the weight of the chain termination over the chain branching. The reason for which the oscillating period is reduced can be explained recalling the dynamic balance of the CSTR. When the "kinetic" term becomes lower than the "convective" contribution, the molar fraction of the reactants grows with a higher slope as the temperature is increased. This can be observed specifying the molar density through the ideal-gas law:

$$\frac{\widetilde{\rho}_0}{\tau}\left(y_i^0 - y_i\right) = \frac{P}{R \cdot T \cdot \tau}\left(y_i^0 - y_i\right) \tag{4.22}$$

Considering that the conversion is increased, the amount of hydrogen and oxygen within the reactor is smaller. So the difference between the inlet and the outlet term is larger. As a result, the time needed to fill the reactor is small and this allows to the system to re-ignite. This is because the weight of the difference in molar fraction is stronger than the temperature increase. To demonstrate the higher reactivity of the system, the temperature dependence of the $\frac{OH}{HO_2}$ and $\frac{O}{HO_2}$ ratios is considered in Figure 4.27.
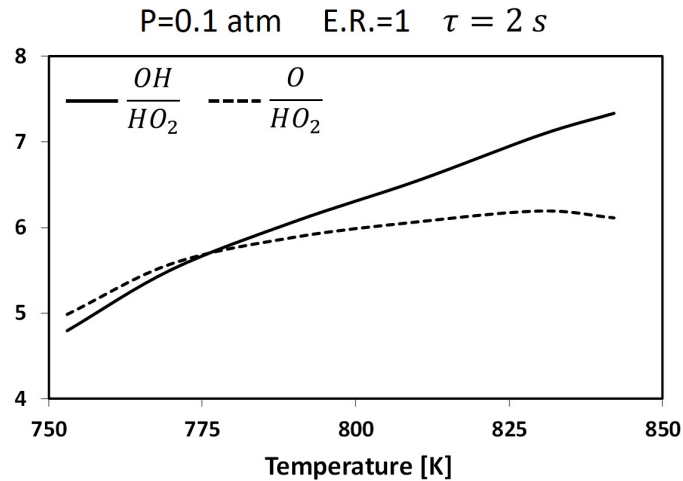


**Figure 4.27:** $\frac{OH}{HO_2}$ and $\frac{O}{HO_2}$ ratios as a function of temperature.

Both quantities are measured in correspondence of the second ignition of the system. As the temperature increases, these ratios increase as well. Therefore, the amount of active radicals O and OH produced are higher and the $HO_2$ released are lower. This occurs because the weight of the branching reaction over the third-body one grows with temperature.

### 4.2.6   Pressure variation: from LOL to UOL

The transition from the Lower to the Upper Oscillating Limit can be studied not only through temperature, but also through pressure variation. In particular, once fixed a temperature, the pressure must be reduced in order to observe such switch. Concerning the case at 753 K analysed in a well-stirred reactor with a residence time of 2 s, the Lower and Upper Oscillating Limits for the stoichiometric mixture of hydrogen and oxygen are 0.1 atm and 0.035 atm. Figure 4.28 depicts the effects of the pressure variation: as it decreases, the oscillations show an increase of the frequency and conversion while the amplitude is progressively reduced.
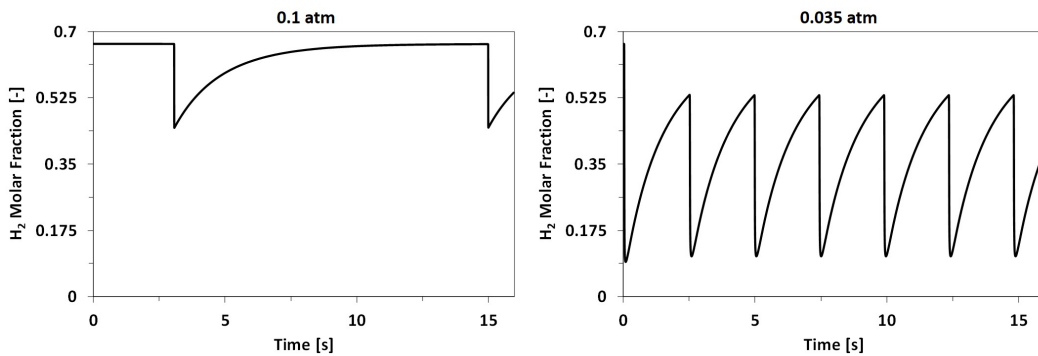
**Figure 4.28:** Temporal hydrogen molar fraction profiles obtained at the LOL (0.1 atm) and UOL (0.035 atm) for a temperature of 753 K and a residence time of 2 s.

Also in this case, the kinetic competition between the branching and third-body reaction is the cause of such behavior. In Figure 4.29 the kinetic constant of the branching reaction is compared with the third-body one evaluated at 0.1 atm and 0.035 atm. As depicted, moving towards the UOL, the weight of the chain termination is progressively reducing over the chain branching. Therefore, for the same temperature, the system can develop a higher reactivity up to a condition suitable for the steady-state achievement. Thus, below the upper-limit pressure, the amount of water developed within the reactor volume keeps the branching reaction sufficiently favored to avoid the inhibition of the system reactivity. As a result, the oscillations do not occur and for all the species, the "kinetic" contribution matches the "convective" one.

111
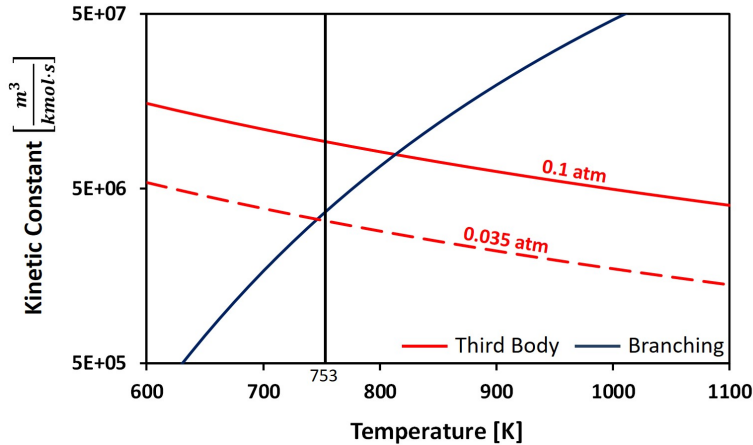
**Figure 4.29:** Kinetic constant of branching (blue solid line) and third-body reaction (red lines) as a function of temperature. Two pressures are investigated for the third-body process: 0.1 atm (red solid line) and 0.035 atm (red dashed line). Vertical black solid line indicate the operating temperature analysed in the example proposed.

This analysis can be also confirmed by the study of the $\frac{OH}{HO_2}$ and $\frac{O}{HO_2}$ ratios in correspondence of the second ignition with pressure variation as reported in Figure 4.30.
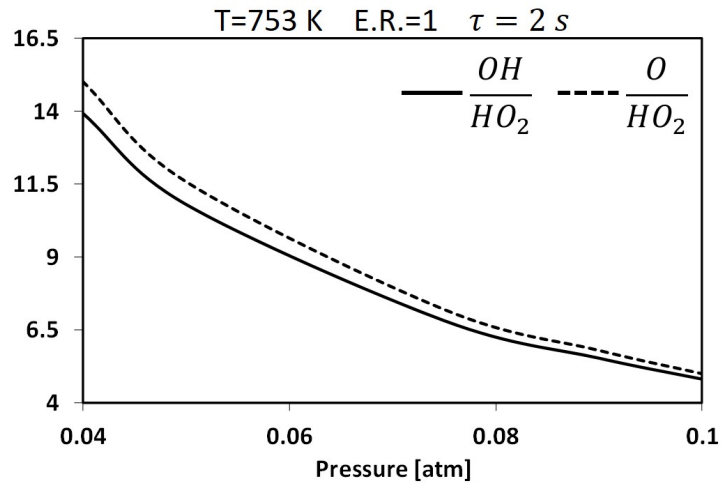


**Figure 4.30:** $\frac{OH}{HO_2}$ and $\frac{O}{HO_2}$ ratios as a function of pressure.

With the increase of pressure the amount of active radicals as OH and O released are progressively smaller, while the $HO_2$ produced are higher. This demonstrates the increasing weight of the third-body reaction over the branching with the pressure growth and, consequently, the decrease of the two ratios under analysis.

### 4.2.7 Upper Oscillating Limit

Considering a stoichiometric mixture of hydrogen and oxygen within a well-stirred reactor, the oscillating field can be identified in a P-T diagram. Two curves delimit such area: the Lower Oscillating Limit and the Upper Oscillating Limit. Above such temperature or below that pressure the system stops oscillating. Figure 4.31 couples LOL and UOL for a continuously stirred tank reactor with a residence time equal to 2 s.
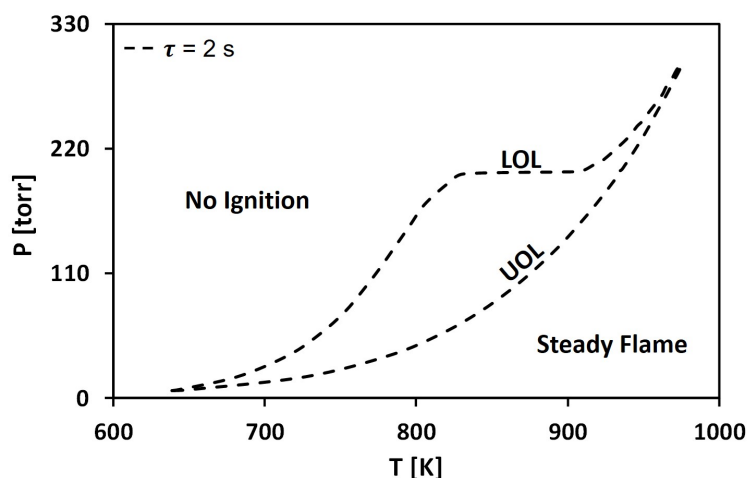


**Figure 4.31:** Oscillating field for a stoichiometric mixture of $H_2$ and $O_2$ obtained in a well-stirred reactor with a residence time of 2 s.

The Upper Oscillating Limit curve, for the same residence time tends to increase progressively with temperature and pressure. This is still controlled by the equilibrium between the third-body and the branching reaction. As seen in the previous section, only when a sufficient amount of active radicals as H, OH and O are released and kept in the reactor, the system can achieve the stationary state. Otherwise, when the chain termination generates a relevant scavenging of hydroxyl and hydrogen radicals, the reactivity is inhibited and an oscillating regime can be established.

As seen for LOL, for the same temperature and pressure, by increasing the residence time, the switch to the oscillating phenomena occurs. In fact, since the flow rate exchanged by the reactor with the external environment is reduced, the amount of H radicals removed is smaller; in this way, the ignition of the mixture occurs and the inhibition of the reactivity happens as the water is produced. Also for the Upper Oscillating Limit, the increase of residence time causes the switch from the steady to the oscillating state. In this case, the causes are different. In fact, the analysis must be performed considering the amount of $H_2$ and $O_2$

introduced in the reactor per unit of time. With respect to the LOL, the temperature and pressure conditions are such that the weight of the chain branching over the chain termination is high. In this way, the H radical is branched causing the reactivity increase. Since such path is sustained by the consumption of fresh reactants, if their flow rate is reduced, within the reactor volume the reactivity vanishes because the active radicals are consumed by the termination reactions. As a result, the inhibition of the system occurs and the switch from the "kinetic" to the "convective" region is observed.

When the operating conditions are modified such that the system stops oscillating, the mode through which the stationary state is achieved is a middle ground between the two regimes. Therefore, a damping phenomenon can be observed. Figure 4.32 shows an example of damping a case.
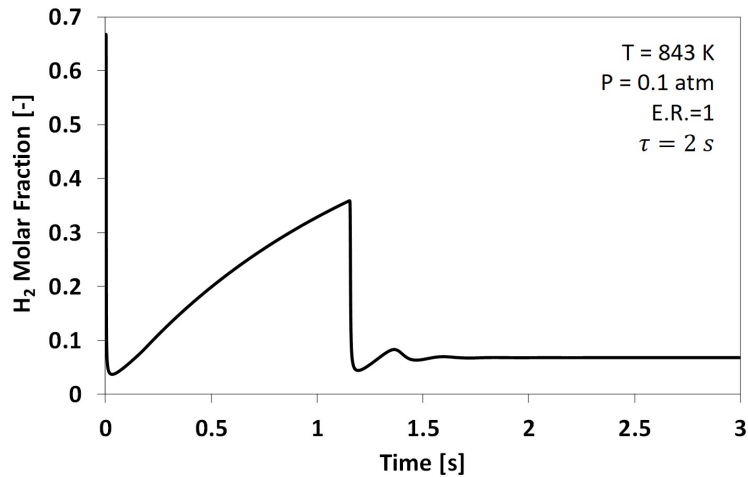


**Figure 4.32:** Hydrogen molar fraction profile as a function of time.

After the first ignition, within the reactor there is the switch from the "kinetic" to the "convective" region. The inhibition is caused by the high amount of active radicals developed during this first stage compared with the low amount of fresh reactants accumulated in the reactor volume. Therefore, a re-accumulation of the $H_2$ and $O_2$ occurs up to a second ignition. After this event, a new inhibition of the system can be observed; but, with respect to the previous one, the amount of radicals kept in the system are larger due to the higher weight of the branching over the the termination chain. As a result, the system can reach the stationary state after a damping phenomenon characterized by the continuous alternating of ignition and inhibition of the chemistry up to a matching condition between the "kinetic" and "convective" contributions for each species. At this point, the fresh reactants introduced in the reactor are continuously consumed by the reactivity

114

present in the system.

When temperature is further increased, or pressure is decreased, the damping state disappears. Figure 4.33 shows an example of steady-state oxidation for a $H_2/O_2$ mixture at stoichiometric conditions.
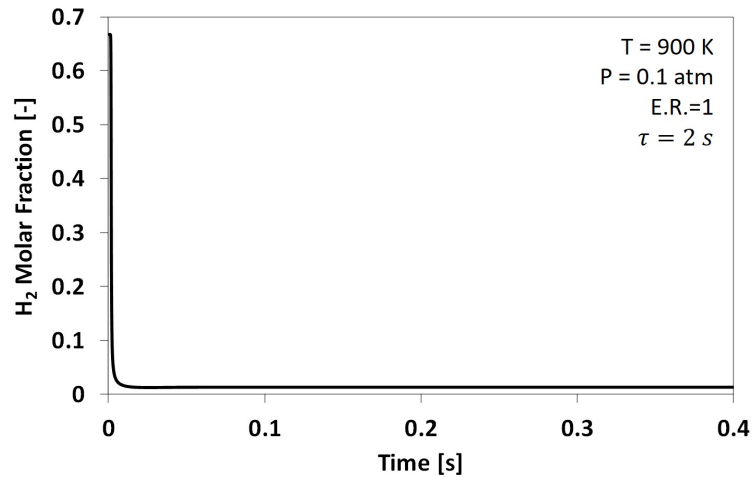


**Figure 4.33:** $H_2$ molar fraction profile as a function of time for a steady-state case.

After the first ignition, the system reaches a minimum in terms of hydrogen molar fraction. After this point, the stationary state is reached because for all the species the matching between the "kinetic" and the "convective" terms occurs. The operating conditions in terms of pressure and temperature are such that the branching reaction is more favored than the third-body one. This causes the development of a reactivity able to sustain the continuous consumption of the fresh reactants introduced in the reactor. The conversion is high, but not complete. Increasing further the temperature or decreasing the pressure, the steady-state molar fraction of the hydrogen is progressively smaller. In order to demonstrate such concept, the dynamic CSTR material balance must be recalled. With this variation of the operating conditions, the reactive term is progressively increased; in fact, the higher the temperature, the higher the reaction rates. The lower the pressure, the higher the weight of the branching reaction and the amount of active radicals developed in the system. The "convective" contribution must be further analysed:

$$\frac{P}{R \cdot T \cdot \tau} \left( y^{in} - y \right) \tag{4.23}$$

The term out of the brackets is smaller. Therefore, the difference in molar fraction must be higher in order to satisfy the matching condition between the "kinetic" and the "convective" term. This means that the molar fraction of hydrogen kept

in the reactor is progressively smaller with the increase of temperature or the decrease of pressure. Likewise, the conversion is gradually greater.

### 4.2.8   P-T-$\tau$ map

Figure 4.34 collects all the pressure, temperature and residence time dependencies of the oscillations analysed in the previous sections. In particular, the P-T map for the stoichiometric mixture of hydrogen and oxygen is provided for four residence times.
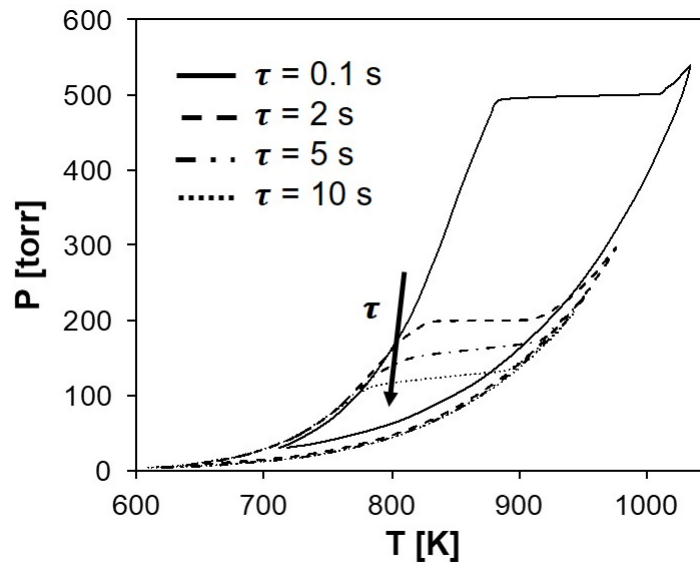


**Figure 4.34:** P-T oscillating fields computed at four residence times: 0.1, 2, 5 and 10 s.

As $\tau$ is increased, the extension of the oscillating field is reduced and confined to lower temperatures and pressures. As depicted in the figure, the part which is mainly modified is the "flat" zone. This is the part of the Lower Oscillating Limit where the pressure is kept almost constant with the temperature variation. Such region moves vertically downward with the residence time growth. For the cases from 2 to 10 s, the UOL curves are rather overlapped; the same consideration can be done for the part located at small temperatures and pressures of LOL curves. Therefore, the chemical characteristic times are much smaller than the fluid dynamic ones. This means that the convection does not affect the spatial position of the Upper and the Lower Oscillating Limits in the P-T diagram for this window of residence times. The only relevant difference lies in the "flat" curve. For the same temperature, e.g. 850 K, this line moves to lower temperatures with the residence time increase. On the other hand, for the same residence time, reducing the pressure, the system oscillates, while when increasing it the

stationary state occurs. In this last regime, in particular, after the first ignition, the fresh reactants re-accumulation can be observed by keeping the system in the slow reaction. Therefore, in case of sufficiently high residence times, there is a middle region which separates the ignition curve from the Lower Oscillating Limit in the high pressure region. In Figure 4.35, the ignition curve computed for the well-stirred reactor with a residence time of 2 s is reported.
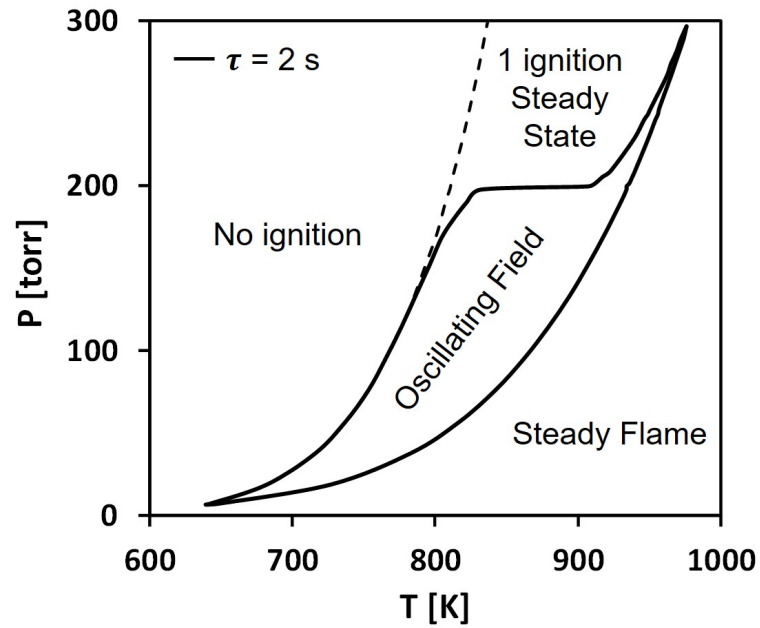
**Figure 4.35:** P-T diagram for the stoichiometric mixture of $H_2$ and $O_2$ for a well-stirred reactor with a residence time of 2 s.

## 4.3  Syngas

In the previous section, the kinetic analysis of the causes which determine the oscillating oxidation of the hydrogen within isothermal well-stirred reactors has been provided.

In order to progressively move to the study of methane oscillations, the analysis of syngas oscillating combustion must be first considered. The word syngas indicates a mixture of hydrogen and carbon monoxide with a specific $H_2$-to-CO ratio as a function of its origin. Typically, in addition to these main components, other species as $CO_2$ and methane are present. In this work, the objective in studying syngas is to understand which are the kinetic effects of the carbon monoxide addition on the oscillating oxidation of hydrogen. Therefore, a mixture of only CO and $H_2$ is considered as fuel. Several ratios of the two reactants will be examined in order to study the most important chemical paths in the different inlet mixture conditions. Also for syngas, the analysis of isothermal well-stirred reactors is performed in order to decouple all the effects of the temperature variation from kinetics.

All the reactors analysed in the following sections have a fixed volume of 550 cm$^3$ [82, 83]; the $H_2$-to-CO ratio of the several syngas mixtures investigated is always considered in molar terms.

### 4.3.1   Impact of the CO addition on the hydrogen oscillations

An initial analysis must take into account the effects on the oscillations of a small addition of CO in the inlet mixture. Therefore, an initial $H_2$-to-CO molar ratio of 100 is assumed. This corresponds to a dilution of about 6% molar of carbon monoxide. The presence of this species causes a very small variation of the extension of the oscillating field with respect to the hydrogen oxy-combustion. Considering a stoichiometric mixture of $H_2/O_2$ in an isothermal PSR with a residence time of 2 s and a pressure of 0.1 atm, oxidation occurs in an oscillating way between 753 K and 843 K. By adding CO, the ignition temperature is slightly increased to 754 K, while the Upper Oscillating Limit is almost the same. This variation is related to the third-body efficiency different from 1 of the new molecule added. Considering the Reaction (4.7):

$$H + O_2(+M) \leftrightarrow HO_2(+M) \tag{4.24}$$
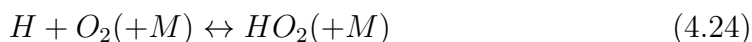
a H atom and a $O_2$ molecule react producing a $HO_2$ radical; for this process, carbon monoxide has a slightly higher capacity in stabilizing the excited $HO_2$

species than hydrogen. In fact, its third-body efficiency for this reaction is 1.9. The increase of the relative amount of CO with respect to $H_2$ in the inlet mixture causes the shift of LOL to higher temperatures. This is because for the same operating conditions, the weight of the third-body over the branching reaction is slightly higher than the case with only hydrogen; hence, an higher temperature is required in order to observe the initial switch from the slow to the fast chemistry.

During the reaction occurrence, CO is oxidized to $CO_2$. Also this molecule has an impact on such third-body reaction, since its efficiency is 3.8. But, around the ignition, the increase of the weight of the third-body over the branching reaction is smaller with respect to the case without carbon monoxide in the inlet mixture. In fact, the lower amount of hydrogen fed to the reactor causes a smaller production of water. On the contrary, $CO_2$ is highly produced and the value assumed by the molar concentration of the third body $M$ is lower than the $H_2/O_2$ system analysed in the same conditions. This can be explained recalling Equation (4.16). For the oxidation of hydrogen, the only two species with a third-body efficiency different from 1 are $H_2$ (1.3) and $H_2O$ (10). In case of syngas also CO and $CO_2$ must be taken into account. The presence of carbon monoxide causes the initial increase of the weight of the third-body over the branching reaction. For the same amount of fuel, $y_{fuel} = 0.666667$, in case of the $H_2/O_2$ system, the quantity $\sum_{i=1}^{NC} y_i \cdot \varepsilon_i$ amounts to 1.20; in case of syngas with a $H_2$-to-CO ratio of 100, the correction factor of the third-body molar concentration is 1.79. Therefore, this relatively small amount of CO causes a slight increase of the LOL. In order to generalize this concept, Figure 4.36 shows the trend of the $\sum_{i=1}^{NC} y_i \cdot \varepsilon_i$ quantity as a function of $H_2$-to-CO ratio.
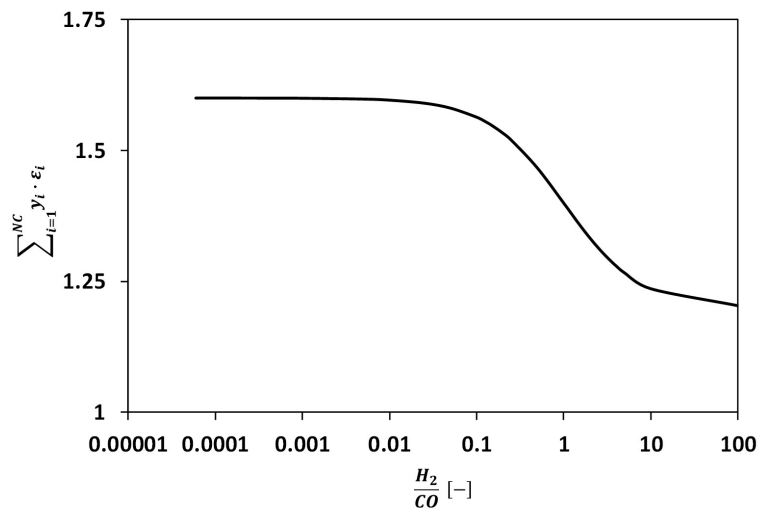


**Figure 4.36:** Correction factor for $H + O_2(+M) \leftrightarrow HO_2(+M)$ third-body reaction as a function of the inlet $H_2$-to-CO ratio.

As the carbon monoxide in the inlet mixture increases, the weight of the third-body reaction progressively grows.

The comparison between the correction factors for hydrogen and syngas is now performed around the ignition, assuming a reactants conversion of 10 %. In case of the $H_2/O_2$ system, the amount of water produced in molar fraction is about $y_{H_2O} = 0.0666667$. In correspondence of the minimum of the $H_2$ molar fraction, the quantity $\sum_{i=1}^{NC} y_i \cdot \varepsilon_i$ amounts to 1.78. Instead, for syngas, the amount of water produced is less because of the $CO_2$ presence: $y_{H_2O} = 0.066007$ and $y_{CO_2} = 0.00066007$. Then, the correction factor assumes a value equal to 1.7795, which is slightly smaller than in case of pure hydrogen. Again, the trend of the $\sum_{i=1}^{NC} y_i \cdot \varepsilon_i$ function can be studied in relation to the $H_2$-to-CO ratio through Figure 4.37. In this case, such quantity has been considered in correspondence of the minimum of the molar fraction of the reactants for the conditions of the Upper Oscillating Limit.
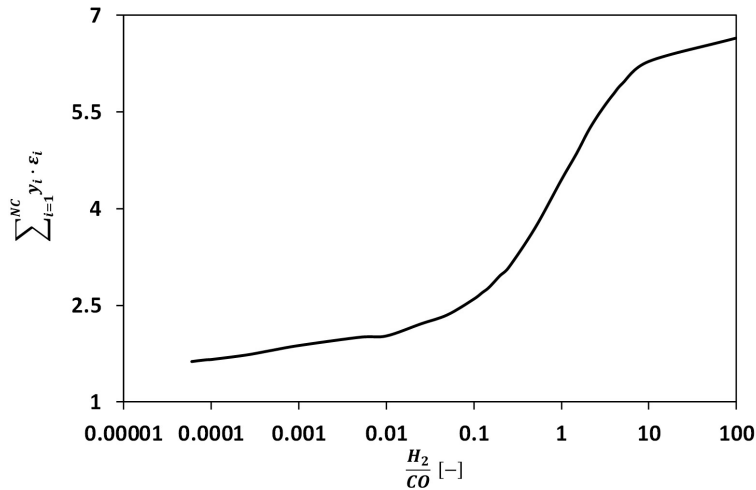


**Figure 4.37:** Trend of the correction factor for the $H + O_2(+M) \leftrightarrow HO_2(+M)$ third-body reaction as a function of the inlet $H_2$-to-CO ratio obtained in correspondence of the $H_2$ and CO minimum molar fraction in UOL conditions.

Increasing the amount of carbon monoxide in the inlet mixture, the $CO_2$ progressively produced is higher than water. Therefore, the weight of the third-body reaction progressively reduces with respect to higher $H_2$-to-CO ratio.

Coupling the two observed effects, both the Lower and the Upper Oscillating Limits are increased. The first is much more affected by this change, while the last is less sensitive since the two phenomena act in the opposite direction. Therefore, the variation of UOL is smaller than that observed for LOL. In addition, with the decrease of the $H_2$-to-CO ratio in the inlet mixture, also the $H_2O$-to-$CO_2$ ratio at the reactor outlet is progressively reduced. As a consequence, there is a condition

where the higher initial increase of the weight of the third-body over branching reaction, caused by the CO, no longer is able to counteract the lower increase of such quantity around the ignition. As a result, the Upper Oscillating Limit decreases, while the LOL increases. This can be observed by switching from a $H_2$-to-CO ratio of 2.5 to 2. UOL changes from 846 K to 845 K. Reducing again such ratio, lower temperatures are progressively needed to allow the oscillations vanishing. This is valid only until a certain value of the ratio itself; in fact, with a further decrease, the UOL returns to increase monotonously as the Lower Oscillating Limit. The cause of such behavior is related to the CO oxidation chemistry, whose importance than the hydrogen one becomes progressively more relevant.

In Figure 4.38, both the Oscillating Limits are shown as a function of $H_2$-to-CO ratio.
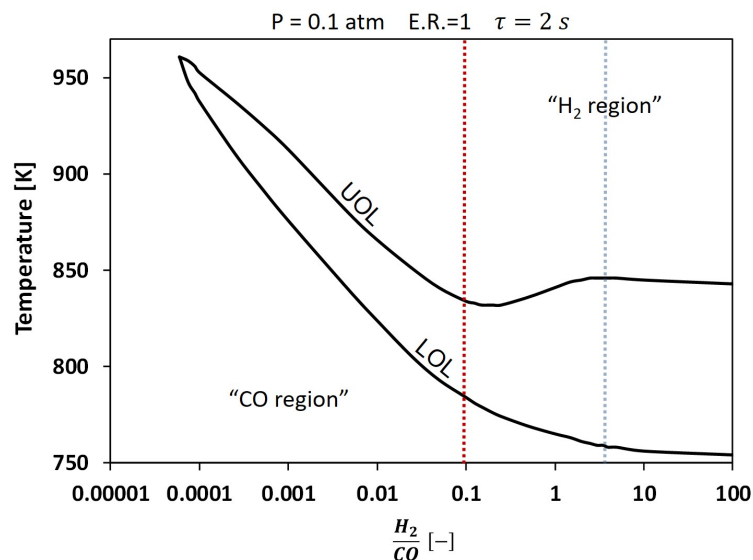


**Figure 4.38:** Lower and Upper Oscillating Limits as a function of the syngas $H_2$-to-CO ratio. They have been obtained within an isothermal CSTR with a residence time of 2 s, at 0.1 atm for a stoichiometric mixture of $H_2/CO/O_2$.

The dotted red line splits the x-axis in two regions: in the left one, the oscillations are caused by termination reactions belonging to both the hydrogen and the CO oxidation chemistry. In the next sections, such part is called "CO region". Instead, in the right part, the oscillations are controlled only by the termination reactions of the hydrogen chemistry and the CO and $CO_2$ behave as diluents in influencing such phenomenon. For this reason, it is defined "$H_2$ region". It is split up in a zone where UOL increases and one where it decreases with the $H_2$ content.

In conclusion, in this section, the analysis of both the diluent and the chemical

effects of the CO addition has been considered. This species influences the weight of the third-body over the branching reaction, causing the oscillating field variation. Its extension decreases with the increase of the relative amount of carbon monoxide than hydrogen in the inlet mixture. In this direction, LOL progressively increases; conversely, UOL has a non-linear variation which depends on the syngas $H_2$-to-CO ratio.

### 4.3.2   Kinetic mechanism in the "CO region"

If in the "$H_2$ region" the oscillating phenomenon is controlled by hydrogen chemistry and, in particular, only by the competition between the $H+O_2$ branching and third-body reaction, in the "CO region" the system is slightly more complicated.

When the syngas composition is characterized by an excess of carbon monoxide, the kinetic mechanism is mainly controlled by the reactions which convert the CO into $CO_2$. In fact, since the molar concentration of hydrogen in the inlet mixture is small, the reaction rates which involve the $H_2$ are, then, low. Therefore, as done for the analysis of the hydrogen oscillating oxidation, also for syngas, the most relevant reactions in influencing such phenomenon are proposed.

Performing a Rate of Production Analysis at a time instant immediately after the beginning of the integration, the most relevant reaction which is active in the system is the initiation reaction between a carbon monoxide and an oxygen molecule:

$$CO + O_2 \leftrightarrow CO_2 + O \qquad (4.25)$$

Since a small amount of $H_2$ is present in the inlet mixture, also the initiation reaction between an oxygen and a hydrogen molecule appears in the analysis, but with a reaction rate which is four/five orders of magnitude lower. Figure 4.39 confirms such analysis proposing the ROPA computed for the oxygen.

Rate of Production Analysis - $O_2$

| | | |
|---|---|---|
| | $O_2 + CO = O + CO_2$ | - 2.67e-11 |
| | $O_2 + H_2 = H + HO_2$ | - 6.69e-16 |
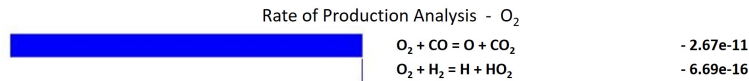
**Figure 4.39:** Example of a Rate of Production Analysis performed at the beginning of the integration for the oxygen molecule.

Therefore, in the system, at the beginning, the production and an initial accumulation of $CO_2$ molecules and O radicals occurs. This last active species can interact with both CO and $H_2$. In this first time interval, the most favored process is the reaction with the carbon monoxide because its molar concentration is much

higher than the hydrogen one:

$$CO + O(+M) \leftrightarrow CO_2(+M) \tag{4.26}$$
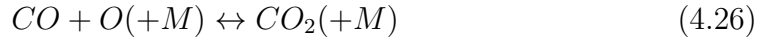
This is a termination reaction which needs to a third body to stabilize the excited $CO_2$ molecule produced. Such process is in competition with the following reaction:

$$H_2 + O \leftrightarrow OH + H \tag{4.27}$$

A hydrogen molecule is consumed by the O atom, releasing an hydroxyl and an H radical. Due to the small amount of $H_2$ present in the reactor volume, such reaction has a small rate. Therefore, the amount of active radicals as H and OH are slowly produced in the reactor. Therefore, at the beginning, the most important reactions are the initiation process which releases O radicals, immediately converted by a CO molecule to give $CO_2$. In parallel and with a smaller velocity, there is the development of a reactivity caused by the presence of hydrogen molecules. The H radical is very rapidly converted by an oxygen molecule through the branching reaction:

$$H + O_2 \leftrightarrow OH + O \tag{4.28}$$

An hydroxyl and the bi-radical O are produced. This reaction contributes to increase the system reactivity and also to ignite the system; in fact, the OH is converted principally by the CO molecule through the propagation reaction:

$$CO + OH \leftrightarrow CO_2 + H \tag{4.29}$$
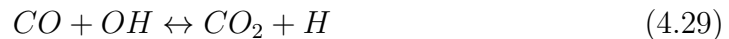
In this way, another H radical is released within the reactor volume favoring a further consumption of the oxygen molecule through the branching (4.28). Also for syngas, the third-body reaction between the hydrogen radical and the $O_2$ molecule competes with the branching itself:

$$H + O_2(+M) \leftrightarrow HO_2(+M) \tag{4.30}$$
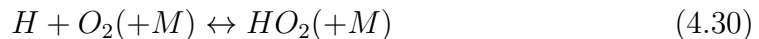
Therefore, a quite high production of $HO_2$ radicals occurs. The most important reactive paths which involve this last species after the system ignition are:

$$O + HO_2 \leftrightarrow O_2 + OH \tag{4.31}$$

$$H + HO_2 \leftrightarrow 2\,OH \tag{4.32}$$

$$H + HO_2 \leftrightarrow H_2 + O_2 \tag{4.33}$$

$$OH + HO_2 \leftrightarrow H_2O + O_2 \tag{4.34}$$

$$HO_2 + HO_2 \leftrightarrow H_2O_2 + O_2 \tag{4.35}$$
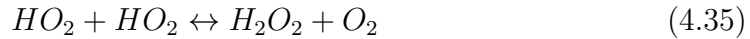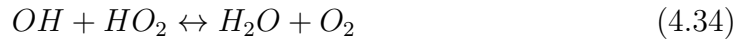
In the "CO region", with the $H_2$-to-CO ratio decrease, the O species becomes progressively the most concentrated active radical. In fact, the reduction of the amount of hydrogen in the inlet mixture causes a gradual decrease of OH and H produced. Therefore, the first reaction which consumes the $HO_2$ radical involves O, producing an oxygen molecule and an hydroxyl radical. It can be assumed as a pseudo-propagation reaction because the net number of radicals released is less than zero, but among products a radical is present. Conversely, the (4.32) is a real propagation reaction where the $HO_2$ is converted into two OH radicals through the reaction with a H atom. Finally, the last three reactions are termination processes. Their importance changes as a function of the syngas $H_2$-to-CO ratio. In Reaction (4.33) and (4.34), the $HO_2$ consumes respectively a H and a OH radical, producing hydrogen, oxygen and water molecules. Both are also present in the hydrogen mechanism and they are the cause of inhibition of the system reactivity after the ignition of the mixture in case of pure $H_2$ oxidation. On the other hand, for syngas, there is a further termination which gains importance with respect to the previous two. The recombination of the $HO_2$ radicals giving $H_2O_2$ and $O_2$ contributes to reduce the system reactivity thanks to the relative stability of the molecules produced. Compared to the $H_2/O_2$ system, in case of syngas, the termination reactions which involve the H and OH are less favored. In fact, the molar concentration of such species is smaller, due to the lower amount of hydrogen fed to the reactor.

As done for pure hydrogen oxidation, some sub-mechanisms can be identified in order to describe the causes of the oscillations. Also for the "CO region" a "chain branching" and a "chain termination" can be recognized. Different are the reactions which belong to each group.

**"Chain Branching"**

The "chain branching" has the (4.28) as first reaction. The OH radical produced is consumed by the carbon monoxide releasing a H radical and a $CO_2$ molecule. On the other hand, the O radical can interact both with CO and $H_2$. This competition is the first source of the system inhibition. In fact, the (4.26) is a termination reaction responsible of the reactivity vanishing. Therefore, from one H radical, another one is obtained and the "chain branching" becomes a "chain propagation".

Conversely, Reaction (4.27) leads to produce a new H atom and a hydroxyl radical, which is immediately consumed by a CO molecule to give a $CO_2$ and another H radical. This last process is then responsible of the development of the system reactivity. In fact, from one H radical, three are obtained. This analysis can be graphically analysed in Figure 4.40 where the schematic representation of the reactions involved in this sub-mechanism is provided.
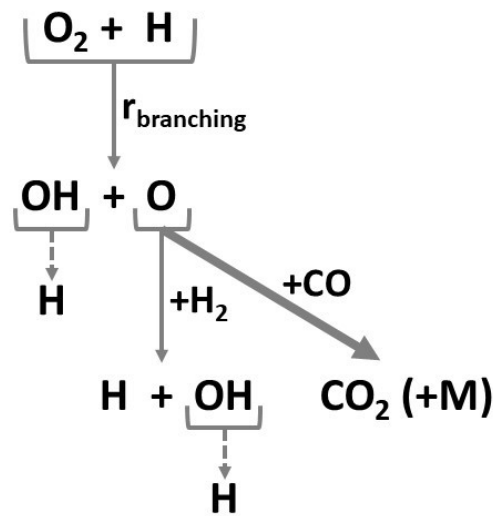


**Figure 4.40:** Schematic representation of the "chain branching" for syngas oxidation.

The difference with respect to the $H_2/O_2$ system lies in the presence of the $CO + O$ third-body reaction as alternative path for the O radical consumption to the (4.27).

In order to better understand the way these two reactions are influencing the oscillations, their competition must be further analysed. A first comparison is reported in Figure 4.41. It shows the profiles of the two kinetic constants as a function of temperature, obtained at 0.1 atm of pressure. Changing the $H_2$-to-CO ratio in the range of the "CO region", only the kinetic constant of the third-body reaction is influenced by this variation. Yet, the sensitivity of such quantity on this parameter is very small, and graphically, no differences can be observed. Therefore, only one line for the kinetic constant of Reaction (4.26) is reported.
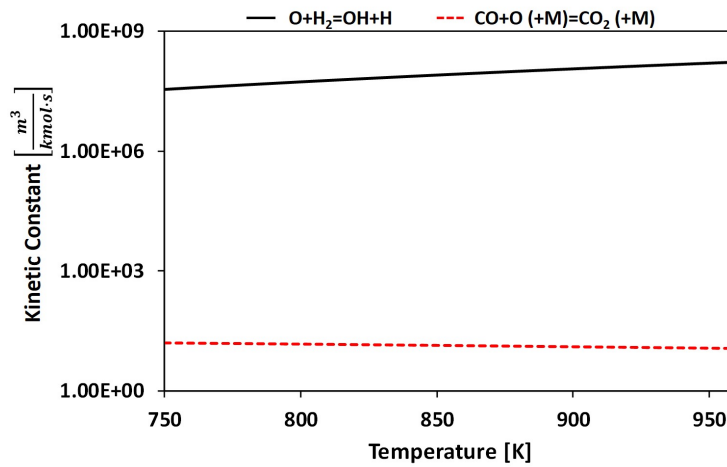
**Figure 4.41:** Kinetic constant profiles for the $H_2 + O$ (solid black line) and $CO + O(+M)$ (dashed red line) reactions as a function of temperature. The operating pressure is 0.1 atm and the syngas/$O_2$ mixture has been investigated at stoichiometric conditions.

As clearly depicted, propagation Reaction (4.27) has a kinetic constant which is much higher than the third-body one. Therefore, such analysis must be coupled with the time profile of the corresponding reaction rates obtained for an oscillating case. Several diagrams have been obtained as a function of different $H_2$-to-CO ratio in the "CO region". In fact, the weight of the third-body reaction over the propagation increases with the decrease of such ratio. This is due to the lower amount of hydrogen and progressively higher quantity of carbon monoxide. In order to confirm such analysis, the temporal profile of the ratio between the third-body and the propagation reaction has been provided. Figure 4.42 shows such comparison for three different $H_2$-to-CO ratios obtained for a corresponding temperature such that the system oscillates. As depicted, with the increase of the CO content in the inlet mixture, the first ignition is located at higher time instants even if the temperature is increased. This effect is due to the higher weight of the third-body reaction with the carbon monoxide growth in the inlet mixture. Therefore, a temperature increase is required to allow a development of a sufficiently high amount of active radicals able to ignite the system.
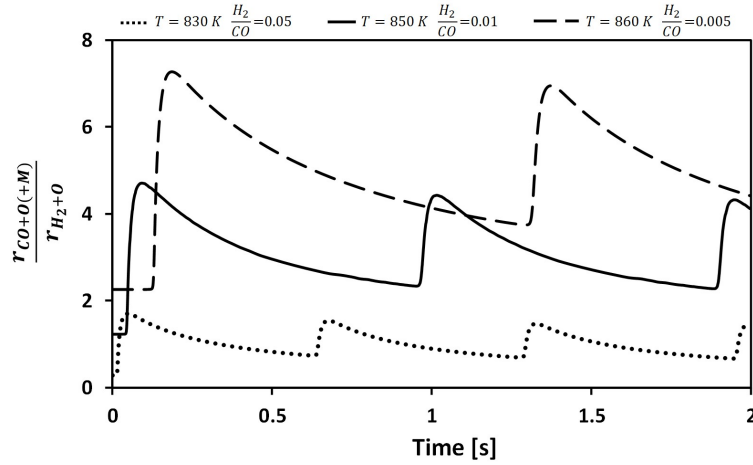
**Figure 4.42:** Ratios of the CO+O third-body reaction over $H_2$+O propagation reaction as a function of time. Three $H_2$-to-CO ratios for the inlet mixture have been considered: 0.05 at 830 K (dotted line), 0.01 at 850 K (solid line) and 0.005 at 860 K (dashed line).

The ratio of the two competing reactions grows with the reduction of the hydrogen fed to the reactor. As a consequence, the weight of the third-body reaction over propagation becomes progressively higher, causing a stronger inhibition of the system reactivity. Through this analysis, the higher the inlet content of CO, the higher the importance of Reaction (4.26) in determining the oscillations. Considering a single curve, the ratio between the two reaction rates of concern increases around the system ignition. Considering the mathematical formulation of this quantity:

$$\frac{k_{CO+O(+M)} \cdot y_{CO}}{k_{H_2+O} \cdot y_{H_2}} \tag{4.36}$$

since both the numerator and the denominator are decreasing, the growth of the ratio is guaranteed by a higher reduction of the $H + O_2$ reaction rate. Since the reactor operates in isothermal conditions, the kinetic constant of such reaction does not change with the mixture composition. Therefore, the variation of the denominator is caused only by the hydrogen molar fraction. On the other side, in the numerator if the CO molar fraction reduces, the kinetic constant of the third-body reaction grows. This is caused by the appearance of $CO_2$ and $H_2O$ within the reactor volume, whose third-body efficiencies are particularly high. Figure 4.43 shows the temporal behavior of the kinetic constant of the $CO + O$ third-body reaction for the three $H_2$-to-CO ratios of concern.
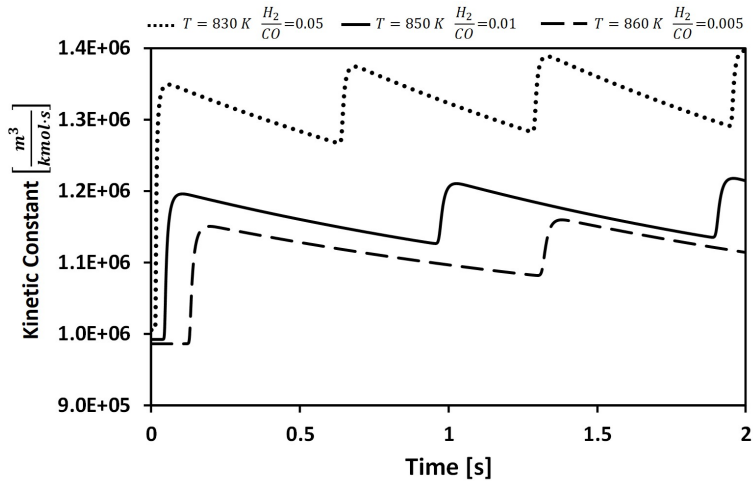
**Figure 4.43:** Time profile of the kinetic constant of the $CO + O$ third-body reaction obtained for three $H_2$-to-CO ratios: 0.05 at 830 K, 0.01 at 850 K and 0.005 at 860 K.

Instead, Figure 4.44 compares the variation of the numerator and denominator during the integration time.
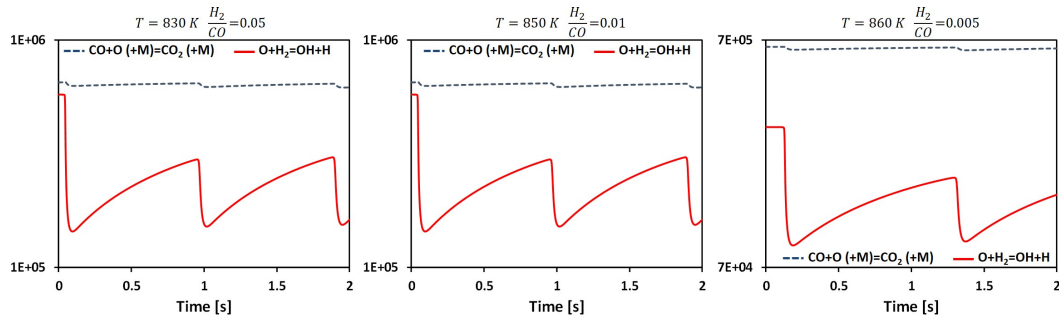


**Figure 4.44:** Time trends of the product between the kinetic constant of the $CO+O$ third-body reaction and the CO molar fraction (dashed blue lines) and of the product of $H_2 + O$ kinetic constant and $H_2$ molar fraction (solid red lines). Three diagrams are reported for three $H_2$-to-CO ratios and temperatures: 0.05 at 830 K, 0.01 at 850 K and 0.005 at 860 K.

As shown, the variation in the third-body reaction rate in the neighborhood of the system ignition is much smaller if compared to the propagation.

**"Chain termination"**

On the other side, the "chain termination" has the (4.30) as first reaction. As for pure hydrogen oxidation, the $HO_2$ radical production is the source of inhibition of the system reactivity. Figure 4.45 shows a schematic representation of the most important reactions involved in this sub-mechanism.
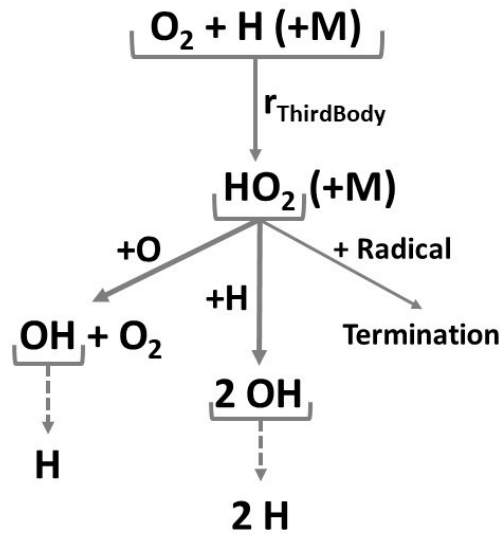
**Figure 4.45:** Schematic representation of the most important reactions involved in the "chain termination". The inlet mixture is characterized by a $H_2$-to-CO ratio belonging to the "CO region".

With respect to the $H_2/O_2$ system, in case of syngas with a $H_2$-to-CO ratio belonging to the "CO region", the $HO_2$ radical is consumed not only by Reaction (4.32), but also through the (4.31), as confirmed by Figure 4.46.
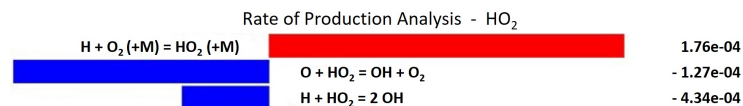


**Figure 4.46:** Rate of Production Analysis for the $HO_2$ in the "kinetic" region of a generic "limit cycle".

The first path is responsible of the consumption of one H radical, producing two OH rapidly consumed by two CO molecules to re-obtain two H atoms. It is a propagation reaction since at net, starting from the H radical consumed by the $HO_2$, another one is obtained at the end. Instead, the pseudo-propagation reaction removes a O radical releasing a new oxygen molecule and a hydroxyl radical which is immediately converted by a CO to a new H radical. Also this process can be assumed as a propagation since from the original H atom, another one is obtained at the end of the chain. The relative importance of these two reactions changes with the decrease of the amount of $H_2$ in the inlet mixture. In fact, through this variation, the H radicals produced in relation to the O atoms are progressively smaller. As a consequence, the weight of the (4.31) over the (4.32) gradually increases. In addition to these two paths, there are other processes

responsible of the $HO_2$ consumption. They are all termination reactions because they convert the $HO_2$ itself and another radical into oxygen, hydrogen and water molecules. Through these paths, the system reactivity is reduced since active species are turned into stable ones. Figure 4.47 shows these three terminations.
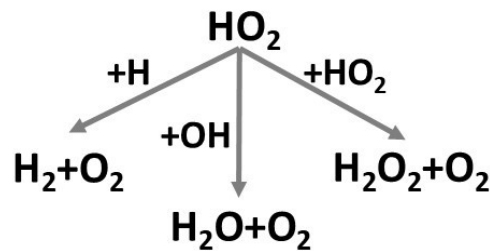


**Figure 4.47:** Termination reactions of the $HO_2$ radical.

The relative importance of these last processes changes as a function of the $H_2$-to-CO ratio. As already seen, in the "CO region", the decrease of such quantity causes the relative increase of the O radicals over H and OH. In addition, the overall amount of the active radicals produced is progressively smaller. This causes the gradual increase of the weight of the Reaction (4.35) over (4.33) and (4.34). In this way, along with $H_2$, $O_2$ and $H_2O$ also $H_2O_2$ is released in the system. For very small values of the $H_2$-to-CO ratio, $HO_2$ recombination is the main responsible of the system inhibition. In order to demonstrate such analysis, the kinetic constant of each reaction multiplied by the molar fraction of the radical which interacts with the $HO_2$ is reported in Figure 4.48 as a function of time. With the relative increase of the amount of CO with respect to the $H_2$, there is the increase of the importance of Reaction (4.31) than the (4.32). Instead, among terminations in correspondence of the reaction rate peaks, the (4.33) and the (4.34) become less relevant than the $HO_2$ radical recombination.

In conclusion, in case of syngas oxidation, for $H_2$-to-CO ratios belonging to the "CO region", the oscillations are the result of the competition of two couple of reactions. The first is between the $H + O_2$ third-body and branching reaction, while the second regards the O radical consumption through the CO and $H_2$ molecules.
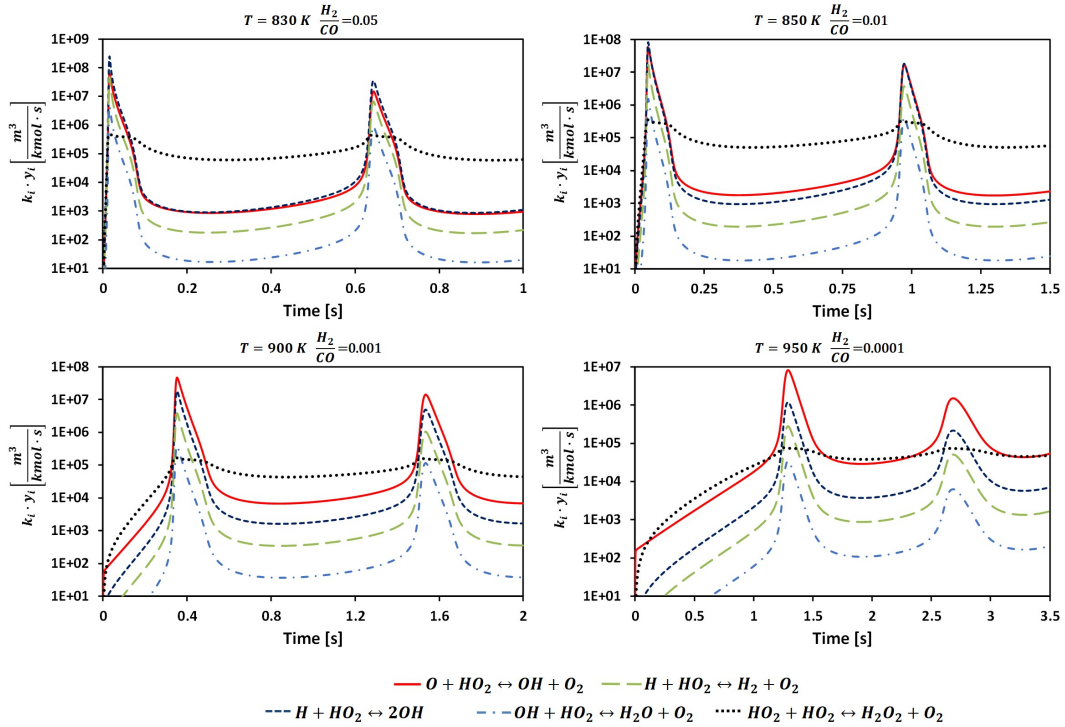
**Figure 4.48:** Time profile of the kinetic constant of each reaction multiplied by the molar fraction of the radical which interacts with the $HO_2$.

### 4.3.3 Analysis of the LOL temperature as a function of the $H_2$-to-CO ratio

In Figure 4.38, the Lower Oscillating Limit has been depicted as a function of the $H_2$-to-CO ratio at 0.1 atm. In particular, it decreases with the increase of the inlet mixture hydrogen content. Therefore, in this direction, the ignition occurs progressively at smaller temperatures. The fast conversion of the reactants can occur only if a sufficiently high amount of active radicals is developed in the reactor volume. This is controlled by two competitions:

- The $H + O_2$ branching and third-body reaction;

- $O$ consumption through $CO$ and $H_2$ molecules.

Therefore, with respect to the pure hydrogen oxidation, increasing the weight of the branching Reaction (4.28) over the third-body (4.30) is not enough in order to have the system ignition. In fact, if the $CO + O(+M)$ was favored over the competing propagation (4.26), the "chain branching" would not be able to develop a sufficiently high amount of radicals to allow the switch from slow to fast chemistry.

Concerning the "$H_2$ region", as seen above, the Lower Oscillating Limit in-

creases reducing the $H_2$-to-CO ratio. In fact, the progressively higher amount of CO behaves as diluent causing an increase of the weight of the $H + O_2$ third-body over branching reaction for the same temperature. In Figure 4.49, the comparison of the kinetic constants of these two reactions as a function of temperature is reported for the $H_2$-to-CO ratio between 0.1 and 100.
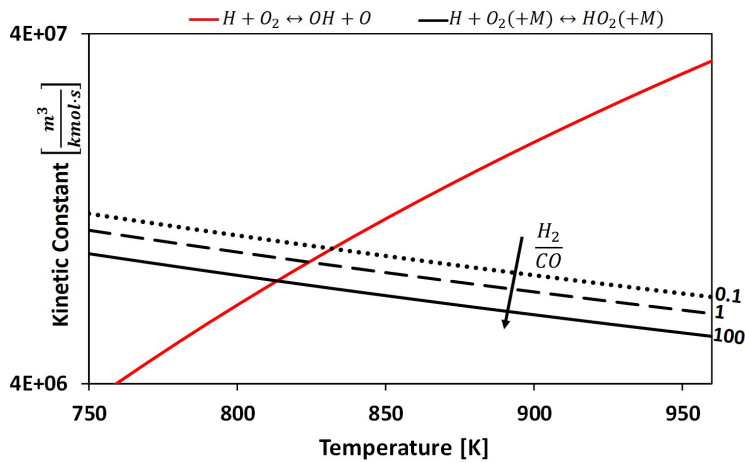


**Figure 4.49:** Kinetic constant of the branching (solid red line) and third-body (black lines) reaction as a function of temperature. Three $H_2$-to-CO ratios have been investigated: 100 (solid black line), 1 (dashed black line) and 0.1 (dotted black line).

By decreasing such parameter, the intersection point of the two curves shifts to higher temperatures. In addition, in this region, LOL is determined only by this competition. In fact, the O is preferentially consumed by the propagation Reaction (4.27) which involves the hydrogen molecule. Figure 4.50 confirms this analysis. Here, the comparison of the quantity $k_{CO+O(+M)} \cdot y_{CO}$ with the $k_{H_2+O} \cdot y_{H_2}$ is performed as a function of temperature changing the $H_2$-to-CO ratio from 0.1 to 100. As depicted, with the increase of the amount of CO in the inlet mixture, the weight of the $H_2 + O$ propagation keeps higher with respect to the $CO + O$ third-body reaction, but the relative weight progressively reduces. Therefore, once the branching Reaction (4.28) is favored over the third-body (4.30), the system can ignite, because through the "chain branching" an enough reactivity is developed in the reactor volume.
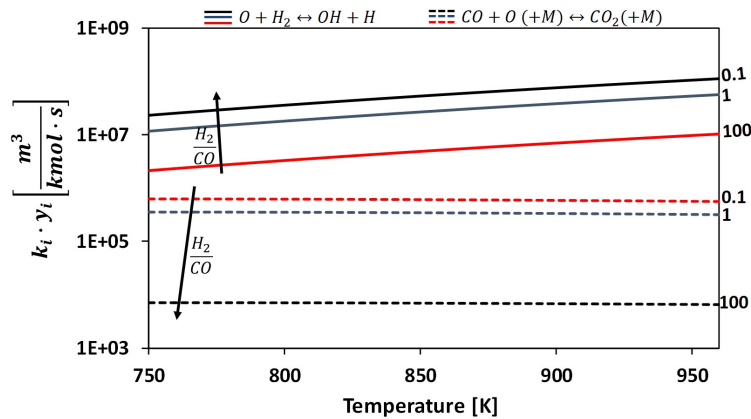
**Figure 4.50:** Comparison of the product between the kinetic constant of the $O + CO(+M)$ or $H_2 + O$ and the molar fraction of the reactant CO or $H_2$ as a function of temperature. Three $H_2$-to-CO ratios have been investigated: 100 (black lines), 1 (blue lines) and 0.1 (red lines).

Conversely, in the "CO region" with the further decrease of the $H_2$-to-CO ratio, the progressive increase of the Lower Oscillating Limit occurs. The switch from slow to fast chemistry is controlled by a different competition. In particular, the balance between the $H + O_2$ branching and third-body reaction is not responsible of the system ignition. Figure 4.51 demonstrates such analysis.
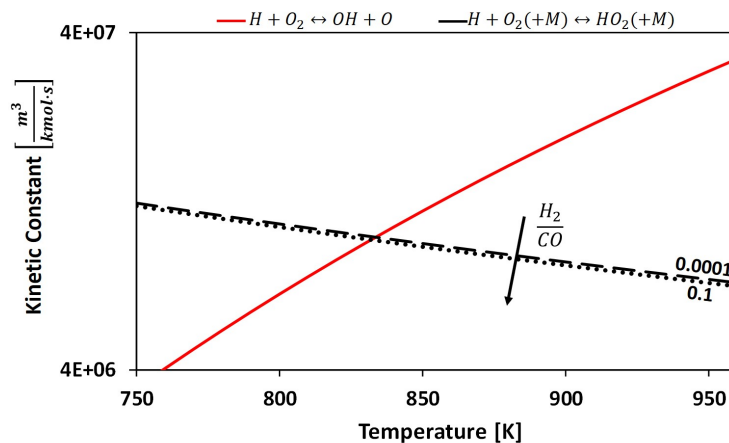


**Figure 4.51:** Kinetic constants of the $H + O_2$ branching (red line) and third-body (black lines) reaction as a function of temperature. Two $H_2$-to-CO ratios have been investigated: 0.1 (dotted line) and 0.0001 (dashed line).

It contains the comparison between the kinetic constants of these two reactions as a function of temperature for the variation of the $H_2$-to-CO ratio from 0.1 to 0.0001. The third-body kinetic constant curve slightly changes, shifting upward of a small quantity. Therefore, the competition for the $O$ radical consumption through $H_2$ and CO molecules is controlling the variation of the Lower Oscillating Limit. Figure 4.52 shows the comparison between the two quantities, $k_{CO+O(+M)} \cdot$

$y_{CO}$ and $k_{H_2+O} \cdot y_{H_2}$, as a function of temperature.
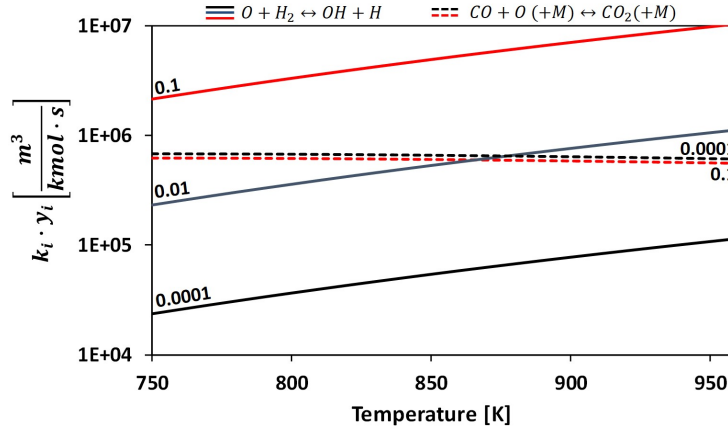


**Figure 4.52:** Comparison of the product between the kinetic constant of the $O+CO$ or $H_2+O$ and the molar fraction of the reactant CO or $H_2$ as a function of temperature. Three $H_2$-to-CO ratios have been investigated: 0.1 (red lines), 0.01 (blue line) and 0.0001 (black lines).

With the decrease of the $H_2$-to-CO ratio, the $CO + O$ third-body reaction experiences a very small variation. On the contrary, the $H_2 + O$ propagation reaction reduces very much, since the molar fraction of the hydrogen at the reactor inlet is progressively smaller. Therefore, the weight of this last process over the third-body for the same temperature is reducing. As a result, a higher temperature is required to allow to the system to develop the sufficient reactivity able to guarantee the switch from slow to fast chemistry. LOL changes from a value around 790 K for a $H_2$-to-CO ratio of 0.1 to 960 K for 0.0001. In this last point, the third-body Reaction (4.26) is more favored than propagation (4.27). Nevertheless, the system ignites because the amount of H radicals developed through the second process is equal to 2. This means that at 960 K, the O consumption through the hydrogen molecule is however able to ignite the system.

### 4.3.4   Upper and Lower Oscillating Limits of pressure

Figure 4.53 shows the Lower and the Upper Oscillating Limit in terms of pressure as a function of the syngas $H_2$-to-CO ratio. They have been obtained in a well-stirred reactor with a residence time of 2 s and an operating temperature of 800 K for a stoichiometric mixture of syngas/$O_2$.
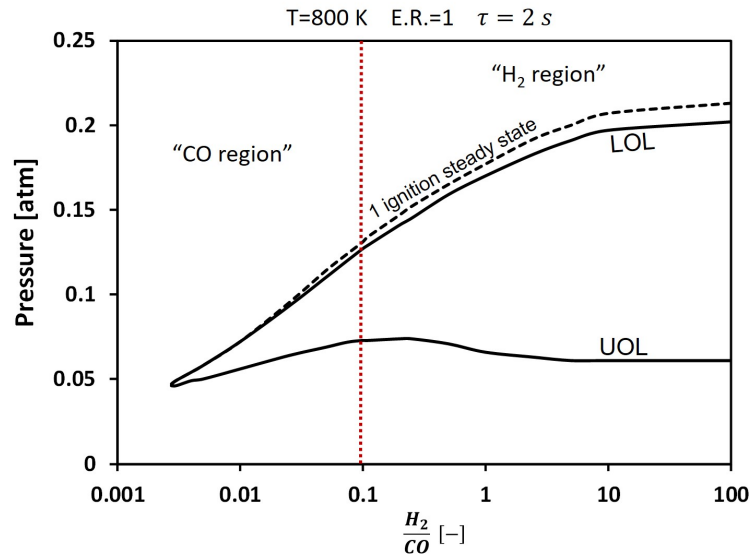
**Figure 4.53:** Lower and Upper (solid lines) Oscillating Limit curves and "1 ignition steady-state" as a function of the H$_2$-to-CO ratio.

In this case, also the "1 ignition steady-state" curve is reported. It delimits the conditions where the system shows a first ignition and, after the reactivity inhibition, the stationary state is achieved in the "convective region" (Section 4.2.4). For a fixed composition of the inlet mixture, varying the pressure from LOL to that value, the system shows a first ignition, then followed by a "convective region" within which the stationary conditions are reached. As seen for hydrogen, in this part, the "kinetic" term grows slowly up to match the "convective" contribution. The residence time is high enough, consequently the molar flow rate is sufficiently small to avoid the development of a reactivity able to re-ignite the system.

The Lower and the Upper Oscillating Limits show a behavior which is similar to the one observed for temperature. In particular, as the H$_2$-to-CO ratio is reduced, LOL reduces as well. e UOL, instead, shows a non linear behavior with the relative content of the hydrogen with respect to the carbon monoxide. Both the trends can be explained performing a kinetic analysis, similar to the one done for the temperature case. Also for pressure, the oscillating field can be divided in the "H$_2$ region" and in the "CO region". The dotted vertical red line represents the boundary which divides these two parts. For a H$_2$-to-CO ratio higher than 0.1, the oscillating phenomenon is controlled by the hydrogen oxidation chemistry. Therefore, the kinetic competition between the $H + O_2$ branching and third-body reaction causes the reactivity inhibition of the system. Hence, with the increase of the relative amount of CO, the weight of the reaction which produces the HO$_2$ radical increases due to the higher third-body efficiency of the inlet mixture. As

a result, the pressure must be decreased in order to allow an enough reactivity through the branching reaction. Figure 4.54 shows the kinetic constants of the two competing reactions as a function of pressure for a $H_2$-to-CO ratio variation from 0.1 to 100.
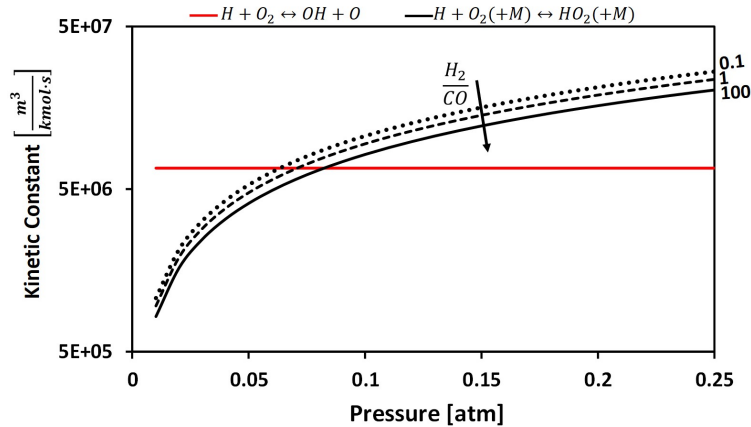


**Figure 4.54:** Kinetic constant of the $H+O_2$ branching (solid red line) and the third-body (black lines) kinetic constants as a function of pressure. Three $H_2$-to-CO ratios have been investigated: 100 (solid black line), 1 (dashed black line) and 0.1 (dotted black line).

The kinetic constant of the branching reaction does not change during the time since it is independent on pressure. Conversely, for the third-body reaction, an increase of such operating parameter causes the growth of the corresponding kinetic constant. In addition, as above explained, for the same pressure, the higher the CO content in the inlet mixture, the higher the kinetic rate. This explains the progressive reduction of LOL in terms of pressure.

For the "$H_2$ region", as the $H_2$-to-CO ratio reduces, the UOL in terms of pressure increases. This is caused by the gradual replacement of water by $CO_2$. In order to demonstrate such concept, along the Upper Oscillating Limit, the conversion in terms of both CO and $H_2$ in correspondence of their minimum has been analysed. In this way, in this position the $\sum_{i=1}^{NC} y_i \cdot \varepsilon_i$ has been computed for different $H_2$-to-CO ratios. In Figure 4.55 the behavior is represented. With the increase of the relative amount of CO in the inlet mixture, the correction factor of the third-body molar concentration decreases. This means that the weight of the third-body reaction over the branching is smaller with respect to higher $H_2$-to-CO ratios. Therefore, higher pressures allow the achievement of the stationary state.
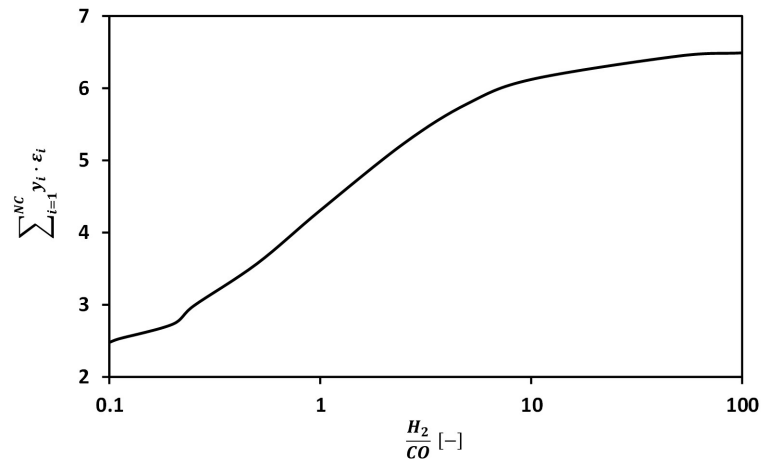
**Figure 4.55:** Correction factor of the third-body molar concentration as a function of the $H_2$-to-CO ratio for the "$H_2$ region" along UOL in terms of pressure.

The behavior of UOL and LOL in the "CO region" is thus considered. In this part, as seen for the temperature variation, they are controlled by the interaction of hydrogen with the carbon monoxide chemistry. In particular, the Lower Oscillating Limit in terms of pressure continuously decreases with the $H_2$-to-CO ratio reduction. Such behavior is not anymore controlled by competition between the $H + O_2$ branching and third-body reaction. In fact, Figure 4.56 shows how the second reaction does not significantly change with the decrease of the relative amount of hydrogen with respect to CO.
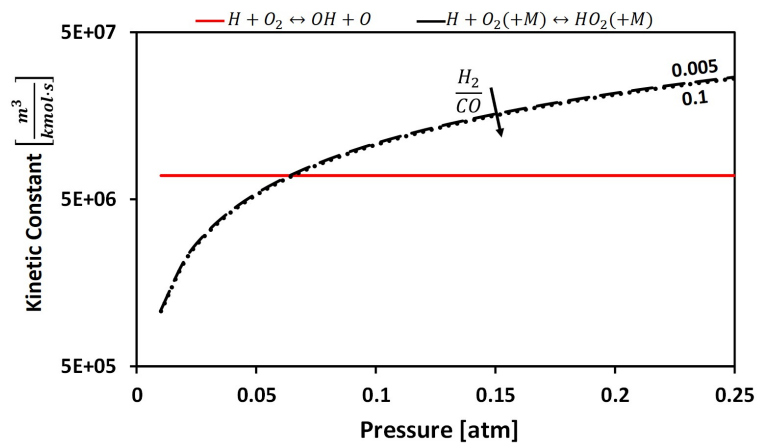


**Figure 4.56:** Kinetic constants of the $H + O_2$ branching (solid red line) and third-body reactions as a function of pressure for two $H_2$-to-CO ratios: 0.1 (dotted black line) and 0.005 (dashed black line).

Therefore, the switch from slow to fast chemistry and the location of the Lower Oscillating Limit is controlled by the competition of the $O$ radical consumption through carbon monoxide and hydrogen molecules. Figure 4.57 shows the pressure

variation of the product between the kinetic constant and the molar fraction of $H_2$ or CO for the $H_2 + O$ and $CO + O(+M)$ reactions.
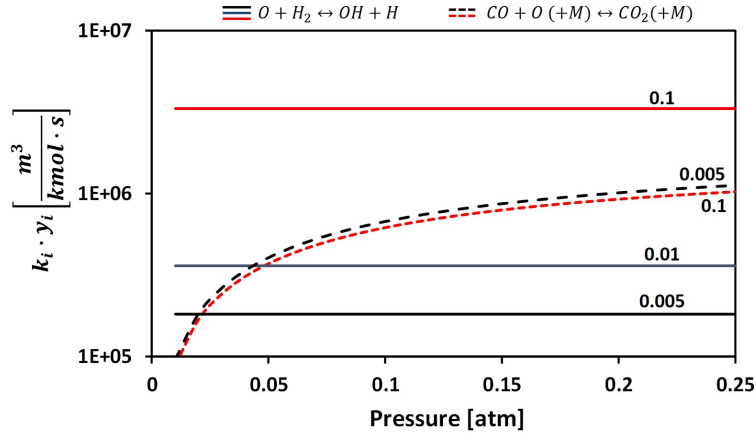


**Figure 4.57:** $k_{CO+O(+M)} \cdot y_{CO}$ (dashed lines) and $k_{H_2+O} \cdot y_{H_2}$ (solid lines) profiles as a function of pressure. Three $H_2$-to-CO ratios have been investigated: 0.1 (red line), 0.01 (blue line) and 0.005 (black line).

With the decrease of the $H_2$-to-CO ratio from 0.1 to 0.005, the third-body reaction curve is shifted upward of a relatively small quantity if compared to the variation of the propagation reaction. This last, in fact, is moved downward of a quite high amount. This is due to the progressive reduction of hydrogen content in the inlet mixture. Therefore, near the boundary with the "$H_2$ region", LOL is determined both by the hydrogen and the carbon monoxide oxidation chemistry. As the relative amount of $H_2$ is reduced with respect to the CO, the importance of the competition between the $H_2 + O$ and $CO + O(+M)$ reactions causes the gradual reduction of LOL in terms of pressure.

In the "CO region", indeed, the Upper Oscillating Limit is a continuously decreasing curve with the $H_2$-to-CO ratio reduction. This behavior can be again explained considering Figure 4.57. With the increase of the amount of CO in the inlet mixture, the intersection point between the two curves progressively moves down to lower pressures. In addition, such point is located in a position of the third-body curve which has a rather high slope. Therefore, decreasing the pressure of a small quantity, the weight of the third-body over the propagation reduces rapidly with respect to higher $H_2$-to-CO ratios. This justifies the smaller extension of the oscillating field with the decrease of the hydrogen content. As a result, the pressure must be reduced of a small amount to allow the steady state achievement because of the increased weight of the propagation reaction over the third-body one.

### 4.3.5  P-T-$\tau$ maps for syngas oscillations

As seen for the $H_2/O_2$ system, also for syngas oxidation the P-T-$\tau$ oscillating maps have been obtained. In particular, two diagrams are proposed: one for the "$H_2$ region" and one for the "CO region".

Figure 4.58 shows the map of the oscillations of a syngas/$O_2$ stoichiometric mixture with a $H_2$-to-CO ratio equal to 2. Three residence times have been investigated: 0.1 s, 2 s and 10 s.
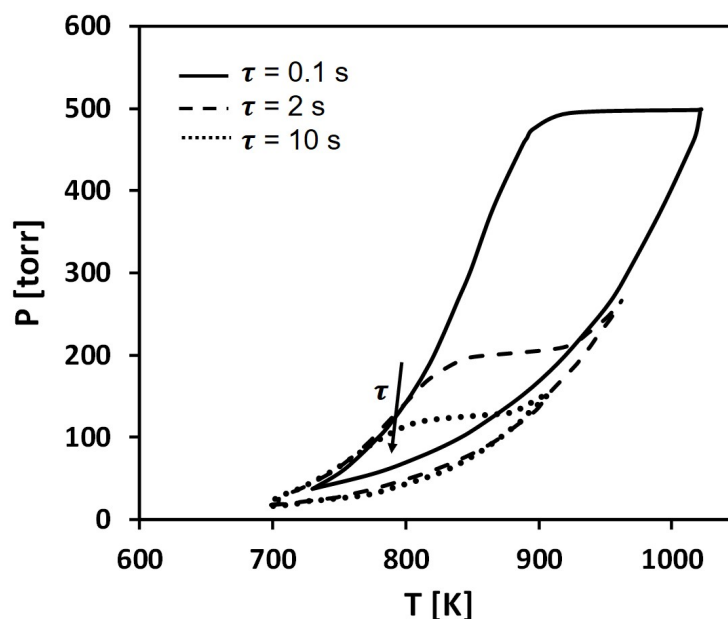


**Figure 4.58:** P-T-$\tau$ oscillating maps obtained for a syngas/$O_2$ mixture at stoichiometric condition for a $H_2$-to-CO ratio equal to 2. Three residence times have been considered: 0.1 s (solid line), 2 s (dashed line) and 10 s (dotted line).

With respect to the map obtained for the pure hydrogen oxidation, this is characterized by a smaller extension of the different oscillating fields. Such effect has been explained in the previous sections. The replacement of a part of the $H_2$ with CO causes the increase of LOL in terms of temperature for the same pressure due to the higher third-body efficiency of the inlet mixture. On the other hand, UOL is slightly reduced with respect to hydrogen case, since the weight of the $H + O_2$ third-body reaction over the relative branching is less favored; in fact, part of the water is replaced by $CO_2$ whose third-body efficiency is smaller. This results in a lower increase of the weight of the third-body over the branching reaction allowing a lower temperature for the steady state achievement.

Instead Figure 4.59 shows the P-T oscillating fields obtained for a stoichiometric mixture of syngas and oxygen with a $H_2$-to-CO ratio equal to 0.001. Three

residence times have been considered: 0.1 s, 2 s and 10 s.
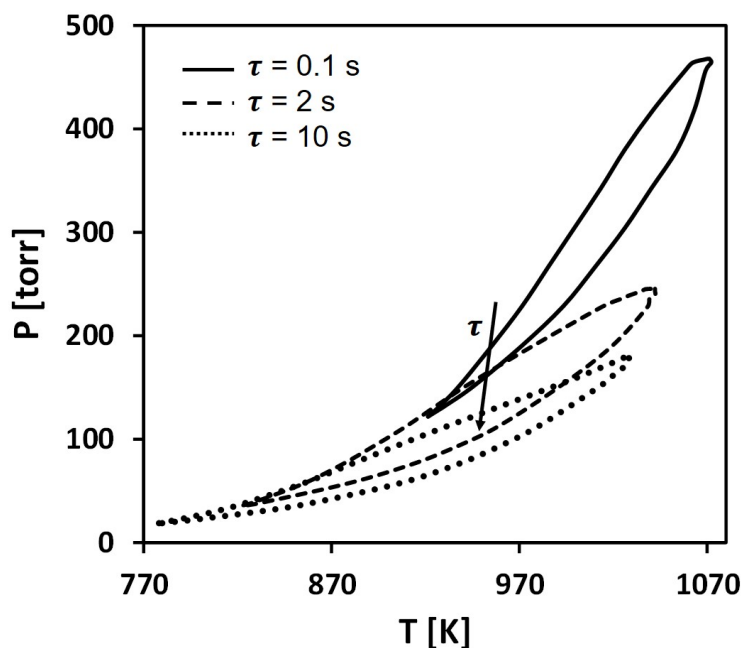


**Figure 4.59:** P-T oscillating fields for a syngas/$O_2$ mixture with a $H_2$-to-CO ratio equal to 0.001 at stoichiometric conditions obtained in a well-stirred reactor for three residence times: 0.1 s (solid line), 2 s (dashed line) and 10 s (dotted line).

With respect to the maps obtained for the pure hydrogen and for syngas with a $H_2$-to-CO ratio belonging to the "$H_2$ region", in this case, the extension of the fields is smaller. In addition, always for the same pressure, LOL and UOL in terms of temperature are higher. This is related to the different chemical competition which controls the oscillating phenomenon. The higher concentration of CO increases the importance of the $O$ radical consumption through Reaction (4.26) with respect to the one which involves the $H_2$ molecule.

Finally, the dependence of the oscillating fields on the residence time is parallel. The variation of such parameter influences the molar flow rate exchanged by the reactor with the external environment: as $\tau$ increases, the flow rate reduces. Therefore, in case of syngas with a $H_2$-to-CO ratio equal to 0.001, the sensitivity of the Upper and Lower Oscillating Limit curves to the residence time variation is higher. In particular, in this direction, they are shifted to smaller temperatures and pressures. This behavior can be explained considering separately LOL and UOL. For this last element, for the same pressure, e.g. 100 torr, for a temperature around 970 K, passing from 2 s to 10 s of residence time, the oscillations appear. As a consequence, the system is not able to develop a sufficient reactivity to sustain the fast reaction. Therefore, the system inhibition occurs as well as the

switch from "kinetic" to "convective" region. On the other hand, in case of 100 torr of pressure, the temperature corresponding to LOL is decreasing shifting from 10 s to 2 s. If these two curves coincided with the ignition curves, the opposite behavior would be expected. Instead, they represent the minimum temperature at which the system shows oscillations. Therefore, at $\tau = 10\,s$ the mixture is able to ignite for temperatures lower than the LOL obtained at 2 s of residence time, but during the first "convective" region the system achieves the stationary state. In fact, in such region, the reactants accumulation is too slow to allow the development of a reactivity able to make the system re-ignite. The region within such behavior can be observed is named as "1 ignition steady-state". Therefore, a comparison between the Lower Oscillating Limits obtained at different residence times is meaningless. For this reason, the "1 ignition steady-state" regions are provided in Figure 4.60. The higher the residence time, the higher the extension of such regions.
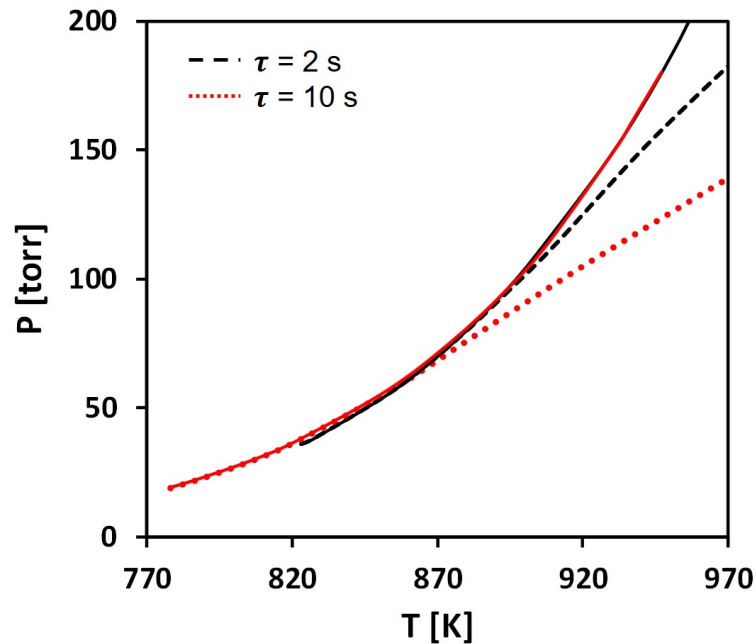


**Figure 4.60:** "1 ignition steady-state" (solid lines) and LOL (dotted lines) curves in the P-T diagram for residence times equal to 2 s (black lines) and 10 s (red lines).

### 4.3.6 Syngas oscillations for small H$_2$-to-CO

In this section, the analysis of the oscillations shapes for very small H$_2$-to-CO ratios is considered. In Figure 4.61, the time profile of the hydrogen molar fraction is reported for two oscillating cases: the first corresponds to the pure hydrogen oxidation, while the second regards the combustion of syngas with a relatively

high amount of CO.
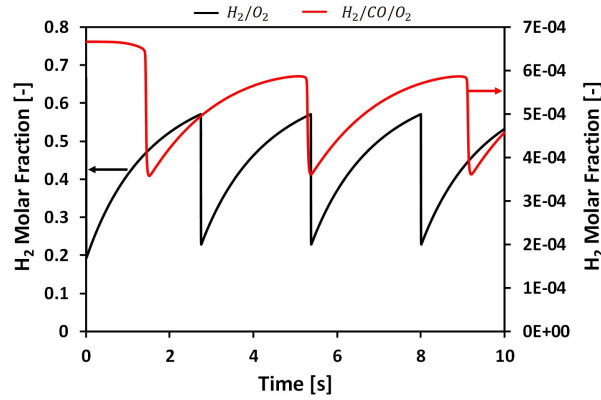


**Figure 4.61:** $H_2$ molar fraction as a function of time obtained for the $H_2/O_2$ system (black line) and syngas/$O_2$ mixture with a very small $H_2$ content (red line).

The main difference between the two curves can be observed around the ignition region. In fact, in case of $H_2/O_2$ system, the maximum point of the hydrogen is sharp: the switch from "kinetic" to "convective" region is immediate, demonstrated by the very high slope of the curve in such position. Conversely, in case of syngas, the system reactivity is lower and mainly controlled by CO oxidation chemistry. Therefore, the hydrogen molar fraction, after the peak, shows a first smooth decrease followed by a more rapid conversion of such reactant which has a lower slope if compared with the previous case. As a result, with a relatively high amount of CO than $H_2$, the oscillations assume a bell-shaped form. This is caused by the lower reactivity of the carbon monoxide with respect to the hydrogen. In order to further analyze such concept, the pure CO oxidation is considered. In this case, without hydrogen, the oscillations can not establish because the kinetic mechanism is formed only by two steps. The first is the initiation reaction:

$$CO + O_2 \leftrightarrow CO_2 + O \tag{4.37}$$

The chemical interaction of the carbon monoxide with an oxygen molecule produces a $CO_2$ and a O radical. This is immediately converted by a new CO to give carbon dioxide through a third-body reaction:

$$CO + O(+M) \leftrightarrow CO_2(+M) \tag{4.38}$$
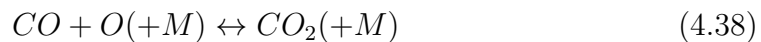
Since no branching reaction appears in the scheme, the switch from slow to fast chemistry does not occur. In fact, such chemical process is the responsible of the exponential growth of reactivity. Without such phenomenon, the fast conversion of

the reactants can not be observed and only a slow partial conversion of the carbon monoxide occurs. Such quantity is very small and around 10 %. This value can be reached only with rather high temperatures. Only in this way, the concentration of the O radicals can reach a value sufficient to allow the CO conversion, even if of a small amount. The two reactions are completely shifted to the products. The equilibrium constants are, in fact, much higher than 100 as confirmed by Figure 4.62.
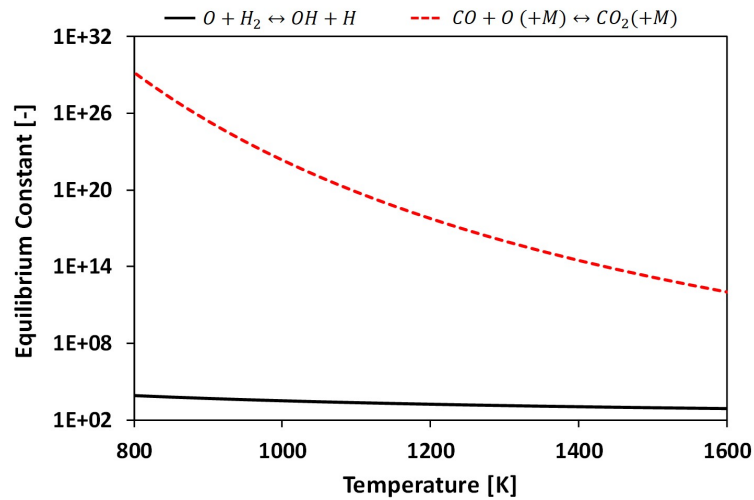


**Figure 4.62:** Equilibrium constants as a function of temperature for the $H_2 + O$ and $CO + O(+M)$ reactions.

Therefore, the backward kinetic constants are much lower than the forward ones. Coupling this analysis with the small concentration of the products themselves, the forward reaction rates are greater than the reverse. Therefore, no competition between the direct and inverse reactions is present. In conclusion, in such a system, the oscillations can not be observed because of the absence of competing reactive paths both in terms of branching-termination and forward-backward reactions.

Therefore, a small amount of hydrogen is needed to observe the switch from slow to fast chemistry. In fact, the presence of this species causes the development of the H radical in the reactor volume. Such species is consumed mainly by the oxygen molecule through the two competing reactions: the branching (4.28) and the third-body (4.30). Both the processes are responsible of the OH appearance which are source of the CO consumption as well as further H production. In this way, the progressive development of these radicals is responsible of the development of reactivity. In particular conditions of temperature, pressure and residence time, the system can ignite causing the fast consumption of the reac-

tants. Therefore, thanks to the presence of competitions between branching and termination reactions, oscillations can establish. Considering the case of very high relative amount of CO than $H_2$ in the inlet mixture, the source of the oscillating phenomenon is related to the competition in the O radical consumption, which can not be related to the third-body effects. Then, the oscillations are developed only by the chemical competition of these two reactions and since the third-body molar concentration does not change very much during the time, the only way to remove the periodic ignition and extinction of the mixture is to move to operating conditions such that this competition disappears.

## 4.4  Methane

In the previous sections, the causes determining the oscillating oxidation within isothermal well-stirred reactors have been identified for the hydrogen and syngas. Therefore, once understood all the properties for the oscillations for these two fuels, the analysis regards the methane, which is also the basis of the chemistry of all the combustion processes. The interest in such phenomenon began with the study of the methane MILD combustion. This process is able to guarantee very low $NO_x$, CO, $CO_2$ and soot emissions thanks to the relatively small operating temperature. In the last few decades, the research studies have focused their attention on investigating this alternative combustion mode [39, 85]. Several experimental data have been developed in order to try to model it; among them, the continuous-flow stirred tank reactors are present. In this devices, MILD combustion can occur in an oscillating way avoiding the achievement of a stationary state. A qualitative analysis of oscillations have been performed by the experimental activities of "Istituto di Ricerca sulla Combustione" (IRC) of Naples [78]. Experimental results have been also published by de Joannon et al. [80] and Sabia et al. [86] where they analysed the oscillating phenomenon within their non-isothermal well-stirred reactor. They built maps showing the different shapes of the oscillations in several operating temperaures, equivalence ratios and $CO_2$ and $N_2$ dilution levels of the inlet mixture. All the experiments were performed at atmospheric pressure with a measured heat exchange with the external environment of $1.3 \cdot 10^{-3} \frac{cal}{cm^2 \cdot s \cdot K}$. Recent experimental data [87] are here modeled using the "POLIMI 1702" kinetic mechanism developed at Chapter 3. Figure 3.29 shows the good agreement of the simulated with experiments in predicting the temperature window within the system oscillates.

Similar activity was carried out at the laboratory of "Centre National de la Recherche Scientifique" (CNRS) of Nancy [88], making available its data obtained in a different non-isothermal perfectly-stirred reactor. The volume is of 85 $cm^3$, the operating pressure of 800 torr and the residence time is 2 s. They investigated the combustion of $CH_4/O_2/He$ and $CH_4/O_2/CO_2$ mixtures for equivalence ratios in the range of 0.5-2 and inlet temperatures between 875-1225 K. Three inlet methane molar fractions have been investigated: 0.01, 0.025 and 0.05. As for the data of Naples, they have been simulated. In Figure 4.63, two of the six maps which compare the experimental and simulated data are reported. The model is able to predict rather well the experimental oscillating fields.
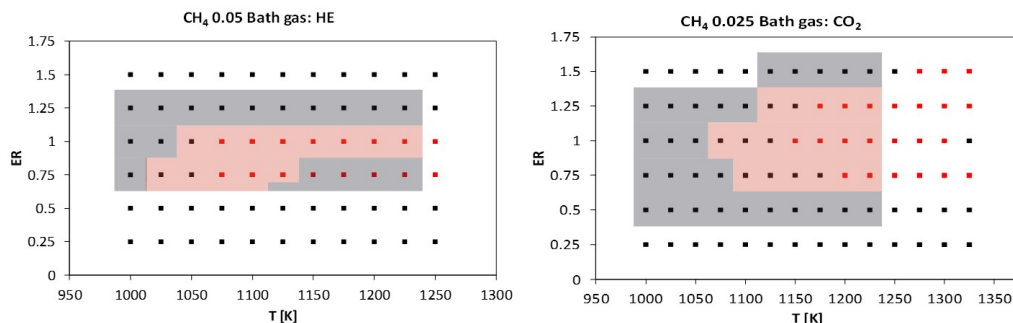
**Figure 4.63:** Oscillating maps obtained in Equivalence Ratio-Temperature diagrams for $CH_4/O_2/He$ and $CH_4/O_2/CO_2$ mixtures. The points are the simulated data, red in case of oscillations and black for stationary state achievement. The colored areas represent the experimental data: the red squares indicate the oscillations, while the grey the steady states.

Therefore, since the available model is able to well predict these data, through this tool the oscillating phenomenon is investigated in isothermal well-stirred reactors. In this way, it is possible to perform a kinetic analysis of the system decoupling the temperature variation from the kinetics itself. In all the examples proposed in the following sections, the reactor volume is 550 cm³ in order to be consistent with the analysis performed for the hydrogen and syngas oscillations.

### 4.4.1 Methane and hydrogen oscillations

Before entering in the kinetic details, an initial analysis of the shapes of the oscillating combustion of methane must be performed. Figure 4.64 shows the shape of the oscillations with the temperature variation. The investigated mixture is constituted by a molar fraction of methane equal to 0.01, at stoichiometric conditions, diluted with nitrogen. The well-stirred reactor analysed has a residence time of 2 s and it is operated in isothermal conditions. Four temperatures have been investigated. The first, 1089 K, is below the Lower Oscillating Limit. In fact, the methane is slowly reduced and it is only partially converted. Therefore, no switch from slow to fast chemistry occurs and the stationary state is achieved. Increasing of one degree the temperature, the system starts oscillating. 1090 K represents, thus, the LOL in terms of temperature for this mixture.
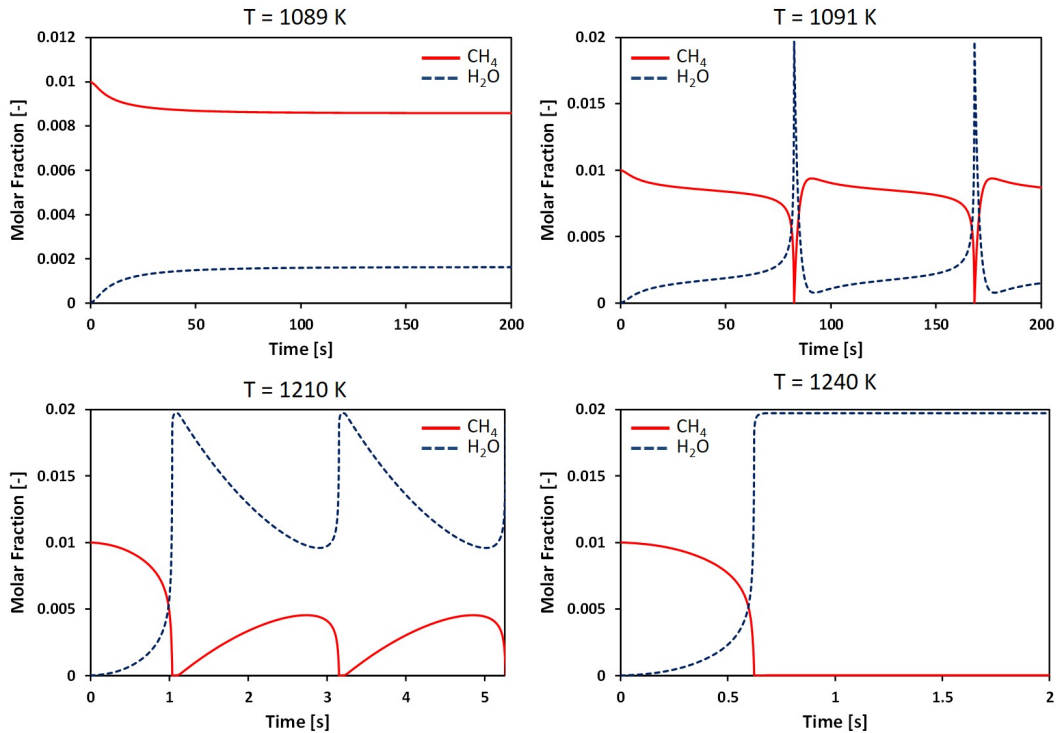
**Figure 4.64:** Methane and water molar fractions as a function of time within an isothermal well-stirred reactor with a residence time of 2 s, at atmospheric pressure for a $0.01$ $CH_4/O_2/N_2$ mixture at stoichiometric conditions.

As depicted in the figure, in correspondence of the first ignition, the methane conversion is complete. The produced water reaches a molar fraction which is near 0.02, since also the oxygen shows a consumption which is close to the 100%. This behavior is repeated equal in the second ignition. By increasing further the temperature, the time scale is reduced. This means that the oscillations frequency is higher, while the amplitude is smaller. The time interval interested by a methane molar fraction near to 0 is progressively increased. The last case considered has been obtained at a temperature above the Upper Oscillating Limit (1232 K). At 1240 K, after the first ignition, the stationary state is achieved; the conversion in terms of methane is almost complete.

Therefore, with respect to the hydrogen and syngas, the system behaves differently. In fact, the oscillations can be observed only for a practically complete oxidation of methane. If only a partial conversion of the $CH_4$ occurs, the system does not oscillate, reaching the steady state. In order to show this concept, the amount of nitrogen is progressively reduced. Switching to a methane molar fraction of 0.1, while keeping the other operating conditions unchanged, Figure 4.65a provides the time profiles of the same two species previously analysed below the LOL (1075 K).
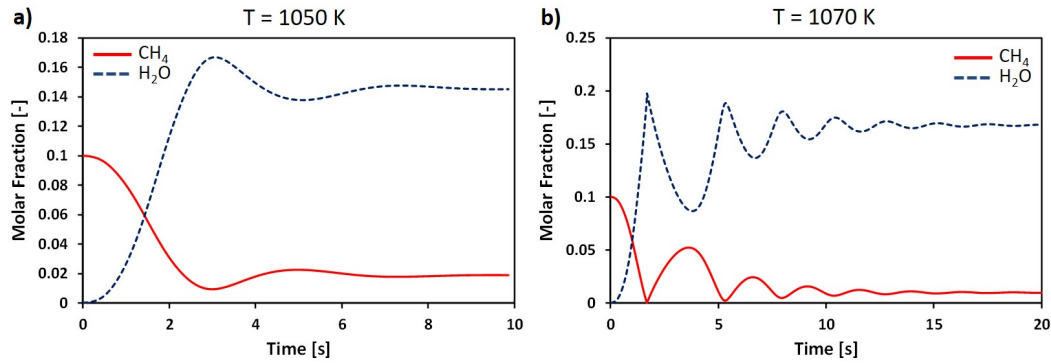
**Figure 4.65:** Methane and water profiles as a function of time. They are obtained in a well-stirred reactor with a residence time of 2 s, at atmospheric pressure, for a mixture of 0.1 $CH_4/O_2/N_2$ mixture at stoichiometric conditions.

The system achieves the stationary state in a damping way, around a methane conversion of 90%. Finally, in Figure 4.65b, the profiles are shown for a temperature near the Lower Oscillating Limit, in particular at 1070 K. In correspondence of the first ignition, $CH_4$ reaches close-to-zero molar fraction; instead, in the second one, this condition does not occur and a damping causes the steady state achievement. This is because the temperature is not sufficiently high to allow a further switch from slow to fast chemistry since the reactivity developed is small.

Another difference with respect to the hydrogen is related to the shape of the oscillations, in particular, around the ignition. As seen, the switch from slow to fast chemistry in case of $H_2$, is very rapid. Therefore, as enough reactivity is developed, the rapid reduction of the molar fraction of reactants can be immediately observed. Moreover, the slope of the curve is negative and near infinite. On the other hand, for methane, its consumption is slower as observed in the previous figures. The molar fraction of the reactants decreases gradually, giving a bell-shaped form to the oscillations. Figure 4.66 shows the comparison of the two kinds of oscillations.
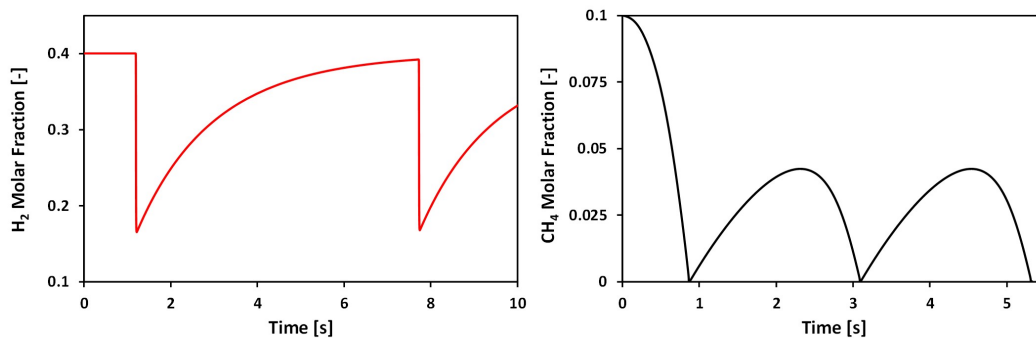


**Figure 4.66:** Hydrogen (on the left) and methane (on the right) molar fraction as a function of time.

In this first section, the main differences in terms of oscillations shape between the hydrogen, syngas and methane oxidation have been identified. They allow to conclude that the phenomenon is not controlled by the same competitions observed for the other two fuels. In fact, the system is more complicated and the analysis of several operating conditions is first performed in the next sections before entering in the kinetic details.

### 4.4.2 Limit cycle for methane oscillations

Also for methane oscillations, a limit cycle can be recognized. It is always characterized by a "kinetic" and a "convective" region. With respect to hydrogen and syngas oxidation, in this case, the "kinetic" part interests a higher time interval. In fact, the $CH_4$ is more stable and, thus, less reactive than $H_2$; therefore, the switch from slow to fast chemistry does not occur rapidly. Hence, the oscillations have a bell-shaped form, with a relatively small slope of the methane and oxygen molar fraction curves. Figure 4.67 shows an example of the limit cycle for methane oscillations.
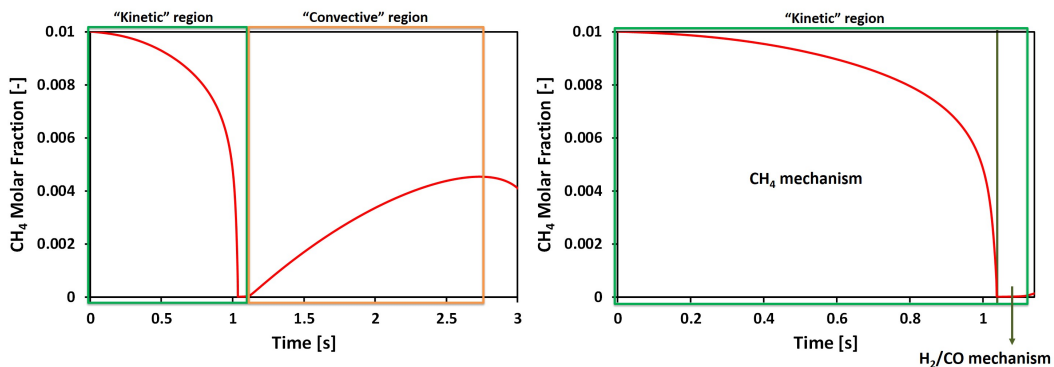


**Figure 4.67:** On the left: example of a limit cycle for the methane molar fraction time profile. The "kinetic" (green box) and "convective" (orange box) regions are shown. On the right: zooming of the kinetic region; it is divided in two parts: the left one where dominates the methane chemistry, while the right one where the $H_2/CO$ chemistry is prevailing.

In particular, on the right, the zooming of the "kinetic" region is provided. This part can be divided in two more as a function of the dominant mechanism. In the first, $CH_4$ chemistry controls the system dynamics, while in the other, when the methane is close to zero, the $H_2/CO$ kinetic scheme is dominant. In fact, in the time interval immediately before the switch from "kinetic" to "convective" region, methane and methyl radical have concentrations close to zero and the reactions which involve such species have very small rates. Conversely, H, OH and O radicals reach their molar fraction peaks and they control the chemical behavior of the system in this region, along with $O_2$, CO and $H_2O$. Figure 4.68

shows the molar fraction temporal profiles of these species in the "kinetic" region.
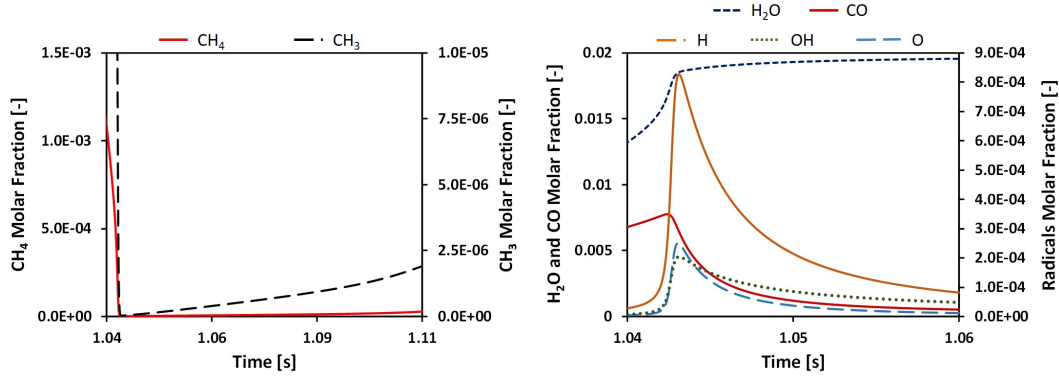


**Figure 4.68:** On the left: $CH_4$ and $CH_3$ molar fractions as a function of time in the $H_2/CO$ part of the "kinetic" region. On the right: H, OH, O, $H_2O$ and CO molar fraction profiles as a function of time always in the $H_2/CO$ part of the "kinetic" region.

### 4.4.3 Kinetic mechanism

As done for the hydrogen and syngas, also for methane, the most relevant reactions which control the system have been identified in order to find the kinetic causes of the oscillating combustion of this fuel. In this case, however, the kinetic scheme is more complicated. In fact, there are a very high number of reactions which involve a lot of different species. For this reason, the time interval interested by the "kinetic" region has been divided in two parts, as seen in the previous section. In the first, the system is dominated by the methane chemistry, while in the second by the $H_2/CO$ mechanism.

**CH$_4$ mechanism**

A small interval after the beginning of the integration, the only active reaction is the initiation which involves a methane and an oxygen molecule:

$$CH_4 + O_2 \leftrightarrow CH_3 + HO_2 \tag{4.39}$$
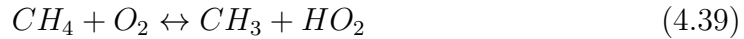
The methyl and $HO_2$ radicals start to accumulate in the reactor volume. In parallel, another initiation reaction is present, even if it is less favored; it is the third-body reaction which converts a methane molecule into a methyl and a hydrogen radical:

$$CH_4(+M) \leftrightarrow CH_3 + H(+M) \tag{4.40}$$
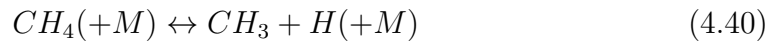
Therefore, also the H atom is released in the reactor volume. Since it is particularly reactive, it interacts immediately with methane and oxygen molecules due to their

high concentration:

$$CH_4 + H \leftrightarrow CH_3 + H_2 \tag{4.41}$$

$$H + O_2 \leftrightarrow OH + O \tag{4.42}$$

In this way, the reactivity starts developing within the reactor volume, with the accumulation of also OH and O radicals. These two species are responsible of the methane consumption:

$$CH_4 + O \leftrightarrow OH + CH_3 \tag{4.43}$$

$$CH_4 + OH \leftrightarrow H_2O + CH_3 \tag{4.44}$$
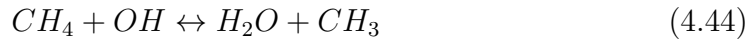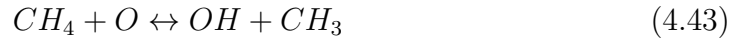
with the consequent further production of methyl radicals, which are, at this point the most concentrated species after the reactants. Figure 4.69 shows the schematic representation of the initiation where the high production of $CH_3$ radicals can be easily recognized.
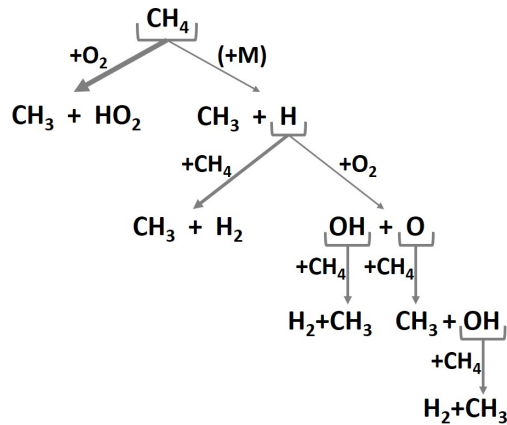


**Figure 4.69:** Schematic representation of the initiation scheme which dominates at the beginning.

In parallel, also the production of $H_2$ molecules can be observed. They start to accumulate within the reactor volume.

After the ignition, the pool of methyl radicals starts to interact with the $O_2$ molecules:

$$O_2 + CH_3 \leftrightarrow CH_2O + OH \tag{4.45}$$

As a result, further OH radicals are developed in the system and an initial accumulation of formaldehyde begins. This species interacts with the radicals present in the reactor; in this way, $CH_2O$ is converted through several reactions into HCO

Rate of Production Analysis - $O_2$

| | |
|---|---|
| $HCO + O_2 = CO + HO_2$ | - 0.030 |
| $H + O_2 = O + OH$ | - 0.013 |
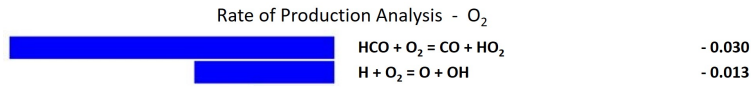
**Figure 4.70:** Rate of Production analysis for the Oxygen molecule in the "CH$_4$ mechanism" region of the "limit cycle".

radicals. This is then consumed by two paths:

$$HCO + M \leftrightarrow H + CO + M \tag{4.46}$$

$$HCO + O_2 \leftrightarrow CO + HO_2 \tag{4.47}$$
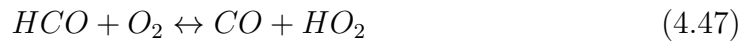
These reactions are responsible of the carbon monoxide appearing in the reactor volume. Progressively, the (4.47), along with the (4.42), becomes the most relevant paths for the oxygen consumption for this part of the "kinetic" region, as shown in Figure 4.70. The HO$_2$ radical produced tends to interact preferentially with the CH$_3$:

$$HO_2 + CH_3 \leftrightarrow CH_3O + OH \tag{4.48}$$

The CH$_3$O radical, then, is converted to give CH$_2$O through two reactions:

$$CH_3O(+M) \leftrightarrow H + CH_2O(+M) \tag{4.49}$$

$$CH_3O + O_2 \leftrightarrow CH_2O + HO_2 \tag{4.50}$$
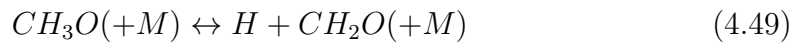
where the first is more favored than the second, causing also the development of higher reactivity due to the H radical released at place of the HO$_2$.
In competition with the (4.48), there is the termination which is the reverse of the first initiation reaction:

$$HO_2 + CH_3 \leftrightarrow CH_4 + O_2 \tag{4.51}$$
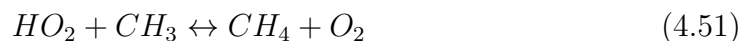
In the time interval immediately before the switch from the CH$_4$ to the H$_2$/CO chemistry, there is a further termination reaction which interests the system; it is the reverse of the second initiation:

$$CH_3 + H(+M) \leftrightarrow CH_4(+M) \tag{4.52}$$
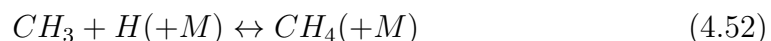
A third termination can be identified in this first part of the "kinetic" region; it is the consequence of the high production and accumulation of the CH$_3$ radicals. Their third-body recombination takes place causing the production of the ethane

molecule:

$$CH_3 + CH_3(+M) \leftrightarrow C_2H_6(+M) \tag{4.53}$$
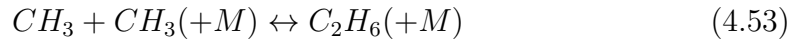
The interaction of this species with active radicals causes the release of $C_2H_5$. As soon as it appears in the system, it is immediately converted through the third-body reaction to give the ethylene molecule:

$$C_2H_5(+M) \leftrightarrow H + C_2H_4(+M) \tag{4.54}$$
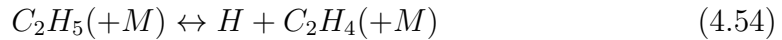
This last relatively stable molecule interacts mainly with O and OH through different paths whose products are mainly $CH_3$ and CO. This last reaction, furthermore, is one of the main source of the H radicals for the methane mechanism section. In conclusion, the mechanism which controls the methane consumption is then reported in Figure 4.71.
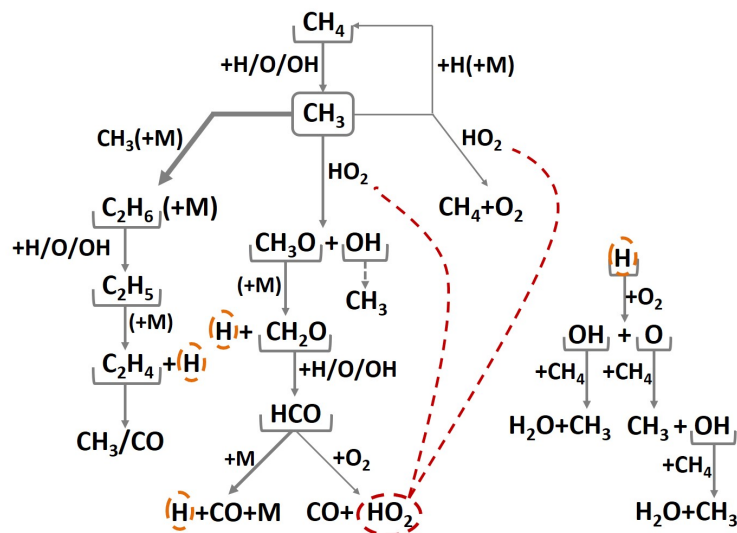


**Figure 4.71:** Schematic representation of the kinetic mechanism which controls the methane conversion. On the right the main mechanism responsible of the H radical consumption.

The switch from "$CH_4$ mechanism" to "$H_2$/CO mechanism" occurs when methane and methyl molar concentrations are near to zero in the reactor volume.

## $H_2$/CO mechanism

The name given to this section of the "kinetic" region is related to the kinetic mechanism which controls the system. In fact, when methane reaches a molar fraction close to zero, also methyl radicals, ethane, ethylene disappear from the system. On the other side, the reactivity continuously increases. This is related to the presence of a relatively high amount of $H_2$, $O_2$ and CO, along with a pool of

H, OH and O radicals. At this point, a fast consumption of the oxygen, hydrogen and carbon monoxide occurs, with the rapid increase of water and $CO_2$.

At the beginning, since methane is not present anymore, the hydroxyl radicals are consumed mainly by hydrogen molecules:

$$H_2 + OH \leftrightarrow H_2O + H \qquad (4.55)$$
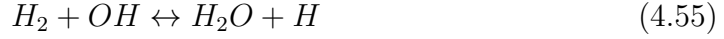
OH consumption occurs also through the reaction with the CO molecule:

$$CO + OH \leftrightarrow CO_2 + H \qquad (4.56)$$

Initially, this second process is less favored than the first since its kinetic constant is lower. Anyway, the amount of developed H radicals is increasing. They are consumed principally by the oxygen still present in the reactor, through the branching Reaction (4.42). With respect to the "$CH_4$ mechanism", here the hydroxyl and O radicals are consumed by different reactions; the OH is still converted by $H_2$ and CO, while O through $H_2$ itself and water:

$$O + H_2 \leftrightarrow OH + H \qquad (4.57)$$

$$O + H_2O \leftrightarrow 2\,OH \qquad (4.58)$$

In competition to the branching reaction which is responsible of the growth of the system reactivity, the third-body reaction between the H radical and $O_2$ molecule occurs:

$$H + O_2(+M) \leftrightarrow HO_2(+M) \qquad (4.59)$$
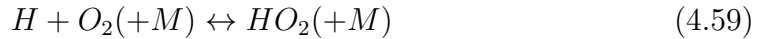
It is responsible of the conversion of the two reactants into the $HO_2$ radical, which is relatively stable if compared with OH and O produced through the (4.42). Therefore, the same competition seen for hydrogen and syngas occurs in this small time interval. The $HO_2$ radicals produced are very rapidly consumed through several reactions, since the reactivity in the system is high:

$$H + HO_2 \leftrightarrow 2\,OH \qquad (4.60)$$

$$H + HO_2 \leftrightarrow H_2 + O_2 \qquad (4.61)$$

$$O + HO_2 \leftrightarrow OH + O_2 \qquad (4.62)$$

$$OH + HO_2 \leftrightarrow H_2O + O_2 \qquad (4.63)$$
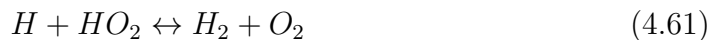
The first is a propagation reaction which releases two OH radicals; the second is

in competition with the previous one and it is a termination because produces a hydrogen and an oxygen molecule. On the other hand, the third reaction is a pseudo-propagation; in fact, among reactants three radicals are present, while only one can be recognized in between products. Finally, the last process is another termination which consumes a OH radical producing a water and an oxygen molecule. Figure 4.72 shows the schematic representation of the kinetic mechanism which controls the system dynamics in this second part of the "kinetic" region.
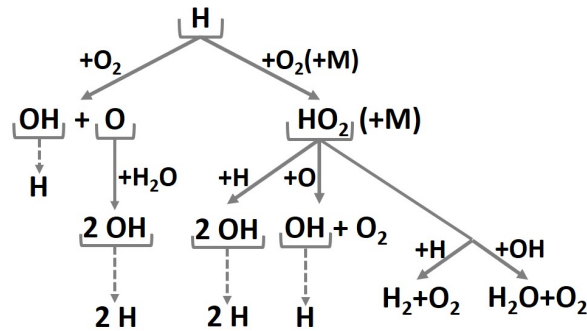


**Figure 4.72:** Schematic representation of the "$H_2$/CO mechanism" of the "kinetic" region of the methane limit cycle. The dashed arrows indicate the fast conversion of OH radicals through the interaction with $H_2$ and CO.

The competition between the third-body and the branching reaction must be further analysed. With respect to the hydrogen and syngas systems, in case of methane, the behavior of these two reactions is different. Around the peaks of the H, OH and O radicals, the time profile of the two reactions can be observed in Figure 4.73. In the first time interval, both the net reaction rates grow with a similar slope; the third-body is less favored than the branching and this allows the active radicals development and accumulation. Around the time instant equal to 1.04 s, the two quantity under analysis reach the corresponding peaks and the relative weight of the (4.59) over (4.42) is still lower than 1, but higher than the previous time instants. After the maximum points, the net rate of the branching reaction reduces with a particularly high slope, becoming lower than the third-body one.
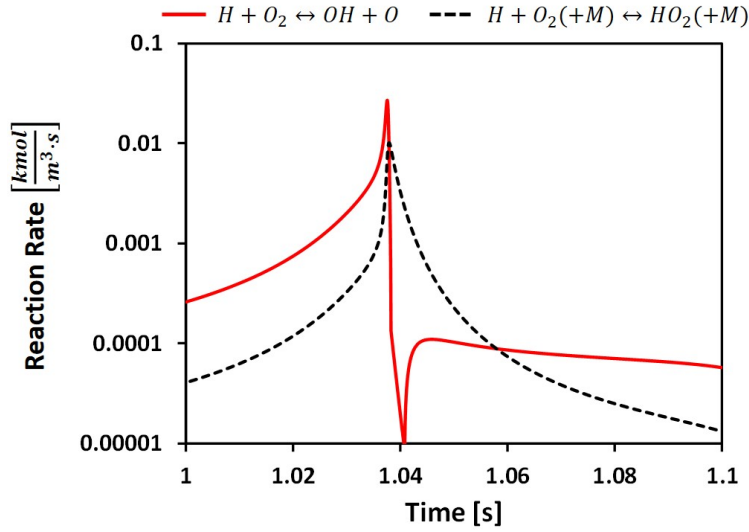
**Figure 4.73:** Branching (solid red line) and third-body (dashed black line) reaction rates as a function of time around the OH, O and H peaks.

In this region, thus, recalling Figure 4.68, the H, OH and O radicals reach their maximum molar fraction values. In fact, the weight of the backward reaction of the branching grows reducing the overall production of these radicals. As a result, the consumption of the oxygen molecule to produce a $HO_2$ radical becomes more favored. Since this path can only propagate the H radical consumed, the reactivity developed in the system is progressively reduced. Therefore, the slope of the molar fraction of these three active radicals decreases up to zero. In parallel, the molar fractions of $H_2$, CO and $O_2$ become progressively small and also their consumption with active radicals is less favored. As a result, the termination reactions acquire importance in reducing the H, OH and O radicals contributing to the occurrence of the maximum molar fraction values. Then, their slopes become negative, but the amount of such quantity in absolute value is much smaller than that recorded before the peaks. Recalling the dynamic CSTR material balance, the slope of the molar fraction of each species is defined through two terms: the "convective" and the "kinetic". For the species of concern, the first is only negative, since they are not present in the inlet mixture; instead, the second can be split in a production and in a consumption term. In the region of slow decrease of the molar fraction of H, OH and O radicals, their difference is smaller than the convective. In fact, some termination reactions acquire importance over the branching. Performing a ROP Analysis in the second part of the "kinetic" region, the two most relevant termination processes are:

$$H + OH + M \leftrightarrow H_2O + M \qquad (4.64)$$

156

which converts one hydrogen and one hydroxyl radical into a water molecule. The second is another third-body reaction responsible of the OH radicals recombination to give a $H_2O_2$ molecule:

$$OH + OH(+M) \leftrightarrow H_2O_2(+M) \qquad (4.65)$$
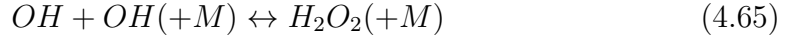
At this point, the reactivity decrease, caused by the $HO_2$ production along with termination reactions, allows a gradual slow re-accumulation of methane continuously fed to the reactor. Most part of this species is consumed by interaction with H, OH and O radicals with the consequent release of $CH_3$. This analysis is reported in Figure 4.68 already considered in Section 4.4.2. Studying the Rate Of Production Analysis for the H radical, the (4.52) is the third most important third-body reaction responsible of the consumption of such radical. In parallel, also the termination which converts a OH and $CH_3$ radicals into methanol has a quite high importance in determining the reactivity inhibition of the system:

$$CH_3 + OH(+M) \leftrightarrow CH_3OH(+M) \qquad (4.66)$$
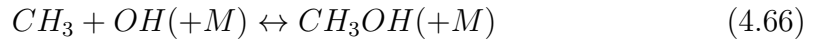
In conclusion, as soon as methane reaches a molar fraction close to zero, the dynamics of the system is controlled by the $H_2$/CO chemistry which causes the fast development of the reactivity, in terms of H, OH and O radicals. A rapid consumption of oxygen can be observed; once it reaches a small molar concentration, the $H + O_2$ third-body reaction becomes more relevant than the branching, causing their production decrease. In parallel, the termination reactions acquire importance converting reactive species into stable molecules. The reactivity progressively vanishes determining the inhibition of the system. When H, OH and O radicals are totally consumed and removed from the reactor, the switch to the slow chemistry occurs and the "kinetic" region ends. Therefore, the "convective" part begins and here, concerning the dynamic CSTR material balance, the "kinetic" term can be neglected with respect to the "convective" contribution. Consequently, since water is not present in the inlet flow rate, its molar fraction reduces during the time. The same analysis can be also performed for carbon dioxide, the other main product of the process under analysis. On the other hand, methane shows a growth of the slope through which it is accumulating in the reactor volume.

### 4.4.4 Kinetic analysis of the causes of oscillations

In the previous sections, the reduced mechanisms which control the two parts in which the "kinetic" region is split have been described. In addition, for the second, also the analysis of the most important termination reactions which cause the reactivity vanishing have been selected. They represent the recombination paths which show a higher growth of their reaction rate with respect to the branching reaction. They are reported below in order of importance in determining the active radicals consumption:

1. $H + O_2(+M) \leftrightarrow HO_2(+M)$

2. $H + OH + M \leftrightarrow H_2O + M$

3. $CH_3 + H(+M) \leftrightarrow CH_4(+M)$

4. $OH + OH(+M) \leftrightarrow H_2O_2(+M)$

They have been defined as the cause of the system inhibition and, consequently, of the oscillations appearance. In fact, considering the oxidation of a stoichiometric mixture of 0.01 $CH_4$ and $O_2$ diluted with nitrogen, the oscillating field is between 1149 K and 1224 K. By removing the four previous reactions from the kinetic mechanism, the oscillations disappear. The temperature for the switch from slow to fast chemistry is 1123 K. Keeping the inlet mixture at stoichiometric conditions, but reducing the dilution level, the stationary state is always guaranteed. Figure 4.74 shows the different behaviors of the methane molar fraction as a function of time by removing the four termination reactions.
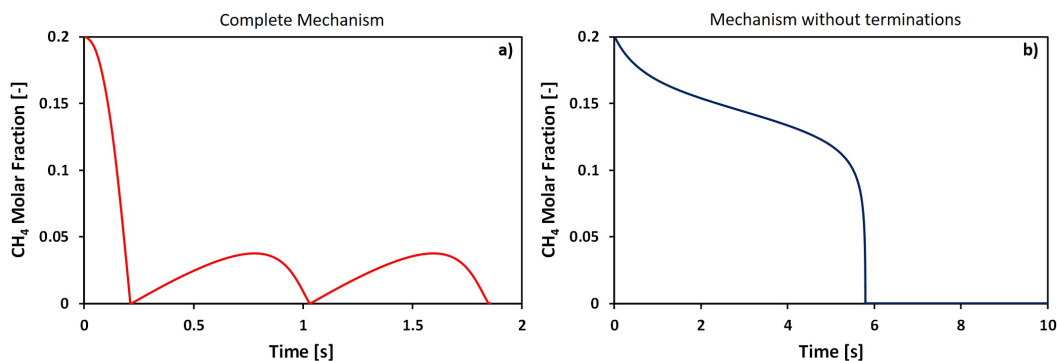


**Figure 4.74:** On the left: methane molar fraction as a function of time obtained at 1150 K with the complete kinetic mechanism. On the right, instead, the same profile has been obtained for the modified kinetic mechanism.

On the other hand, changing the equivalence ratio of the inlet mixture, the hierarchy of termination reactions changes. Switching from stoichiometric to lean

conditions, at place of the (4.65), the termination which consumes a methyl and a hydroxyl radical to give a methanol molecule becomes more important:

$$CH_3 + OH(+M) \leftrightarrow CH_3OH(+M) \tag{4.67}$$
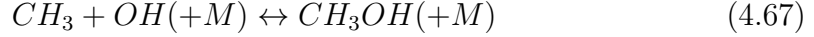
When in the inlet mixture there is an excess of the oxygen with respect to methane, the system becomes more reactive. In fact, with respect to the stoichiometric case, for the same methane molar fraction, the LOL decreases and, thus, smaller temperatures are required in order to observe oscillations. For this reason, methanol production becomes more important than the $H_2O_2$ one. In particular, this last species preferentially decomposes at temperatures around LOL. In addition, the lower amount of OH radicals accumulated reduces the probability to have their recombination. On the contrary, the methyl radical is more concentrated and this increases the importance of the $CH_3OH$ production. In case of slightly rich conditions, the system shows an increase of the LOL for the same methane molar fraction. In this case, studying the ROP Analysis in the region of the oscillations controlled by the $H_2/CO$ mechanism, the fourth termination reaction responsible of the reactivity inhibition is the hydroxyl radicals recombination which acquires more importance than methanol production. In fact, with respect to the stoichiometric conditions, the amount of active radicals developed is a little higher and, at net, the reaction rate of such process is more favored than the methanol production.

Therefore, these 5 reactions have been selected as the cause of the system inhibition and of the oscillations occurrence. Yet, also all the other termination processes cover a role in influencing such phenomena. With respect to the previous ones, they have reaction rates which are smaller and their sum is not enough to counteract the reactivity development of the branching. Therefore, there is a threshold in terms of reaction rate which the sum of the terminations must overcome in order to inhibit the system and allow the switch to the "convective" region. This threshold can be identified in the reaction rate of the branching (4.42). This analysis can be demonstrated through the following procedure. Considering a stoichiometric mixture of methane and oxygen, the initial removal of the first four termination reactions above listed from the kinetic mechanism is able to eliminate the oscillating phenomenon. In this way, changing the operating conditions in terms of temperature, the system does not show oscillations anymore. At $P = 1\,atm$, with 2 s of residence time and a volume of 550 cm$^3$, 1123 K represents the first temperature at which such system ignites with a complete consumption of methane; at the same time, the stationary state is also reached.

Instead, at 1122 K, only a partial conversion of methane occurs and no switch from slow to fast chemistry can be observed.

Then, a fictitious reaction has been created in the mechanism; fictitious because the kinetic constant is arbitrarily given. In particular, the H and OH irreversible recombination to give water has been re-introduced in the scheme with a temperature independent kinetic constant. Therefore, the only Arrhenius parameter different from zero is the pre-exponential factor. Its value is set equal to a number such that the oscillations appear again in the system for a very small temperature window. Therefore, fixing it at $8 \cdot 10^{16} \frac{cm^6}{mol^2 \cdot s}$, at 1123 K, the oscillating phenomenon occurs and it extends up to 1124 K. Figure 4.75 shows the shape of the oscillations in terms of methane molar fraction. The time interval interested by the "CH$_4$ mechanism" is particularly long; in fact, the temperature is rather small and the system requires a longer time to develop an enough reactivity to allow the first complete conversion of methane. At the same time, the kinetic mechanism has been strongly modified and the purpose now is to demonstrate the chemical competition which causes the oscillations and not reproduce the real behavior of the system.
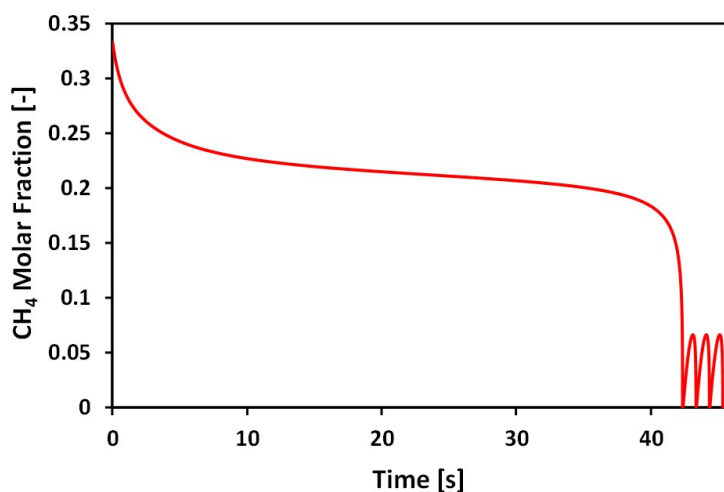


**Figure 4.75:** Methane molar fraction as a function of time. The profile has been obtained through the modified kinetic mechanism in presence of the "fictitious" reaction which causes the oscillations appearing at 1123 K.

At this point, the reaction rate of such process is compared to that of branching. In Figure 4.76, the ratio between the branching and the fictitious reaction rate has been shown as a function of time.
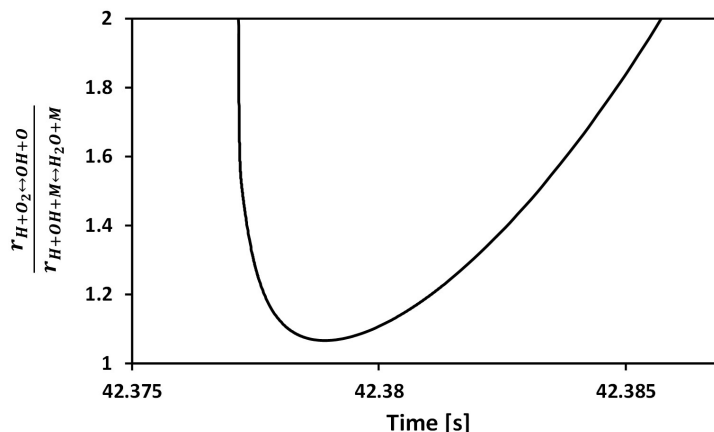
**Figure 4.76:** Time profile of the ratio between the branching and the fictitious reaction rate. Only the time interval around the H, OH and O radicals molar fraction peaks has been provided.

It depicts only a partial time interval which corresponds to the minimum reached by such quantity around the peaks of the H, OH and O radicals. Since the minimum lies above 1 means that reaction rate of the branching is still higher than the fictitious one. At this point, the rates of the terminations not removed from the kinetic mechanism have been added to the one of the fictitious reaction. The terminations involved are all the processes which convert the H, OH and O radicals into stable molecules. There are, however, two exceptions; the first is represented by the third-body reaction which converts hydrogen and oxygen radicals into OH.

$$O + H + M \leftrightarrow OH + M \tag{4.68}$$

Among reactants, three very reactive radicals can be recognized, while only one is present as product. Therefore, such process can be assumed as a pseudo-termination since reduces strongly the system reactivity. The second exception is similar to the previous one and it is based on the interaction between the OH and O radicals, producing $HO_2$.

$$O + OH + M \leftrightarrow HO_2 + M \tag{4.69}$$

Also in this case, from three, only one radical is obtained. In addition, comparing these two reactions, the second contributes to strongly decrease the reactivity since the $HO_2$ radical is much less active than the hydroxyl. On the other hand, from a kinetic point of view, the first process has a higher impact on the system since its reaction rate is higher.

Then, the ratio between the branching reaction and the sum of the terminations

has been computed. Figure 4.77 shows its time profile for the same time interval previously analysed.
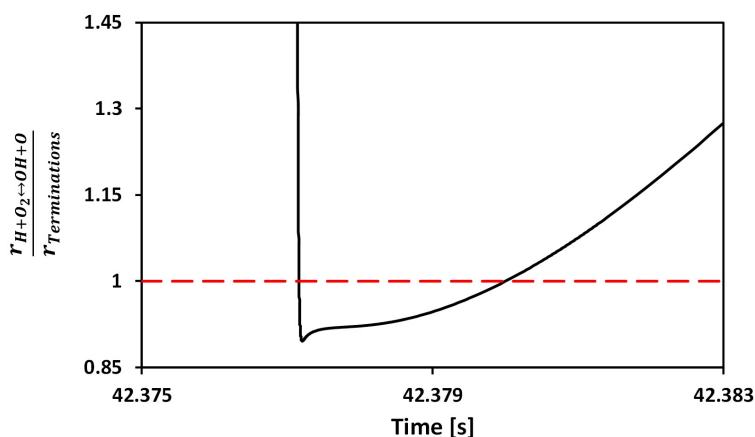


**Figure 4.77:** Temporal profile of the ratio between the branching reaction rate and the sum of the termination processes.

As depicted, the minimum of such ratio is lower than one. In order to complete the analysis, the fictitious reaction is removed from the kinetic mechanism; therefore, the system does not oscillate anymore and at 1123 K it reaches the stationary state. Figure 4.78 provides the time profile of the ratio between the branching and the sum of the termination reactions. As shown, its minimum has always a value higher than 1. This means that the branching prevails on the terminations during the "kinetic" region; this means that the inhibition of the reactivity does not occur and the steady state is achieved. This analysis can confirm the contribution given by all the termination reactions in determining the system inhibition and, therefore, the establishment of oscillations.
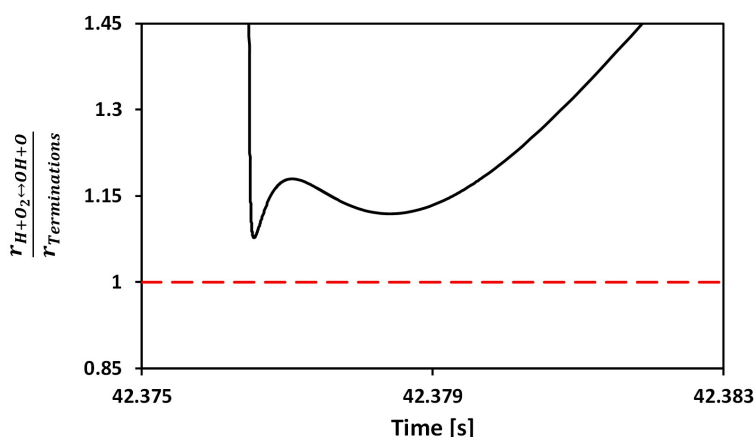


**Figure 4.78:** Temporal profile of the ratio between the branching reaction and the sum of the terminations without the fictitious path.

### 4.4.5 "Branching ratio" as a function of operating conditions

Once understood the importance of all the termination reactions in determining the oscillations, the concept of "branching ratio" is introduced. It indicates the rate of the branching divided by the sum of all the rates of termination reactions which are responsible of the H and OH radicals consumption. Among them, the most relevant reactions in influencing such parameter are listed below in order of importance:

1. $H + O_2(+M) \leftrightarrow HO_2(+M)$

2. $H + OH + M \leftrightarrow H_2O + M$

3. $CH_3 + H(+M) \leftrightarrow CH_4(+M)$

4. $OH + OH(+M) \leftrightarrow H_2O_2(+M)$

5. $CH_3 + OH(+M) \leftrightarrow CH_3OH(+M)$

6. $H + O + M \leftrightarrow OH + M$

7. $OH + O + M \leftrightarrow HO_2 + M$

8. $H + HO_2 \leftrightarrow H_2 + O_2$

9. $OH + HO_2 \leftrightarrow H_2O + O_2$

Considering the inlet mixture at stoichiometric conditions, without diluent and at atmospheric pressure, such ratio is evaluated at several temperatures. At 1170 K, below the Lower Oscillating Limit (1182 K), the system shows a first ignition with an almost 100% of methane conversion and, then, it reaches the stationary state in a "damping" way as depicted in Figure 4.79a.
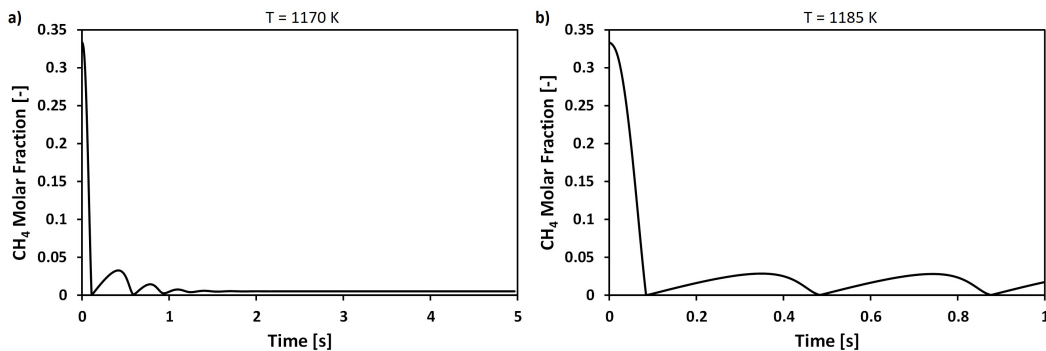


**Figure 4.79:** Methane molar fraction as a function of time evaluated at 1170 K (left) and 1185 K (right).

Figure 4.80a shows the temporal trends of the "branching ratio"; in parallel, also the ratio between the rate of branching reaction and two times the third-body one is displayed. The factor of 2 is a sort of normalization done as a function of the number of net radicals developed by the first process with respect to the second.



**Figure 4.80:** "Branching ratio" (solid black lines) and ratio between branching and $H + O_2$ third-body reaction rates (dotted blue lines) as a function of time at 1170 K (left) and 1185 K (right).

In correspondence of the first minimum of the $CH_4$ molar fraction, the "branching ratio" reaches a value lower than 0.5. Therefore, in this position, the termination reactions become more important than the branching and the reactivity of the system is vanished. The switch to the "convective" region occurs and a re-accumulation of the reactants is observed. When methane and oxygen reach their maximum molar fractions, the "branching ratio" assumes values larger than 1. This means that the weight of the termination processes is lower than the previous time interval. In this way, considering that the branching reaction increases exponentially the amount of radicals, a new reactivity is developed. The second "kinetic" region begins and the reactants are progressively consumed. As seen in Figure 4.79a, methane does not reach a minimum molar fraction as small as the previous cycle. This is due to the relatively small temperature which causes, during the methane conversion, the greater production of $HO_2$ than active radicals. In fact, the weight of the $H + O_2$ third-body reaction is stronger. This is related also to the quite high amount of water, accumulated in the reactor, whose third-body efficiency is particularly high. Therefore, the system does not show anymore the switch to the "$H_2/CO$" mechanism and it is only controlled by the $CH_4$ mechanism, keeping it in slow chemistry. When methane reaches its minimum, the system is again inhibited since the "branching ratio" assumes values lower than 0.5. A new cycle begins, but it shows a smaller amplitude than the

previous. Therefore, the weight of the branching reaction is progressively reduced and, at the end, the system achieves the stationary state. The "branching ratio" keeps lower than one, around 0.65. This demonstrates that the operating conditions are not suitable to develop and sustain a reactivity able to keep the system turned on.

Instead, at 1185 K, the temperature is sufficiently high to allow the establishment of the oscillating phenomenon as depicted in Figure 4.79b. On the other hand, in Figure 4.80b, the two ratios are shown as a function of time. As seen for the previous example, the "branching ratio" reaches its first minimum in correspondence of a value equal to the one observed at 1170 K. With respect to that case, at 1185 K, such quantity grows up to a maximum point which is slighlty lower, but the weight of the branching over the third-body reaction is higher. This allows the development of a larger reactivity in the second "kinetic" region which guarantees the further complete consumption of methane. Therefore, with respect to lower temperatures, the system can show a second switch from "$CH_4$" to "$H_2/CO$" chemistry. This is related to the higher weight of the branching with respect to the $H + O_2$ third-body reaction which allows a greater development of active radicals. In this way, the "branching ratio" decreases up to a very small value, close to 0.4, allowing a new system inhibition and the beginning of a new limit cycle which repeats periodically during the time. Therefore, the higher temperature allows the production in each "limit cycle" of a larger reactivity in terms of active radicals; in this way, also in the following cycles the switch from "$CH_4$" to "$H_2/CO$" mechanism can be observed. Since the temperatures are not extremely high, the termination reactions have still a strong impact on the reactivity allowing the inhibition of the system and, as a result, the oscillations establishment.

Passing to 1250 K, the oscillations are still present but they show a smaller amplitude in terms of methane molar fraction as observable in Figure 4.81a.
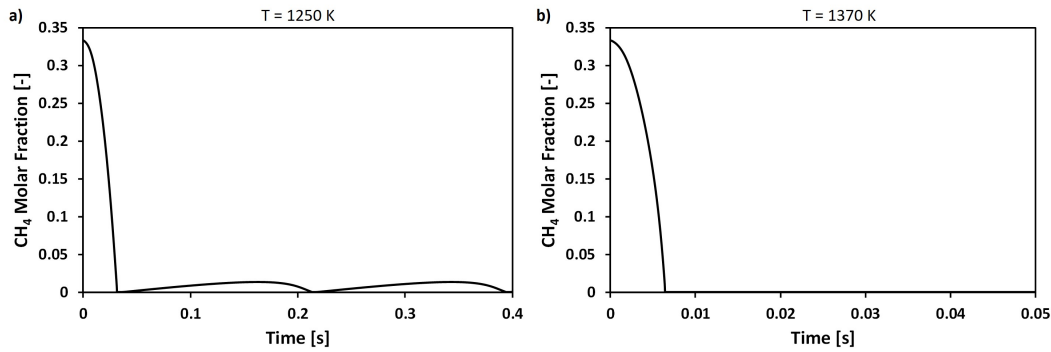
**Figure 4.81:** Methane molar fraction as a function of time at 1250 K (left) and 1370 K (right).

The analysis of the "branching ratio" during the integration time is proposed through Figure 4.82a.
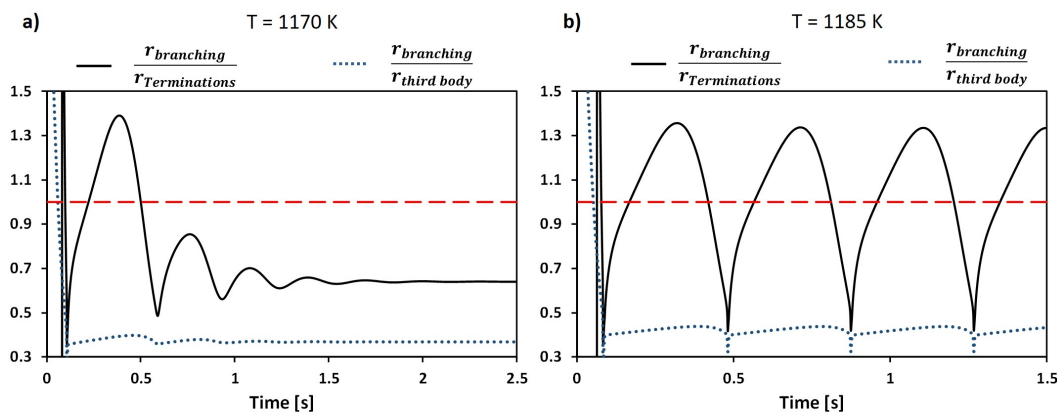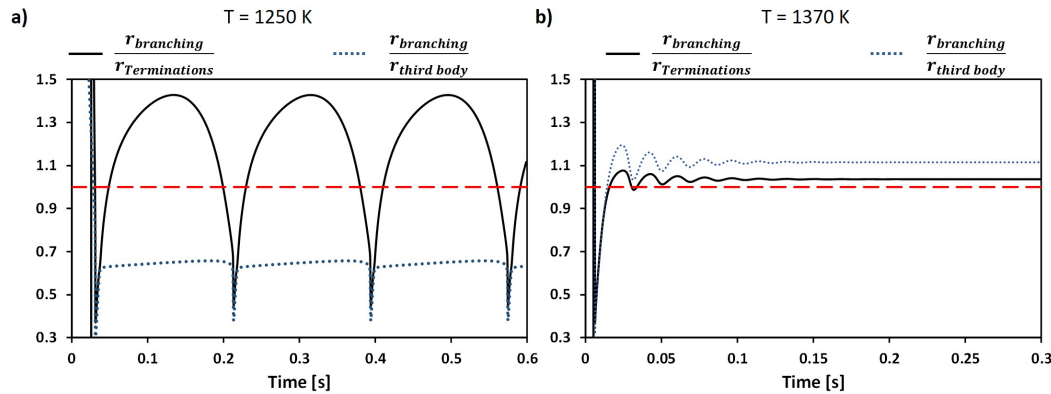


**Figure 4.82:** "Branching ratio" (solid black lines) and ratio between branching and $H + O_2$ third-body reaction rates (dotted blue lines) as a function of time at 1250 K (left) and 1370 K (right).

In parallel, also the trend of the branching weight with respect to the $H + O_2$ third-body reaction is provided. The system dynamics is similar to the one observed at 1185 K. The first minimum point of the "branching ratio" is equal to the ones observed in the other cases. Then, it grows up to a maximum which is about 1.4. In fact, the increased temperature determines the gradual increase of the branching reaction with respect to all the termination processes. But when there is the complete consumption of methane and, consequently, the switch to the "H$_2$/CO" mechanism, the operating conditions are such that the system reactivity is vanished as demonstrated by the minimum value of the "branching ratio" lower than 0.5. Therefore, at this temperature the weight of the terminations is high enough to remove in an efficient way the active radicals, inhibiting the system. Therefore, the oscillations can establish.

The last temperature analysed is above 1367 K, which is the Upper Oscillating

Limit for this system. In Figure 4.81b, the temporal profile of the methane molar fraction is shown at 1370 K. The operating conditions allow the steady state achievement which corresponds to a complete consumption of methane and a system which is turned on. Figure 4.82b shows, instead, the "branching ratio" and the weight of the branching over the $H + O_2$ third-body reaction as a function of time. After the first minimum which is equal to the ones observed at the other temperatures, both the two quantities investigated grow above 1, and in a damping way, they approach their stationary value always higher than 1. Therefore, the weight of the branching reaction at this temperature is higher than the sum of the termination reaction rates and this condition is kept during the time. As a result, the $HO_2$ production is disadvantaged than the OH and O one, and the termination reactions are not able to inhibit the reactivity of the system as at lower temperatures.

Experimentally, for temperature belonging to the oscillating field, within the reactor, periodic ignition and extinction can be observed through flashes of light. Above the upper oscillating limit, this phenomenon is not registered anymore and the light is always present and fixed during the time once achieved the stationary state.

### 4.4.6   Methane oscillations vs diluent

The reduction of the amount of diluent in the inlet mixture modify the extension of the oscillating field. Figure 4.83 proposes the LOL and UOL in terms of temperature obtained as a function of diluent molar fraction at 1 atm of pressure. The well-stirred reactor is operated in isothermal conditions with a residence time of 2 s and a volume of 550 cm$^3$. Four diluents have been investigated. They have been chosen as a function of their average third-body efficiencies. Helium has a lower than 1 efficiency, nitrogen is a neutral species in these terms, while water and $CO_2$ have third-body efficiencies higher than 1.

As depicted, switching from He to carbon dioxide, starting from a 0 diluent molar fraction, the limits show a smaller slope. For the same inlet mixture composition, higher temperatures are required to observe the oscillations appearing and vanishing. In case of $H_2O$, instead, the Lower Oscillating Limit has a positive slope, while the Upper behaves similarly to those of other diluents.

Changing the third component of the inlet mixture, the oscillating field changes. This because the weight of the third-body reactions changes with the variation of the diluent added to the reactants. In fact, as seen above, in order to observe the oscillations, it is necessary to have a system inhibition in the last part of the

"kinetic" region of each limit cycle. This is caused by the termination reactions and, among them, the most important ones are also third-body processes.
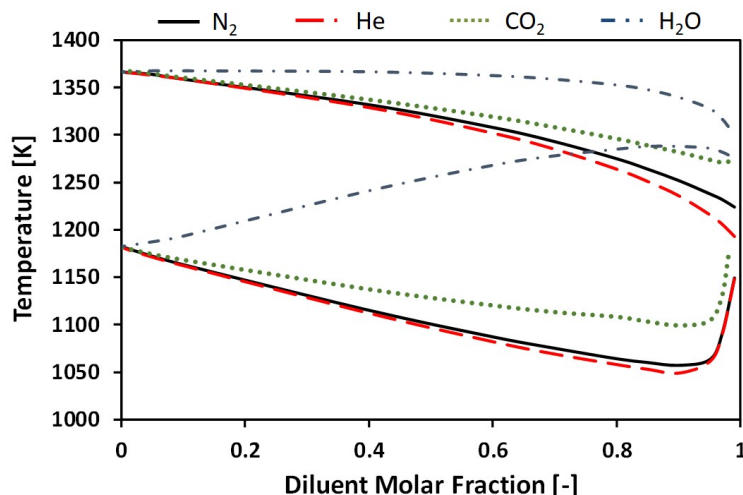


**Figure 4.83:** Lower and Upper Oscillating Limits as a function of diluent molar fraction obtained at 1 atm of pressure in an isothermal well-stirred reactor with a residence time of 2 s and a volume of 550 cm$^3$. The inlet mixture is evaluated at stoichiometric conditions.

Consequently, passing from a diluent with a higher efficiency, for the same inlet mixture composition, the LOL and UOL moves to greater temperatures. The first because higher temperatures are required in order to allow a near to 100 % of conversion of methane in the part of the "kinetic" region controlled by the CH$_4$ mechanism. On the other hand, the Upper Oscillating Limit corresponds to operating conditions such that the branching process is more favored than termination reactions, which are influenced by the efficiencies of the diluent adopted. In particular, recalling the "branching ratio", with the increase of the weight of third-body reactions, such quantity reduces and higher temperatures are needed in order to make the branching more favored.

Analyzing, moreover, the Lower and Upper Oscillating Limit curves for the helium, nitrogen and carbon dioxide, they decrease with the increase of the dilution level in the inlet mixture. This is again an effect related to the third-body reactions. In fact, higher is the amount of the diluent, lower is the molar fraction of methane and oxygen; therefore, the amount of products as CO$_2$ and H$_2$O produced within the reactor are smaller. Hence, their impact on these kinds of reactions is progressively smaller and this allows lower temperatures to show the oscillations appearance and vanishing. Always in terms of "branching ratio", since the weight of the third-body reactions is gradually lower, such ratio is higher and, for the same pressure, lower temperatures allow to achieve the stationary state.

On the other hand, in case of water, LOL curve changes in the opposite direction than the other diluents. In fact, its third-body efficiency is able to counteract the lower amount of $H_2O$ produced in the reactor with the dilution level increase. This occurs up to a percentage of diluent of about 95%, above which it is reduced along with the extension of the oscillating field due to the small reactivity of the system caused by the very small concentration of the reactants.

Considering, in conclusion, the behavior of LOL and UOL for a single diluent, nitrogen for example, for a dilution level until a value around 0.9, both the curves monotonously decreases. Instead, above this point, the oscillating field reduces its extension. This is related to the drastic decrease of the amount of reactants introduced in the system which causes the gradual reduction of the reactivity developed in the reactor; in addition, the diluent shows a too high concentration and it is responsible, at the end, of the recombination and extinction of the reaction itself.

### 4.4.7 P-T-$\tau$ map

As done for hydrogen and syngas, also for methane the P-T oscillating fields have been obtained at three different residence times: 0.1 s, 2 s and 10 s. Figure 4.84 shows these diagrams obtained for a stoichiometric mixture of methane and oxygen within a well-stirred reactor of 550 cm³.
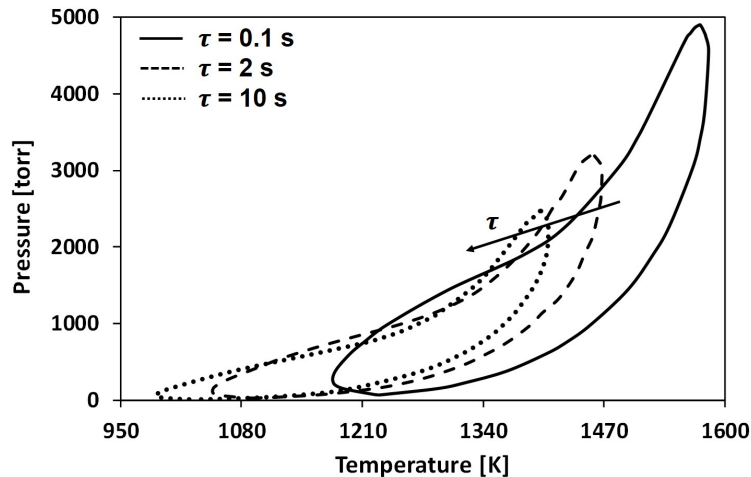


**Figure 4.84:** P-T maps obtained for a stoichiometric mixture of methane and oxygen, without diluent at three residence times: 0.1 s, 2 s and 10 s.

With the decrease of the residence time, the oscillating region is shifted to higher temperatures interesting a larger pressure window. Moving to 0.1 s, in addition, also the extension of the field is increased. In order to explain such behavior, the concept of residence time must be again considered. Its variation influences the flow rate exchanged by the reactor with the external environment. In fact, it results from the ratio between the volume and the volumetric flow rate. For the same reactor volume, by decreasing $\tau$, the flow rate increases. Therefore, concerning the dynamic CSTR material balance for the active radicals as H, OH and O, the higher the flow rate, the higher the "convective" term. Such contribution is negative for these species and, therefore, it contributes, along with the termination reactions, to reduce and to inhibit the system reactivity. Therefore, with the reduction of the residence time, for the same pressure, an higher temperature is required to observe both the ignition and the inhibition of the oscillating phenomenon. So, the "convective" contribution can be placed at the denominator of the "branching ratio"; an increase of the residence time means lower radicals removed per unit of time and, consequently, the ratio assumes values which are higher for the same operating conditions. Hence, fixed the pressure, the temperature window within the system oscillates is shifted to lower temperatures.

CHAPTER $5$

# Conclusions and outlooks

I N this Thesis, the analysis of methane combustion in MILD oxy-fuel conditions has been investigated. In particular, the development of a detailed kinetic mechanism to model such unconventional conditions has been performed. Starting from the state-of-the-art scheme developed by the CRECK Modeling group at "Politecnico di Milano", the updated "POLIMI 1702" has been obtained. The "AramcoMech1.3" has been adopted as core for the new mechanism and the thermodynamic database has been updated through the Burcat [56]. In this way, the huge collection of experimental data concerning the oxy-combustion of methane in presence of high dilution levels of $CO_2$ and $H_2O$ has been simulated, showing a good accuracy in predicting several operating conditions of temperature, pressure and composition. Different reactors have been considered: laminar flame speeds, plug-flow reactors and well-stirred reactors. In particular, perfectly-stirred reactors, studied in conditions intermediate between the low and the high temperature, showed an oscillatory behavior, characterized from a periodic extinction and re-ignition of the mixture, resulting in a discontinuous phenomenon. Therefore, a theoretical analysis and study from a kinetic point of view of this problem has been performed to get an insight on the underlying causes of the establishment of such limit cycles. Due to the relatively high complexity of the kinetic mecha-

nism of methane, the preliminary analysis of the hydrogen and syngas has been carried out. In fact, their oxidation is based on a number of reactions in the order of tens and they show an oscillatory combustion within well-stirred reactors at low-pressure conditions, too. In case of hydrogen, the role of $H_2O$ in controlling the chemical competition between the $H + O_2$ branching and third-body reaction has been identified as the cause of the system inhibition. This, coupled with the continuous mass exchange of the reactor with the external environment, causes the return of reactivity and the beginning of a new "limit cycle". In case of syngas, when the molar fraction of CO becomes sufficiently higher than the $H_2$, the inhibition of the system reactivity after the ignition is guaranteed by a further competition with respect to the previous. In particular, the consumption of the O radical through the hydrogen or carbon monoxide represents a second source of the oscillations. In this way, it has been possible to understand the important role of the termination reactions in determining the consumption of the active radicals as H, OH and O with respect to the branching reaction, which is the only process responsible of their exponential increase. Afterwards, starting from the analysis of such fuels, the causes of the oscillating combustion for methane could be defined. The chemical competition between the $H + O_2$ branching and the main termination reactions responsible of the active radical consumption is the cause of the reactivity inhibition and, consequently, of the oscillations establishment. In order to explain such concept the "branching ratio" has been created, as a measure to weight the branching over the termination reactions. It has been observed that below the LOL it keeps smaller than 1, while above UOL it is higher than 1. On the other hand, in the oscillating field, it periodically changes by alternating from a very small value to a maximum, close to or higher than 1. In this way, the chemical competition between the branching and the termination channels has been demonstrated through such parameter.

Starting from the kinetic mechanism developed and from the kinetic analysis performed for fuel up to methane, further work can be developed on these bases. This Thesis ends with a short mention to some of them.

## 5.1 "POLIMI 1702" extension

Describing the chemistry of the methane combustion in several conditions is the basis for the extension of a kinetic model to higher hydrocarbons as well as to pollutants. In fact, the dynamics of the combustion of these species is strongly influenced by the oxidation of methane. Therefore, "POLIMI 1702" represents the basis for the future extension of the model. First of all, the extension to higher

hydrocarbon, including also the oxygenated ones must be done. In parallel, the introduction of the subset of reactions describing the $NO_x$ production must be performed. These operations require a procedure similar to the one investigated in this Thesis, based on a huge collection of experimental data on which perform testing and validation of the model in development.

At the end, a reduction of the scheme can be performed in order to recover a model able to be implemented within large CFD simulations. In this way, such tool can be used in the modeling of industrial units like the innovative steam cracking furnaces investigated by IMPROOF. Therefore, it will be used to estimate the amount of $NO_x$ really emitted along with the impact on adopting alternative fuels as bio-gas on the net $CO_2$ produced.

## 5.2 Higher hydrocarbon oscillations

Heavier hydrocarbons, as ethane and ethylene, show an oscillating combustion within well-stirred reactors. Since the chemistry of such species is characterized by reactions involved in the "POLIMI 1702" kinetic mechanism, such model can be used to perform a kinetic study of such phenomenon also for these species. In addition, considering that the most relevant termination reactions involved in the "branching ratio" are mostly the same, a similar behavior for such parameter is expected, too.

In addition, a further extension of the analysis of the "branching ratio" can be performed within non-isothermal well-stirred reactors. In this way, the dependence of the heat exchange on the oscillations can be studied allowing to define the conditions which make the system oscillate.

Finally, once understood all the causes also for higher hydrocarbons and in non-isothermal conditions, the development of a model able to predict the oscillating combustion in well-stirred reactors can be developed. In this way, the obtained tool could be used to define the operating conditions in an industrial unit to avoid the oscillations establishment along with all the related negative consequences.

# Bibliography

[1] H. Zimmermann, R. Walzl, Ethylene, Wiley-VCH Verlag GmbH & Co. KGaA, 2000.

[2] S. A. Miller, Ethylene and its industrial derivatives, Benn, 1969.

[3] W. R. True, Global ethylene capacity poised for major expansion, Oil & gas journal 111 (7) (2013) 90–95.

[4] T. Ren, M. K. Patel, K. Blok, Steam cracking and methane to olefins: energy use, co 2 emissions and production costs, Energy 33 (5) (2008) 817–833.

[5] A. Chauvel, G. Lefebvre, Petrochemical Processes...., Editions OPHRYS, 1989.

[6] C. E. Baukal Jr, The john zink hamworthy combustion handbook: Volume 1-Fundamentals, CRC press, 2012.

[7] C. Tien, S. Lee, Flame radiation, Progress in Energy and Combustion Science 8 (1) (1982) 41 – 59.

[8] M. R. Djokic, K. M. Van Geem, G. J. Heynderickx, S. Dekeukeleire, S. Vangaever, F. Battin-Leclerc, G. Bellos, W. Buysschaert, B. Cuenot, T. Faravelli, Improof: Integrated model guided process optimization of steam cracking furnaces, in: International Conference on Sustainable Design and Manufacturing, Springer, 2017, pp. 589–600.

[9] T. Ren, M. Patel, K. Blok, Olefins from conventional and heavy feedstocks: Energy use in steam cracking and alternative processes, Energy 31 (4) (2006) 425–451.

## Bibliography

[10] Y. Zhang, F. Qian, C. M. Schietekat, K. M. Van Geem, G. B. Marin, Impact of flue gas radiative properties and burner geometry in furnace simulations, AIChE Journal 61 (3) (2015) 936–954.

[11] B. Adams, J. Olver, Impact of high-emissivity coatings on process furnace heat transfer, in: AIChE Spring Meeting, 2015.

[12] G. D. Stefanidis, K. M. Van Geem, G. J. Heynderickx, G. B. Marin, Evaluation of high-emissivity coatings in steam cracking furnaces using a non-grey gas radiation model, Chemical Engineering Journal 137 (2) (2008) 411–421.

[13] C. Schietekat, M. M. Van Goethem, K. Van Geem, G. Marin, 3d swirl flow reactor technology for pyrolysis processes: Hydrodynamic and computational fluid dynamic study, in: XX International conference on chemical reactors (Chemreactor-20), 2012.

[14] P. A. Reyniers, C. M. Schietekat, D. J. Van Cauwenberge, L. A. Vandewalle, K. M. Van Geem, G. B. Marin, Necessity and feasibility of 3d simulations of steam cracking reactors, Industrial & Engineering Chemistry Research 54 (49) (2015) 12270–12282.

[15] A. Oasmaa, B. van de Beld, P. Saari, D. C. Elliott, Y. Solantausta, Norms, standards, and legislation for fast pyrolysis bio-oils from lignocellulosic biomass, Energy & Fuels 29 (4) (2015) 2471–2484.

[16] S. R. Turns, An introduction to combustion, Vol. 287, McGraw-hill New York, 1996.

[17] G. Williams, Combustion theory.

[18] M. Chaos, F. L. Dryer, Syngas combustion kinetics and applications, Combustion Science and Technology 180 (6) (2008) 1053–1096.

[19] R. Rota, Fondamenti di termodinamica dell'ingegneria chimica, Pitagora, 2015.

[20] K. K. Kuo, Principles of combustion.

[21] J. I. Steinfeld, J. S. Francisco, W. L. Hase, Chemical kinetics and dynamics, Vol. 3, Prentice Hall Englewood Cliffs (New Jersey), 1989.

[22] A. Linan, F. A. Williams, Fundamental aspects of combustion.

[23] B. Lewis, G. Von Elbe, Combustion, flames and explosions of gases, Elsevier, 2012.

[24] e. a. Ahren W. Jasper, Third-body collision efficiencies for combustion modeling: hydrocarbons in atomic and diatomic baths, Proceedings of the Combustion Institute 35.

[25] F. A. De Capitani, F., Flammability limits computation through laminar flame speed method.

[26] B. Bolin, B. Doos, Greenhouse effect, New York, NY (USA); John Wiley and Sons Inc., 1989.

[27] R. D. Brook, S. Rajagopalan, C. A. Pope, J. R. Brook, A. Bhatnagar, A. V. Diez-Roux, F. Holguin, Y. Hong, R. V. Luepker, M. A. Mittleman, et al., Particulate matter air pollution and cardiovascular disease, Circulation 121 (21) (2010) 2331–2378.

[28] M. K. Hubbert, Energy from fossil fuels, Science 109 (2823) (1949) 103–109.

[29] I. E. Agency, Key world energy statistics, International Energy Agency, 2007.

[30] M. Hoel, S. Kverndokk, Depletion of fossil fuels and the impacts of global warming, Resource and Energy Economics 18 (2) (1996) 115 – 136.

[31] I. E. A. (IEA), CO2 Emissions from Fuel Combustion (2017 edition), Internal Energy Agency (IEA), 2017.

[32] S. Solomon, G.-K. Plattner, R. Knutti, P. Friedlingstein, Irreversible climate change due to carbon dioxide emissions, Proceedings of the National Academy of Sciences 106 (6) (2009) 1704–1709.

[33] K. L. Demerjian, J. A. Kerr, J. G. Calvert, The mechanism of photochemical smog formation, Wiley, 1974.

[34] R. M. Harrison, J. Yin, Particulate matter in the atmosphere: which particle properties are important for its effects on health?, Science of The Total Environment 249 (1) (2000) 85 – 101.

[35] M. Frenklach, Reaction mechanism of soot formation in flames, Physical Chemistry Chemical Physics 4 (11) (2002) 2028–2037.

[36] T. Jayaraman, T. Kanitkar, The paris agreement, Economic and Political Weekly 51 (3).

[37] A. Cavaliere, M. de Joannon, Mild combustion, Progress in Energy and Combustion science 30 (4) (2004) 329–366.

[38] J. Wünning, J. Wünning, Flameless oxidation to reduce thermal no-formation, Progress in energy and combustion science 23 (1) (1997) 81–94.

[39] M. Noor, A. P. Wandel, T. Yusaf, A review of mild combustion and open furnace design consideration, International Journal of Automotive and Mechanical Engineering 6 (1) (2012) 730–754.

[40] Y. B. Zeldovich, P. Y. Sadovnikov, D. Frank-Kamenetskii, Oxidation of nitrogen in combustion, translation by m, Shelef, Academy of Sciences of USSR, Institute of Chemical Physics, Moscow-Leningrad.

[41] H. Tsuji, A. K. Gupta, T. Hasegawa, M. Katsuki, K. Kishimoto, M. Morita, High temperature air combustion: from energy conservation to pollution reduction, CRC press, 2002.

[42] P. Li, F. Hu, B. Xiong, J. Zhang, J. Mi, Chapter 14 - {MILD} oxy-fuel combustion, in: C. Zheng, Z. Liu (Eds.), Oxy-Fuel Combustion, Academic Press, 2018, pp. 289 – 324.

[43] A. Cuoci, A. Frassoldati, T. Faravelli, E. Ranzi, Opensmoke++: An object-oriented framework for the numerical modeling of reactive systems with detailed kinetic mechanisms, Computer Physics Communications 192 (2015) 237–264.

[44] G. Buzzi-Ferraris, F. Manenti, Bzzmath: Library overview and recent advances in numerical methods.

[45] Creck modeling.
URL www.creckmodeling.chem.polimi.it

[46] E. Ranzi, A. Frassoldati, R. Grana, A. Cuoci, T. Faravelli, A. Kelley, C. Law, Hierarchical and comparative kinetic modeling of laminar flame speeds of hydrocarbon and oxygenated fuels, Progress in Energy and Combustion Science 38 (4) (2012) 468 – 501.

[47] D. M. Smooke, J. A. Miller, R. J. Kee, Determination of adiabatic flame speeds by boundary value methods, Combustion Science and Technology 34 (1-6) (1983) 79–90.

[48] S. Liao, D. Jiang, Z. Huang, Q. Cheng, J. Gao, Y. Hu, Approximation of flammability region for natural gas-air-diluent mixture, Journal of Hazardous Materials 125 (1) (2005) 23 – 28.

[49] R. J. Kee, J. A. Miller, T. H. Jefferson, Chemkin: A general-purpose, problem-independent, transportable, fortran chemical kinetics code package, Tech. rep. (1980).

[50] R. Design, Chemkin software input manual, San Diego, CA.

[51] e. a. Lindemann, Discussion on the radiation theory of chemical action, Transactions of the Faraday Society 17 (1922) 598–606.

[52] R. Gilbert, K. Luther, J. Troe, Theory of thermal unimolecular reactions in the fall-off range. ii. weak collision rate constants, Berichte der Bunsengesellschaft für physikalische Chemie 87 (2) (1983) 169–177.

[53] S. et al., Pressure and temperature dependence of reactions proceeding via a bound complex. 2. application to 2ch3=c2h5+h, Combustion and Flame 75 (1) (1989) 25–31.

[54] R. Design, Chemkin theory manual, San Diego, CA.

[55] A. Burcat, Thermochemical data for combustion calculations, Combustion chemistry (1984) 455–473.

[56] A. Burcat, B. Ruscic, Third millenium ideal gas and condensed phase thermochemical database for combustion with updates from active thermochemical tables, Argonne National Laboratory Argonne, IL, 2005.

[57] Napoli, Istituto di ricerche sulla combustione.
URL http://www.irc.cnr.it/

[58] Nancy, Centre national de la recherche scientifique.
URL http://www.cnrs.fr/centre-est/

[59] A. N. Mazas, D. A. Lacoste, T. Schuller, Experimental and numerical investigation on the laminar flame speed of ch4/o2 mixtures diluted with co2 and h2o (2010).

[60] A. A. Konnov, I. V. Dyakov, Measurement of propagation speeds in adiabatic cellular premixed flames of ch4+o2+co2, Experimental Thermal and Fluid Science 29 (8) (2005) 901 – 907.

[61] A. A. Konnov, I. V. Dyakov, Experimental study of adiabatic cellular premixed flames of methane (ethane, propane)+oxygen+carbon dioxide mixtures, Combustion Science and Technology 179 (4) (2007) 747–765.

**Bibliography**

[62] F. H. Coppens, A. A. Konnov, The effects of enrichment by h2 on propagation speeds in adiabatic flat and cellular premixed flames of ch4+o2+co2, Fuel 87 (13) (2008) 2866 – 2870.

[63] Y. Xie, J. Wang, M. Zhang, J. Gong, W. Jin, Z. Huang, Experimental and numerical study on laminar flame characteristics of methane oxy-fuel mixtures highly diluted with co2, Energy & Fuels 27 (10) (2013) 6231–6237.

[64] A. Keromnes, W. K. Metcalfe, K. A. Heufer, N. Donohoe, A. K. Das, C.-J. Sung, J. Herzler, C. Naumann, P. Griebel, O. Mathieu, M. C. Krejci, E. L. Petersen, W. J. Pitz, H. J. Curran, An experimental and detailed chemical kinetic modeling study of hydrogen and syngas mixture oxidation at elevated pressures, Combustion and Flame 160 (6) (2013) 995 – 1011.

[65] S. M. Burke, W. Metcalfe, O. Herbinet, F. Battin-Leclerc, F. M. Haas, J. Santner, F. L. Dryer, H. J. Curran, An experimental and modeling study of propene oxidation. part 1: Speciation measurements in jet-stirred and flow reactors, Combustion and Flame 161 (11) (2014) 2765 – 2784.

[66] S. M. Burke, U. Burke, R. M. Donagh, O. Mathieu, I. Osorio, C. Keesee, A. Morones, E. L. Petersen, W. Wang, T. A. DeVerter, M. A. Oehlschlaeger, B. Rhodes, R. K. Hanson, D. F. Davidson, B. W. Weber, C.-J. Sung, J. Santner, Y. Ju, F. M. Haas, F. L. Dryer, E. N. Volkov, E. J. Nilsson, A. A. Konnov, M. Alrefae, F. Khaled, A. Farooq, P. Dirrenberger, P.-A. Glaude, F. Battin-Leclerc, H. J. Curran, An experimental and modeling study of propene oxidation. part 2: Ignition delay time and flame speed measurements, Combustion and Flame 162 (2) (2015) 296 – 314.

[67] C.-W. Zhou, Y. Li, E. O'Connor, K. P. Somers, S. Thion, C. Keesee, O. Mathieu, E. L. Petersen, T. A. DeVerter, M. A. Oehlschlaeger, G. Kukkadapu, C.-J. Sung, M. Alrefae, F. Khaled, A. Farooq, P. Dirrenberger, P.-A. Glaude, F. Battin-Leclerc, J. Santner, Y. Ju, T. Held, F. M. Haas, F. L. Dryer, H. J. Curran, A comprehensive experimental and modeling study of isobutene oxidation, Combustion and Flame 167 (2016) 353 – 379.

[68] Y. Li, C.-W. Zhou, K. P. Somers, K. Zhang, H. J. Curran, The oxidation of 2-butene: A high pressure ignition delay, kinetic modeling study and reactivity comparison with isobutene and 1-butene, Proceedings of the Combustion Institute 36 (1) (2017) 403 – 411.

180

[69] W. K. Metcalfe, S. M. Burke, S. S. Ahmed, H. J. Curran, A hierarchical and comparative kinetic modeling study of c1-c2 hydrocarbon and oxygenated fuels, International Journal of Chemical Kinetics 45 (10) (2013) 638–675.

[70] C. Olm, I. G. Zsely, R. Palvolgyi, T. Varga, T. Nagy, H. J. Curran, T. Turanyi, Comparison of the performance of several recent hydrogen combustion mechanisms, Combustion and Flame 161 (9) (2014) 2219 – 2234.

[71] C. Olm, I. G. Zsely, T. Varga, H. J. Curran, T. Turanyi, Comparison of the performance of several recent syngas combustion mechanisms, Combustion and Flame 162 (5) (2015) 1793 – 1812.

[72] D. F. Davidson, M. D. Di Rosa, E. J. Chang, R. K. Hanson, C. T. Bowman, A shock tube study of methyl-methyl reactions between 1200 and 2400 k, International journal of chemical kinetics 27 (12) (1995) 1179–1196.

[73] P. Stewart, C. Larson, D. Golden, Pressure and temperature dependence of reactions proceeding via bound complex., Combustion and Flame 75 (1) (1989) 25 – 31.

[74] E. Goos, A. Burcat, B. Ruscic, Extended third millennium ideal gas and condensed phase thermochemical database for combustion with updates from active thermochemical tables.

[75] S. J. Klippenstein, From theoretical reaction dynamics to chemical modeling of combustion, Proceedings of the Combustion Institute 36 (1) (2017) 77 – 111.

[76] A. B. Bendtsen, P. Glarborg, K. Dam-johansen, Low temperature oxidation of methane: the influence of nitrogen oxides, Combustion Science and Technology 151 (1) (2000) 31–71.

[77] P. Glarborg, L. L. B. Bentzen, Chemical effects of a high co2 concentration in oxy-fuel combustion of methane, Energy & Fuels 22 (1) (2007) 291–296.

[78] P. de Joannon, M. Sabia, Istituto di ricerche sulla combustione, Private Communications.

[79] COST, 3rd general meeting and workshop on secs in industry of smartcats action, 2017.

[80] M. de Joannon, A. Cavaliere, T. Faravelli, E. Ranzi, P. Sabia, A. Tregrossi, Analysis of process parameters for steady operations in methane mild com-

bustion technology, Proceedings of the Combustion Institute 30 (2) (2005) 2605 – 2612.

[81] D. Baulch, J. Griffiths, A. J. Pappin, A. F. Sykes, Stationary-state and oscillatory combustion of hydrogen in a well-stirred flow reactor, Combustion and Flame 73 (2) (1988) 163 – 185.

[82] D. L. Baulch, J. F. Griffiths, A. J. Pappin, A. F. Sykes, Third-body interactions in the oscillatory oxidation of hydrogen in a well stirred flow reactor, Journal of the Chemical Society, Faraday Transactions 1: Physical Chemistry in Condensed Phases 84 (5) (1988) 1575–1586.

[83] D. L. Baulch, J. F. Griffiths, B. Johnson, R. Richter, Hydroxyl radical concentrations and reactant temperature profiles during oscillatory ignition of hydrogen: experimental measurements by laser resonance absorption spectroscopy and comparisons with numerical calculations, in: Proceedings of the Royal Society of London A: Mathematical, Physical and Engineering Sciences, Vol. 430, The Royal Society, 1990, pp. 151–166.

[84] P. Gray, J. Griffiths, S. Scott, Branched-chain reactions in open systems: theory of the oscillatory ignition limit for the hydrogen+ oxygen reaction in a continuous-flow stirred-tank reactor, Proceedings of the Royal Society of London. Series A, Mathematical and Physical Sciences (1984) 243–258.

[85] M. de Joannon, P. Sabia, A. Tregrossi, A. Cavaliere, Dynamic behavior of methane oxidation in premixed flow reactor, Combustion Science and Technology 176 (5-6) (2004) 769–783.

[86] P. Sabia, G. Sorrentino, A. Chinnici, A. Cavaliere, R. Ragucci, Dynamic behaviors in methane mild and oxy-fuel combustion. chemical effect of co2, Energy & Fuels 29 (3) (2015) 1978–1986.

[87] M. de Joannon, Private communication, Istituto di Ricerche sulla Combustione, Napoli, 2017.

[88] F. Battin-Leclerc, Private communication, Centre National de la Recherche Scientifique, Nancy, 2017.